Thesis

Imprints of the primordial Universe in the Cosmic Microwave and gravitational wave backgrounds

FENU, Elisa

Abstract

La recherche présentée dans cette thèse représente d'importantes briques sur le chemin de la construction d'une compréhension plus complète et profonde des mécanismes physique caractéristiques des premières secondes après la création de notre Univers, un régime de température et d'énergies autrement inaccessibles en laboratoire. De plus, ceci souligne également les questions ouvertes qui restent non résolues.

Reference

FENU, Elisa. *Imprints of the primordial Universe in the Cosmic Microwave and gravitational wave backgrounds*. Thèse de doctorat : Univ. Genève, 2011, no. Sc. 4329

UNIVERSITÉ DE GENÈVE
Département de physique théorique

FACULTÉ DES SCIENCES
Prof. Ruth DURRER

Imprints of the primordial Universe in the Cosmic Microwave and Gravitational Wave Backgrounds

THÈSE

présentée à la Faculté des sciences de l'Université de Genève
pour obtenir le grade de
Docteur ès sciences, mention physique

par

Elisa Fenu

de

Bologna (Italie)

Thèse N° XXXXXX

GENÈVE

Atelier de reproduction de la Section de physique

2011

Résumé

L'objet d'étude de la cosmologie est notre propre Univers conçu comme un système physique obéissant aux lois de la physique valides sur Terre. Dès lors, le dessein des cosmologistes est de parvenir à la compréhension des origines de notre Univers et de son évolution au travers de stages temporels distincts par leurs dynamiques propres. Un des aspects les plus stimulants de la cosmologie moderne est la possibilité pour les physiciens d'avoir un aperçu et finalement de tester un éventail d'énergies si hautes qu'elles ne peuvent pas être atteintes en laboratoire. Cet objectif peut être réalisé par l'étude de processus physiques caractéristiques des premiéres secondes suivant le Big-Bang, alors que la température était extrêmement haute et que des mécanismes n'ayant pas encore de confirmation physique ont pu joué un rôle important.

Dans cette thèse, j'ai étudié l'Univers jeune au travers des empreintes que des mécanismes à hautes énergies ont pu laisser dans le fonds diffus cosmologique et dans le fonds des ondes gravitationnelles. A l'aide des nouvelles données, nous sommes sur le point d'atteindre, d'ici quelques années, un niveau de précision nous permettant d'accéder à une compréhension plus profonde des processus typiques de l'Univers issu directement du Big-Bang, et ainsi, de tester la physique aux très hautes températures d'alors. J'ai en particulier concentré mes recherches sur deux traits fondamentaux différents qui ont pu caractériser l'Univers jeune: les champs magnétiques primordiaux et les défauts cosmologiques.

D'un côté, nous nous intéressons à la question qui concerne l'origine des champs magnétiques observés aujourd'hui dans les galaxies et les clusters: il demeure flou de savoir si de tels champs ont été générés par un champs primordial provenant de l'Univers jeune et de ses processus à hautes énergies ou s'il s'agit du résultat de scénarios de séparation de charges lors de la formation tardive des structures. Selon la première option, nous devrions alors pouvoir détecter les empreintes d'un tel champs dans le fonds diffus. Une telle analyse a déjà permis d'obtenir d'importantes contraintes sur les caractéristiques du champs primordial avant la recombinaison, telle son amplitude initiale. Nous avons d'abord analysé les interactions entre les champs magnétiques et les ondes gravitationnelles, confirmant que ces interactions ne sont pas une cause d'amplification de ces deux quantités physiques, au moins jusqu'au second ordre dans les perturbations. Concernant d'autres conséquences de cette interaction, nous avons suivi une idée présentée auparavant dans la littérature selon laquelle nous pouvons obtenir des limites supérieures plus sévères qu'au travers d'une analyse du fonds diffus sur l'amplitude du champs primordial, à supposer qu'il provienne de mécanismes causaux. Appliquant les limites de la nucléosynthèse sur la densité d'énergie des ondes gravitationnelles produites par un champs primordial alors que l'Univers est encore très jeune, nous avons pu exclure la plupart des mécanismes primordiaux proposés pour générer des champs magnétiques. En effet, nous avons confirmé que des champs générés de manière causale n'ont pas assez de puissance à grande échelle même s'ils présentent initialement une composante hélicoïdale les faisant évoluer par cascade inverse. Les limites dans le cas de champs hélicoïdaux sont plus souples que celles obtenues pour des champs standards non hélicoïdaux, mais ils ne peuvent pas avoir générés les champs observés dans les galaxies et les clusters, même si la plus efficace amplification dynamo est admise. Seuls des champs magnétiques apparus durant l'inflation avec un spectre rouge, ou ceux produits durant une transition de phases QCD tardive peuvent avoir assez de puissance pour produire le champ présent aujourd'hui. Pour traiter d'un autre chapitre concernant la génération d'un champs magnétique primordial dans l'Univers je-

une, nous avons étudié la possibilité de produire un champs faible à travers une dynamique non linéaire créant des courants vorticaux lorsque l'approximation du couplage fort entre les photons et les baryons n'est plus valide, proche de la surface de dernière diffusion. Ce mécanisme est nécessairement présent dans l'Univers primordial et a déjà été analysé par différents auteurs. Dans le but de reconsidérer ce processus dans toute sa complétude, nous avons pris en compte, pour la première fois dans la littérature scientifique, toutes les contributions au spectre de puissance du champs magnétique résultant. A l'aide d'un calcul numérique, nous avons obtenu une amplitude du champs trop faible pour soutenir les mécanismes d'amplification nécessaires afin d'expliquer le champs observé aujourd'hui. Ceci signifie que le champs faible généré par la magnéto-genèse autour de la recombinaison n'a pas assez de puissance pour expliquer le champs magnétique que nous observons aujourd'hui. Un autre pas important dans l'énigme des champs magnétiques consiste en l'analyse de l'influence des particules relativistes, non sujettes aux interactions avec le fluide cosmique avant la recombinaison, sur les empreintes qu'un champs magnétique constant laisse sur les anisotropies du fonds diffus. Alors qu'un failbe champs initial produit principalement un quadrupole, nous observons comment ce quadrupole peut être effacé par compensation des tensions anisotropes du champs et des particules relativistes circulant librement dans un Univers anisotrope. Cette compensation résulte en une isotropisation de l'Univers et, dans le cas pour lequel ceci reste vrai même durant la recombinaison, dans une annulation complète du quadrupole généré par le champs magnétique. Si nous prenons les neutrinos primordiaux dans le rôle des particules relativistes, cet argument dépend bien entendu de leur masse, et la suppression finale sera d'autant plus efficace si les neutrinos restent longtemps relativistes. Même si aucune compréhension définitive concernant l'origine des champs magnétiques observés aujourd'hui n'a été atteinte, des réponses plus claires ont pu être apportées à quelques questions fondamentales de l'option primordiale. Il est évident que davantage de recherches sont nécessaires pour résoudre complétement l'énigme des champs magnétiques.

Un autre aspect de mes recherches était concentré sur les ondes gravitationnelles produites par un champs scalaire ayant brisé une symétrie globale. Nous obtenons que la partie du spectre qui concerne les longueurs d'ondes plus grandes que l'horizon lors de la génération est plat avec une amplitude qui, pour quelques valeurs d'espérance de vide, est dans la fourchette de sensibilité de certaines observations. En d'autres mots, ce spectre est très semblable à celui produit par des perturbations tensorielles primordiales générées durant l'inflation. Ainsi, il est important de trouver une façon efficace de démêler ces deux spectres dans le cas d'amplitudes similaires. Ceci est la motivation nous ayant poussés à entreprendre l'analyse de la polarisation B du spectre produit par les défauts, ceci dans le cadre d'un second projet sur ce même sujet. Dans le but de détecter ou de mieux contraindre la contribution des défauts cosmologiques au fonds diffus, nous avons étudié la polarisation B locale du fonds diffus comme étant produite par différentes sortes de défauts cosmologiques et par des perturbations inflationnaires primordiales. Nous soulignons d'abord qu'étant donné que les expériences réelles du fonds diffus ne sont pas des échantillons idéals des anisotropies de la température couvrant tout le ciel, l'analyse de modes B locaux, qui ne dépend pas des conditions aux bords, confère de grands avantages par rapport aux modes B standards non locaux. En effet, dans la polarisation locale, le signal du défaut est substantiellement augmenté par apport à l'inflationnaire, alors que, si nous considérons le cas non local, ce n'est pas le cas, car le rapport signal/bruit pour deux modèles est presque équivalent. De plus, nous avons aussi montré que la comparaison

de ce rapport entre deux signaux correspondant à des portions du ciel de taille différente indique que, lorsque nous agrandissons la taille d'une portion observée du ciel, le rapport de l'inflation augmente significativement, alors que celui du défaut ne change pas. Ceci est une conséquence de la nature non causale de l'inflation, qui présente ses caractères principaux dans un éventail d'angles correspondant à des distances plus grandes que le rayon de Hubble à la recombinaison. Si nous considérons donc des morceaux de ciel correspondant à des angles plus petits, nous nous attendons à extraire le signal correspondant aux processus causaux comme la génération des perturbations des défauts. Avec notre proposition d'analyse du ciel, nous prévoyons une amélioration des limites supérieures sur la contribution des défauts aux anisotropies du fonds cosmologique de plusieurs ordres de grandeurs.

La recherche présentée dans cette thèse représente d'importantes briques sur le chemin de la construction d'une compréhension plus complète et profonde des mécanismes physique caractéristiques des premières secondes après la création de notre Univers, un régime de température et d'énergies autrement inaccessibles en laboratoire. De plus, ceci souligne également les questions ouvertes qui restent non résolues.

The jury members are:

- Dr. Chiara Caprini, CEA-Saclay (France)
- Dr. Torsten Ensslin, Max-Planck-Insitute for Astrophysics (Garching, Germany)
- Dr. Martin Kunz, Département de Physique Théorique de l'Université de Genève (Switzerland)
- Prof. Andrii Neronov, Data Centre for Astrophysics , Université de Genève (Switzerland)

I want to thank them again for having accepted to be part of the jury for my Thesis.

To my grandfather, il nonno Lino.
I hope he would be proud of me.

Contents

Chapter 1

Introduction

After almost four years of Ph.D. in Cosmology, I have achieved the unquestionable ability of listing the first most frequently asked questions about my field of research. Most of these questions are very difficult to be answered and often the physical community is still doubting about a concluding common understanding of the physical mechanism responsible for a given phenomenon. Personally, I always feared them: being a physicist, I am part of the group of few people that is supposed to know almost all the answers, while most of the time the real state of the art obliges us to reply that no conclusive interpretation is yet known. Moreover, on the personal point of view, I have to admit that most of these questions were and are questions that I ask myself still today.

Here are the top three: "*Is the Universe finite of infinite?*" and "*Is the Universe going to collapse again and finish?*", not to mention the most scaring one: "*What is Cosmology useful for?*".

The aim of the next few pages of this introduction is to provide my personal answer to the most fundamental and complicated among the above queries concerning why we should study Cosmology today. I will provide a broad picture of this field of research in order to underline the scientific characteristics that make Cosmology be part of Physics and that, in my opinion, are the origin of its fascination.

1.1 The basis of Cosmology

The first reasonable answer that highlights the importance of Cosmology and that could be provided to the leading question quoted above stands in the clear evidence that this discipline has been subject of study since hundreds of years. It is more than two millennia that researchers and ancient time thinkers are involved in trying to understand and predict the evolution of the Universe that surrounds us. Of course, the "Universe" under analysis changed through the years, as well as the theoretical and mathematical techniques at disposal for scientists and researchers. But the aim of the cosmological investigation has always been the common need of exploring the sky around us and of providing the most scientific answers to the fundamental question concerning the origin of our Universe.

Stating without doubts the epoch corresponding to the birth of Cosmology as the scientific discipline studied today is not an easy task [1, 2]. Already in the ancient Greece, Plato, Aristotle and Ptolemy were involved in a sort of cosmological pseudo-science intended as a search for a picture of the Universe that would have made sense with no mention of divine beings. Their cosmological model of the Universe consisted in a stationary Earth

around which the Sun and all the planets were rotating. This model has been replaced by a more sophisticated heliocentric model by Copernicus in 1543 and later emphasized and partially confirmed by Galileo through his new telescopic observations in 1632. In the 17th century, Kepler, using Tycho Brahe's observational data, showed that the Earth and the other planets all travel around the Sun in elliptical orbits. The issue concerning how the planets continued to retrace the same paths forever around the Sun remained a central problem of Cosmology until Isaac Newton explained how objects move under gravity. He accomplished this, with the help of other mathematicians as Euler and Laplace, by showing how motions in the sky obey the same laws that determine the movement of bodies on Earth. During the 19th century, remarkable new observational techniques, photography and spectroscopy, did address cosmological questions: for the first time, scientists could investigate what the Universe was made of and this was a major turning point in the development of Cosmology. Another fundamental improvement towards modern Cosmology is represented by the capability of precisely measuring distances, that remains one of the more challenging difficulties even today. In the 20th century the astronomers started to use basic properties of a type of variable stars called Cepheids, that are characterized by a particular period-luminosity relation. Considering that their apparent magnitude is directly related to their absolute magnitudes (brightness diminishes with the square of the distance), astronomers succeeded in inferring their distances from Earth.

Another turning point in the history of Cosmology is represented by the gravitational field equations with which Einstein provided a compact mathematical tool that could describe the general configuration of matter and space taking the Universe as a whole. By the early 1920s most leading scientists agreed that Einstein's field equations provide the foundation for Cosmology. Finding realistic solutions to these equations in order to produce a model of the Universe was a very difficult task. After a large debate, the scientific community agreed on a dynamical expanding model that has been worked out independently first by Friedmann and later by Lemaître, Robertson and Walker. This Friedmann-Robertson-Walker (FRW) solution was in agreement with Hubble's observations of a linear relation between velocities and distances of galaxies in the Universe and set the birth of the so-called Big Bang theory of the origin of the Universe, scenario that corresponds to the background of modern Cosmology still today. The deciding experimental confirmation supporting this model comes from 1965, when Arno Penzias and Robert Wilson, studying the sky's microwave "noise" for Bell Telephone Laboratories, detected microwaves coming from all around the sky as an universal background [3]. Indeed, back in 1948 Gamov had argued that the Big Bang Universe would be permeated by a radiation background with a temperature barely above the absolute zero. This radiation, that now people refer to as Cosmic Microwave Background (CMB) was initially dominating the expansion of the Universe and then it cooled down reaching very low energies. By the early 1970s, Cosmology became increasingly an observational science, even if philosophical considerations remain a central issue for a long time afterwards.

Nevertheless, despite the old history behind modern Cosmology, someone can still doubt about whether it is a useful and scientific subject to be studied or not: the only fact that, from a very ancient time, people has always been involved in exploring the visible Universe does not prove unambiguously its deep importance for Science. Neglecting digressions concerning the definition of "usefulness" of a discipline, that is not the aim of this Thesis, one

fundamental aspect that places in the present epoch Cosmology at the center of Theoretical Physics is given by the insights that scientists gain through the study of the primordial Universe: they can investigate and understand laws of Physics at energies and temperatures so high that can not be reached otherwise in laboratories. Behind the fascinating charme of Cosmology as a discipline that studies the most fundamental and mysterious physical system one can think of, our Universe, there is the capacity of Physics to interpret and understand what we see in the deep sky. The above claim alone makes clear in my opinion how far is human understanding gone up to today and how much it is important to keep questioning in a scientific way about a Universe that seemed obscure and unachievable until some decades ago.

Indeed, through the discovery of the CMB and the observation that it follows a black body distribution at a temperature of $2.725\,^{\circ}\mathrm{K}$, corresponding to a frequency of $\simeq 160\,\mathrm{GHz}$, physicists are now able to constrain and get information concerning physical processes that take place at energies close to the Planck scale, $M_{\mathrm{P}} \simeq 10^{19}\,\mathrm{GeV}$, roughly 13.7 billions of years ago.

This represents the main aim of my research: I have been trying to extract information about physical mechanisms that may have taken place in a primordial Universe through the imprints that they have left in the cosmological observables that we are investigating today.

In order to be able to constrain most of the high energy processes that may characterize the primordial Universe, we consider mainly two different important observables: the anisotropies of the CMB and the Gravitational Wave Background (GWB). In the last few decades the level of accuracy with which people is able to measure the CMB is improving significantly, therefore cosmologists have been able to reject and constrain an increasing number of theoretical models. On the other hand, we also need more accurate theoretical predictions in order to understand the nature of our measurements of the sky temperature and polarization maps.

As I already mentioned above, the CMB is a prediction of the hot Big Bang model of Cosmology and it has been first detected by Penzias and Wilson back in 1965 [3]. This is the result of the free-streaming of photons from a redshift $z \simeq 1100$ towards us as a consequence of recombination, a process that takes place at a temperature of about $0.2\,\mathrm{eV}$, or 3×10^5 years after the Big Bang. Before this epoch the CMB photons are tightly coupled to the baryons and therefore they are not free to travel toward us. Once the Universe cools down while expanding, the hydrogen and helium nuclei can bind electrons into neutral atoms and photons start free-stream. Therefore, the CMB gives us a snapshot of the Universe when it is only 10^5 years old.

Of course, from this snapshot we can also gain information concerning processes that take place in an earlier Universe. Indeed, COBE satellite discovered in 1992 [4] the presence of small fluctuations on top of the isotropic and homogeneous background of the CMB temperature. These variations of temperature from one part of the CMB sky to another, to which we refer to as CMB anisotropies, seem to be compatible with the predictions given from inflation, an early stage in the evolution of the Universe during which it expanded exponentially fast. In this scenario density perturbations are generated in the very early Universe, only about $10^{-43}\,\mathrm{sec}$ after the Big Bang, and propagate until photon decoupling, where we detect their imprint on the uniform CMB sky. In inflationary models [5] pertur-

bations are generated by quantum fluctuations of the inflaton field which are set by the energy scale of inflation. Through this mechanism, both scalar and tensor anisotropies are generated and they need to be tested against experimental data in order to gain a deeper understanding of the physics behind inflation.

Given the importance of the information that is contained in these anisotropies, after their first discovery there has been a lot of activity in increasing the accuracy of the sky maps in order to reach enough sensitivity to enable us to discriminate and constrain several theoretical models proposed as possible mechanisms to generate such perturbations. With this purpose, in 2001 a new NASA satellite, the Wilkinson Microwave Anisotropy Probe (WMAP) [6], was launched and has been taking data for 7 years. The WMAP data, together with other astrophysical data (Supernovae, Baryonic Acoustic Oscillations, Lyman Alpha, Weak Lensing...), have lead to a stunning confirmation of the Standard Model of Cosmology and to quite precise constraints on a minimal set of cosmological parameters. CMB anisotropies turn out to have an amplitude of 10^{-5} over a wide range of angular scales and they do not show a preferred direction in the sky. The best fit to the data is given at the present stage of our knowledge by the so-called ΛCDM model, which tells us that the expansion history of our Universe is now dominated by a unexpectedly small cosmological constant $M_{\rm Pl}^2\Lambda \simeq 10^{-47}\,{\rm GeV}^4$. This "new" unknown source of energy is thought to be responsible for the recent acceleration of the Universe as it is shown by data up to redshifts of about $z \simeq 1$. This picture is also consistent with almost gaussian adiabatic initial conditions for the density perturbations generated during inflation. The relative abundance of tensor anisotropies produced in the early stages of the Universe through a similar scenario is measured by the tensor-to-scalar r, whose measure is important since it is directly related to the scale at which inflation took place. This is a model dependent quantity, but in general it is predicted to be smaller than unity, making the primordial gravitational waves (GWs) coming from inflationary tensor perturbations very difficult to be detected. Present constraints on the tensor-to-scalar ratio are $r < 0.43$ using WMAP (5 years analysis) alone and get tight as $r < 0.22$ once we include other experimental data [7].

In order to enrich Cosmology with even more precise measurements, a new European satellite, Planck [8] has been launched by ESA in May 2009 and it is now taking data. With Planck we expect to have a significant improvement concerning the data that we will have soon at our disposal: it will resolve the CMB temperature anisotropies up to multipoles corresponding to $\ell \simeq 2500$ (while WMAP resolution was reaching ℓ's of about 700), increasing the angular resolution by 3 times and the sensitivity by 10 times with respect to its American precursor. Concerning the polarization measurements, Planck is performing as well as WMAP was measuring temperature anisotropies.

Since Thomson scattering of an anisotropic radiation field also generates polarization, the CMB is predicted to be polarized roughly at 5% level of the temperature anisotropies. This polarization signal is usually decomposed in E-modes (parity even) and B-modes (parity odd). Since scalar perturbations have no handedness, B-modes can only be sourced by vector and tensor modes. As we already mentioned above, inflation generates both scalar and tensor perturbations, while vectors are not generated and if they are they decay after inflation in the radiation dominated Universe. Therefore the detection of a non-zero B-mode signal is a way to measure the GW contribution given by primordial tensor

anisotropies, even if it is rather weak. This translates in a determination of the tensor-to-scalar ratio r and in a consequent derivation of the energy scale of inflation.

In a sense, primordial GWs can be understood as being the gravitational analog of the CMB for photons and as a consequence they carry fundamental information about the early Universe. The reason behind this comparison stands in the fact that particles with only gravitational interaction decouple much earlier than particles which have also electroweak or strong interactions. Therefore, gravitons decoupled at scales below the Planck scale, namely already 10^{-44} sec after the Big Bang. This means that a GWB encodes in its frequency spectrum all the information concerning the conditions in which it is created. In other words, their extremely small cross section represents on one hand the reason why GWs are so interesting but on the other hand this is the reason why they are so difficult to be detected and until today we only have an indirect probe of their existence [9].

A huge effort is focused into GW detection in the present epoch: terrestrial interferometers as LIGO [10, 11] and VIRGO [12] are now being upgraded and are likely to detect the first GW signal in the years to come. Their range of frequency is $10 - 1000$ Hz, while the space interferometer LISA [13, 14, 15, 16], which is expected to be lunched in 2020 or even later, will have its best sensitivity around 10^{-3} Hz. Even more futuristic detectors with a much more deep sensitivity as BBO or DECIGO are under study [17]. Another very promising experiment for the GW detection is represented by the pulsar timing arrays which use high accuracy timing of a collection of low timing noise pulsars to search for GWs in the μhz to $n$hz frequency bands [18, 19].

As mentioned above, GWs represents the smoking-gun for inflation models, since they are expected to be produced during the early exponential expansion of the Universe and therefore we should be able to detect a B-mode signal of primordial origin. But not only inflation sources GWs and therefore B-modes: there are many other cosmological mechanisms that are thought to give rise to a GWB that in some case, for some values of parameters describing these models, may be seen by present or future GW detectors.

One important but model-dependent mechanism that may characterize the early stages of our Universe is pre-heating. This takes place just after inflation, roughly 10^{-32} sec after the hot Big Bang, when the inflaton field has decayed and leads to a thermal bath of mainly standard model particles. It is quite hard to work out the details of this mechanism works but it can generate inhomogeneities leading to GWs [20, 21, 22]. The typical frequency that characterizes the peak of the spectrum of such a GWB is $\omega \gtrsim 10^{10}$ Hz and unfortunately there are no GW detectors at so high frequencies.

Another proposed mechanism that may lead to a production of a significant GWB is represented by first order phase transitions. While expanding adiabatically, the Universe may have undergone several phase transitions due to the temperature decrease. The nature of these transitions depends mainly on the theoretical models that describe particle physics interactions and if they are first order transitions, they proceed via bubble nucleation. This violent and inhomogeneous process represents an efficient source of GWs. More in detail, during a first order phase transition, true-vacuum bubbles nucleate and collide, breaking the spherical symmetry of the bubble walls. On one hand this generates anisotropic stresses that source GWs, and on the other hand we have injection of energy in the plasma with the consequent formation of magnetohydrodynamic (MHD) turbulence in the fluid. This turbulence generates itself GWs and amplifies small magnetic fields (MFs) generated by charge separation at bubble walls. MFs themselves are a possible source of GWs, given the fact that they have non-zero anisotropic stresses, and this aspect represents one of the

pillars of my research, as it will be described in the next section.

In the standard model of particle physics the electroweak (EW) phase transition is not even a second order transition, but only a cross-over [23, 24]. But in some scenarios beyond the standard model, see e.g. [20, 21, 22], the transition may be first order. In this last case, a strongly first order EW phase transition can produce a GWB that peaks at a characteristic frequency corresponding to a 1% of the Hubble time during the transition, $\omega \sim 10^{-3}\,\mathrm{Hz}$ [25]. That means that the signal falls into the sensitivity range expected for the future GW detector LISA.

Moreover, standard lattice simulations predict QCD phase transition to be a simple crossover [26, 27]. But, considering a sufficiently large neutrino chemical potential [28], this confinement transition may become first order [29]. In this case, GW's typical frequency, $\omega \sim 10^{-7}\,\mathrm{Hz}$, is in the range of sensitivity of pulsar timing-array

Finally, another important source of GW backgrounds is represented by topological or non-topological defects. They might form during early Universe phase transitions or reheating and have been considered in a first stage as possible candidate for seeding structure formation [30, 31]. A later comparison with CMB anisotropies [32, 33] show that they do not reproduce the observed dependence of the anisotropies from the multipole momenta. This allowed us to put constraints on their contribution to density perturbations: they can not contribute more than 10% to the total CMB anisotropies [34]. Given the fact that defects have non vanishing anisotropic stresses, they also source GWs, whose frequency strongly depends on the scale at which these defects are created. I will focus on the GWBs produced by defects in Section 1.3.

Let me stress again, before describing in more detail my research, that the main aim of this Thesis is to study some of the imprints that important physical mechanisms which may have occurred in the primordial Universe have left in the CMB and to predict the main features of the GW spectrum starting from a description of the sources that produced it in order to be able to detect or constrain models and parameters that govern high energy physics, which would not be accessible otherwise. More in detail, one of the topics on which I concentrated my research is the investigation of a possible production of seed MFs in the early Universe, through which we can explain the existence of the MF that is measured today and which permeates all the galaxies and clusters reachable by our observations. Another subject on which I centered my interest are topological and non-topological defects, with the attempt to better constrain them through a more careful and clever investigation of the GWB that they generate.

This fundamental interest in investigating and understanding better several scenarios that might have happened in our primordial Universe is supported and needed by new incoming data provided by several more accurate detectors.

1.2 Magnetic fields in the Universe: primordial or late origin?

Since their discovery in the 1950s, MFs have been detected on larger and larger scales in our Universe [35, 36]. Initially MFs with a strength of some μGauss have been measured in our galaxy and, more recently, in other more distant galaxies [37, 38, 39, 40] up to a redshift $z \simeq 2$. They have a correlation length of some kpc. There is also evidence of MFs

with an amplitude of $1-10^{-2}\mu$Gauss on a scale of some Mpc in clusters of galaxies [41, 42]. Finally, measurements also detected MFs in superclusters [43].

MF measurements are in general quite challenging: Zeeman splitting detection can be used in nearby galaxies, but once high redshift measurements are needed people usually uses synchrotron radiation or Faraday rotation evaluations. However, through these estimation methods, we obtain information only concerning regions of the sky where free electrons are present with a somehow known or predictable number density. Only recently new evidence has been achieved for intergalactic MFs [44, 45, 46, 47]. Indeed, these MFs can deflect the charged particles resulting from electromagnetic pair cascades of high energetic gamma rays coming from distant point sources once they interact with background photons. This deflection causes a dispersion of lower energy gamma rays coming from inverse Compton scattering from the beam and the lack of GeV signals highlighted by the latest FERMI data suggests a lower bound of 10^{-16} Gauss for the MF amplitude in filaments and voids.

During the years and motivated by the improvements in detecting and measuring MFs throughout more distant regions of the Universe, various mechanisms have been proposed in the literature in order to explain their origin [36, 48, 49, 50]. The main question that I addressed and tried to answer during these years is whether these MFs are generated in late Universe through charge separation processes during structure formation or by ejection from stars and galaxies, or whether they are the result of an amplification of a seed field generated in a primordial Universe. The final part of the story is that up to today there is yet not clear conclusive answer to this fundamental question and more work is needed on both theoretical and experimental sides.

Concerning the first mentioned scenario related to astrophysical processes that take place during nonlinear collapse of galaxies and clusters, there are still some difficulties in understanding how this mechanism can lead to fields which have the observed coherence scales and amplitudes. On the other hand, there are several high energy scenarios able to produce MFs in the early Universe, from EW [51, 52, 53] or even QCD [54] phase transitions to inflationary options [55, 56, 57, 58, 59].

There are still several problems and doubts even concerning how MFs can be generated in a primordial Universe: unknown physics must be invoked in order to justify the non-minimal coupling of the electromagnetic field to the inflation sector through which a MF can be produced on all scales during inflation. Similarly, MFs generated during phase transitions, through the mechanism that I briefly pictured in the previous section, seem not to have enough power on large scales in order to explain the observed large coherence of the fields. This argument will be deeply investigated in Chapter 3.
A third possible primordial mechanism that generates a small seed MF is related to magnetogenesis induced by charge separation processes before recombination. This is a rather standard mechanism through which a MF is inevitably produced on scales larger than the ones interested by earlier phase transitions but it seems too weak to represent the concluding explanation to the MF puzzle. Chapter 4 will investigate this option in detail.

I have focused my research on the hypothesis that the observed MFs are seeded by a primordial field generated in the very early Universe. Clearly, seed primordial fields have a very tiny amplitude and, once they are generated, they need to be amplified. Two mainly different physical mechanisms have been proposed in order to reach this aim during the

evolution of the Universe and it is not yet clear which one of the two is the key for the MF amplification.
On one hand there is the adiabatic contraction, which is related to the fact that during structure formation the cosmic plasma is a good conductor and the MHD approximation holds. The MF lines are therefore frozen in while galaxies and clusters grow and its amplitude scales as $\rho^{2/3}$, where ρ denotes the matter density of the cosmic plasma. This means that the MF strength is enhanced by roughly 3 orders of magnitude by simple contraction, therefore MFs of nGauss are needed initially to explain the observational data in galaxies and clusters.
Alternatively, seed fields might have been amplified by the so-called nonlinear dynamo mechanism, that is able to exponentially enhance the MF amplitude by a factor up to 10^{15}, combining the turbulent motion of the ionized gas with the differential rotation of galaxies [48]. In this case the initial MF strength can be as small as 10^{-21}Gauss. However, this mechanism is exponentially sensitive to the age of the Universe, therefore it is not clear how it can amplify MFs in galaxies at higher redshifts. Indeed, at a redshift $z \simeq 1$ the age of the Universe is half of its present value and this would reduce the enhancement factor to less than 10^8.

As I already discussed above, we can obtain information concerning the amplitude and the structure of a MF present in our Universe before recombination through the investigation of the imprints that have been left in the CMB and GWB.

Since the MF stress energy tensor contains scalar, vector and tensor perturbations, it might leave signatures in all the possible CMB and large scale structure observables and, even if the small temperature anisotropies are fully accounted for by initial small fluctuations which are generated during inflation, small deviations from these predictions are used to limit other sources of perturbations that might be present in the early Universe. These bounds on primordial MFs have been deeply studied in the literature and limits of the order of 10^{-9} Gauss have been derived from CMB anisotropies [60, 61, 62, 63], non-gaussianties [64, 65, 66] and structure formation [67]. The fundamental point behind this relaxed upper-bound is that CMB limits cannot get more stringent than the nGauss and the main reason is that CMB anisotropies give information on scales larger than those that characterize correlation lengths of MFs produced during causal processes as phase transitions, that are much smaller [68]. In other words, large scale CMB anisotropies are not so sensitive to fluctuations that may be produced by a primordial MF on a very small scale. This is summarized by the following general expression representing the MF energy density parameter Ω_B in terms of CMB anisotropies $\Omega_{\rm rad}$ [69]

$$\Omega_B \simeq 10^{-5}\Omega_{\rm rad}\left(\frac{B}{10^{-8}\text{Gauss}}\right)^2 . \tag{1.1}$$

Through the above equation we understand how a primordial MF of the order of 10^{-9} Gauss would contribute to the CMB anisotropies with a 1% effect and therefore it is clear that a MF amplitude as small as 10^{-22} Gauss will never be detectable in the CMB.

On the other hand, GWs are much more efficient compared to the CMB in setting upper-bounds on initial MF amplitudes. The reason is that they give an integrated bound on the additional amount of relativistic energy density that may have been present at the moment of nucleosynthesis and therefore they are able to probe also much smaller scales with respect to CMB anisotropies. This aspect is briefly discussed below and will be in-

vestigated in detail in the following Chapter 3.

Summarizing, the main point of this research stands in the evidence that investigating and eventually probing the existence of cosmic MFs can provide us with important information about processes that took place at the time when such a field was generated, as well as knowledge about turbulent dynamo scenarios that characterize structure formation and that might amplify the seed MFs in recent stages of the Universe. Only more and more precise measurements can help us understanding their real origin, and a big experimental improvement is expected in the next years, given the application of new techniques as the one proposed by Refs.[44, 45, 46, 47] or the radio observations that will be performed by the Square Kilometre Array telescope [70], that allow us to detect the presence of MFs in the intergalactic medium. Therefore, more research is required in order to investigate different reasonable mechanisms for MF generation.

1.2.1 Interaction between gravitational waves and primordial magnetic fields

As a first step in the investigation of primordial MFs, we focus on the interaction between MFs and GWs following an idea proposed in [71]. Here the author addresses this small nonlinear effect and claims to have found conditions under which a resonant amplification of the second order MF can take place due to the interaction with the GWB. Similar conclusions have been found in [72, 73].

We review this MF-GW interaction up to second order in [74], studying the modifications induced by this interaction on the MF spectrum. More precisely, we investigate the growth of second order MF and GW energy densities on super horizon scales finding no enhancement of both second order quantities. In contrast with the previous literature, our results are expressed in terms of measurable physical quantities that makes them immediately understandable and clear, as it is confirmed by our following final equations

$$\Omega_B^{(2)} \simeq \Omega_B^{(1)}\Omega_{\rm GW}^{(1)} \simeq \Omega_B^{(1)}\left(\frac{H_{\rm inf}}{M_{\rm P}}\right)^2 \ll \Omega_B^{(1)} \,, \tag{1.2}$$

$$\Omega_{\rm GW}^{(2)} \simeq \left[\Omega_B^{(1)}\right]^2 + \left[\Omega_{\rm GW}^{(1)}\right]^2 \,. \tag{1.3}$$

The above expressions summarize our conclusive results and represent the energy density parameters of the second order MF and GW induced by first order quantities once the scales cross the horizon. We find that the sub-horizon amplification is negligible and, as it is clear from Eq. (1.2), that no enhancement of the second order MF is induced by the interaction with first order GWs. The reason is that, since tensor perturbations grow on super-horizon scales, the first order density parameter $\Omega_{\rm GW}^{(1)}$ grows as well and reaches a constant value only inside the horizon. For perturbation theory to be valid, we have to require that this constant value at horizon crossing is much smaller than unity, and in particular it turns out to be of the order of $(H_{\rm inf}/M_{\rm P})^2 \ll 1$, where $H_{\rm inf}$ stands for the Hubble parameter at the end of inflation. Equivalently, we obtain comparable results concerning the second order production of GWs, as shown by Eq. (1.3).

Finally, we underline that, since the growth comes from super-horizon evolution, conductivity and other large scales plasma properties are not relevant in this analysis. This is justified by the argument that currents are generated on sub-horizon scales, since they

are induced by electromagnetic causal fields. Despite this simple argument, this seems a controversial topic and has already been discussed in [75, 76].

1.2.2 Helical primordial magnetic fields: a feasible option?

Continuing with the investigation concerning the interaction between MFs and GWs, we extend a computation first presented in [77]. Here the authors obtain very stringent upper-bounds on primordial MFs produced by causal mechanisms, applying the nucleosynthesis constraint on the GWs produced by the MF itself. These limits suggest that causally generated MFs do not have enough power on large scale and therefore cannot seed the observed MF in galaxies and clusters, even considering the most efficient dynamo amplification. In ref. [77] the authors also conclude that only MFs generated during an inflationary stage could have enough power on large scales if their spectrum was very red.

The reason behind these strong constraints on causal MFs relies on the fact that causality implies a blue MF spectrum on large super horizon scales, whose corresponding energy density scales like

$$\frac{\mathrm{d}\rho_B(k)}{\mathrm{d}\log k} \propto k^5\,, \tag{1.4}$$

where k is the wave number. As a consequence, the nucleosynthesis limit on the GWs produced by such a MF, even if it is a relaxed limit, is dominated mostly by the contribution of the smallest scales where the MF amplitude is maximal. Indeed, the spectrum of GWs generated by primordial MFs turns out to have a blue large scale tail whose peak corresponds roughly to the initial magnetic correlation length, that for causal processes is well inside the Hubble radius at the time of MF generation. This sets very strong limits on the MF amplitude on such scales.

In order to obtain conservative constraints, [77] and ourselves afterwards consider only GWs produced by primordial MFs as candidates to which we should apply the nucleosynthesis bound, however no other primordial sources of GWs are taken into account for this computation. The more one adds up different contributions to the GW production, the more the limits on the primordial MF amplitude become stringent.

In more detail, in [77] the authors assume that the primordial MF evolves via direct cascade: it is damped on very small scales due to its interaction with the cosmic plasma, while on scales larger than its correlation length its flux is conserved, namely the MF spectrum scaled to today remains constant on large scales. This evolution can be summarized by the following expressions for the time variation of the MF correlation scale $L(t)$ and energy density $\rho_B(t)$

$$L(t) \propto t^{2/(n+5)}, \qquad \rho_B(t) \propto t^{-2(n+3)/(n+5)}, \tag{1.5}$$

where n is the spectral index that characterizes the slope of the MF power spectrum on large scales ($n = 2$ for a causal MF spectrum).

The GW energy obtained through this computation amounts on [77]

$$\Omega_{\mathrm{GW}} \propto \frac{(\Omega_B^*)^2}{\Omega_{\mathrm{rad}}}\,, \tag{1.6}$$

with a prefactor that depends on the detail of the mechanism that generates the MF. This equation underlies how the final GW density parameter directly depends on the initial

amount of MF energy Ω_B^* responsible for its generation. With this it becomes clear how, applying the nucleosynthesis bound on $\Omega_{\rm GW}$, we get information about the initial maximal allowed strength of the primordial MF, B_λ^*.

Finally, in ref. [77] the authors estimate the suppression of the magnetic field amplitude on a comoving scale λ with respect to its initial strength B_λ^* due to its direct cascade evolution to be given by the following analytical expression

$$B_\lambda \simeq B_{L^*} \left(\frac{L_*}{\lambda}\right)^{(n+3)/2} . \tag{1.7}$$

Considering that the initial magnetic correlation scale L_* is always many orders of magnitude smaller than the scale λ at which we estimate the MF amplitude, that we consider for example to correspond to the cluster correlation length $\lambda = 0.1\,$Mpc, the above equation translates into upper-bounds of the order of $B_\lambda < 10^{-31}$ Gauss for a causal MF produced during the EW phase transition. For red MFs generated during inflation ($n \simeq -1.8$) the limits weaken down to $B_\lambda < 10^{-19}$ Gauss, allowing them to be possible candidates for dynamo amplification, as already explained above.

In order to escape these strong upper-bounds on the seed field strength, a MF with an initial non-zero helicity has been proposed as a possible way out [78]. Indeed, helical MFs evolve via inverse cascade during a turbulent phase of the expansion of the Universe and the transfer of power from small to larger scales has been argued to be a possible solution to relax these constraints, given the fact that the magnetic correlation length grows much faster than during a direct cascade evolution. This can be seen by the following expressions of the time dependent quantities $L(t)$ and $\rho_B(t)$ during an inverse cascade evolution, as obtained from numerical simulations of helical MFs in a turbulent MHD evolution during a radiation dominated phase [79]

$$L(t) \propto t^{2/3}, \qquad \rho_B(t) \propto t^{-2/3}. \tag{1.8}$$

Slightly different results have been obtained in Refs. [80, 78].

In Ref. [81] we compute the amount of GWs produced by an helical MF during the inverse cascade evolution [79] and we apply the nucleosynthesis bound on these GWs.

The first difference with respect the previous treatment is given by the fact that in this case the MF spectrum contains also an antisymmetric part corresponding to the non-vanishing helicity of the MF. This anyway does not contribute to its energy density but it only influences the time evolution of $L(t)$ and $\rho_B(t)$.

In addition to the above evolution equations (1.8), we also model in a simple way the initial MF evolution in which its energy density grows from a zero initial value to the moment in which the MHD turbulence is fully developed. The reason for doing this is that, as it is proven in the article, the time continuity of the GW source affects not only the slope of the power spectrum on small scales, but also the peak position and the amplitude of the final resulting GW spectrum.

We concentrate our analysis on the GWs produced during the turbulent stage, since it is in this regime that an helical MF is characterized by the inverse cascade evolution. This turbulent stage ends when the dissipation scale, at which we have the UV cutoff of the MF spectrum, growing more rapidly than $L(t)$, reaches the correlation scale. After this turbulent stage we consider the source of GWs to vanish. This is not completely correct,

since the MF is still present and able to source GWs and the only difference is that now it evolves via flux conservation on large scales. Since this later evolution only influences scales that are larger than the horizon at the moment in which turbulence stops, this does not affect the peak of the GWs that is the main responsible of our constraints on the MF amplitude, and therefore we can safely ignore it.

It is important to underline that an explicit computation concerning the duration of the turbulent regime related to the different scenarios that we consider as possible candidates for the MF production (EW and QCD phase transitions and inflation) shows that turbulence lasts for many Hubble times. This classifies this GW generation mechanisms as long-lasting processes, as referred by in Ref. [82], and this justifies a completely coherent approximation for the magnetic anisotropic stress, which represents the actual source of GWs. Moreover, numerical simulations of colliding bubbles have proven that the totally coherent approximation, that corresponds in a deterministic time evolution, is in good agreement with numerical results [83].

The resulting GW energy density produced by a primordial helical MF is similar in its form to the result previously obtained for the direct cascade evolution case, Eq. (1.6). The GW spectrum presents a blue large-scale slope and the final resulting amplitude of the GW peak obviously depends, as before, on the initial MF energy density at our disposal to generate GWs. We underlined in the paper that, for a reasonable initial magnetic density parameter $\Omega_B^* \simeq 0.1$, the GWs produced by a blue MF originated during the EW phase transition can almost reach the level of sensitivity of the LISA experiment. On the other hand, GWs produced by red inflationary MFs are much below any proposed experiment.

Finally, our result can be summarized, as for the direct cascade evolution, by the following equation, representing the dependence of the maximal allowed MF amplitude on a comoving scale λ by the initial MF B_λ^*

$$B_\lambda \simeq B_{L^*} \left(\frac{L_*}{\lambda}\right)^{(n+3)/2} \left(\frac{T_{\rm in}}{T_{\rm fin}}\right)^{(n+2)/3} . \tag{1.9}$$

The difference from the results obtained by [77] is encoded in the last factor, which is the one that exactly comes from the inverse cascade evolution of the MF. This last term is also the responsible for the mitigation of the limits that we obtained for helical MFs produced by causal mechanisms with respect to non-helical primordial MFs: considering for example the EW phase transition with a spectral index $n = 2$ one gets a relaxation on the constraint B_λ of roughly 7 orders of magnitude. This is obtained considering the initial temperature of the EW phase transition to be $T_{\rm in} = 100\,\text{GeV}$ and computing the final temperature at which turbulence ends to correspond to 21 MeV. On the other hand, constraints on red MFs such as the ones produced during inflation are not strongly influenced by the inverse cascade evolution. This is mainly due to their negative spectral indices that reduce the importance of the mitigating term coming from the inverse cascade evolution.

Two other brief comments are important at this point: first, we considered until now the smoothing scale λ to correspond to the cluster correlation scale $\lambda = 0.1\,\text{Mpc}$. This choice is also justified by the fact that this scale corresponds roughly to the smallest scale the survived damping at recombination [84, 85]. However, the authors of [78], following numerically the evolution of a primordial MF, find a smaller dissipation scale at recombination. Since the above bounds strongly depend on the smoothing scale at which we compute the amplitude B_λ, we have a huge relaxation of the limits if we decrease the smoothing scale, in particular for blue MF spectra. Indeed, the scaling of the maximally allowed MF

amplitude B_λ with the length λ reads

$$B_{\tilde{\lambda}} = B_\lambda \left(\frac{\lambda}{\tilde{\lambda}}\right)^{(n+3)/2} . \tag{1.10}$$

This makes clear that, considering a smaller smoothing scale $\tilde{\lambda} = 1\,\mathrm{kpc}$, the bounds are relaxed by 5 orders of magnitude for the EW phase transition ($n = 2$) and only by a factor of 16 for inflation with a red spectral index $n = -1.8$.

The second important remark is that we get much more stringent constraints imposing the limit of not overcoming the 10% of the radiation amount during all its evolution directly to the initial MF energy density

$$\Omega_B^* \leq 0.1\,\Omega_{\mathrm{rad}} . \tag{1.11}$$

Considering the usual example of the EW phase transition, the above limit translates in an improvement of 2 orders of magnitude with respect to the bounds imposed by nucleosynthesis. We did not explore this possibility from the beginning since we know that the only moment of the evolution of the Universe where this prescription has necessarily to hold corresponds to nucleosynthesis. In this way we left space to some unexplored mechanisms where the initial MF energy density may overpass the 10% of the radiation amount at some initial time prior to nucleosynthesis.

To summarize, the important results that we obtain from the computation presented above are a slight relaxation of the bounds on the initial MF amplitude in the case of inverse cascade evolution. We are able to reject most of the proposed causal primordial high energy mechanisms able to produce MFs in the early Universe even if they have a non-zero helicity: the observed field in galaxies and cluster are either not seeded by primordial MFs or these primordial fields have been generated during inflation and have a red spectrum. They can also be the remnant of a later QCD phase transition, even if it is unlikely to be a first order transition, that would be the only case where a sufficient MF can be generated.
To evade this conclusion, another possibility would be to argue that MFs with a correlation scale as small as 1 kpc are sufficient to be amplified and seed the field observed today in galaxies and clusters.

1.2.3 Seed magnetic fields from recombination

As I have already mentioned above, we also investigate the production of second order MFs during recombination through the so-called Harrison mechanism [86]. Indeed, non-linear dynamics can create vortical currents when the tight-coupling approximation between photons and baryons breaks down near the last scattering surface. This mechanism is necessarily present in the early Universe and it has been already analyzed by several authors [87, 88, 89, 90, 91, 92, 93, 94].

The main idea behind this scenario is related to a sort of competition between the different interactions governing the primordial plasma, namely the Thomson scattering between electrons and photons (whose cross-section is much bigger than the cross-section for the same interaction between protons and photons, that can therefore be safely ignored) and the Coulomb interaction between electrons and protons. A careful analysis of the characteristic time scales involved in the problem shows that the Coulomb scattering is

always inefficient with respect to the Thomson interaction and this results in a electric field generation. This electric field is the main responsible for keeping electrons and protons always tightly coupled and its main contribution is represented by the velocity difference between baryons and photons. This has been already pointed out in Ref. [94].

From the computation of the electric field curl generated by this effect, we obtain the following three different contributions that source the MF

$$\left(a^2 B\right)' = S_1\left[\Delta v_{\mathrm{b}\gamma}^{(2)}\right] + S_2\left[\left\{\delta_\gamma^{(1)} + \Phi^{(1)} - \Psi^{(1)}\right\}\Delta v_{\mathrm{b}\gamma}^{(1)}\right] + S_3\left[\Theta_\gamma^{(1)} v_{\mathrm{b}}^{(1)}\right], \tag{1.12}$$

where Φ, Ψ are first order metric perturbations, $\Delta v_{\mathrm{b}\gamma} = v_{\mathrm{b}} - v_\gamma$ is the photon-baryon velocity difference, and Θ_γ is the photon quadrupole moment, from anisotropic stress. The first part of the source is a purely second order term in perturbation theory, while the other two are quadratic first order contributions. We take into account for the first time in the literature all the three above contributions to the resulting MF power spectrum in [95].

In more detail, due to the presence of the electric field, electrons and protons are very tightly coupled and from the point of view of photons they can be considered as a single fluid of baryons. In this sense the analysis of this evolution can be addressed as a two-fluid dynamics of photons and baryons, whose equations are very close to the CMB dynamics. We use therefore the second-order Boltzmann code of [96], through which we consider a full tight-coupling treatment and a second order expansion of cosmological perturbations.

The numerical computation, whose steps have been followed and checked analytically in regimes where the power spectrum behavior could have been predicted through some reasonable approximations, gives as final result a MF amplitude of 10^{-29} Gauss on a comoving smoothing scale of 1 Mpc. This means that the seed field generated by magnetogenesis around recombination is too weak to sustain the amplification mechanisms that can amplify it in order to explain the observed field today.

However, this is not the only relevant conclusion that we obtain through this analysis. We also understand the reason behind the importance of considering all the terms that source the MF generation. Indeed, on large scales we observe some cancelation among all the terms and neglecting this cancelation would lead to wrong over-estimating results. We also understand this effect from an analytical point of view as a suppression of the resulting quadratic terms by a factor $(k\eta)^2$, that at early times and large scales reduces the resulting MF power.

We also point out how the MF continues to be created even after photon decoupling, as the output of our numerical integration clearly shows. The reason is that, even if the majority of electrons and protons combine to give hydrogen atoms, a non-zero residual ionization fraction of free electrons is present. This translates in an increasing of the MF production at the recombination instant and stopping the numerical integration at recombination, as previous authors did, under-estimates the final MF amplitude by one order of magnitude.

Finally, we get an inside understanding of the physical process responsible for this generation that allowed us to compare our computation with other previous approaches. We interpret the magnetogenesis scenario produced by second order perturbations in the tight coupling regime as summarized by the following equation

$$(a^2 B)' \sim \omega_{\mathrm{b}} + \mathcal{O}(\mathrm{quad})\,. \tag{1.13}$$

This tells us that the contributions sourcing the MF through the Harrison mechanism are of two different kinds: the first term represents the vorticity of baryons, which can not be generated even at second order in perturbation theory in the tight coupled regime. This is already pointed out in [97] and in [98] through a first order computation. The second term encodes a purely second order contribution that is present even in the tight coupled regime and this is the main responsible for the MF generation in the case we analyze: these quadratic terms can source the MF even if there is no initial vorticity.

1.2.4 Constant magnetic fields and free-streaming particles

As a last step concerning my research on primordial MFs, we focus our attention on constant MFs, namely MFs coherent over Hubble scales. Upper-bounds concerning such fields have already been obtained in the literature: Refs. [99, 100, 101] set limits of the order of $B \leq 10^{-9}$ Gauss, considering both the anisotropies produced in the CMB and the Faraday rotation generated by these homogeneous fields.

We review these limits imposed by CMB perturbations, considering also the presence in a primordial Universe of free-streaming massless particles such as neutrinos after their decoupling before recombination ($T \simeq 1.4\,\mathrm{MeV}$). We conclude that the above CMB limits are invalid in the case where a massless free-streaming particle is present before photon decoupling. The reason behind this conclusion is that massless free-streaming particles traveling in an anisotropic Universe develop anisotropic stresses which scale exactly as the anisotropic stress of the MF. This results in a compensation of the two anisotropic stresses and in an isotropization of the Universe. Therefore, the quadrupole of the CMB anisotropies is canceled.

In detail, we mimic the presence of a constant MF in the primordial Universe via a modification of the Friedmann background geometry. Such a Universe is described by a Bianchi I geometry and we compute the effects that this anisotropic background produces on the CMB multipoles. The analytical computation is performed at leading order in the MF energy density $\Omega_B \ll 1$ and this is justified by the fact that Faraday rotation constraints are not influenced by our analysis. This can be understood as a small deviation from the homogeneous and isotropic Friedmann background.

As a first case, we consider only the MF as a source of CMB perturbation, without taking into account the presence of free-streaming neutrinos. The result shows, as expected, that the CMB quadrupole is then proportional to the MF energy density parameter

$$C_2 \propto \left(\frac{\Omega_B}{\Omega_{\mathrm{rad}}}\right)^2, \tag{1.14}$$

allowing us to constrain its amplitude via this imprint in the CMB.

However, as the Universe reaches the temperature of 1.4 MeV, neutrinos decouple and start to free-stream. Their distribution function in momentum-space is affected by the anisotropic expansion caused by the presence of the MF and therefore they develop an anisotropic stress, which, at the leading order in our expansion around a Friedmann Universe, scales like their pressure with the expansion of the Universe. This means that this anisotropic stress scales as the one of the MF ($\propto a^{-4}$) as long as neutrinos can be considered massless relativistic particles and this turns out to be the main ingredient behind the compensation argument explained above. In other words, once the anisotropic stress

of neutrinos is adjusted to the one of the MF after a few Hubble times, they redshift in the same way and their sum remains zero. The Universe expands therefore as in a Friedmann background and the CMB quadrupole is erased.

It is important to underline that this effect depends on the absolute value of the energy density parameter characterizing the massless relativistic particles responsible for the compensation. Namely, in the case of neutrinos it is efficient only because we have $\Omega_\nu \sim 0.4 > 5/32$. Any other free-streaming relativistic component contributing with an energy density $\Omega_x < 5/32$, as for example primordial GWs from inflation, is not able to damp the anisotropy efficiently enough to cancel the quadrupole. On the other hand, the GW contribution from another source like for example phase transitions in a later Universe are constrained only by the nucleosynthesis to be such that $\Omega_{\rm GW} < 0.2$ and can therefore compensate the MF anisotropy. In this case neither photons nor neutrinos would have experienced any anisotropic expansion and the only evidence of a constant MF would be present in the GWB quadrupole.

Neglecting an eventual compensation due to GWs from phase transitions, the isotropization provided by relativistic free-streaming neutrinos is maintained until neutrinos become non relativistic and this depends on their masses: this happens when their temperature drops below their mass scale. For the temperature anisotropies of the CMB it is relevant whether this happens before or after photon decoupling. Once neutrinos become non relativistic, their pressure drops drastically ($\propto a^{-5}$) and their anisotropic stress is no more able to counteract the MF anisotropy. In order to quantify the effect due to this transition, we repeat the same computation for the CMB quadrupole considering that the neutrinos are almost degenerate. We have then to distinguish between two different cases: if their mass is high enough that they became non relativistic before photon decoupling, the isotropization effect is not present and the CMB will be affected by the MF anisotropy as if these massless particles were not present. In other words, photons result to be unable to counteract the MF anisotropic stress, even if their energy density is high enough to overpass the limiting value 5/32. The reason is that they decouple only in a matter dominated background, preventing the compensation mechanism to take place. On the other hand, if neutrino masses are small enough such that they were relativistic even after photon decoupling, the CMB quadrupole is noticeably reduced due to the compensation illustrated above. Indeed they will maintain the expansion of the Universe isotropic until they become non relativistic. In this last scenario, the final resulting quadrupole turns out to be reduced with respect the previous case by several orders of magnitude, loosening the constraints on the MF amplitude as obtained from the CMB anisotropies.

Finally, we point out that, considering non-degenerate neutrinos, as soon as we are left with only one neutrino species that is still relativistic, this effect of compensation can no more be guaranteed. The reason is that, as it was the case for photons, once the equilibrium between the anisotropic stresses of neutrinos and MF is broken, it can not be re-established in a matter dominated background.

We check our approximated computation through a numerical evolution of the exact equations, confirming the significant suppression of the CMB quadrupole in the case of massless free streaming neutrinos that become non relativistic long after photon decoupling, as explained above.

With our qualitative analysis we make clear how the mechanism of compensation between the anisotropic stresses of a MF and free-streaming neutrinos works in the simple case of a large scale coherent MF.

1.3 Cosmological defects: how much can they contribute to the CMB fluctuations?

Another source of perturbations that might be present in the early Universe and that might leave detectable imprints in the CMB anisotropies is represented by the so-called cosmological defects. They may originate at the end of hybrid inflation scenarios or by a first order phase transition that takes place in a later Universe. Indeed, spontaneous symmetry breaking which can happen during expansion and cooling of the Universe can lead to the formation of defects, regions of space where a large potential energy is concentrated and cannot relax to the vacuum due to topological obstruction.

For example, they represent the $N-1$ Goldstone modes resulting from a global $\mathcal{O}(N)$ phase transition of a N-component symmetric scalar field that might be present in the early Universe. After the global symmetry breaking, these Goldstone modes start to order on the horizon scale, as it is the case for a typical causal process. This originates in a nearly scale invariant spectrum of CMB anisotropies for temperature perturbations at very large scales. The same prediction is given by inflation and a first confirmation of the solidity of these forecasts has been provided by the COBE satellite, who initially detected the flat large scale plateau of the CMB spectrum. This is the reason why in the '80s many researches focused on the analysis of the anisotropies produced by cosmological defects.

Defects have been for the first time excluded as main cause for the fluctuations of the CMB by [32]: they have been discovered to give rise to a different first acoustic peak in the temperature power spectrum with respect to perturbations generated during inflation. The defect acoustic peak is too small with respect to the Sachs-Wolfe plateau and its peak position in ℓ-space corresponds to smaller scales, as it is the case for isocurvature perturbations, than the peak predicted by adiabatic perturbations from inflation. The main reason behind this difference is related to the fact that only scalar perturbations contribute to the peak amplitude, while the amplitude of the plateau is influenced by all kinds of perturbations. Defects generate, contrary to inflation, all kinds of perturbations, scalar, vector and tensor and the main feature of these perturbations is that the amplitude of vector anisotropies is comparable to the tensor strength [30, 102, 103, 104, 105]. Therefore, the presence of vector anisotropies for defects explains the difference of these two amplitudes. Another cause of the disagreement in the peaks of the TT-power spectrum between defects and inflation is given by the fact that defects represent an incoherent source of cosmological perturbations, while inflation generates coherent anisotropies. Naively one can picture this as a cancelation on super-horizon scales of the perturbations sourced by defects and this causes a smaller signal than the one given by inflation mechanisms. Testing this different prediction against incoming experimental data, the defect contribution to CMB anisotropies has been constrained to be less than 10% [102, 103, 104, 105, 34].

Decoherence is also the main responsible for the suppression of the EE- and TE-correlation peaks produced by defects in comparison with inflation. Refs. [106, 107] point out how it destroys cross-correlations of defects perturbations. This is another efficient way to constrain the defect contribution to the CMB perturbations.

However, in order to improve the existing upper-bounds for this contribution, we concentrate our attention on the polarization signal produced by defects. Indeed, their BB-power spectrum presents fundamental differences with respect to the inflationary one, mainly due to the fact that the vector contribution modifies the B-polarization signal coming from defects. It peaks at smaller scales ($\ell \sim 500$) and its amplitude is larger than the

polarization generated during inflation, when we set the temperature anisotropies of defects to be the allowed proportion of 10% of the total CMB anisotropies. Finally, since polarization is not influenced by the ISW effect, it represents a direct probe of super-horizon correlations at the recombination epoch. This would be a discriminating signal able to invalidate a defect contribution or any other purely causal generation process.
These are the main reasons that suggested us to focus our research on a deeper analysis of the GWB and B-polarization signals sourced by defects.

1.3.1 Gravitational wave background generated by a self-ordering scalar field

The GWB generated during hybrid preheating [108, 109, 110, 111, 112, 113, 114, 115] or during first order phase transitions [51, 116, 52, 53, 117, 118] has been investigated in great detail in the literature. These causal processes usually originate GW spectra that peak at wavelengths that are well inside the Hubble horizon during their generation. Therefore, most of the past analysis were focused on characterizing the GWBs produced on wavelengths smaller than the causal horizon at time of production.

Our first aim concerning the defect analysis is to investigate the tail of the GW spectrum involving wavelengths that are still outside of the Hubble radius while these GWs are produced. We consider therefore a N-component scalar field that undergoes a global phase transition and we focused on the large-scale analysis of the system. In this limit, once the transition is finished, we can consider the field to be fixed in its vacuum expectation value, neglecting its oscillations. Therefore, the only scales that characterize this system are the mass scale of the field that breaks the symmetry and the Hubble radius during the GW generation. The equation of motion of the field components in the large-scale limit can be approximated by the so-called "non-linear sigma model" (NLSM) equation [119]. In order to solve analytically this equation, we consider the number of the field components N to be large (numerical simulations showed that $N > 4$ is large enough for this approximation to hold). In the large-N limit the NLSM equation becomes liner and can be solved analytically in terms of simple Bessel functions depending on the background evolution of the Universe.

Therefore, in this large-N limit we are able to follow analytically all the steps that lead to the GW generation, obtaining finally the spectral shape of the GWB generated by self-ordering scalar fields on scales that are super-horizon at the time of production. The result is presented in [120] for two different cases, short- and long-lasting sources, depending on whether the source of GWs was decaying while Universe expanded or not. We focus our computation on wavelengths that were entering the horizon during a radiation dominated background, namely whose frequencies are in the range of sensitivity of most of the proposed GW experiments (a similar computation focused on a matter dominated background has been performed in [121]).

The main result of this computation is represented by a scale invariant spectrum of GWs whose amplitude in the case of a long-lasting source is

$$\frac{\mathrm{d}\Omega_{\mathrm{GW}}(k,t_0)}{\mathrm{d}\log k} \propto \frac{\Omega_{\mathrm{rad}}}{N}\left(\frac{v}{M_{\mathrm{P}}}\right)^4 . \tag{1.15}$$

Depending of course on the value of the true vacuum expectation value v of the scalar field which is breaking the symmetry, this GWB is in some scenarios within the the range of sensitivity of some GW experiments. The reason behind the flatness of the spectrum is that

the GW energy density continues to grow until horizon crossing and saturates thereafter, reaching its constant value.

Finally, it is important to compare this GWB with the one generated by primordial tensor perturbations from inflation. The ratio of these two backgrounds gives

$$\mathcal{R} \simeq \frac{256}{N} \left(\frac{v}{M}\right)^4, \tag{1.16}$$

that depends on the number of field components N and on the value of its vacuum expectation value v. However, the most important point of this analysis is that the power spectrum characterizing the GWs generated by a self-ordering scalar field is very similar to the one coming from inflation. Therefore, it is important to find an efficient way to disentangle these two spectra in the case they turn out to have also similar amplitudes. This is the motivation that push us toward the analysis of the B-polarization spectrum produced by defects that is briefly summarized in the following subsection.

1.3.2 B-polarization: defects vs. inflation

With the initial aim of finding a powerful tool able to help us distinguishing between the scale-invariant GWB produced by a self-ordering scalar field from a global phase transition in the early Universe and an inflationary background of primordial GWs, we focus our attention on the B-polarization power spectra produced by these two different scenarios.

I already mentioned above, the several differences between the two B-polarization spectra, whose main causes are the presence of vector defect perturbations and the causal nature of the defect generation process. We concentrate our attention on a deeper investigation of these differences with the attempt of building a sort of template that could be used by present and future experiments to detect or better constrain the defect contribution to CMB anisotropies.

In detail, we want to find a way to exploit the higher amplitude of the small-scale defect B-mode peak, characteristic that is even more pronounced in the real space angular correlation function. Indeed, plotting this function for defects and for inflation, it is immediately clear which scales are of most interest for the two different processes: defect signals, being a causal source of perturbations, are more pronounced on scales that were causally connected at recombination, corresponding to small angles $\theta \in [0^\circ, 1^\circ]$. On the other hand, the a-causal nature of inflation is evident from the large scale features of its correlation function, whose oscillations have a smaller amplitude but are on angles corresponding to scales that were super-horizon during recombination, $\theta \in [2^\circ, 4^\circ]$. Therefore, a relevant issue that we want to address was whether the defect peak on small scales could be measured by full or partial sky experiments.

Instead of examining the usual B-modes for the CMB polarization signal, we consider the so-called local $\tilde{B}$-modes, that are defined locally in every small patch of the sky and are directly related to the measured Stokes parameters. The usual non-local B-modes are obtained by a inverse Laplacian operation on the local $\tilde{B}$-modes, and this operation depends significantly on the boundary conditions. Therefore, even if on the theoretical point of view these two quantities contain the same amount of information, the real CMB experiments are not full sky ideal probes of the temperature anisotropies and this makes a big difference. Indeed, CMB experiments measure temperature and polarization on a given patch of the sky with fixed noise level and resolution, depending on the instruments. The

analysis of local $\tilde{B}$-modes does not suffer from the inversion of the differential operators, that depends on boundary conditions and affects the final result for local observations.

In Ref. [122] we compute, following Ref. [123], the signal-to-noise ratio (S/N) for the local $\tilde{B}$-polarization sourced by defects and by inflation. In order to reflect and extract the importance of the defect signal that is concentrated on the small scale part of the spectrum, we consider first small patches of the sky corresponding to angles $\theta \in [0^\circ, 1^\circ]$, sampling this interval with a fixed number of equal bins. Then, we compare this first result with the S/N for the two sources considering bigger patches of the sky, $\theta \in [0^\circ, 4^\circ]$ and keeping fixed the number of bins of our sampling. The comparison between the two S/N corresponding to different sky patch sizes shows that, once we enlarge the patch of the sky that we observe, the inflation S/N increases significantly, while the one for defects does not change much. This corresponds to fact that angles above $\sim 1^\circ$ do not contain more information concerning defects, while large scales encode the most characteristic features of inflation, as it is evident from the real space angular correlation function discussed above.

Moreover, in order to compare the efficiency of the local $\tilde{B}$-modes with respect the usual non-local ones, we compute the S/N for local $\tilde{B}$- and usual non-local B-modes for both generation mechanism, defects and inflation, fixing the sky patch size. The result shows that in the local polarization the defect signal is substantially enhanced with respect the inflationary one, while, if we consider the non-local one, this is not the case, namely the S/Ns for the two models are almost equivalent.

Summarizing, our contribution is relevant since with our proposed method, for clever choices of smoothing scale and observed angle patch sizes, we expect to be able to improve the current upper-bounds on the defect contribution to the CMB anisotropies by several orders of magnitude.

Chapter 2

Interactions of cosmological gravitational waves and magnetic fields

PHYSICAL REVIEW D **79**, 024021 (2009)

Interactions of cosmological gravitational waves and magnetic fields

Elisa Fenu and Ruth Durrer

The energy momentum tensor of a magnetic field always contains a spin-2 component in its anisotropic stress and therefore generates gravitational waves. It has been argued in the literature (Caprini & Durrer [77]) that this gravitational wave production can be very strong and that back-reaction cannot be neglected. On the other hand, a gravitational wave background does affect the evolution of magnetic fields. It has also been argued (Tsagas et al. [124], [71]) that this can lead to a very strong amplification of a primordial magnetic field. In this paper we revisit these claims and study back reaction to second order.

DOI: 10.1103/PhysRevD.79.024021 **PACS** numbers 04.50.+h, 11.10.Kk, 98.80.Cq

2.1 Introduction

Wherever we can measure them in the Universe, magnetic fields of 0.5 to several micro Gauss are present. They have been found in ordinary galaxies [37, 38] like ours, but also in galaxies at relatively high redshift [39] and in galaxy clusters [41, 42]. It is still unknown where these cosmological magnetic fields come from. Are they primordial, *i.e.* generated in the early universe [93, 125, 98], or did they form later on by some non-linear aspect of structure formation, like the Harrison mechanism which works once vorticity or, more generically, turbulence has developed [126]?

In addition, once initial fields are generated, it is still unclear whether they are strongly amplified by a dynamo mechanism or only moderately by contraction. Since the cosmic plasma is an excellent conductor, the magneto-hydrodynamic (MHD) approximation can be employed which implies that the magnetic field lines are frozen in during structure formation. Therefore, as long as non-linear magnetic field generation can be neglected, the magnetic field scales inversely proportional to the area, so that $B/\rho^{2/3}$ is roughly constant during structure formation. Here ρ is the energy (or matter) density of the cosmic plasma. For galaxies, with a density of about $\rho_{\rm gal} \sim 10^5\bar\rho$ this means that simple contraction will enhance magnetic fields by approximately 10^3, $\bar\rho$ is the mean density. Hence, if no dynamo is active during galaxy formation, initial fields of $B_{\rm in} \sim 10^{-9}$Gauss are needed. On the other hand, non-linear dynamo action can enhance the magnetic field exponentially by a factor up to 10^{15}, so that initial fields as tiny as $B_{\rm in} \sim 10^{-21}$Gauss might suffice [**?**]. However, since this enhancement is exponentially sensitive to the age of the Universe, it remains unclear how it can generate the magnetic fields in galaxies at redshifts of $z \sim 1$ or more, where the age of the Universe was at most half its present value reducing the amplification factor to less than 10^8.

Another problem of cosmic magnetic fields is that primordial generation of fields usually leads to a very blue magnetic field energy spectrum,

$$\frac{\mathrm{d}\rho_B}{\mathrm{d}\log k} \propto k^{M+3} \,, \tag{2.1}$$

where $M = 2$ for "causally" produced magnetic fields [68] and $M \sim 0$ for typical inflationary production mechanisms [55]. Such blue magnetic field spectra are strongly constrained by their gravity wave production [77] and cannot lead to the large scale fields observed today. The only solution to the problem might lie in an "inverse cascade" by which energy is transferred from small to larger scales. Since within the linearized approximation each Fourier mode evolves independently, such a cascade is inherently non-linear. Within standard MHD is has been shown that only helical magnetic fields can lead to inverse cascade [48].

In this work, we want to address a weakly non-linear effect which has not been considered in [48], namely the interaction of gravitational waves and magnetic fields. We shall study how this interaction can modify the magnetic field spectrum. We also re-interpret a finding by Tsagas [71], where the interaction between gravitational waves and magnetic fields has been interpreted as "resonant amplification". Similar conclusions are drawn in Refs. [72], [73]. However, in this last article it is noted that the amplification can take place only on super-horizon scales. And even though Ref. [73] does mention that there is no amplification in the long-wavelength limit, they do not really quantify this statement.

We show that the build up of magnetic fields due to their interaction with gravitational waves is at most logarithmic and thus comparable to the generation of gravitational waves by magnetic fields.

Furthermore, in Ref. [73] it has also been pointed out that the super-horizon "amplification" is independent of the fact whether the plasma is highly conducting or not. This seems physically reasonable as currents generated by electromagnetic fields can act only causally, *i.e.* on sub-horizon scales. An animated discussion on this subject follwed the above publications and can be found in Refs. [75], [76]. Here the role of a finite conductivity in an expanding Universe is addressed but controversal final conclusions have been reached.

The main advantage of our treatment is that we express the relevant results entirely in terms of physical, measurable quantities, which renders the interpretation straight forward. We actually find for the density parameters of second order perturbations that, once the scales considered are inside the horizon,

$$\Omega_B^{(2)} \simeq \Omega_B^{(1)}\Omega_{\mathrm{GW}}^{(1)} \simeq \Omega_B^{(1)} \left(\frac{H_{\mathrm{inf}}}{M_{\mathrm{P}}}\right)^2 \,, \tag{2.2}$$

$$\Omega_{\mathrm{GW}}^{(2)} \simeq \left[\Omega_B^{(1)}\right]^2 + \left[\Omega_{\mathrm{GW}}^{(1)}\right]^2 \,, \tag{2.3}$$

as one probably would expect naively. Even though most parts of this result can already be found in the above cited papers, they are interpreted there in a different way, and especially in Eq. (2.2) it is not always noted that the factor $\Omega_{\mathrm{GW}}^{(1)}$ always has to remain small.

The paper is organized as follows. In the next section we set up the fully non-linear equations for the evolution of magnetic fields in the relativistic MHD approximation. We use the 3+1 formalism and closely follow the derivation given in Ref. [127]. Since we

are mainly interested in gravitational waves, we specialize to the vorticity free case. In Section III we consider linear perturbations. We solve the linear perturbation equations for gravitational waves and magnetic fields with given initial conditions. We also derive the evolution of the corresponding energy densities. This part is not new and mainly included for completeness and to fix the notation for the subsequent Section IV, where we solve the second order equations. On this level the gravitational waves interact with the magnetic field. We calculate the second order magnetic field generated by this interaction and show that for reasonable values for the first order perturbations, its energy density remains always much smaller than the energy density of the first order contributions. In this sense, one cannot speak of resonant amplification. In Section V we summarize our results and draw some conclusions.

Throughout this work we use the metric signature $(-,+,+,+)$. Conformal time is denoted by t and we neglect the background curvature of the Universe, $K = 0$. Spacetime indices are denoted by lower case Greek letters, μ, ν, while lower case Latin letters, i, j are used for spatial indices. Most of our calculations are performed in the radiation dominated era and we shall often use the expression

$$a(t) = H_{\rm in} a_{\rm in}^2 t$$

for the scale factor.

2.2 The basic equations

We work in the MHD approximation, where we assume high conductivity. The electric field is then small compared to the magnetic field in the baryon rest-frame which we take to be the frame of our "fundamental observer". In addition, we assume the velocity u^μ of this fundamental observer to be vorticity-free and we neglect acceleration. According to Frobenius' theorem u is hyper-surface orthogonal and we can choose spatial coordinates in the three-space orthogonal to u. Furthermore, in the early Universe which is of interest to us, the dominant radiation and baryons are tightly coupled so that the energy flux is also given by u and we can set the heat flux $q = 0$. In our vorticity free frame, the magnetic part of the Weyl tensor, H_{ij} is related to the shear simply by

$$H_{ij} = {\rm curl}\sigma_{ij} \ ,$$

where curl is the 3-dim curl on the hyper-surface normal to u. Here σ is the shear of u given by

$$\begin{aligned} \sigma_{\mu\nu} &\equiv \tfrac{1}{2}\left(u_{\mu;\nu} + u_{\mu;\nu}\right) - \tfrac{1}{3}\Theta\tilde{p}_{\mu\nu} \qquad , \\ \Theta &\equiv u^{\mu}_{;\mu} \quad \text{and} \quad \tilde{p}_{\mu\nu} \equiv g_{\mu\nu} + u_\mu u_\nu \quad . \end{aligned}$$

Note that the normalization of u implies $0 = u^\nu u_{\nu;\mu} \propto u_{0;\mu}$. The gravito-magnetic interaction can then be described by the following equations, see [127]

$$\begin{aligned}
\nabla_u E_{ij} &= -\Theta E_{ij} - \frac{1}{2}\kappa\left(\rho + p + \frac{1}{6\pi}B^2\right)\sigma_{ij} - D^2\sigma_{ij} - \kappa\frac{1}{2}\nabla_u \Pi_{ij} - \frac{1}{6}\Theta\kappa\Pi_{ij} \\
&\quad +3\sigma_{\langle i}{}^n E_{j\rangle n} - \frac{1}{2}\kappa\sigma_{\langle i}{}^n\Pi_{j\rangle n}\,, \qquad (2.4)\\
\nabla_u \sigma_{ij} &= -E_{ij} + \frac{1}{2}\kappa\Pi_{ij} - \sigma_{\langle i}{}^n\sigma_{j\rangle n} - \frac{2}{3}\Theta\sigma_{ij}\,, \qquad (2.5)\\
\nabla_u B_i &= -\frac{2}{3}\tilde{p}_{ij}\Theta B^j + \sigma_{ij}B^j\,, \qquad (2.6)\\
\nabla_u \Theta &= -\frac{1}{3}\Theta^2 - \frac{1}{2}\kappa\left(\rho + 3p + \frac{1}{4\pi}B^2\right) - 2\sigma^2\,. \qquad (2.7)
\end{aligned}$$

Here E_{ij} is the electric part of the Weyl tensor, ρ and p are the energy density and pressure of the cosmic fluid which is assumed to follow the motion of the baryons (like, *e.g.* radiation before decoupling), $\kappa = 8\pi G$ is the gravitational coupling constant and B_i is the magnetic field. We have neglected the electric field in the above equations, since we assumed it to be much smaller that the magnetic field, *i.e.* $B^2 \gg E^2$. The covariant derivative in direction u is denoted by ∇_u and the brackets indicate symmetrization and trace subtraction,

$$X_{\langle ij\rangle} = \frac{1}{2}\left(X_{ij} + X_{ji}\right) - \frac{1}{3}\tilde{p}_{ij}X_m{}^m\,.$$

D^2 is the Laplace operator on the hyper-surface orthogonal to u. The scalars B^2 and σ^2 are simply $\sigma^2 \equiv \sigma_{ij}\sigma^{ij}/2$ and $B^2 \equiv B_iB^i$.

In addition to this we have the Einstein equation, the spatial part of which yields

$$\begin{aligned}
\mathcal{R}_{ij} &= E_{ij} + \frac{2}{3}\left(\kappa\rho + \frac{1}{8\pi}\kappa B^2 - \frac{1}{3}\Theta^2 + \sigma^2\right)\tilde{p}_{ij} \\
&\quad +\frac{1}{2}\kappa\Pi_{ij} - \frac{1}{3}\Theta\sigma_{ij} + \sigma_{n\langle i}\sigma^n{}_{j\rangle}\,, \qquad (2.8)
\end{aligned}$$

and its trace, the generalized Friedmann equation,

$$\frac{1}{3}\Theta^2 + \frac{1}{2}\mathcal{R} = \kappa\rho + \frac{1}{8\pi}\kappa B^2 + \sigma^2\,. \qquad (2.9)$$

Here $\mathcal{R}_{ij}$ is the Ricci tensor on the spatial hyper-surface and $\mathcal{R}$ is its trace.

From this system we can derive second order equations for σ_{ij} and B_i which are

$$\begin{aligned}
&\nabla_u\nabla_u\sigma_{ij} - D^2\sigma_{ij} + \frac{5}{3}\Theta\nabla_u\sigma_{ij} + \left(\frac{4}{9}\Theta^2 - \frac{3}{2}\kappa p - \frac{5}{6}\kappa\rho - \frac{1}{6\pi}\kappa B^2 - \frac{4}{3}\sigma^2\right)\sigma_{ij} = \\
&\qquad \kappa\nabla_u\Pi_{ij} + \frac{2}{3}\Theta\kappa\Pi_{ij} + \frac{2}{3}\kappa B^2\sigma_{ij} + \Theta\sigma_{\langle i}{}^n\sigma_{j\rangle n} + 2\sigma_{\langle i}{}^n\nabla_u\sigma_{j\rangle n} - \nabla_u\sigma_{\langle i}{}^n\sigma_{j\rangle n} \\
&\qquad -\kappa\sigma_{\langle i}{}^n\Pi_{j\rangle n} + \frac{1}{3}\sigma^2\sigma_{ij} + 3\sigma_{\langle i}{}^n\left[\frac{1}{2}\left(\sigma_{j\rangle}{}^m\sigma_{nm} + \sigma_n{}^m\sigma_{j\rangle m}\right) - \frac{2}{3}\delta_{j\rangle n}\sigma^2\right]\,, \qquad (2.10)
\end{aligned}$$

and

$$\nabla_u\nabla_u B_i - D^2 B_i + \frac{5}{3}\Theta\nabla_u B_i + \left(\frac{1}{3}\kappa\rho - \kappa p + \frac{2}{9}\Theta^2 + \frac{1}{12\pi}\kappa B^2 + \frac{2}{3}\sigma^2\right) B_i = \\ \sigma_{ij}\nabla_u B^j + 2\Theta\sigma_{ij}B^j + 2(\nabla_u\sigma_{ij})B^j - \frac{3}{2}\kappa\Pi_{ij}B^j + \sigma^n_{\langle i}\sigma_{j\rangle n}B^j + \mathrm{curl}J_i \,. \tag{2.11}$$

Eq. (2.11) can be obtained from Eq. (40) of [128] when setting $A_i = 0$, $\omega_{ij} = 0$ and $q_i = 0$. J_i stands for the 3-dimensional current. Eq. (2.11) is obtained without neglecting the electric field. The term $\mathrm{curl}E_i$, which is present in the original Maxwell equation which reduces to Eq. (2.6) if $E_i = 0$ [127] results in the Laplacian term D^2B_i and terms proportional to the wavenumber k times the electric field [see Eq. (40) of [128]]. We have neglected these latter contributions in the above equation, since they are only relevant inside the horizon ($kt \gg 1$), where we can neglect the source term of the equations, as we shall argue in the following.

In a regime of low conductivity we can neglect also the current in Eq. (2.11) and the magnetic field obeys to the above wave equation, while in a very hight conductivity case we should directly set the electric field $E_i = 0$ from the beginning and solve Eq. (2.6), obtaining a power-low behaviour with respect to time for B_i. In both cases we find that the behaviour in time of the induced second order magnetic field $B_i^{(2)}$ is the same on super-horizon scales (up to uncertain logarithmic corrections). We interpret this as the insensitivity of super-horizon perturbations to plasma properties like conductivity.

Inside the horizon, we neglect the source term. This is motivated by the Green function of the damped wave equation obtained when linearizing (2.11), which rapidly oscillates on sub-horizon scales. For Eq. (2.6) it is not the Green function but the source term $\sigma^{(1)}_{ij}B^j_{(1)}$ which oscillates when $kt \gg 1$, since gravity waves start oscillating at horizon crossing. Therefore again, the sub-horizon amplification is unimportant. The same conclusion is actually drawn in Ref. [73], where the fluid velocities are not neglected.

In the following we shall consider these equations in first and second perturbative orders with respect to a spatially flat Friedmann background,

$$\mathrm{d}s^2 = a^2(-\mathrm{d}t^2 + \delta_{ij}\mathrm{d}x^i\mathrm{d}x^j)\,.$$

We neglect a possible spatial curvature of the background and work with conformal time t. The time dependence of the scale factor a is determined by the Friedmann equation,

$$\left(\frac{\dot{a}}{a}\right)^2 = \frac{\kappa}{3}\rho a^2 \quad \text{and} \\ \dot{\rho} = -3(1+w)\rho\left(\frac{\dot{a}}{a}\right) \,, \quad w = p/\rho \,.$$

2.3 First order perturbations

2.3.1 Magnetic fields

A background Friedmann Universe can of course not contain a magnetic field since the latter always generates anisotropic stresses $\Pi_{ij} \neq 0$ which break isotropy. When considering a

magnetic field as a first order perturbation, Eq. (2.6) leads in first order to

$$\dot{B}_i^{(1)} = -\frac{\dot{a}}{a} B_i^{(1)} \ . \tag{2.12}$$

For this we use that to lowest order $u = a^{-1}\partial_t$ and $(\nabla_u B)_i = a^{-1}(\partial_t - \dot{a}/a)B_i$. Furthermore $\tilde{p}_{ij} = g_{ij} = a^2\delta_{ij}$ and $\Theta = 3\dot{a}/a^2$. This is solved by

$$B_i^{(1)}(\mathbf{x},t) = B_{i\,\mathrm{in}}^{(1)}(\mathbf{x})\frac{a_{\mathrm{in}}}{a(t)} \ , \qquad B^{i(1)}(\mathbf{x},t) = B_{\mathrm{in}}^{i(1)}(\mathbf{x})\frac{a_{\mathrm{in}}^3}{a^3(t)} \ . \tag{2.13}$$

The average energy density of the first order magnetic field is then given by

$$\langle \rho_B^{(1)} \rangle = \frac{1}{8\pi}\langle B_{(\mathrm{in})}^{(1)2}(\mathbf{x})\rangle \frac{a_{\mathrm{in}}^4}{a^4(t)} \ . \tag{2.14}$$

Here, we assume that the first order magnetic field has been generated by some random process. Hence $B_{i\,\mathrm{in}}^{(1)}$ is a random variable and $\langle\cdots\rangle$ denotes the expectation value. We assume also that this random process is statistically homogeneous so that $\langle \rho_B^{(1)} \rangle$ is independent of position.

2.3.2 Gravitational waves

For the gravity wave equation we consider a Fourier component

$$\begin{aligned} \sigma_{ij}^{(1)k}(\mathbf{x},t) &= \sigma^{(1)}(\mathbf{k},t) Q_{ij}(\hat{\mathbf{k}}) \exp(i\mathbf{k}\cdot\mathbf{x}) \ , \\ D^2\sigma_{ij}^{(1)k}(\mathbf{x},t) &= -\frac{k^2}{a^2(t)}\sigma_{ij}^{(1)k}(\mathbf{x},t) \ . \end{aligned}$$

Here $Q_{ij}(\hat{\mathbf{k}})$ is a transverse traceless polarization tensor. We assume that the gravity waves are statistically isotropic and parity invariant so that both polarizations have the same averaged square amplitudes. For the amplitude $\sigma^{(1)}(\mathbf{k},t)$ we obtain to first order the usual tensor perturbation propagation equation (neglecting anisotropic stresses of the cosmic fluid)

$$\ddot{\sigma}^{(1)} + \left[k^2 - \frac{3}{2}(1+w)\mathcal{H}^2\right]\sigma^{(1)} = 0 \ , \tag{2.15}$$

where $\mathcal{H} = \dot{a}/a$ denotes the co-moving Hubble parameter, $\mathcal{H} = aH$, where H is the physical Hubble parameter. We now rewrite this equation in terms of the dimensionless variable $\Sigma_{(1)}(\mathbf{k},t) \equiv \sigma_{(1)}(\mathbf{k},t)/(a_{\mathrm{in}}^2\Theta) = \sigma_{(1)}(\mathbf{k},t)/(3Ha_{\mathrm{in}}^2)$. We have normalized by the factor $1/a_{\mathrm{in}}^2$ in order for the quantity Σ to be independent of the normalization of the scale factor. This is not true for σ which is $\sigma \propto a_{\mathrm{in}}^2$. In this way, Σ can be directly related to observable quantities which are of course independent of the normalization of the scale factor. Equivalently, we will make use of the variable $\mathcal{B}$ that is defined as $\mathcal{B} \equiv \sqrt{\kappa}B/(3Ha_{\mathrm{in}})$ in order to be independent of the normalization of the scale factor, as well as Σ. In terms of Σ the above equation becomes

$$\ddot{\Sigma}_{(1)} - 3(1+w)\mathcal{H}\dot{\Sigma}_{(1)} + \left[k^2 + \left(\frac{3}{2} + 6w + \frac{9}{2}w^2\right)\mathcal{H}^2\right]\Sigma_{(1)} = 0 \ . \tag{2.16}$$

In the matter or radiation era, the solutions to this linear homogeneous differential equation are well known in terms of Bessel functions. We are mainly interested in the radiation epoch, where $w = 1/3$. During radiation domination the Universe expands like $a(t) \propto t$ such that $\mathcal{H} = Ha = 1/t$. We can therefore express the scale factor as

$$a(t) = H_{\rm in} a_{\rm in}^2 t \ . \tag{2.17}$$

In the radiation dominated Universe Eq. (2.16) reduces to

$$\ddot{\Sigma}_{(1)} - \frac{4}{t}\dot{\Sigma}_{(1)} + \left(k^2 + \frac{4}{t^2}\right)\Sigma_{(1)} = 0 \ , \tag{2.18}$$

with solution

$$\Sigma_{(1)} \propto (kt)^3 \left[j_1(kt) + y_1(kt)\right] \ , \tag{2.19}$$

where j_n and y_n denote the spherical Bessel functions of index n [129].

We distinguish the super- and sub-horizon behaviors. In the long wavelengths limit, $z \equiv kt \ll 1$, we have

$$\lim_{z\to 0} z^3 j_1(z) \simeq \frac{z^4}{3} \ , \qquad \lim_{z\to 0} z^3 y_1(z) \propto -z \ .$$

Taking into account only the faster growing mode, we obtain

$$\Sigma_{(1)}(t) \simeq \Sigma_{(1)}^{\rm in} \left(\frac{kt}{kt_{\rm in}}\right)^4 \ , \qquad kt \ll 1 \ , \tag{2.20}$$

or equivalently

$$\Sigma_{(1)}(t) \simeq \Sigma_{(1)}^{\rm in} \left(\frac{a}{a_{\rm in}}\right)^4 \ , \qquad kt \ll 1 \ . \tag{2.21}$$

The quantity directly related to gravity waves is however given by $\sigma_{(1)} = 3Ha_{\rm in}^2\Sigma_{(1)}$, for which we obtain on super-horizon scales

$$\sigma_{(1)}(t) \simeq \sigma_{(1)}^{\rm in} \left(\frac{a}{a_{\rm in}}\right)^2 \ , \qquad kt \ll 1 \ . \tag{2.22}$$

A direct consequence of this is that the "gravity wave energy density" is constant in time outside the horizon, as we show in the next sub-section. Of course the notion of "gravity wave energy density" and "gravity wave" is not strictly well defined for wavelengths larger than the size of the Hubble horizon. We shall just use the expression which is valid inside the horizon and call this the "gravity wave energy density" by analogy. It has a physical interpretation as a true energy density only once it enters the horizon. However, whenever this quantity becomes of the order of the background energy density, we know that perturbations become large and we can no longer trust linear perturbation theory.

Let us also consider the short wavelengths limit where $kt \gg 1$. In this limit we can approximate

$$\Sigma_{(1)}(t) \simeq (kt)^2 \frac{\cos(kt)}{\cos(1)} \Sigma_{(1)}(kt = 1) \ , \qquad kt \gg 1 \ , \tag{2.23}$$

where the initial constant $\Sigma_{(1)}(kt = 1)$ stands for the value of $\Sigma_{(1)}$ when it enters the

horizon and can be obtained from Eq. (2.20),

$$\Sigma_{(1)}(kt=1) \simeq \Sigma_{(1)}^{\rm in}\left(\frac{1}{kt_{\rm in}}\right)^4 .$$

The behavior of gravity waves on sub-horizon scales, $kt \gg 1$, is then given by

$$\sigma_{(1)}(t) \simeq 3a_{\rm in}^2 H(kt)^2 \frac{\cos(kt)}{\cos(1)}\Sigma_{(1)}(kt=1) . \tag{2.24}$$

We shall see that in this case the gravity waves energy density decreases like $1/a^4$, as it has to be for true gravity waves which are massless modes.

2.3.3 Energy Densities

As a first physically important quantity, let us discuss the energy densities of these first order perturbations and the corresponding density parameters.

The magnetic energy density is

$$\rho_B^{(1)} \equiv \frac{B_{(1)}^2}{8\pi} = \frac{B_i^{(1)}B_{(1)}^i}{8\pi} , \tag{2.25}$$

with Eq. (2.14), this becomes

$$\rho_B^{(1)}(t) = \frac{1}{8\pi}B_{(1)\,\rm in}^2\left(\frac{a_{\rm in}^4}{a^4}\right) . \tag{2.26}$$

In the radiation dominated universe under consideration, the density parameter of the first order magnetic field is therefore given by

$$\Omega_B^{(1)}(t) \equiv \frac{\rho_B^{(1)}}{\rho_c} = \frac{8\pi G\rho_B^{(1)}}{3H^2} = \frac{G}{3}\frac{B_{(1)\,\rm in}^2}{H_{\rm in}^2} = \Omega_{B\,\rm in}^{(1)} . \tag{2.27}$$

The density parameter $\Omega_B^{(1)}$ is constant in time. Both, the background radiation and the magnetic field which is frozen in, scale in the same way with the expansion of the Universe. As long as the magnetic field density parameter $\Omega_B^{(1)}$ is much smaller than 1, the magnetic field can be considered a small perturbation.

This is the result for a constant magnetic field. We also want to consider a stochastic magnetic field. In this case $\mathbf{B}(x)$ is a random variable and its spectrum is given by [77]

$$a^2(t)\mathbf{B}(\mathbf{x},t) = \frac{1}{(2\pi)^3}\int {\rm d}^3k\mathbf{B}(\mathbf{k})e^{i\mathbf{x}\cdot\mathbf{k}} , \tag{2.28}$$

$$\langle B_i(\mathbf{k})B_j^*(\mathbf{q})\rangle = (2\pi)^3\delta(\mathbf{k}-\mathbf{q})\mathcal{P}_{ij}(\hat{\mathbf{k}})\mathcal{P}_{B\,\rm in}^{(1)}(k) . \tag{2.29}$$

Here the basic time evolution of the magnetic field $\propto a^{-2}$ has been removed so that, to first order $\mathbf{B}(\mathbf{k})$ is independent of time. $\mathcal{P}_{ij}(\hat{\mathbf{k}}) = \delta_{ij} - k^{-2}k_ik_j$ is the projection tensor onto the plane normal to $\mathbf{k}$. The tensorial form of the spectrum is dictated by statistical isotropy which also requires that $\mathcal{P}_{B\,\rm in}^{(1)}$ depends only on the absolute value $k = |\mathbf{k}|$, and by the fact

that $\mathbf{B}$ is divergence free. The Dirac delta is a consequence of statistical homogeneity[1]. In this case we obtain

$$\begin{aligned}\langle\rho_B^{(1)}\rangle &= \frac{1}{(2\pi)^6 8\pi}\int \mathrm{d}^3k\int \mathrm{d}^3q\langle\mathbf{B}(\mathbf{k})\mathbf{B}(\mathbf{q})\rangle e^{i\mathbf{x}\cdot(\mathbf{k}-\mathbf{q})}\\ &= \frac{1}{(2\pi)^3}\int\frac{\mathrm{d}k}{k}k^3\mathcal{P}^{(1)}_{B\,\mathrm{in}}(k) = \int\frac{\mathrm{d}k}{k}\frac{\mathrm{d}\rho_B^{(1)}(k)}{\mathrm{d}\log k}\ .\end{aligned}$$

For the magnetic field density parameter at scale k this yields

$$\frac{\mathrm{d}\Omega_B^{(1)}(k,t)}{\mathrm{d}\log k} = \frac{8\pi G}{3(2\pi)^3}\frac{k^3\mathcal{P}^{(1)}_{B\,\mathrm{in}}(k)}{H_{\mathrm{in}}^2} = \frac{\mathrm{d}\Omega^{(1)}_{B\,\mathrm{in}}(k)}{\mathrm{d}\log k}\ . \tag{2.30}$$

Let us now consider gravity waves. The gravity wave energy density in real space is given by

$$\rho^{(1)}_{GW} \equiv \frac{\langle\dot{h}_{ij}\dot{h}^{ij}\rangle}{8\pi G}\frac{1}{a^2}\ , \tag{2.31}$$

where the factor $1/a^2$ comes from the fact that the dot denotes the derivative with respect to conformal time and the difference of a factor 4 in the normalization as compared *e.g.* to [131] comes from our definition of the perturbation variable [$g_{ij} = a^2(\delta_{ij} + 2h_{ij})$]. In Eq. (2.31) h_{ij} is considered as tensor field with respect to the spatial metric δ_{ij} so that there are no scale factors involved in raising or lowering indices, $h_{ij} = h_i{}^j = h^{ij}$. For simplicity we shall keep this convention is this section for all spatial tensors.

To lowest order the shear is given by $\sigma^{(1)}_{ij} = a\dot{h}_{ij}$. Furthermore, the fact that $\sigma^{(1)}_{ij}$ is transverse and traceless together with statistical isotropy determines entirely the tensor structure of the power spectrum.

$$\begin{aligned}&\langle\sigma_{ij}^{(1)\,\mathrm{in}}(\mathbf{k})\sigma_{lm}^{(1)\,\mathrm{in}}(\mathbf{q})\rangle =\\ &\qquad(2\pi)^3\delta(\mathbf{k}-\mathbf{q})\mathcal{M}_{ijlm}(\hat{\mathbf{k}})\mathcal{P}^{(1)}_{\sigma\,\mathrm{in}}(k)\ ,\end{aligned}$$

where [77]

$$\begin{aligned}\mathcal{M}_{ijlm}(\hat{\mathbf{k}}) \equiv\ & \delta_{il}\delta_{jm} + \delta_{im}\delta_{jl} - \delta_{ij}\delta_{lm} + k^{-2}(\delta_{ij}k_lk_m +\\ & \delta_{lm}k_ik_j - \delta_{il}k_jk_m - \delta_{im}k_lk_j - \delta_{jl}k_ik_m\\ & -\delta_{jm}k_lk_i) + k^{-4}k_ik_jk_lk_m\ .\end{aligned} \tag{2.32}$$

We have $\mathcal{M}^{ij}{}_{ij} = 4$, which takes into account the two polarization degrees of freedom. Therefore, considering that also for the shear we do not multiply by the scale factor while raising or lowering indices, $\sigma_{ij} = \sigma^{ij}$, we can write the gravity waves energy density in terms of σ_{ij} as

$$\rho^{(1)}_{GW} = \frac{\langle\sigma_{ij}\sigma^{ij}\rangle}{8\pi G}\frac{1}{a^4}\ . \tag{2.33}$$

[1] One could also add a term which is odd under parity but we disregard this possibility in this work [130].

For the contribution to the energy density per logarithmic frequency interval we then obtain

$$\begin{aligned}\frac{\mathrm{d}\rho^{(1)}_{GW}(k,t)}{\mathrm{d}\log k} &= \frac{2}{(2\pi)^3 G}\left[k^3\mathcal{P}^{(1)}_{\sigma}(k,t)\right]\frac{1}{a^4} \\ &= \frac{18}{(2\pi)^3 G}\left[k^3\mathcal{P}^{(1)}_{\Sigma}(k,t)\right]H^2\left(\frac{a_{\rm in}}{a}\right)^4 , \end{aligned} \tag{2.34}$$

where we have used the relation $\sigma_{ij} = 3Ha_{\rm in}^2\Sigma_{ij}$ or equivalently $\mathcal{P}^{(1)}_{\sigma}(k,t) = 9H^2a_{\rm in}^4\mathcal{P}^{(1)}_{\Sigma}(k,t)$. Finally, we can write the gravity wave density parameter as

$$\frac{\mathrm{d}\Omega^{(1)}_{\rm GW}(k,t)}{\mathrm{d}\log k} \equiv \frac{1}{\rho_c}\frac{\mathrm{d}\rho^{(1)}_{GW}}{\mathrm{d}\log k} = \frac{48\pi}{(2\pi)^3}\left[k^3\mathcal{P}^{(1)}_{\Sigma}(k,t)\right]\left(\frac{a_{\rm in}}{a}\right)^4 . \tag{2.35}$$

We have now to distinguish between super- and sub-horizon modes. Using our super-horizon result for $\Sigma_{(1)} = \sigma_{(1)}/(3Ha_{\rm in}^2)$ where $kt \ll 1$

$$\Sigma^{(1)}_{ij}(\mathbf{k},t) \simeq \Sigma^{(1)}_{ij\,\rm in}(\mathbf{k})\left(\frac{t}{t_{\rm in}}\right)^4 ,$$

we find

$$\begin{aligned}\frac{\mathrm{d}\rho^{(1)}_{GW}(k,t)}{\mathrm{d}\log k} &= \frac{18}{(2\pi)^3 G}\left[k^3\mathcal{P}^{(1)}_{\Sigma\,\rm in}(k)\right]\left(\frac{a}{a_{\rm in}}\right)^8 H^2\left(\frac{a_{\rm in}}{a}\right)^4 \\ &= \frac{18}{(2\pi)^3 G}\left[k^3\mathcal{P}^{(1)}_{\Sigma\,\rm in}(k)\right]H_{\rm in}^2 = \frac{\mathrm{d}\rho^{(1)}_{GW\,\rm in}}{\mathrm{d}\log k} . \end{aligned} \tag{2.36}$$

For the last equal sign we made use of Eq. (2.17). Hence on super-horizon scales the "gravity wave energy density" is time independent. Then, of course the gravity wave density parameter grows like a^4,

$$\frac{\mathrm{d}\Omega^{(1)}_{\rm GW}(k,t)}{\mathrm{d}\log k} = \frac{\mathrm{d}\Omega^{(1)\,\rm in}_{GW}}{\mathrm{d}\log k}\left(\frac{a}{a_{\rm in}}\right)^4 , \quad kt \ll 1 , \tag{2.37}$$

where

$$\frac{\mathrm{d}\Omega^{(1)\,\rm in}_{GW}(k)}{\mathrm{d}\log k} = \frac{48\pi}{(2\pi)^3}\left[k^3\mathcal{P}^{(1)}_{\Sigma\,\rm in}(k)\right] . \tag{2.38}$$

Inside the horizon, $kt \gg 1$, we have to insert the expression of $\Sigma_{(1)}$ given by Eq. (2.23) in Eq. (2.34), which yields

$$\frac{\mathrm{d}\rho^{(1)}_{GW}(k,t)}{\mathrm{d}\log k} \simeq \frac{9}{(2\pi)^3 G}\left[k^3\mathcal{P}^{(1)}_{\Sigma\,\rm in}(k)\right]\frac{H_{\rm in}^2}{(kt_{\rm in})^4}\left(\frac{a_{\rm in}}{a}\right)^4 \propto \frac{1}{a^4} . \tag{2.39}$$

For the density parameter we obtain in a radiation dominated background

$$\begin{aligned}\frac{\mathrm{d}\Omega^{(1)}_{GW}(k)}{\mathrm{d}\log k} &\simeq \frac{24\pi}{(2\pi)^3}\left(\frac{1}{kt_{\rm in}}\right)^4\left[k^3\mathcal{P}^{(1)}_{\Sigma\,\rm in}(k)\right] \\ &\simeq \frac{1}{2}\left(\frac{1}{kt_{\rm in}}\right)^4\frac{\mathrm{d}\Omega^{(1)\,\rm in}_{GW}}{\mathrm{d}\log k} , \quad kt \gg 1 . \end{aligned} \tag{2.40}$$

Inside the horizon, the gravity wave density parameter is constant in time as is natural in a radiation dominated Universe. Note that this agrees, up to the factor 1/2 which comes from averaging $\cos^2(kt)$, with Eq.(2.37) at horizon entry, where $(a/a_{\rm in})^4 = (kt_{\rm in})^{-4}$. Large scale gravity waves from inflation, are "amplified" for a long time before entering the horizon, *i.e.* they have $kt_{\rm in} \ll 1$. Only if $\left[{\rm d}\Omega^{(1)}_{GW}(k)/{\rm d}\log k\right]$ is small for all values of k, perturbation theory is justified. Therefore it is not sufficient if $\left[{\rm d}\Omega^{(1)\,{\rm in}}_{GW}/{\rm d}\log k\right]$ is small, but we actually need that $(kt_{\rm in})^{-4}\left[{\rm d}\Omega^{(1)\,{\rm in}}_{GW}/{\rm d}\log k\right]$ be small. This is better understood if we write the energy density in terms of the metric perturbation. In a radiation dominated Universe the "growing" (not decaying) mode solution for the metric perturbation is

$$h_{ij}(k,t) = e_{ij}(\mathbf{k}) h_{\rm in} j_0(kt) \ ,$$

where $e_{ij}(\mathbf{k})$ is transverse traceless and j_0 is the spherical Bessel function of order 0. Using $j_0' = -j_1$ and Eq. (2.31) yields

$$\rho^{(1)}_{GW} = k^3 \frac{k^2 \langle |h_{\rm in}|^2 \rangle j_1^2(kt)}{8\pi G a^2}$$

With $\rho_c = 3H^2/(8\pi G) = 3/(8\pi G a^2 t^2)$ and $\langle |h_{\rm in}|^2\rangle \equiv \mathcal{P}_h$, we find

$$\frac{{\rm d}\Omega_{GW}}{{\rm d}\log k} = 3[(kt)^2 j_1^2(kt)] k^3 P_h \simeq 3(kt)^4 k^3 \mathcal{P}_h \ , \quad \text{if } kt \ll 1 \ . \tag{2.41}$$

Hence if the metric perturbations are small for all values of k, *i.e.* $k^3\mathcal{P}_h \ll 1$ this implies

$$\frac{{\rm d}\Omega_{GW}}{{\rm d}\log k} \ll (kt)^4 \ .$$

Therefore the requirement $(kt_{\rm in})^{-4}\left[{\rm d}\Omega^{(1)\,{\rm in}}_{GW}/{\rm d}\log k\right] \ll 1$ is equivalent to the requirement that the metric perturbations be small on super horizon scales [note that $j_0(z) \simeq 1$ for $z \ll 1$].

Before we go to the second order, let us stress this point once more, because it is the origin of the confusion in the literature. Inflation generates gravitational waves with an amplitude

$$k^3\mathcal{P}_h \simeq \left(\frac{H_{\rm inf}}{M_{\rm P}}\right)^2 \leq 10^{-10} \ ,$$

where $M_{\rm P}$ is the Planck mass and $H_{\rm inf}$ denotes the scale factor during inflation. The maximum value of 10^{-10} is the maximum tensor fluctuation from inflation allowed by the cosmic microwave background anisotropies.

However, the density parameter on super-horizon scale is given by, see Eq. (2.41)

$$\frac{{\rm d}\Omega^{(1)}_{GW}}{{\rm d}\log k} \simeq (kt)^4 \left(\frac{H_{\rm inf}}{M_{\rm P}}\right)^2 , \qquad kt \ll 1 \ .$$

This equation is correct for any power law background, $a \propto t^q$, also for matter and even for inflation. 0nly at horizon crossing, can the density parameter become of the order 10^{-10}. Inside the horizon it stays constant if the background is radiation. Hence Eq. (2.40) can

be written as

$$\frac{\mathrm{d}\Omega_{GW}^{(1)}(k)}{\mathrm{d}\log k} \simeq \left(\frac{H_{\rm inf}}{M_{\rm P}}\right)^2 , \qquad kt \gg 1 . \tag{2.42}$$

2.4 Second order perturbations

In this section we include all terms of second order in the perturbations, and we shall insert our first order results for them; *i.e.* in terms of the form $\sigma_{ij}B^j$ we insert $\sigma_{ij}^{(1)}B_{(1)}^j$ or for Π_{ij} we insert the first order magnetic fields, $\Pi_{ij}^{(1)} = B_i^{(1)}B_j^{(1)} - (1/3)\tilde{p}_{ij}^{(0)}B^{(1)2}$ in Eqs. (2.10) and (2.11). We obtain the following differential equations for the evolution of the second order perturbations $B_i^{(2)}(\mathbf{x},t)$ and $\sigma_{ij}^{(2)}(\mathbf{x},t)$:

$$\begin{aligned}
&\nabla_u\nabla_u B_i^{(2)} - D^2 B_i^{(2)} + \frac{5}{3}\Theta\nabla_u B_i^{(2)} + \frac{1}{3}\Theta^2(1-w)B_i^{(2)} = \\
&\quad \sigma_{ij}^{(1)}\nabla_u B_{(1)}^j + 2\Theta\sigma_{ij}^{(1)}B_{(1)}^j + 2\nabla_u\sigma_{ij}^{(1)}B_{(1)}^j \\
&\quad +(D^2)^{(1)}B_i^{(1)} + \mathrm{curl}J_i , \qquad (2.43)\\
&\nabla_u\nabla_u\sigma_{ij}^{(2)} - D^2\sigma_{ij}^{(2)} + \frac{5}{3}\Theta\nabla_u\sigma_{ij}^{(2)} + \frac{1}{6}\Theta^2(1-3w)\sigma_{ij}^{(2)} = \\
&\quad \kappa\nabla_u\Pi_{ij}^{(1)} + \frac{2}{3}\Theta\kappa\Pi_{ij}^{(1)} + \Theta\sigma_{\langle i(1)}{}^n\sigma_{j\rangle n}^{(1)} + (D^2)^{(1)}\sigma_{ij}^{(1)} \\
&\quad +2\sigma_{\langle i}^{n(1)}\nabla_u\sigma_{j\rangle n}^{(1)} - \nabla_u\sigma_{\langle i(1)}{}^n\sigma_{j\rangle n}^{(1)} . \qquad (2.44)
\end{aligned}$$

Taking into account that $\nabla_u B_{i(1)} = -(2/3)\Theta B_{i(1)}$ together with $\nabla_u\Pi_{ij}^{(1)} = -(4/3)\Theta\Pi_{ij}^{(1)}$, Eqs. (2.43), (2.44) can be simplified to

$$\begin{aligned}
&\nabla_u\nabla_u B_i^{(2)} - D^2 B_i^{(2)} + \frac{5}{3}\Theta\nabla_u B_i^{(2)} + \frac{1}{3}\Theta^2(1-w)B_i^{(2)} = \\
&\quad \left[\frac{4}{3}\Theta\sigma_{ij(1)} + 2\nabla_u\sigma_{ij}^{(1)}\right]B_{(1)}^j + (D^2)^{(1)}B_i^{(1)} , \qquad (2.45)\\
&\nabla_u\nabla_u\sigma_{ij}^{(2)} - D^2\sigma_{ij}^{(2)} + \frac{5}{3}\Theta\nabla_u\sigma_{ij}^{(2)} + \frac{1}{6}\Theta^2(1-3w)\sigma_{ij}^{(2)} = \\
&\quad -\frac{2}{3}\Theta\kappa\Pi_{ij}^{(1)} + \Theta\sigma_{\langle i(1)}{}^n\sigma_{j\rangle n}^{(1)} + (D^2)^{(1)}\sigma_{ij}^{(1)} \\
&\quad +2\sigma_{\langle i}^{n(1)}\nabla_u\sigma_{j\rangle n}^{(1)} - \nabla_u\sigma_{\langle i(1)}{}^n\sigma_{j\rangle n}^{(1)} . \qquad (2.46)
\end{aligned}$$

We have also neglected the term $\mathrm{curl}J_i$ in Eq. (2.43). Since it is proportional to k in the Fourier space, its contribution is important only on sub-horizon scales, where we anyway neglect the source part. Outside the horizon, $kt \ll 1$, it is negligible.

2.4.1 The second order magnetic field from gravity waves and a constant magnetic field

For simplicity, and to gain intuition, we first consider a constant first order magnetic field,

$$B_i^{(1)}(\mathbf{x},t) = B_{i\,\rm in}^{(1)}\frac{a_{\rm in}}{a} , \qquad B_i^{(1)}(\mathbf{k},t) = B_{i\,\rm in}^{(1)}\frac{a_{\rm in}}{a}\delta^3(\mathbf{k}) .$$

In this case, the convolution of $B_{(1)}$ and $\sigma_{(1)}$ into which the products in ordinary space transform under Fourier transformation, become normal products and the second order magnetic field $B_i^{(2)}$ has the same wavelength as the first order gravity wave which generates it.

Remembering that $\sigma_{ij} \propto a^{-4}\sqrt{\mathcal{P}_\sigma^{(1)}} \equiv a^{-4}\sigma^{(1)}$ one obtains

$$\ddot{B}_i^{(2)} + 2\mathcal{H}\dot{B}_i^{(2)} + B_i^{(2)}\left[k^2 + \frac{1}{2}\mathcal{H}^2(1-3w)\right] = 2\dot{\sigma}_{ij}^{(1)} B_{j\,\mathrm{in}}^{(1)} \frac{a_{\mathrm{in}}}{a^2}\ . \tag{2.47}$$

In principle, one has to consider the corrections to the orthogonal spatially projected covariant derivative $(D^2)^{(1)}B_i^{(1)}$ due to the tensor perturbations h_{ij} in the metric tensor $g_{\mu\nu}$. Computing these corrections, they turn out to be equal to zero, since the magnetic field is transverse. This remains valid even if $\mathbf{B}^{(1)}$ is not constant.

Considering the expansion-normalized dimensionless variable $\mathcal{B}_i^{(2)} \equiv \sqrt{\kappa}B_i^{(2)}/(\Theta a_{\mathrm{in}})$, we obtain

$$\begin{aligned}
&\ddot{\mathcal{B}}_i^{(2)} - \mathcal{H}(1+3w)\dot{\mathcal{B}}_i^{(2)} + \mathcal{B}_i^{(2)}\left[k^2 + \mathcal{H}^2\left(\frac{1}{2} + 3w + \frac{9}{2}w^2\right)\right] = f_i\,,\\
&f_j \equiv 2\sqrt{\kappa}\left[\dot{\Sigma}_{ij}^{(1)} - \frac{3}{2}\mathcal{H}(1+w)\Sigma_{ij}^{(1)}\right] B_{j\,\mathrm{in}}^{(1)}\left(\frac{a_{\mathrm{in}}}{a}\right)^2\ .
\end{aligned} \tag{2.48}$$

We investigate the behavior of the second order perturbation in the radiation dominated phase.

Moreover, since the source $f_i(\mathbf{k},t)$ and therefore also $\mathcal{B}_i^{(2)}(\mathbf{k},t)$ are random variables, we want to determine their spectra. The first order gravity wave spectrum is

$$\begin{aligned}
\langle \Sigma_{ij}^{(1)\,\mathrm{in}}(\mathbf{k})\Sigma_{ln}^{*(1)\,\mathrm{in}}(\mathbf{q})\rangle &= (2\pi)^3\mathcal{M}_{ijln}(\hat{\mathbf{k}})\delta^3(\mathbf{k}-\mathbf{q})\mathcal{P}_{\Sigma\,\mathrm{in}}^{(1)}(k)\,,\\
\langle \Sigma_{ij}^{(1)\,\mathrm{in}}(\mathbf{k})\Sigma_{(1)\,\mathrm{in}}^{*ij}(\mathbf{q})\rangle &= 4(2\pi)^3\delta^3(\mathbf{k}-\mathbf{q})\mathcal{P}_{\Sigma\,\mathrm{in}}^{(1)}(k)\,,
\end{aligned}$$

where $\mathcal{M}_{ijlm}$ is the gravity waves polarization tensor defined in Eq. (2.32). It can also be expressed in terms of the projection tensor $\mathcal{P}_{ij}(\hat{\mathbf{k}})$, $\mathcal{M}_{ijlm} \equiv \mathcal{P}_{il}\mathcal{P}_{jm} + \mathcal{P}_{im}\mathcal{P}_{jl} - \mathcal{P}_{ij}\mathcal{P}_{lm}$. Actually $(1/2)\mathcal{M}_{ij}{}^{lm}$ is the projection tensor onto the two transverse traceless modes of a rank 2 symmetric tensor. The power spectrum of the second order magnetic field $\mathcal{B}_{(2)}$ is of the form

$$\langle \mathcal{B}_i^{(2)}(\mathbf{k},t)\mathcal{B}_j^{*(2)}(\mathbf{p},t)\rangle = (2\pi)^3\mathcal{P}_{ij}(\hat{\mathbf{k}})\delta^3(\mathbf{k}-\mathbf{p})\mathcal{P}_{\mathcal{B}}^{(2)}(k,t)\ . \tag{2.49}$$

We obtain the solution for $\mathcal{B}_i^{(2)}(\mathbf{k},t)$ with the help of Green function method,

$$\mathcal{B}_i^{(2)}(\mathbf{k},t) = \int_{t_{\mathrm{in}}}^{t} \mathrm{d}t'\mathcal{G}(t,t',\mathbf{k})f_i(\mathbf{k},t')\,. \tag{2.50}$$

Here $\mathcal{G}$ is the Green function of the second order linear differential operator acting on $\mathcal{B}_i^{(2)}$ which depends on the cosmological background. It can be determined in terms of the homogeneous solutions which in the radiation dominated era are simply spherical Bessel functions and powers. More precisely, in terms of $z = kt$, Eq. (2.48) in the radiation

dominated case, $w = 1/3$, becomes

$$\mathcal{B}_i^{(2)\prime\prime} - \frac{2}{z}\mathcal{B}_i^{(2)\prime} + \left(1 + \frac{2}{z^2}\right)\mathcal{B}_i^{(2)} = k^{-2} f_i(z, \mathbf{k}) \ , \tag{2.51}$$

where the prime denotes a derivative w.r.t. z. Two homogenous solutions to this equation are $P_1(z) = z^2 j_0(z)$ and $P_2(z) = z^2 y_0(z)$. Defining the Wronskian, $W(z) = P_1'(z)P_2(z) - P_1(z)P_2'(z) = z^2$, a possible Green function is

$$\mathcal{G}(z, z', \mathbf{k}) = \frac{P_1(z')P_2(z) - P_1(z)P_2(z')}{W(z')} \ . \tag{2.52}$$

The solution obtained by integrating with this Green function satisfies the initial condition $\mathcal{B}_i^{(2)}(z_{\rm in}, \mathbf{k}) = \mathcal{B}_i^{(2)\prime}(z_{\rm in}, \mathbf{k}) = 0$. Any other solution can be obtained by adding a homogeneous solution to this one. We discuss the physically correct choice of initial conditions in more detail in the Appendix 2.6.1. For the magnetic field, the initial conditions chosen with this Green function seem adequate to us. We can now write the magnetic field spectrum as

$$\begin{aligned}\langle \mathcal{B}_i^{(2)}(\mathbf{k}, t)\mathcal{B}_j^{*(2)}(\mathbf{p}, t)\rangle = \int_{z_{\rm in}}^{z} {\rm d}z' \int_{z_{\rm in}}^{z} {\rm d}z'' k^{-2} p^{-2} \times \\ \mathcal{G}(z, z', \mathbf{k})\mathcal{G}^*(z, z'', \mathbf{p})\langle f_i(\mathbf{k}, z') f_j^*(\mathbf{p}, z'')\rangle \ .\end{aligned} \tag{2.53}$$

We solve Eq. (2.51), distinguishing the sub- and super-horizon regimes. In the long wavelength limit, $kt = z \ll 1$, we have to insert the solution obtained for gravity waves $\Sigma_{ij}^{(1)}$ on super-horizon scales and given in Eq. (2.20). Therefore, the source term $f_i(\mathbf{k}, t)$ reads

$$f_i(\mathbf{k}, t') = 4\sqrt{\kappa}\mathcal{P}_i^s(\hat{\mathbf{k}}) \left[\Sigma_{sn}^{(1)\,\rm in}(\mathbf{k}) B_n^{(1)\,\rm in}\right] (H_{\rm in} a_{\rm in})^2 t' \ , \tag{2.54}$$

and equivalently for $f_j^*(\mathbf{q}, t'')$. The power spectrum of f_i can then be written as

$$\begin{aligned}\langle f_i(\mathbf{k}, z') f_j^*(\mathbf{p}, z'')\rangle &= 16\kappa \mathcal{P}_i^s(\hat{\mathbf{k}})\mathcal{P}_j^l(\hat{\mathbf{q}})\langle \Sigma_{sn}^{(1)\,\rm in}(\mathbf{k})\Sigma_{lr}^{*(1)\,\rm in}(\mathbf{k})\rangle B_n^{(1)\,\rm in} B_r^{*(1)\,\rm in} (H_{\rm in} a_{\rm in})^4 z' z'' k^{-2} \\ &\equiv (2\pi)^3 \delta^3(\mathbf{k} - \mathbf{p})\mathcal{P}_{ij}(\hat{\mathbf{k}}) h(z', z'', k) \ .\end{aligned} \tag{2.55}$$

For the function $h(z', z'', k)$ we obtain the following expression

$$\begin{aligned} h(z', z'', k) &\simeq F(k) g(z') g(z'') \ , \\ F(k) &= \kappa B_{(1)\,\rm in}^2 \mathcal{P}_{\Sigma\,\rm in}^{(1)}(k) k^{-2} \ , \\ g(z') &= 4 H_{\rm in}^2 a_{\rm in} z' \ . \end{aligned}$$

The solution for the power spectrum of the second order perturbation of the magnetic field can then be written as

$$\begin{aligned}\langle \mathcal{B}_i^{(2)}(\mathbf{k}, t)\mathcal{B}_j^{*(2)}(\mathbf{p}, t)\rangle = (2\pi)^3 \mathcal{P}_{ij}(\hat{\mathbf{k}})\delta^3(\mathbf{k} - \mathbf{p}) \times \\ \left[\int_{z_{\rm in}}^{z} {\rm d}z' \mathcal{G}(z, z', \mathbf{k}) \sqrt{F(k)} g(z')\right]^2 \ .\end{aligned} \tag{2.56}$$

The square $[\cdots]^2$ is simple the power spectrum $\mathcal{P}_{\mathcal{B}}^{(2)}(k,t)$ which we want to determine. Of course, the integrals in the square bracket are solutions to our magnetic field Eq. (2.51) with source $\sqrt{F(k)}g(z)$. Hence $\sqrt{\mathcal{P}_{\mathcal{B}}^{(2)}}$ satisfies the equation

$$\begin{aligned} &P'' - \frac{2}{z}P' + \left(1 + \frac{2}{z^2}\right)P = \frac{\alpha}{k^3}z \ , \\ &|P| \equiv \sqrt{\mathcal{P}_{\mathcal{B}}^{(2)}(k,t)} \ , \qquad z \equiv kt \ , \\ &\alpha \equiv 4H_{\rm in}^2 a_{\rm in}\sqrt{\kappa B_{(1)\,\rm in}^2 \mathcal{P}_{\Sigma\,\rm in}^{(1)}(k)} \ . \end{aligned} \tag{2.57}$$

Solving the above equation with the Wronskian method in the regime $z = kt \ll 1$, one finds

$$P(z) \simeq \frac{\alpha}{2k^3}z^3 \ , \qquad z = kt \ll 1 \ .$$

This yields

$$k^3\mathcal{P}_{\mathcal{B}}^{(2)}(k,t) \simeq 4\kappa\frac{B_{(1)}^{\rm in\,2}}{H_{\rm in}^2}\left[k^3\mathcal{P}_{\Sigma\,\rm in}^{(1)}(k)\right]\left(\frac{a}{a_{\rm in}}\right)^6 \ , \qquad kt \ll 1 \ . \tag{2.58}$$

This is the second order magnetic field power spectrum induced by the presence of a first order field and a gravitational wave. It is the growth $\propto t^6$ of this induced field which has been interpreted in Refs. [124, 71, 72] as strong amplification. But before drawing such conclusions, we want to compare the energy density parameter of $B^{(2)}$ with the one of $\sigma^{(1)}$ and $B^{(1)}$ inside the horizon, where these quantities have a simple physical interpretation.

Inside the horizon, $kt \gg 1$, we can no longer use the above simple approximation for the source term. The solution of Eq. (2.57) with a generic source term,

$$\left[\sqrt{\mathcal{P}_{\mathcal{B}}^{(2)}(k,z)}\right]'' - \frac{2}{z}\left[\sqrt{\mathcal{P}_{\mathcal{B}}^{(2)}(k,z)}\right]' + \left[\sqrt{\mathcal{P}_{\mathcal{B}}^{(2)}(k,z)}\right] = \mathcal{S}(k,z) \ , \tag{2.59}$$

can be written as

$$\sqrt{\mathcal{P}_{\mathcal{B}}^{(2)}(k,z)} = \int_{z_{\rm in}}^{z} dz' \mathcal{S}(k,z')\mathcal{G}(z,z',\mathbf{k}) \, . \tag{2.60}$$

But, once the gravity waves enter the horizon, the source and the Green function start oscillating and the contribution to the above integral becomes negligible. We therefore neglect the source inside the horizon and simply match the solution at horizon crossing with the homogeneous solutions of Eq. (2.57) given above, that are $P_1(z) = z^2 j_0(z)$ and $P_2(z) = z^2 y_0(z)$ ($z = kt$). Considering the limit $z \gg 1$, this yields

$$k^3\mathcal{P}_{\mathcal{B}}^{(2)}(k,t) \simeq 2\kappa\frac{B_{(1)}^{\rm in\,2}}{H_{\rm in}^2}\left[k^3\mathcal{P}_{\Sigma\,\rm in}^{(1)}(k)\right]\left(\frac{a}{a_{\rm in}}\right)^2\frac{1}{(kt_{\rm in})^4} \ , \qquad kt \gg 1 \ . \tag{2.61}$$

2.4.1.1 The energy density

To analyze this amplification which happens mainly on super-horizon scales, let us compare energy densities after horizon entry. The energy density of our second order magnetic field

is

$$\frac{\mathrm{d}\rho_B^{(2)}(k,t)}{\mathrm{d}\log k} \equiv \frac{1}{(2\pi)^3}\left[k^3\mathcal{P}_B^{(2)}(k,t)\right]\frac{1}{a^2} = \frac{1}{(2\pi)^3}\left[k^3\mathcal{P}_{\mathcal{B}}^{(2)}(k,t)\right]\frac{9H^2}{\kappa}\left(\frac{a_{\rm in}}{a}\right)^2 . \tag{2.62}$$

The factor $1/a^2$ comes from the fact that we have to raise one index of $\langle B_i^{(2)}B_i^{(2)}\rangle$ in order to compute the energy density, while $a_{\rm in}^2$ is due to the definition of $\mathcal{B}_i^{(2)} \propto B_i^{(2)}/a_{\rm in}$ that we gave above. The density parameter for $B^{(2)}$ then reads

$$\frac{\mathrm{d}\Omega_B^{(2)}(k,t)}{\mathrm{d}\log k} = \frac{3}{(2\pi)^3}\left(\frac{a_{\rm in}}{a}\right)^2\left[k^3\mathcal{P}_{\mathcal{B}}^{(2)}(k,t)\right] . \tag{2.63}$$

With $H = H_{\rm in}a_{\rm in}^2/a^2$ we find that even though $\mathcal{P}_{\mathcal{B}}^{(2)}(k,t)$ is growing like t^6 on super-horizon scales, the density parameter grows like $\Omega_{\rm GW}^{(1)}$. After horizon entry, this growth stops and $\Omega_B^{(2)}$ remains constant. Inserting the solutions (2.58) and (2.61) for $k^3\mathcal{P}_{\mathcal{B}}^{(2)}(k,t)$ gives

$$\frac{\mathrm{d}\Omega_B^{(2)}(k,t)}{\mathrm{d}\log k} = 6\frac{d\Omega_{\rm GW}^{(1)}(k,t)}{d\log k}\Omega_B^{(1)} \tag{2.64}$$

on super- and sub-horizon scales.

Hence, even though the second order magnetic field $\mathcal{B}_{(2)}$ is growing considerably, this reflects only the growth of the unphysical density parameter $\Omega_{\rm GW}^{(1)}$ on super-horizon scales. Once this is factored in, the magnetic field density parameter is not. The values for both, $\left[\mathrm{d}\Omega_{\rm GW}^{(1)\,\rm in}(k)/\mathrm{d}\log k\right](kt_{\rm in})^{-4} = \left[\mathrm{d}\Omega_{\rm GW}^{(1)}(k)/\mathrm{d}\log k\right]$ and $\Omega_B^{(1)}$ are at most of the order of 10^{-5} and smaller. For the gravity waves, we have seen that $\left[\mathrm{d}\Omega_{\rm GW}^{(1)\,\rm in}(k)/\mathrm{d}\log k\right](kt_{\rm in})^{-4}$ is just the square amplitude of the metric perturbations on super horizon scales, which has to be $k^3P_h \lesssim 10^{-10}$ in order not to overproduce CMB anisotropies on large scales (integrated Sachs–Wolfe effect). Similar arguments yield $\Omega_B^{(1)} < 10^{-5}$ on large scales (see, *e.g.* [60, 63]). Therefore, even though we agree with the calculation in Ref. [71], we do not agree with the interpretation. If the gravitational wave energy density is as small as required by the measurements of CMB anisotropies, $\Omega_B^{(2)}$ always remains smaller than $\Omega_B^{(1)}$. Furthermore, up to logarithmic corrections, $B^{(2)}$ inherits the spectrum of the first order gravity waves.

In the next section we show that this conclusion persists also if we allow for a stochastic magnetic field. Just the computation becomes more involved.

2.4.2 The second order magnetic field from gravity waves and a stochastic magnetic field

In the case in which the first order magnetic field is not spatially constant, all the products $\Sigma_{ij}^{(1)}(\mathbf{x},t)B_{(1)}^j(\mathbf{x},t)$ become convolutions in Fourier space

$$\int \mathrm{d}^3x e^{i\mathbf{k}\cdot\mathbf{x}}\Sigma_{ij}^{(1)}(\mathbf{x},t)B_{(1)}^j(\mathbf{x},t) = \frac{1}{(2\pi)^3}\mathcal{P}_i{}^n(\hat{\mathbf{k}})\int \mathrm{d}^3q\Sigma_{nj}^{(1)}(\mathbf{q},t)B_{(1)}^j(\mathbf{k}-\mathbf{q},t) ,$$

where the projector $\mathcal{P}_i{}^n \equiv \delta_i^n - \hat{k}_i\hat{k}^n$ projects onto the transverse modes. The result of this convolution is a magnetic field and therefore transverse. Hence this projector is not strictly necessary. But as we shall see, it simplifies the calculations.

Our equations are written in terms of the dimensionless expansion-normalized variables $\mathcal{B}_i^{(2)}(\mathbf{x},t)$ and $\Sigma_{ij}^{(2)}(\mathbf{x},t)$, and we want to express their power spectra in terms of the power spectra of the first order random variables $B_i^{(1)}(\mathbf{x},t)$ and $\Sigma_{ij}^{(1)}(\mathbf{x},t)$ for which we assume simple power laws,

$$\begin{aligned}
&B_i^{(1)}(\mathbf{k},t) = B_{i(1)}^{\rm in}(\mathbf{k})\frac{a_{\rm in}}{a}\ ,\\
&B^i_{(1)}(\mathbf{k},t) = B^{{\rm in}\,i}_{(1)}(\mathbf{k})\frac{a_{\rm in}^3}{a^3}\ ,\\
&a_{\rm in}^2\langle B_i^{(1)\,{\rm in}}(\mathbf{k})B_j^{*(1)\,{\rm in}}(\mathbf{q})\rangle = (2\pi)^3\mathcal{P}_{ij}(\hat{\mathbf{k}})\delta^3(\mathbf{k}-\mathbf{q})\mathcal{P}^{(1)}_{B\,{\rm in}}(k)\ ,\\
&\langle B_i^{(1)\,{\rm in}}(\mathbf{k})B^{*i}_{(1)\,{\rm in}}(\mathbf{q})\rangle = 2(2\pi)^3\delta^3(\mathbf{k}-\mathbf{q})\mathcal{P}^{(1)}_{B\,{\rm in}}(k)\ ,\\
&\mathcal{P}^{(1)}_{B\,{\rm in}}(k) = \begin{cases} [B^2_{(1)\,{\rm in}}\lambda^3](\lambda k)^M & \text{for } k<k_d,\\ 0 & \text{for } k>k_d,\end{cases}
\end{aligned} \tag{2.65}$$

where k_d is the damping scale which we assume to be always much smaller than the Hubble scale. The scale λ is arbitrary, e.g., the scale at which we want to calculate the magnetic field. With this normalization $B^{\rm in}_{(1)}$ is simply the amplitude of the magnetic field at scale λ at time $t_{\rm in}$. At any other moment, the magnetic field at scale λ is given by $B^{\rm in}_{(1)}a_{\rm in}^2/a^2(t)$.

Equivalently we have for the gravity wave power spectrum

$$\begin{aligned}
&\Sigma_{ij}^{(1)}(\mathbf{k},t) = \Sigma_{ij}^{(1)\,{\rm in}}(\mathbf{k})T(k,t)\ ,\\
&\langle\Sigma_{ij}^{(1)\,{\rm in}}(\mathbf{k})\Sigma_{ln}^{*(1)\,{\rm in}}(\mathbf{q})\rangle = (2\pi)^3\mathcal{M}_{ijln}(\hat{\mathbf{k}})\delta^3(\mathbf{k}-\mathbf{q})\mathcal{P}^{(1)}_{\Sigma\,{\rm in}}(k)\ ,\\
&\langle\Sigma_{ij}^{(1)\,{\rm in}}(\mathbf{k})\Sigma^{*ij}_{(1)\,{\rm in}}(\mathbf{q})\rangle = 4(2\pi)^3\delta^3(\mathbf{k}-\mathbf{q})\mathcal{P}^{(1)}_{\Sigma\,{\rm in}}(k)\ ,\\
&\mathcal{P}^{(1)}_{\Sigma\,{\rm in}}(k) = [\Sigma^2_{(1)\,{\rm in}}\lambda^3](\lambda k)^A\ .
\end{aligned} \tag{2.66}$$

Here the transfer function $T(k,t)$ keeps track of the deterministic time-dependence of the gravity waves. In the previous section we have derived the well known behavior of the gravity wave transfer function which oscillates on sub-horizon scales, $kt \gg 1$, and behaves like a power law on super-horizon scales. For the radiation dominated case,

$$T(k,t) \ \simeq\ \left(\frac{a}{a_{\rm in}}\right)^4\ , \qquad kt \ll 1\ . \tag{2.67}$$

Starting from Eq. (2.45), we can write the following evolution equation for the second order perturbation

$$\begin{aligned}
&\ddot{B}_i^{(2)}(\mathbf{x},t) + 2\mathcal{H}\dot{B}_i^{(2)}(\mathbf{x},t) - a^2D^2B_i^{(2)}(\mathbf{x},t) +\\
&\qquad\frac{1}{2}\mathcal{H}^2(1-3w)B_i^{(2)}(\mathbf{x},t) = 2a\dot{\sigma}_{ij}^{(1)}(\mathbf{x},t)B^j_{(1)}(\mathbf{x},t)\ .
\end{aligned} \tag{2.68}$$

Replacing $B_i^{(2)} = 3Ha_{\rm in}\mathcal{B}_i^{(2)}/\sqrt{\kappa}$ and $\sigma_{ij}^{(1)} = 3Ha_{\rm in}^2\Sigma_{ij}^{(1)}$, we obtain

$$\ddot{\mathcal{B}}_i^{(2)}(\mathbf{x},t) - (1+3w)\mathcal{H}\dot{\mathcal{B}}_i^{(2)}(\mathbf{x},t) - a^2D^2\mathcal{B}_i^{(2)}(\mathbf{x},t) + \left(\frac{1}{2}+3w+\frac{9}{2}w^2\right)\mathcal{H}^2\mathcal{B}_i^{(2)}(\mathbf{x},t) = 2\sqrt{\kappa}a_{\rm in}aB_{(1)}^j(\mathbf{x},t)\left[\dot{\Sigma}_{ij}^{(1)}(\mathbf{x},t) - \frac{3}{2}\mathcal{H}(1+w)\Sigma_{ij}^{(1)}(\mathbf{x},t)\right] . \tag{2.69}$$

This is the same differential equation as for the constant magnetic field. In Fourier space this equation becomes

$$\ddot{\mathcal{B}}_i^{(2)}(\mathbf{k},t) - (1+3w)\mathcal{H}\dot{\mathcal{B}}_i^{(2)}(\mathbf{k},t) + \mathcal{B}_i^{(2)}(\mathbf{k},t)\times \left[k^2 + \left(\frac{1}{2}+3w+\frac{9}{2}w^2\right)\mathcal{H}^2\right] = f_i(\mathbf{k},t)\,, \tag{2.70}$$

where the source $f_i(\mathbf{k},t)$ is now given by a convolution

$$f_i(\mathbf{k},t) \equiv \frac{2}{(2\pi)^3}\sqrt{\kappa}a_{\rm in}a\mathcal{P}_i{}^r(\hat{\mathbf{k}})\times \left[\int \mathrm{d}^3q\dot{\Sigma}_{rj}^{(1)}(\mathbf{q},t)B_{(1)}^j(\mathbf{k}-\mathbf{q},t) - \frac{3}{2}(1+w)\mathcal{H}\times\int \mathrm{d}^3q\Sigma_{rj}^{(1)}(\mathbf{q},t)B_{(1)}^j(\mathbf{k}-\mathbf{q},t)\right] . \tag{2.71}$$

In terms of the variable $z = kt$ we obtain again Eq. (2.51). As in the previous section we solve it with the Green function method. Therefore, the power spectrum of $\mathcal{B}_i^{(2)}$ is given by

$$\langle\mathcal{B}_i^{(2)}(\mathbf{k},t)\mathcal{B}_j^{*(2)}(\mathbf{p},t)\rangle = (2\pi)^3\delta^3(\mathbf{k}-\mathbf{p})\times(\delta_{ij}-\hat{k}_i\hat{k}_j)\mathcal{P}_{\mathcal{B}}^{(2)}(k,t)\ ,$$

with

$$\mathcal{P}_{\mathcal{B}}^{(2)}(k,t) \;=\; \int_{z_{\rm in}}^{z}\mathrm{d}z'\int_{z_{\rm in}}^{z}\mathrm{d}z''\mathcal{G}(z,z',\mathbf{k})\times\mathcal{G}^*(z,z'',\mathbf{p})\langle f_i(\mathbf{k},z')f_j^*(\mathbf{p},z'')\rangle\ ,$$

where $z = kt$. In the radiation dominated epoch ($w = 1/3$) the source term reads

$$\begin{aligned} f_i(\mathbf{k},t') &= \frac{2}{(2\pi)^3}\sqrt{\kappa}a_{\rm in}a(t')\mathcal{P}_i{}^r(\hat{\mathbf{k}})\times \\ &\quad\left[\int \mathrm{d}^3q\dot{\Sigma}_{rm}^{(1)}(\mathbf{q},t')B_{(1)}^m(\mathbf{k}-\mathbf{q},t') - 2\mathcal{H}(t')\int \mathrm{d}^3q\Sigma_{rm}^{(1)}(\mathbf{q},t')B_{(1)}^m(\mathbf{k}-\mathbf{q},t')\right] \\ &= \frac{2}{(2\pi)^3}\sqrt{\kappa}\frac{a_{\rm in}^2}{a^2(t')}\mathcal{P}_i{}^r(\hat{\mathbf{k}})\times \\ &\quad\left[\int \mathrm{d}^3q\Sigma_{rm}^{(1)\,\rm in}(\mathbf{q})\dot{T}(q,t')B_m^{(1)\,\rm in}(\mathbf{k}-\mathbf{q}) - \right. \\ &\qquad\left. 2\mathcal{H}(t')\int \mathrm{d}^3q\Sigma_{rm}^{(1)\,\rm in}(\mathbf{q})T(q,t')B_m^{(1)\,\rm in}(\mathbf{k}-\mathbf{q})\right]\ , \end{aligned} \tag{2.72}$$

and equivalently for $f_j^*(\mathbf{p},t'')$. To determine the power spectrum of f_i we assume that the

magnetic field $B_{(1)}$ and gravity waves $\sigma_{(1)}$ are uncorrelated, so that

$$\langle f_i(\mathbf{k},t')f_j^*(\mathbf{p},t'')\rangle \equiv (2\pi)^3\delta^3(\mathbf{k}-\mathbf{p})\mathcal{P}_{ij}(\hat{\mathbf{k}})h(t',t'',k) = \frac{16\kappa}{(2\pi)^6}\mathcal{H}(t')\mathcal{H}(t'')\left[\frac{a(t')a(t'')}{a_{\rm in}^2}\right]^2 \mathcal{P}_i{}^r(\hat{\mathbf{k}})\mathcal{P}_j{}^n(\hat{\mathbf{p}}) \times \int \mathrm{d}^3q \int \mathrm{d}^3s \langle \Sigma^{(1)\,\rm in}_{rm}(\mathbf{q})\Sigma^{*(1)\,\rm in}_{nl}(\mathbf{s})\rangle \times \langle B^{(1)\,\rm in}_m(\mathbf{k}-\mathbf{q})B^{*(1)\,\rm in}_l(\mathbf{p}-\mathbf{s})\rangle \ . \tag{2.73}$$

The function $h(t',t'',k)$ is given by [77]

$$h(t',t'',k) = \frac{8\kappa}{(2\pi)^3}\mathcal{H}(t')\mathcal{H}(t'')\left[\frac{a(t')a(t'')}{a_{\rm in}^2}\right]^2 I(k)\,,$$
$$I(k) \equiv \int \mathrm{d}^3q(1+\gamma^2)(1+\alpha^2)\mathcal{P}^{(1)}_{\Sigma\,\rm in}(q)\mathcal{P}^{(1)}_{B\,\rm in}(|\mathbf{k}-\mathbf{q}|)\ , \tag{2.74}$$

where $\alpha \equiv \hat{k}\cdot\widehat{(k-q)}$ and $\gamma \equiv \hat{k}\cdot\hat{q}$. We neglect the angular dependence of $(1+\gamma^2)$ and $(1+\alpha^2)$ and simply set

$$(1+\gamma^2)(1+\alpha^2) \simeq 1\ .$$

We then have to solve the following integral,

$$I(k) = 4\pi\Sigma^2_{(1)\,\rm in}B^2_{(1)\,\rm in}\lambda^{A+M+6}\int_0^{1/\max(t',t'')}\mathrm{d}q q^{A+2}\int_{-1}^{1}\mathrm{d}\mu(k^2+q^2-2\mu kq)^{M/2}\ .$$

Here we evaluate the integral only up to the scale q which enters the horizon at the later of the two times. All scales $q < 1/\max(t',t'')$ are super-horizon from $t_{\rm in}$ to $\max(t',t'')$. A soon as q enters the horizon, the gravity wave transfer function begins to oscillate and the contribution to the integral becomes negligible. The integral over μ can be evaluated; for $M \neq -2$ it yields

$$I(k) \ = \ \frac{8\pi}{2+M}\Sigma^2_{(1)\,\rm in}B^2_{(1)\,\rm in}\lambda^{A+M+6}\int_0^{1/\max(t',t'')}\frac{\mathrm{d}q\ q^{A+2}}{kq}\left(|k+q|^{M+2}-|k-q|^{M+2}\right)\ .$$

We shall not treat the case $M=-2$, where the angular integral introduces a logarithmic dependence on q, separately. This corresponds to approximating $\log(k/q)\sim 1$. We approximate these integrals by their dominant contribution.

- If the spectra are sufficiently red such that $A+M+3<0$, the result is dominated by the region $k<1/\max(t',t'')$ and we obtain

$$I(k) \simeq 16\pi\Sigma^2_{(1)\,\rm in}B^2_{(1)\,\rm in}\lambda^3(\lambda k)^{A+M+3}\left(\frac{1}{A+3}-\frac{1}{A+M+3}\right)\ .$$

- On the other hand, if the spectra are blue such that $A+M+3>0$, the integral is dominated by its value at the upper boundary,

$$I \simeq 16\pi\Sigma^2_{(1)\,\rm in}B^2_{(1)\,\rm in}\lambda^3\frac{1}{A+M+3}\left[\frac{\lambda}{\max(t',t'')}\right]^{A+M+3}\ .$$

If, as in the previous sub-section, we can write the function $h(t', t'', k)$ in the form

$$h(t', t'', k) \simeq F(k) g(t') g(t'') \,, \tag{2.75}$$

we can proceed as we did before to obtain the results (2.58) and (2.61). A source where the time dependence of the unequal time correlator factorizes is called "totally coherent". In the totally coherent case, the power spectrum is simply the square of the solution which has as its source the square root of the power spectrum of the source [31]. In most cases, the unequal time correlator is more complicated than this, but the totally coherent approximation is often quite reasonable [31]. If the source is totally coherent, the square root of the power spectrum $\mathcal{P}_{\mathcal{B}}^{(2)}$ simply satisfies the same evolution equation as $\mathcal{B}_{(2)}$ with source term $\sqrt{F} g$.

- If $A + M + 3 < 0$, we can write

$$F(k) = \frac{128\pi\kappa}{(2\pi)^3} (k\lambda)^{A+M+3} \lambda^3 \times \left(\frac{1}{A+3} - \frac{1}{A+M+3} \right) \,,$$
$$g(t') = \frac{B_{(1)\,\mathrm{in}} \Sigma_{(1)\,\mathrm{in}}}{a_{\mathrm{in}}^2} \mathcal{H}(t') a^2(t') \,.$$

- For $A + M + 3 > 0$, we set

$$F(k) = \frac{128\pi\kappa}{(2\pi)^3} \frac{1}{A+M+3} \lambda^{A+M+6} \,,$$
$$g(t') = \frac{B_{(1)\,\mathrm{in}} \Sigma_{(1)\,\mathrm{in}}}{a_{\mathrm{in}}^2} \mathcal{H}(t') a^2(t') \left(\frac{1}{t'} \right)^{(A+M+3)/2} \,.$$

  This corresponds to replacing

$$\left[\frac{1}{\max(t', t'')} \right]^{(A+M+3)} \quad \text{by} \quad \left(\frac{1}{t' t''} \right)^{(A+M+3)/2}$$

  which is of course not entirely correct and we expect this to over estimate the true result somewhat. However, within the accuracy of our approximations this is sufficient. To obtain a more accurate result we would have to expand the function $h(k, t', t'')$ in eigenfunctions with respect to convolution in time, as it is done in Ref. [31].

Within this totally coherent approximation we can now solve the problem like in the previous sub-section. In the case $A + M + 3 < 0$ we find on super-horizon scales, where the source is active

$$k^3 \mathcal{P}_{\mathcal{B}}^{(2)}(k, t) \simeq \frac{32\pi\kappa}{(2\pi)^3} \frac{\left[k^3 \mathcal{P}_{B\,\mathrm{in}}^{(1)}(k) \right]}{H_{\mathrm{in}}^2} \left[k^3 \mathcal{P}_{\Sigma\,\mathrm{in}}^{(1)}(k) \right] \times \left(\frac{a}{a_{\mathrm{in}}} \right)^6 \,, \quad kt \ll 1 \,. \tag{2.76}$$

On sub-horizon scales, performing the matching at horizon crossing, we obtain

$$k^3 \mathcal{P}_{\mathcal{B}}^{(2)}(k, t) \simeq \frac{16\pi\kappa}{(2\pi)^3} \frac{\left[k^3 \mathcal{P}_{B\,\mathrm{in}}^{(1)}(k) \right]}{H_{\mathrm{in}}^2} \left[k^3 \mathcal{P}_{\Sigma\,\mathrm{in}}^{(1)}(k) \right] \times \left(\frac{a}{a_{\mathrm{in}}} \right)^2 \frac{1}{(k t_{\mathrm{in}})^4} \,, \quad kt \gg 1 \,. \tag{2.77}$$

If $A+M+3>0$, we analyze in in more detail only the case $A\simeq -3$ and $M=2$. The spectral index $A=-3$ correspond to a scale invariant gravity wave power spectrum as it is obtained in slow-roll inflation [132]. The index $M=2$ characterizes a causal magnetic field $B_{(1)}$. In this case, we have to solve the differential equation,

$$P''-\frac{2}{z}P'+\left(1+\frac{2}{z^2}\right)P=\frac{\alpha}{k^2}\ , \tag{2.78}$$
$$\alpha\equiv (a_{\rm in}H_{\rm in})^2 B^{(1)}_{\rm in}\Sigma^{(1)}_{\rm in}\sqrt{\frac{64\pi}{(2\pi)^3}\kappa\lambda^5}\ ,$$

where the source is constant in time. Detailed comments about the initial conditions chosen for the solution of the above equation can be found in Appendix 2.6.1. Finally, we can write the solution for $P(z)$ in the case where $z=kt\ll 1$ as

$$P(z)\simeq\frac{\alpha}{k^2}z^2\log\left(\frac{z}{z_{\rm in}}\right)\ ,\qquad z\ll 1\ .$$

The power spectrum of $\mathcal{B}^{(2)}$ on super-horizon scales is therefore given by

$$\begin{aligned}k^3\mathcal{P}^{(2)}_{\mathcal{B}}(k,t) &\simeq \frac{16\pi\kappa}{(2\pi)^3}\frac{\left[k^3\mathcal{P}^{(1)}_{B\,\rm in}(k)\right]}{H^2_{\rm in}}\left[k^3\mathcal{P}^{(1)}_{\Sigma\,\rm in}(k)\right]\times\\ &\left(\frac{a}{a_{\rm in}}\right)^4\frac{1}{(kt_{\rm in})^2}\log^2\left(\frac{a}{a_{\rm in}}\right)\ ,\qquad kt\ll 1\ .\end{aligned} \tag{2.79}$$

On sub-horizon scales, $z=kt\gg 1$, we match the super-horizon solution at horizon crossing with the homogeneous solution of Eq. (2.78), as we did above, obtaining

$$\begin{aligned}k^3\mathcal{P}^{(2)}_{\mathcal{B}}(k,t) &\simeq \frac{32\pi\kappa}{(2\pi)^3}\frac{\left[k^3\mathcal{P}^{(1)}_{B\,\rm in}(k)\right]}{H^2_{\rm in}}\left[k^3\mathcal{P}^{(1)}_{\Sigma\,\rm in}(k)\right]\times\\ &\left(\frac{a}{a_{\rm in}}\right)^2\frac{1}{(kt_{\rm in})^4}\log^2\left(kt_{\rm in}\right)\ ,\qquad kt\gg 1\ .\end{aligned} \tag{2.80}$$

2.4.2.1 Density parameter

Using Eq. (2.62), we find the following expressions for the energy density of the stochastic second order magnetic field. If $A+M+3<0$, we have on super-horizon scales

$$\frac{{\rm d}\rho^{(2)}_B(k,t)}{{\rm d}\log k}\equiv\frac{1}{(2\pi)^3}k^3\mathcal{P}^{(2)}_B(k,\eta)\left(\frac{a_{\rm in}}{a}\right)^2\simeq\frac{288\pi}{(2\pi)^6}\left[k^3\mathcal{P}^{(1)}_{B\,\rm in}(k)\right]\left[k^3\mathcal{P}^{(1)}_{\Sigma\,\rm in}(k)\right]\ . \tag{2.81}$$

This results in a density parameter for $B_{(2)}$ given by

$$\frac{{\rm d}\Omega^{(2)}_B(k,t)}{{\rm d}\log k}\equiv\frac{1}{\rho_c}\frac{d\rho^{(2)}_B(k,\eta)}{d\log k}\simeq 6\frac{{\rm d}\Omega^{(1)}_{B\,\rm in}(k)}{{\rm d}\log k}\frac{{\rm d}\Omega^{(1)}_{GW}(k,t)}{{\rm d}\log k}\ ,\qquad kt\ll 1\ . \tag{2.82}$$

Inside the horizon we obtain for the second order magnetic field density parameter

$$\frac{\mathrm{d}\Omega_B^{(2)}(k,t)}{\mathrm{d}\log k} \simeq 6\frac{\mathrm{d}\Omega_{B\,\mathrm{in}}^{(1)}(k)}{\mathrm{d}\log k}\frac{d\Omega_{GW}^{(1)}(k)}{d\log k}\ , \qquad kt \gg 1\ . \tag{2.83}$$

The gravity wave density parameter, $\left[\mathrm{d}\Omega_{GW}^{(1)}(k,t)/\mathrm{d}\log k\right]$ is given by Eqs. (2.37) and (2.40) respectively. This corresponds, as in the previous section for a constant magnetic field, to the naively expected result, $\Omega_B^{(2)} \sim \Omega_{\mathrm{GW}}^{(1)}\Omega_B^{(1)}$.

For blue spectra, $A + M + 3 > 0$, the second order magnetic field density parameter reads in the interesting case $A \simeq -3$ and $M = 2$ on super-horizon scales

$$\begin{aligned}\frac{\mathrm{d}\Omega_B^{(2)}(k,t)}{\mathrm{d}\log k} &= \frac{12}{(kt)^2}\frac{\mathrm{d}\Omega_{B\,\mathrm{in}}^{(1)}(k)}{\mathrm{d}\log k}\frac{\mathrm{d}\Omega_{\mathrm{GW}}^{(1)}(k,t)}{\mathrm{d}\log k}\log^2\left(\frac{a}{a_{\mathrm{in}}}\right)\\ &= 12\frac{\mathrm{d}\Omega_{\mathrm{GW}}^{(1)}(k,t)}{\mathrm{d}\log k}\left.\frac{\mathrm{d}\Omega_{B\,\mathrm{in}}^{(1)}(k)}{\mathrm{d}\log k}\right|_{k=1/t}(kt)^3\log^2\left(\frac{a}{a_{\mathrm{in}}}\right)\ , \quad kt \ll 1\ .\end{aligned} \tag{2.84}$$

Note that the value of $\left[\mathrm{d}\Omega_B^{(2)}(k,t)/\mathrm{d}\log k\right]$ on super-Hubble scales is affected by $\left[\mathrm{d}\Omega_B^{(1)}(k_t)/\mathrm{d}\log k_t\right]$ at horizon crossing, $k_t = 1/t$ which may well be larger than $\left[\mathrm{d}\Omega_B^{(1)}(k)/\mathrm{d}\log k\right]$ but of course has also to be much smaller than 1.

This expression grows only logarithmically faster than $\left[\mathrm{d}\Omega_{GW}^{(1)}(k,t)/\mathrm{d}\log k\right]$. The growth stops at horizon entry where the second order magnetic field density parameter has acquired a factor $\log^2(kt_{\mathrm{in}})$. Inside the horizon we obtain a density parameter of

$$\frac{\mathrm{d}\Omega_B^{(2)}(k,t)}{\mathrm{d}\log k} = 12\frac{\mathrm{d}\Omega_{B\,\mathrm{in}}^{(1)}(k)}{\mathrm{d}\log k}\frac{\mathrm{d}\Omega_{\mathrm{GW}}^{(1)}(k)}{\mathrm{d}\log k}\log^2(kt_{\mathrm{in}})\ , \qquad kt \gg 1\ . \tag{2.85}$$

Up to the logarithmic correction, this corresponds to the result for red spectra above.

2.4.2.2 Reheating and matter dominated epochs

In order to make contact with Refs. [124, 71], we now repeat the calculation in a matter dominated background ($w = 0$). We want to point out that the results we obtain are mathematically the same as the ones found in [71]. The only difference lies in the interpretation. In the previous paragraph we have seen that, even though

$$\frac{\mathrm{d}\Omega_{GW}^{(1)}(k)}{\mathrm{d}\log k} \sim \left(\frac{1}{kt_{\mathrm{in}}}\right)^4\left[k^3\mathcal{P}_{\Sigma\,\mathrm{in}}^{(1)}(k)\right]\ ,$$

and even though $(kt_{\mathrm{in}})^{-4}$ can become very large, this product is never larger than about 10^{-10}. We believe that this point has been missed in Ref. [71].
If $w = 0$, the scale factor grows like $a \propto t^2$ so that $\mathcal{H} = 2/t$. As mentioned before, for the super horizon amplification the question whether the conductivity is high or low is not relevant.

From the first order perturbations, we obtain the same behaviour for the magnetic field

$B^{(1)}$ in terms of the scale factor, therefore the density parameter is then given by

$$\frac{\mathrm{d}\Omega_B^{(1)}(k,t)}{\mathrm{d}\log k} = \frac{8\pi G}{3(2\pi)^3}\frac{\left[k^3\mathcal{P}_{B\,\mathrm{in}}^{(1)}(k)\right]}{H_{\mathrm{in}}^2}\frac{a_{\mathrm{in}}}{a}\ . \tag{2.86}$$

The first order gravity waves on super-horizon scales now behaves as

$$\Sigma_{ij}^{(1)}(\mathbf{k},t) = \Sigma_{ij\,\mathrm{in}}^{(1)}(\mathbf{k})\left(\frac{a}{a_{\mathrm{in}}}\right)^3\ . \tag{2.87}$$

Once the gravitational waves enter the horizon, they start oscillating and the energy density decays as radiation. Therefore in this case the relative density parameters for the first order gravity waves is

$$\frac{\mathrm{d}\Omega_{\mathrm{GW}}^{(1)}(k,t)}{\mathrm{d}\log k} = \frac{48\pi}{(2\pi)^3}\left[k^3\mathcal{P}_{\Sigma\,\mathrm{in}}^{(1)}(k)\right]\left(\frac{a}{a_{\mathrm{in}}}\right)^2\ , \qquad kt \ll 1\ . \tag{2.88}$$

On sub-horizon scales we obtain

$$\frac{\mathrm{d}\Omega_{\mathrm{GW}}^{(1)}(k,t)}{\mathrm{d}\log k} = \frac{24\pi}{(2\pi)^3}\left[k^3\mathcal{P}_{\Sigma\,\mathrm{in}}^{(1)}(k)\right]\left(\frac{a_{\mathrm{in}}}{a}\right)\frac{1}{(kt_{\mathrm{in}})^6}\ , \qquad kt \gg 1\ . \tag{2.89}$$

Computing finally the induced second order magnetic field density parameter, we obtain the naively expected result on super-horizon scales

$$\frac{\mathrm{d}\Omega_B^{(2)}(k,t)}{\mathrm{d}\log k} \simeq \begin{cases} \frac{\mathrm{d}\Omega_B^{(1)}(k,t)}{\mathrm{d}\log k}\frac{\mathrm{d}\Omega_{\mathrm{GW}}^{(1)}(k,t)}{\mathrm{d}\log k}\ , \\ \qquad \text{for } A+M+3<0 \\ (kt)^3\left[\frac{\mathrm{d}\Omega_B^{(1)}(k,t)}{\mathrm{d}\log k}\right]_{k=1/t}\times \\ \qquad \frac{\mathrm{d}\Omega_{\mathrm{GW}}^{(1)}(k,t)}{\mathrm{d}\log k}\log^2\frac{a}{a_{\mathrm{in}}}\ , \\ \qquad \text{for } A+M+3>0 \end{cases} \qquad kt \ll 1\ .$$

On sub-horizon scales the density parameter turns out to be given by

$$\begin{aligned} \frac{\mathrm{d}\Omega_B^{(2)}(k,t)}{\mathrm{d}\log k} &\simeq \frac{\mathrm{d}\Omega_B^{(1)}(k,t)}{\mathrm{d}\log k}\frac{\mathrm{d}\Omega_{\mathrm{GW}}^{(1)}(k,t_k)}{\mathrm{d}\log k} \\ &\simeq \frac{\mathrm{d}\Omega_B^{(1)}(k,t)}{\mathrm{d}\log k}\left(\frac{H_{\mathrm{inf}}}{M_{\mathrm{P}}}\right)^2,\ kt \gg 1\,, \end{aligned} \tag{2.90}$$

for both cases $A+M+3<0$ and $A\simeq -3$, $M=2$, up to logarithmic corrections. Here t_k stands for the horizon crossing time, $t_k = 1/k$, and in the last $\simeq$ sign we have used that $\left[\mathrm{d}\Omega_{\mathrm{GW}}^{(1)}(k,t_k)/\mathrm{d}\log k\right] \simeq (H_{\mathrm{inf}}/M_{\mathrm{P}})^2$ is the gravity waves density parameter at horizon crossing, which is smaller than 10^{-10}. This means that the second order magnetic field does not grow larger the the first order one. Inside the horizon they decrease both like $\propto a^{-1}$. $\Omega_B^{(2)}$ stays always much smaller than $\Omega_B^{(1)}$, as we have found in the case of a radiation dominated background.

2.4.3 Second order gravity waves

Starting from Eq. (2.46), we can write the evolution equation for $\sigma_{ij}^{(2)}$ in real space $(\mathbf{x}, t)$ as follows:

$$\ddot{\sigma}_{ij}^{(2)} - a^2 D^2 \sigma_{ij}^{(2)} - \frac{3}{2}\mathcal{H}^2(1+w)\sigma_{ij}^{(2)} = \\ -2\kappa a\mathcal{H}\Pi_{ij}^{(1)} + \left[a\mathcal{H}\sigma_{\langle i(1)}{}^{n}\sigma_{j\rangle n}^{(1)} + 2a\sigma_{\langle i(1)}{}^{n}\dot{\sigma}_{j\rangle n}^{(1)} - a\dot{\sigma}_{\langle i(1)}^{n}\sigma_{j\rangle n}^{(1)}\right]\frac{1}{a^2} \ . \quad (2.91)$$

The factor $1/a^2$ in the source part of the above equation comes from the fact that in Eq. (2.46) we had to add factors $a^2(t)$ in order to lower or rise indices. On the other hand, now we deal with purely spatial tensors such that $\sigma_{ij} = \sigma^{ij}$ and also $\dot{\sigma}_{ij} = \dot{\sigma}^{ij}$.

Introducing again the dimensionless expansion-normalized variable $\Sigma_{ij}^{(2)}$, the previous equation can be written as

$$\ddot{\Sigma}_{ij}^{(2)} - 3(1+w)\mathcal{H}\dot{\Sigma}_{ij}^{(2)} + 3\mathcal{H}^2\left(\frac{3}{2}w^2 + 2w + \frac{1}{2}\right)\Sigma_{ij}^{(2)} - a^2 D^2\Sigma_{ij}^{(2)} = \\ -\frac{2}{3}\kappa\frac{a^2}{a_{\rm in}^2}\Pi_{ij}^{(1)} + \left[-\frac{3}{2}(1+3w)\mathcal{H}^2\Sigma_{\langle i(1)}{}^{n}\Sigma_{j\rangle n}^{(1)} \right. \\ \left. +6\mathcal{H}\Sigma_{\langle i(1)}{}^{n}\dot{\Sigma}_{j\rangle n}^{(1)} - 3\mathcal{H}\dot{\Sigma}_{\langle i(1)}^{n}\Sigma_{j\rangle n}^{(1)}\right]\left(\frac{a_{\rm in}}{a}\right)^2 \ . \quad (2.92)$$

As for $B^{(2)}$, the source is given by the first order perturbations magnetic field $[\Pi_{ij}^{(1)}]$ and the first order gravity waves and does *e.g.* not couple to the second order magnetic field. Since we assume the first order magnetic field and gravity wave fluctuations to be independent, we can add the power spectra for the solutions of the individual source terms,

$$k^3\mathcal{P}_\Sigma^{(2)}(k,t) = k^3\mathcal{P}_\Sigma^{(2)\,\Pi}(k,t) + k^3\mathcal{P}_\Sigma^{(2)\,\rm GW}(k,t) \ .$$

where $\mathcal{P}_\Sigma^{(2)\,\Pi}(k,t)$ is the power spectrum of the solution of Eq. (2.92) with source term $\Pi^{(1)}$ only and $\mathcal{P}_\Sigma^{(2)\,\rm GW}(k,t)$ comes from the source terms containing $\Sigma^{(1)}$.

2.4.3.1 Magnetic field part of the source $\left[k^3\mathcal{P}_\Sigma^{(2)\,\Pi}(k,t)\right]$

Considering first the magnetic field part of the source, we have to solve the following differential equation in the momentum space $(\mathbf{k}, t)$

$$\ddot{\Sigma}_{ij}^{(2)} - 3(1+w)\mathcal{H}\dot{\Sigma}_{ij}^{(2)} + \left[k^2 + 3\mathcal{H}^2\left(\frac{3}{2}w^2 + 2w + \frac{1}{2}\right)\right]\Sigma_{ij}^{(2)} = f_{ij} \ , \quad (2.93)$$

where the source is given by

$$f_{ij}(\mathbf{k}, t) \equiv -\frac{2}{3}\kappa\frac{a^2}{a_{\rm in}^2}\Pi_{ij}^{(1)}(\mathbf{k}, t) \ . \quad (2.94)$$

As before, we have to compute the unequal time correlator:

$$\langle\Pi_{ij}^{(1)}(\mathbf{k}, t')\Pi_{rn}^{*(1)}(\mathbf{p}, t'')\rangle = (2\pi)^3\delta^3(\mathbf{k}-\mathbf{p})\mathcal{M}_{ijrn}(\hat{\mathbf{k}})h(k, t', t'') \ , \quad (2.95)$$

where the anisotropic stresses are given by

$$\Pi_{ij}^{(1)}(\mathbf{k},t') = -\frac{1}{16\pi(2\pi)^3}\mathcal{M}_{ij}{}^{ls}(\hat{\mathbf{k}})\int \mathrm{d}^3q B_l^{(1)}(\mathbf{q},t')B_s^{(1)}(\mathbf{k}-\mathbf{q},t')\,.$$

$(1/2)\mathcal{M}_{ij}{}^{ls}(\hat{\mathbf{k}})$ is the projector on the tensor modes. We have neglected a trace contribution to the magnetic field stress tensor since, once we project with $\mathcal{M}_{ij}{}^{ls}$, the trace vanishes.

After some computation [77], we find for the function $h(k,t',t'')$ the following expression:

$$h(k,t',t'') = \frac{1}{(8\pi)^2}\frac{1}{4(2\pi)^3}I(k)\left[\frac{a_{\rm in}^2}{a(t')a(t'')}\right]^2, \tag{2.96}$$

$$I(k) = \int \mathrm{d}^3q(1+\gamma^2)(1+\alpha^2)\mathcal{P}_{B\,\rm in}^{(1)}(q)\times\mathcal{P}_{B\,\rm in}^{(1)}(|\mathbf{k}-\mathbf{q}|)\,. \tag{2.97}$$

where $\alpha \equiv \hat{k}\cdot\widehat{(k-q)}$ and $\gamma \equiv \hat{k}\cdot\hat{q}$. As before, we approximate $(1+\gamma^2)(1+\alpha^2)\simeq 1$. With this, we obtain the following expression for the expectation value of the source term:

$$\langle f_{ij}(\mathbf{k},t')f_{rn}^*(\mathbf{p},t'')\rangle = \frac{4}{9}\kappa^2\frac{a^2(t')a^2(t'')}{a_{\rm in}^4}\langle\Pi_{ij}^{(1)}(\mathbf{k},t')\Pi_{rn}^{*(1)}(\mathbf{p},t'')\rangle\,. \tag{2.98}$$

The expectation value of the stochastic variable $\Sigma_{ij}^{(2)}$ can be written as

$$\langle\Sigma_{ij}^{(2)}(\mathbf{k},t)\Sigma_{rn}^{*(2)}(\mathbf{p},t)\rangle = (2\pi)^3\delta^3(\mathbf{k}-\mathbf{p})\mathcal{M}_{ijrn}(\hat{\mathbf{k}})\mathcal{P}_\Sigma^{(2)}(k,t)\,. \tag{2.99}$$

If $\langle\Pi_{ij}^{(1)}(\mathbf{k},t')\Pi_{rn}^{*(1)}(\mathbf{p},t'')\rangle$ can be written as a product of a function of (k,t) and (k,t''), this source is totally coherent and we can write the function $h(k,t',t'')$ of Eq. (2.96) in the form

$$\frac{4}{9}\kappa^2\frac{a^2(t')a^2(t'')}{a_{\rm in}^4}h(k,t',t'') = F(k)g(t')g(t'')\,,$$

where we introduced the pre-factor of h since we finally need an expression for the unequal time correlator of the source, as in Eq. (2.98), while the function h alone is only part of the correlator of the anisotropic stress, Eq. (2.95).
The square root of the power spectrum is then a solution of the differential equation (2.93) with source term $\sqrt{F(k)}g(t)$. Written as differential equation for the variable $z=kt$ and setting $w=1/3$, this becomes

$$\left[\sqrt{\mathcal{P}_\Sigma^{(2)\,\Pi}(k,z)}\right]'' - \frac{4}{z}\left[\sqrt{\mathcal{P}_\Sigma^{(2)\,\Pi}(k,z)}\right]' + \left(1+\frac{4}{z^2}\right)\left[\sqrt{\mathcal{P}_\Sigma^{(2)\,\Pi}(k,z)}\right] = \sqrt{F(k)}\frac{g(z/k)}{k^2}\,. \tag{2.100}$$

As for the second order magnetic field, we distinguish between two cases. First we consider $2M+3>0$. The integral I is then dominated by the upper cutoff. The magnetic field is not oscillating and we therefore take damping scale k_d as the upper cutoff. We neglect the slow time dependence of this scale. Using Eq. (2.65) for the magnetic field

power spectrum, I can be approximated by

$$I \simeq \frac{8\pi}{2M+3}\left[B_{\rm in}^{(1)4}\lambda^3\right](\lambda k_d)^{2M+3} .$$

Hence the functions $F(k)$, $g(t')$ are given by

$$F(k) = \frac{\kappa^2}{36(2\pi)^4}\frac{1}{2M+3}(\lambda k_d)^{2M+3}\left[B_{\rm in}^{(1)4}\lambda^3\right] ,$$
$$g(t') = 1 .$$

In the case $2M+3<0$, we obtain

$$I \simeq 8\pi\left[B_{\rm in}^{(1)4}\lambda^3\right](\lambda k)^{2M+3}\left(\frac{1}{M+3}-\frac{1}{2M+3}\right) .$$

This case is totally coherent and we can set

$$F(k) = \frac{\kappa^2}{36(2\pi)^4}\left[B_{\rm in}^{(1)4}\lambda^3\right]\left(\frac{1}{M+3}-\frac{1}{2M+3}\right)(\lambda k)^{2M+3} ,$$
$$g(t') = 1 .$$

We now solve Eq. (2.100) for the two different source terms.

- In the case $2M+3>0$, we can write Eq. (2.100) in the form

$$P'' - \frac{4}{z}P' + \left(1+\frac{4}{z^2}\right)P = \frac{\alpha}{k^2} ,$$
$$z \equiv kt , \qquad |P| \equiv \sqrt{\mathcal{P}_\Sigma^{(2)\,\Pi}(k,t)} , \qquad \alpha \equiv \sqrt{F(k)} .$$

  Solving the above equation on super-horizon scales and following the considerations for the choice of initial conditions explained in Appendix 2.6.1, we find

$$P(z) \simeq -\frac{\alpha}{2k^2}z^2 , \qquad z \ll 1 ,$$

  this gives the second order power spectrum

$$k^3\mathcal{P}_\Sigma^{(2)\,\Pi}(k,t) \simeq \frac{\kappa^2}{36(2\pi)^4(2M+3)}\left[\frac{k^3\mathcal{P}_{B\,\rm in}^{(1)}(k)}{H_{\rm in}^2}\right]^2\left(\frac{a}{a_{\rm in}}\right)^4\left(\frac{k_d}{k}\right)^{2M+3} , \qquad kt \ll 1 . \tag{2.101}$$

  This is equivalent to a density parameter for $\Sigma^{(2)}$ given by

$$\frac{{\rm d}\Omega_{\rm GW}^{(2)\,\Pi}(k,t)}{{\rm d}\log k} \simeq \left[\frac{{\rm d}\Omega_{B\,\rm in}^{(1)}(k)}{{\rm d}\log k}\right]^2\left(\frac{k_d}{k}\right)^{2M+3} \simeq \left[\frac{{\rm d}\Omega_{B\,\rm in}^{(1)}(k_d)}{{\rm d}\log k}\right]^2\left(\frac{k}{k_d}\right)^3 , \qquad kt \ll 1 . \tag{2.102}$$

  Inside the horizon, the Green function oscillates and we can neglect the contribution

from the source. The solution for the power spectrum is then given by

$$k^3\mathcal{P}_{\Sigma}^{(2)\,\Pi}(k,t) \simeq \frac{\kappa^2}{36(2\pi)^4(2M+3)} \left[\frac{k^3\mathcal{P}_{B\,\mathrm{in}}^{(1)}(k)}{H_{\mathrm{in}}^2}\right]^2 \left(\frac{a}{a_{\mathrm{in}}}\right)^4 \left(\frac{k_d}{k}\right)^{2M+3}, \quad kt \gg 1\,. \tag{2.103}$$

Therefore, the second order density parameter is given by the same expression,

$$\frac{\mathrm{d}\Omega_{\mathrm{GW}}^{(2)\,\Pi}(k,t)}{\mathrm{d}\log k} \simeq \left[\frac{\mathrm{d}\Omega_{B\,\mathrm{in}}^{(1)}(k_d)}{\mathrm{d}\log k}\right]^2 \left(\frac{k}{k_d}\right)^3, \qquad kt \gg 1\,. \tag{2.104}$$

Up to logarithmic factors this result agrees with the findings of Ref. [77].

- In the case $2M+3<0$ we have again to solve the equation

$$P'' - \frac{4}{z}P' + \left(1+\frac{4}{z^2}\right)P = \frac{\alpha}{k^2}\,, \tag{2.105}$$

Hence

$$P(z) \simeq -\frac{\alpha}{2k^2}z^2\,, \quad z \ll 1\,.$$

But now

$$\alpha \equiv \frac{\kappa}{6(2\pi)^2}\sqrt{\frac{1}{2}\left(\frac{1}{M+3}-\frac{1}{2M+3}\right)k^{2M+3}} \times \left[B_{\mathrm{in}}^{(1)2}\lambda^3\right]\lambda^M\,,$$

so that

$$k^3\mathcal{P}_{\Sigma}^{(2)\,\Pi}(k,t) \simeq \frac{\kappa^2}{144(2\pi)^4}\left[\frac{k^3\mathcal{P}_{B\,\mathrm{in}}^{(1)}(k)}{H_{\mathrm{in}}^2}\right]^2\left(\frac{a}{a_{\mathrm{in}}}\right)^4, \qquad kt \ll 1\,. \tag{2.106}$$

As in the first case, the density parameter is the same for $kt<1$ and $kt>1$,

$$\frac{d\Omega_{\mathrm{GW}}^{(2)\,\Pi}(k,t)}{d\log k} \simeq \left[\frac{d\Omega_{B\,\mathrm{in}}^{(1)}(k)}{d\log k}\right]^2. \tag{2.107}$$

2.4.3.2 Gravity waves part of the source $\left[k^3\mathcal{P}_{\Sigma}^{(2)\,\mathrm{GW}}(k,t)\right]$

Let us finally consider the part of the source given by first order gravity waves. In this case, we can write the source f_{ij} as:

$$f_{ij}(\mathbf{x},t) = \Big[-\frac{3}{2}(1+3w)\mathcal{H}^2\Sigma_{\langle i}^{(1)\,n}\Sigma_{j\rangle n}^{(1)} + 6\mathcal{H}\Sigma_{\langle i}^{(1)\,n}\dot{\Sigma}_{j\rangle n}^{(1)} - 3\mathcal{H}\dot{\Sigma}_{\langle i}^{(1)n}\Sigma_{j\rangle n}^{(1)}\Big]\left(\frac{a_{\mathrm{in}}}{a}\right)^2\,. \tag{2.108}$$

As before, we ignore the traces that are present in the above products, once we evaluate them in the momentum space, since we project them out with $(1/2)\mathcal{M}_{ij}{}^{lm}$ afterwards. Remembering that $\Sigma_{ij}=\Sigma^{ij}$, we have on super-horizon scales, where the transfer function

is given by Eq. (2.67):

$$\begin{aligned}\left[\Sigma_{\langle i(1)}{}^{n}\Sigma^{(1)}_{j\rangle n}\right](\mathbf{k},t) &= \frac{1}{2(2\pi)^3}\left(\frac{a}{a_{\rm in}}\right)^8 \mathcal{M}_{ij}{}^{lm}(\hat{\mathbf{k}})\int \mathrm{d}^3q\,\Sigma^{(1)\,\rm in}_{ln}(\mathbf{q})\Sigma^{(1)\,\rm in}_{nm}(\mathbf{k}-\mathbf{q})\ ,\\ \left[\Sigma_{\langle i(1)}{}^{n}\dot{\Sigma}^{(1)}_{j\rangle n}\right](\mathbf{k},t) &= \left[\dot{\Sigma}^{n}_{\langle i(1)}\Sigma^{(1)}_{j\rangle n}\right](\mathbf{k},t) = \\ &\quad \frac{2\mathcal{H}}{(2\pi)^3}\left(\frac{a}{a_{\rm in}}\right)^8 \mathcal{M}_{ij}{}^{lm}(\hat{\mathbf{k}})\times\int \mathrm{d}^3q\,\Sigma^{(1)\,\rm in}_{ln}(\mathbf{q})\Sigma^{(1)\,\rm in}_{nm}(\mathbf{k}-\mathbf{q})\ .\end{aligned}$$

These equations are strictly true only on super-horizon scales where $\Sigma\propto 1/a^4$. However, since inside the horizon Σ oscillates and the contribution from the source is negligible, we can use this approximation. Setting $w=1/3$ we can finally write the source in the form

$$f_{ij}(\mathbf{k},t)=\frac{9}{2(2\pi)^3}\mathcal{H}^2\left(\frac{a}{a_{\rm in}}\right)^6\times\mathcal{M}_{ij}{}^{lm}(\hat{\mathbf{k}})\int \mathrm{d}^3p\,\Sigma^{(1)\,\rm in}_{ln}(\mathbf{p})\Sigma^{(1)\,\rm in}_{nm}(\mathbf{k}-\mathbf{p})\ , \qquad (2.109)$$

and the two-point correlation function of the source part reads:

$$\begin{aligned}&\langle f_{ij}(\mathbf{k},t')f^*_{rc}(\mathbf{q},t'')\rangle=(2\pi)^3\delta^3(\mathbf{k}-\mathbf{q})\mathcal{M}_{ijrc}(\hat{\mathbf{k}})h(k,t',t'')\ ,\\ &h(k,t',t'')=\frac{1}{8(2\pi)^3}U(t',t'')I(k)\ ,\\ &U(t',t'')=\frac{81}{4}\mathcal{H}^2(t')\mathcal{H}^2(t'')\left[\frac{a(t')}{a_{\rm in}}\right]^6\left[\frac{a(t'')}{a_{\rm in}}\right]^6\ ,\\ &I(k)=\mathcal{M}_{bdlm}(\hat{\mathbf{k}})\int \mathrm{d}^3p\left[\mathcal{M}_{lnbf}(\hat{\mathbf{p}})\mathcal{M}_{mndf}(\widehat{\mathbf{k}-\mathbf{p}})+\right.\\ &\qquad\left.\mathcal{M}_{lndf}(\hat{\mathbf{p}})\mathcal{M}_{mndf}(\widehat{\mathbf{k}-\mathbf{p}})\right]\mathcal{P}^{(1)}_{\Sigma\,\rm in}(p)\mathcal{P}^{(1)}_{\Sigma\,\rm in}(|\mathbf{k}-\mathbf{p}|)\ .\end{aligned}$$

More details about the computation of $h(k,t't'')$ and of the four point correlation function of the gravity waves can be found in Appendix 2.6.2.
Using the tensor calculus package "xAct" for Mathematica [133], we can compute the above products of the three projectors,

$$\begin{aligned}&\mathcal{M}_{bdlm}(\hat{\mathbf{k}})\left[\mathcal{M}_{lnbf}(\hat{\mathbf{p}})\mathcal{M}_{mndf}(\widehat{\mathbf{k}-\mathbf{p}})+\mathcal{M}_{lndf}(\hat{\mathbf{p}})\mathcal{M}_{mnbf}(\widehat{\mathbf{k}-\mathbf{p}})\right]=\\ &\qquad 2(1+\alpha^2+\beta^2+\alpha^2\beta^2-8\alpha\beta\gamma+\gamma^2+\alpha^2\gamma^2+\beta^2\gamma^2+\alpha^2\beta^2\gamma^2)\simeq 2\ .\end{aligned} \qquad (2.110)$$

where $\alpha\equiv\hat{k}\cdot(\widehat{k-p})$, $\beta\equiv\hat{p}\cdot(\widehat{k-p})$ and $\gamma\equiv\hat{k}\cdot\hat{p}$. Again we have approximated this angular dependence by a constant to simplify the calculations. This approximation is well justified within our accuracy. In order to write the function $h(k,t',t'')\simeq F(k)g(t')g(t'')$, we have to evaluate the integral I as before. We first consider the most interesting case of a scale invariant spectrum, $A\simeq -3$. Up to an infrared log-divergence which we neglect as usual (this divergence can be avoided if we choose $A=-2.99$ instead of $A=-3$), we have

$$\begin{aligned}F(k)&\simeq\frac{81\pi}{2(2\pi)^3}\left[k^3\mathcal{P}^{(1)}_{\Sigma\,\rm in}(k)\right]^2\frac{1}{k^3}\ ,\\ g(t')&\simeq\mathcal{H}^2(t')\left[\frac{a(t')}{a_{\rm in}}\right]^6\ .\end{aligned}$$

Therefore, the equation for $\sqrt{\mathcal{P}_{\Sigma}^{(2)\,\mathrm{GW}}(k,t)}$ in the radiation dominated era becomes

$$
\begin{aligned}
&P''(z) - \frac{4}{z}P' + \left(1 + \frac{4}{z^2}\right) P = \frac{\alpha}{k^6} z^4 \,, \\
&z \equiv kt \,, \qquad |P| \equiv \sqrt{\mathcal{P}_{\Sigma}^{(2)\,\mathrm{GW}}(k,t)} \,, \\
&\alpha \equiv \frac{1}{t_{\mathrm{in}}^6} \sqrt{\frac{81\pi}{2(2\pi)^3} \frac{\left[k^3 \mathcal{P}_{\Sigma\,\mathrm{in}}^{(1)}(k)\right]^2}{k^3}} \,.
\end{aligned}
$$

The super-horizon solution, evaluated always with the help of the Wronskian method and keeping only the non-homogeneous part as explained in the Appendix 2.6.1, is the given by

$$
P(z) \simeq \frac{1}{10} \frac{\alpha}{k^6} z^6 \,, \qquad z \ll 1 \,,
$$

that yields a contribution to the gravity wave power spectrum given by

$$
k^3 \mathcal{P}_{\Sigma}^{(2)\,\mathrm{GW}}(k,t) \simeq 0.4 \frac{\pi}{(2\pi)^3} \left[k^3 \mathcal{P}_{\Sigma\,\mathrm{in}}^{(1)}(k)\right]^2 \left(\frac{a}{a_{\mathrm{in}}}\right)^{12} , \qquad kt \ll 1 \,. \tag{2.111}
$$

For the density parameter on super-horizon scales this yields

$$
\frac{\mathrm{d}\Omega_{\mathrm{GW}}^{(2)\,\Sigma}(k,t)}{\mathrm{d}\log k} \simeq 0.01 \left[\frac{\mathrm{d}\Omega_{\mathrm{GW}}^{(1)}(k,t)}{\mathrm{d}\log k}\right]^2 , \qquad kt \ll 1 \,. \tag{2.112}
$$

Considering now the sub-horizon limit, we obtain for the power spectrum the following expression:

$$
k^3 \mathcal{P}_{\Sigma}^{(2)\,\mathrm{GW}}(k,t) \simeq 0.1 \frac{\pi}{(2\pi)^3} \left[k^3 \mathcal{P}_{\Sigma\,\mathrm{in}}^{(1)}(k)\right]^2 \frac{1}{(kt_{\mathrm{in}})^8} \left(\frac{a}{a_{\mathrm{in}}}\right)^4 , \qquad kt \gg 1 \,, \tag{2.113}
$$

and the density parameter becomes

$$
\frac{\mathrm{d}\Omega_{\mathrm{GW}}^{(2)\,\Sigma}(k,t)}{\mathrm{d}\log k} \simeq 0.02 \left[\frac{\mathrm{d}\Omega_{\mathrm{GW}}^{(1)}(k)}{\mathrm{d}\log k}\right]^2 , \quad kt \gg 1 \,. \tag{2.114}
$$

On the other hand, when $2A + 3 > 0$ we have

$$
\begin{aligned}
&F(k) \simeq \frac{81\pi}{2(2\pi)^3} \Sigma_{(1)\,\mathrm{in}}^4 \lambda^{6+2A} \frac{1}{2A+3} \,, \\
&g(t') \simeq \mathcal{H}^2(t') \left[\frac{a(t')}{a_{\mathrm{in}}}\right]^6 \left(\frac{1}{t'}\right)^{(2A+3)/2} \,.
\end{aligned}
$$

In the radiation epoch the equation for $\sqrt{\mathcal{P}_{\Sigma}^{(2)\,\mathrm{GW}}(k,t)}$ reads:

$$P'' - \frac{4}{z}P' + \left(1 + \frac{4}{z^2}\right) P = \alpha z^{(5/2-A)} \,,$$
$$\alpha \equiv \sqrt{\frac{81\pi}{2(2\pi)^3}\frac{1}{2A+3}} k^{3/2}\mathcal{P}_{\Sigma\,\mathrm{in}}^{(1)}(k)\frac{1}{(kt_{\mathrm{in}})^6} \,.$$

Solving the above equation in the long wavelengths limit, we find:

$$P(z) \simeq \frac{\alpha}{2} z^{9/2-A} \,, \qquad z \ll 1 \,,$$

where the exact pre-factor depends weakly on the value of A. For the power spectrum this results in

$$k^3\mathcal{P}_{\Sigma}^{(2)\,\mathrm{GW}}(k,t) \simeq \frac{81\pi}{8(2\pi)^3}\left[k^3\mathcal{P}_{\Sigma\,\mathrm{in}}^{(1)}(k)\right]^2\left(\frac{a}{a_{\mathrm{in}}}\right)^{12}(kt)^{-2A-3} \,, \qquad kt \ll 1 \,. \tag{2.115}$$

and inside the horizon this reads

$$k^3\mathcal{P}_{\Sigma}^{(2)\,\mathrm{GW}}(k,t) \simeq \frac{81\pi}{16(2\pi)^3}\left[k^3\mathcal{P}_{\Sigma\,\mathrm{in}}^{(1)}(k)\right]^2\left(\frac{a}{a_{\mathrm{in}}}\right)^{4}\frac{1}{(kt_{\mathrm{in}})^8} \,, \qquad kt \gg 1 \,. \tag{2.116}$$

Translating this to the density parameter as above, we obtain

$$\begin{aligned}
\frac{\mathrm{d}\Omega_{\mathrm{GW}}^{(2)\,\Sigma}(k,t)}{\mathrm{d}\log k} &\simeq 0.2\left[\frac{\mathrm{d}\Omega_{\mathrm{GW}}^{(1)}(k)}{\mathrm{d}\log k}\right]^2(kt)^{-2A-3} \\
&\simeq 0.2\left[\left.\frac{\mathrm{d}\Omega_{\mathrm{GW}}^{(1)}(k)}{\mathrm{d}\log k}\right|_{k=1/t}\right]^2(kt)^3 \,, \qquad kt \ll 1 \,, \\
\frac{\mathrm{d}\Omega_{\mathrm{GW}}^{(2)\,\Sigma}(k,t)}{\mathrm{d}\log k} &\simeq 0.1\left[\frac{\mathrm{d}\Omega_{\mathrm{GW}}^{(1)}(k)}{\mathrm{d}\log k}\right]^2 \,, \quad kt \gg 1 \,.
\end{aligned} \tag{2.117}$$

2.5 Summary and conclusions

In this work we have studied the evolution of stochastic cosmic magnetic fields and gravity waves up to second order in the perturbations. We have especially calculated the density parameters of the generated second order perturbations. We start with density parameters $\left[\mathrm{d}\Omega_{\mathrm{B}}^{(1)}(k,t)/\mathrm{d}\log k\right]$ and $\left[\mathrm{d}\Omega_{\mathrm{GW}}^{(1)}(k,t)/\mathrm{d}\log k\right]$ which are related to the first order magnetic field and gravitational wave power spectra in Section 2.3.3. Since tensor perturbations grow on super-horizon scales, the gravity wave density parameter grows on super-Hubble scales and only becomes constant once the perturbations enter the horizon. For perturbation theory to be valid, we have of course to require that these density parameters are much smaller than unity. As we have seen in Section 2.3.3, to require that $\left[\mathrm{d}\Omega_{\mathrm{GW}}^{(1)}(k,t)/\mathrm{d}\log k\right]$

is smaller than one also on sub-Hubble scales, is equivalent to

$$\frac{\mathrm{d}\Omega_{\mathrm{GW}}^{(1)}(k,t_{\mathrm{in}})}{\mathrm{d}\log k}\frac{1}{(kt_{\mathrm{in}})^4} \simeq \left(\frac{H_{\mathrm{inf}}}{M_{\mathrm{P}}}\right)^2 \ll 1\,. \tag{2.118}$$

Here we summarize the new results on the density parameters for second order perturbation on sub-horizon scales. For magnetic fields, we obtain

$$\frac{\mathrm{d}\Omega_{\mathrm{B}}^{(2)}(k)}{\mathrm{d}\log k} \simeq \frac{\mathrm{d}\Omega_{\mathrm{GW}}^{(1)}(k)}{\mathrm{d}\log k}\frac{\mathrm{d}\Omega_{\mathrm{B}}^{(1)}(k)}{\mathrm{d}\log k}\,, \quad tk \gg 1\,, \tag{2.119}$$

up to numerical constants and logarithms which are beyond the accuracy of our approximation. Hence, it is not correct that the presence of gravity waves resonantly enhances a first order magnetic field. The second order density parameter is quite what we would naively expect and it is much smaller than the first order perturbations as long as the latter are small. Also on super-horizon scales, the second order magnetic field density parameter is always much smaller than the first order one, see Eqs.(2.82) and (2.84).

Since the growth comes from super horizon scales, conductivity is not relevant for this result. We have shown that also in a matter dominated background we obtain

$$\begin{aligned}\frac{\mathrm{d}\Omega_{\mathrm{B}}^{(2)}(k)}{\mathrm{d}\log k} &\simeq \left.\frac{\mathrm{d}\Omega_{\mathrm{GW}}^{(1)}(k)}{\mathrm{d}\log k}\right|_{kt=1}\frac{\mathrm{d}\Omega_{\mathrm{B}}^{(1)}(k)}{\mathrm{d}\log k} \\ &\simeq \left(\frac{H_{\mathrm{inf}}}{M_{\mathrm{P}}}\right)^2\frac{\mathrm{d}\Omega_{\mathrm{B}}^{(1)}(k)}{\mathrm{d}\log k} \ll \frac{\mathrm{d}\Omega_{\mathrm{B}}^{(1)}(k)}{\mathrm{d}\log k}\,,\end{aligned} \tag{2.120}$$

hence no significant amplification.

Second order gravity waves are induced on the one hand by the anisotropic stresses of the first order magnetic fields and on the other hand by the quadratic terms in the evolution equation for σ_{ij} which are, e.g., of the form $\sigma_{im}\dot{\sigma}^m_j$ and similar expressions. In Section 2.4.3.1 we have shown that the second order contribution from anisotropic stresses on sub-Hubble scales is of the order of

$$\frac{\mathrm{d}\Omega_{\mathrm{GW}}^{(2)\,\Pi}(k,t)}{\mathrm{d}\log k} \simeq \begin{cases} \left[\frac{\mathrm{d}\Omega_B^{(1)}(k_d)}{\mathrm{d}\log k_d}\right]^2\left(\frac{k}{k_d}\right)^3, & \text{if } 2M+3>0 \\ \left[\frac{\mathrm{d}\Omega_B^{(1)}(k)}{\mathrm{d}\log k}\right]^2, & \text{if } 2M+3<0\,, \end{cases} \tag{2.121}$$

both on super- and sub-horizon scales. Note that the above expression is continuous at $2M+3=0$, where both expressions scale like $(k\lambda)^3$ and are independent of k_d. One should point out that we neglected the slow time dependence of the damping scale. Correctly one has to choose the value of the damping scale at horizon crossing, $k_d(t_k)$ with $t_k = 1/k$. Depending on the magnetic field spectrum, the resulting gravity waves come mainly from the small scale magnetic field, if its spectrum is blue $2M+3>0$. In this case the gravity waves power spectrum is always proportional to k^3. In our case of a simple power law magnetic field spectrum, this behavior is maintained for all $k < k_d$. If the magnetic field spectrum is red, $2M+3<0$, gravity waves depend on the field at scale k and their spectrum is the square of the B-field spectrum. In the first case, the non-linearity leads to

a 'sweeping' of magnetic field power on small scales to gravitational wave power on larger scales. This can be regarded as an 'inverse cascade' of small scale magnetic field power into large scale gravity waves. But in no case can the gravity wave density parameter become larger than the one of the magnetic field, which has to be much smaller than one, for perturbation theory to be valid.

A similar result was already obtained in Ref. [77]. Contrary to this reference we have no logarithmic build-up of gravity waves. This comes from our different treatment; we directly calculate the shear σ_{ij} and not the tensor perturbation of the metric, h_{ij}. In this way we loose the log term which corresponds to the homogeneous $h_{ij} =$ constant solution on super-horizon scales to which we are not sensitive. However, in our more qualitative work, we do not want to insist on log terms which we neglect in this work also in other places.

The second order gravity wave density parameter induced by first order gravity waves is given by

$$\frac{\mathrm{d}\Omega_{\mathrm{GW}}^{(2)\,\Sigma}(k,t)}{\mathrm{d}\log k} \simeq \left[\frac{\mathrm{d}\Omega_{\mathrm{GW}}^{(1)}(k,t)}{\mathrm{d}\log k}\right]^2 , \qquad kt \gg 1 \, , \tag{2.122}$$

on sub-horizon scales.
Adding both contributions we find

$$\frac{\mathrm{d}\Omega_{\mathrm{GW}}^{(2)}(k,t)}{\mathrm{d}\log k} \simeq \begin{cases} \left[\frac{\mathrm{d}\Omega_B^{(1)}(k_d)}{\mathrm{d}\log k_d}\right]^2 \left(\frac{k}{k_d}\right)^3 + \left[\frac{\mathrm{d}\Omega_{\mathrm{GW}}^{(1)}(k,t)}{\mathrm{d}\log k}\right]^2 , \\ \qquad \text{if } 2M+3>0\,, \quad kt \gg 1 \\ \left[\frac{\mathrm{d}\Omega_B^{(1)}(k)}{\mathrm{d}\log k}\right]^2 + \left[\frac{\mathrm{d}\Omega_{\mathrm{GW}}^{(1)}(k,t)}{\mathrm{d}\log k}\right]^2 , \\ \qquad \text{if } 2M+3<0\,, \quad kt \gg 1 \, . \end{cases} \tag{2.123}$$

Acknowledgments

We are grateful to Roy Maartens, Christos Tsagas, Chiara Caprini and Cyril Pitrou for helpful discussions. EF thanks the "EARA Early Stage Training" fellowship for financial support. We acknowledge support by the Swiss National Science Foundation.

2.6 Appendix

2.6.1 General Solution of a Differential Equation with the Wronskian Method

Here we discuss in detail the Wronskian method with which we find the solution of the differential equations in this paper. If we have a inhomogeneous linear second order equation with inhomogeneity $S(z)$, its most general solution is of the form

$$P(z) = c_1(z)P_1(z) + c_2(z)P_2(z) + a_1P_1(z) + a_2P_2(z)\,,$$

where $P_1(z)$ and $P_2(z)$ are two (linearly independent) homogeneous solutions which we suppose to be known, $W(z) = P_1 P_2' - P_1' P_2$ is their Wronskian, and

$$\begin{aligned} c_1(z) &= -\int_{z_{\rm in}}^{z} dx \frac{S(x)}{W(x)} P_2(x) \ , \\ c_2(z) &= \int_{z_{\rm in}}^{z} dx \frac{S(x)}{W(x)} P_1(x) \ . \end{aligned}$$

The particular solution given by the first two terms is such that $P_{\rm inh}(z) = c_1(z)P_1(z) + c_2(z)P_2(z)$ vanishes at $z = z_{\rm in}$ and also $P'_{\rm inh}(z_{\rm in}) = 0$. The general solution is obtained by adding a homogeneous solution, $P_{\rm hom}(z) = a_1 P_1(z) + a_2 P_2(z)$ with arbitrary constants a_1 and a_2.

Let us first consider the example given in Eq. (2.105),

$$P'' - \frac{4}{z} P' + \left(1 + \frac{4}{z^2}\right) P = \frac{\alpha}{k^2} \ ,$$

where α/k^2 is a constant source term. The homogeneous solutions are given by $P_1(z) = z^3 j_1(z)$ and $P_2(z) = z^3 y_1(z)$ and the Wronskian determinant reads

$$W(z) = z^3 \ .$$

In the regime $z \ll 1$ we can approximate the spherical Bessel functions by powers and we find the following general expression for $P(z)$:

$$P(z) = -\frac{\alpha}{3k^2}\left(\frac{z^2}{2} - \frac{z^4}{2z_{\rm in}^2} + z^2 - z z_{\rm in}\right) + a_1 z^4 + a_2 z \ . \tag{2.124}$$

where we have used the fact that, when $z \ll 1$, we can approximate $P_1(z) \simeq z^4$ and $P_2(z) \simeq -z$. Now it is important to notice that the second and the fourth terms of the inhomogeneous solution (2.124) have the same functional behavior as homogeneous solutions and we can always choose a_1 and a_2 such that the homogeneous part cancels them. This is actually always true for the contributions from the lower boundary of the inhomogeneous solution. This may sound pedantic, but it is very important in this specific case as the second term in (2.124) dominates if it is present. In our analysis we have always subtracted such "homogeneous contributions" and only kept the "minimal part", which in this case is

$$P(z) \simeq -\frac{\alpha}{2k^2} z^2 \ , \quad z \ll 1 \, . \tag{2.125}$$

This procedure is important and it is responsible for the results which we have obtained. We justify it also by the fact that the first order solution has exactly the the same time evolution as the homogeneous term and therefore a term $\propto z^4$ present at early times, should be included in the first order perturbations. Once the wave number has entered the horizon, $z \gg 1$, the Green function starts to oscillate and the additional contribution to the integral can be neglected. We then can match the inhomogeneous solution at horizon crossing to the homogenous one at later times. Up to matching details which we have not

considered, this yields

$$P(z) \simeq \frac{\alpha}{2k^2} z^2 \cos z \ , \quad z \gg 1 \ . \tag{2.126}$$

In the same way, we deal with Eq. (2.78)

$$P'' - \frac{4}{z} P' + \left(1 + \frac{4}{z^2}\right) + P = \frac{\alpha}{k^2} \ . \tag{2.127}$$

The homogeneous solutions are $P_1(z) = z^2 j_0(z) \simeq z^2$ and $P_2(z) = z^2 y_0(z) \simeq -z$. These approximations are valid for $z \ll 1$. Using again the Wronskian method, we obtain the following general solution on super-Hubble scales, $z \ll 1$:

$$P(z) \ = \ \frac{\alpha}{k^2} \left(z^2 \log\left(\frac{z}{z_{\rm in}}\right) - z^2 + z z_{\rm in} \right) + a_1 z^2 + a_2 z \ , \qquad z \ll 1 \ , \tag{2.128}$$

Here, the homogeneous solution parts are $-z^2$ and $z z_{\rm in}$, therefore we can identify the solution due to the presence of the source again as

$$P(z) \simeq \frac{\alpha}{k^2} z^2 \log\left(\frac{z}{z_{\rm in}}\right) \ , \quad z \ll 1 \ . \tag{2.129}$$

On sub-horizon scales this becomes, up to matching details which only modify the phase and have an irrelevant effect on the pre-factors,

$$P(z) \simeq \frac{\alpha}{k^2} \log(k t_{\rm in}) z \cos z \ , \quad z \gg 1 \ . \tag{2.130}$$

If the source term depends on z, the details of the calculation as well as the results change somewhat, but the basic argumentation remains the same. We therefore do not repeat the z-dependent examples which arise in this work here.

2.6.2 The four-point correlator of gravity waves

Starting from Eq. (2.109), we compute the two-point correlation function of the source term $\langle f_{ij}(\mathbf{k}, t') f^*_{rn}(\mathbf{p}, t'')\rangle$, which is given by

$$\begin{aligned} \langle f_{ij}(\mathbf{k}, t') f^*_{rc}(\mathbf{q}, t'')\rangle = \frac{1}{(2\pi)^6} U(t', t'') \mathcal{M}_{ij}{}^{lm}(\hat{\mathbf{k}}) \times \\ \mathcal{M}_{rc}{}^{bd}(\hat{\mathbf{q}}) \int \mathrm{d}^3 p \int \mathrm{d}^3 s \langle \Sigma^{(1)\,\rm in}_{ln}(\mathbf{p}) \Sigma^{(1)\,\rm in}_{nm}(\mathbf{k}-\mathbf{p}) \Sigma^{*(1)\,\rm in}_{bf}(\mathbf{s}) \Sigma^{*(1)\,\rm in}_{fd}(\mathbf{q}-\mathbf{s})\rangle, \end{aligned} \tag{2.131}$$

where the function $U(t', t'')$ contains the all time-dependence of the above expression:

$$U(t', t'') = \frac{81}{4} \mathcal{H}^2(t') \mathcal{H}^2(t'') \left[\frac{a(t')}{a_{\rm in}}\right]^6 \left[\frac{a(t'')}{a_{\rm in}}\right]^6 \ . \tag{2.132}$$

To compute the four-point correlator, we assume that the random variables that describe gravity waves are Gaussian, therefore we can apply Wick's theorem. The we can

write the products of four gravity waves $\Sigma^{(1)}$ as

$$\begin{aligned}\langle\Sigma^{(1)\,\mathrm{in}}_{ln}(\mathbf{p})\Sigma^{(1)\,\mathrm{in}}_{nm}(\mathbf{k}-\mathbf{p})\Sigma^{*(1)\,\mathrm{in}}_{bf}(\mathbf{s})\Sigma^{*(1)\,\mathrm{in}}_{fd}(\mathbf{q}-\mathbf{s})\rangle = \\ \langle\Sigma^{(1)\,\mathrm{in}}_{ln}(\mathbf{p})\Sigma^{*(1)\,\mathrm{in}}_{bf}(\mathbf{s})\rangle\langle\Sigma^{(1)\,\mathrm{in}}_{nm}(\mathbf{k}-\mathbf{p})\Sigma^{*(1)\,\mathrm{in}}_{fd}(\mathbf{q}-\mathbf{s})\rangle + \\ \langle\Sigma^{(1)\,\mathrm{in}}_{ln}(\mathbf{p})\Sigma^{*(1)\,\mathrm{in}}_{fd}(\mathbf{q}-\mathbf{s})\rangle\langle\Sigma^{(1)\,\mathrm{in}}_{nm}(\mathbf{k}-\mathbf{p})\Sigma^{*(1)\,\mathrm{in}}_{bf}(\mathbf{s})\rangle + \\ \langle\Sigma^{(1)\,\mathrm{in}}_{ln}(\mathbf{p})\Sigma^{(1)\,\mathrm{in}}_{nm}(\mathbf{k}-\mathbf{p})\rangle\langle\Sigma^{*(1)\,\mathrm{in}}_{bf}(\mathbf{s})\Sigma^{*(1)\,\mathrm{in}}_{fd}(\mathbf{q}-\mathbf{s})\rangle\,. \end{aligned} \tag{2.133}$$

Once the double integration is performed, the last term contributes a constant $\propto \delta^3(\mathbf{k})$ which can be disregarded (a background term). Integrating the remaining two terms over d^3s, we can eliminate one of the two δ-functions which come from the expression of the two point gravity wave correlator. Using the reality condition, $\Sigma^*_{ij}(\mathbf{k}) = \Sigma_{ij}(-\mathbf{k})$, and the expression for the two-point correlation function of gravity waves given in Eq. (2.66), we then obtain

$$\begin{aligned}\int \mathrm{d}^3p \int \mathrm{d}^3s \langle\Sigma^{(1)\,\mathrm{in}}_{ln}(\mathbf{p})\Sigma^{(1)\,\mathrm{in}}_{nm}(\mathbf{k}-\mathbf{p})\Sigma^{*(1)\,\mathrm{in}}_{bf}(\mathbf{s})\Sigma^{*(1)\,\mathrm{in}}_{fd}(\mathbf{q}-\mathbf{s})\rangle = \\ (2\pi)^6\delta^3(\mathbf{k}-\mathbf{q})\int \mathrm{d}^3p \mathcal{P}^{(1)}_{\Sigma\,\mathrm{in}}(p)\mathcal{P}^{(1)}_{\Sigma\,\mathrm{in}}(|\mathbf{k}-\mathbf{p}|)\times \\ \left[\mathcal{M}_{lnbf}(\hat{\mathbf{p}})\mathcal{M}_{mndf}(\widehat{\mathbf{k}-\mathbf{p}}) + \mathcal{M}_{lndf}(\hat{\mathbf{p}})\mathcal{M}_{mnbf}(\widehat{\mathbf{k}-\mathbf{p}})\right]\,. \end{aligned} \tag{2.134}$$

The above equation is symmetric in $\mathbf{k}$ and $\mathbf{q}$, as well as under the exchange of the first and second pairs of indices. Moreover, it is symmetric under the exchange of the first index with the second and the third with the fourth. This suggests us to write the two point correlation function of the source term as

$$\langle f_{ij}(\mathbf{k},t')f^*_{rc}(\mathbf{q},t'')\rangle = (2\pi)^3\delta^3(\mathbf{k}-\mathbf{q})\mathcal{M}_{ijrc}(\hat{\mathbf{k}})h(k,t',t'')\,, \tag{2.135}$$

since the tensor $\mathcal{M}_{ijrc}$ has the same symmetries.

To obtain an expression for the function $h(k,t',t'')$, it is sufficient to calculate the trace of the above two point correlator. We hence should multiply the r.h.s. of the above equation and of Eq. (2.131) by $\mathcal{M}^{ijrc}(\hat{\mathbf{k}})$. Then, setting them to be equal and remembering that $\mathcal{M}^{ijrc}\mathcal{M}_{ijrc} = 8$ [130], we obtain

$$\begin{aligned}8(2\pi)^3\delta^3(\mathbf{k}-\mathbf{q})h(k,t',t'') = \\ U(t',t'')\delta^3(\mathbf{k}-\mathbf{q})\mathcal{M}^{crlm}(\hat{\mathbf{k}})\mathcal{M}^{bd}{}_{rc}(\hat{\mathbf{q}})\int \mathrm{d}^3p\,\mathcal{P}^{(1)}_{\Sigma\,\mathrm{in}}(p)\mathcal{P}^{(1)}_{\Sigma\,\mathrm{in}}(|\mathbf{k}-\mathbf{p}|)\times \\ \left[\mathcal{M}_{lnbf}(\hat{\mathbf{p}})\mathcal{M}_{mndf}(\widehat{\mathbf{k}-\mathbf{p}}) + \mathcal{M}_{lndf}(\hat{\mathbf{p}})\mathcal{M}_{mnbf}(\widehat{\mathbf{k}-\mathbf{p}})\right]\,, \end{aligned} \tag{2.136}$$

with

$$\begin{aligned}h(k,t',t'') = \frac{1}{8(2\pi)^3}U(t',t'')\mathcal{M}_{bdlm}(\hat{\mathbf{k}})\int \mathrm{d}^3p\mathcal{P}^{(1)}_{\Sigma\,\mathrm{in}}(p)\mathcal{P}^{(1)}_{\Sigma\,\mathrm{in}}(|\mathbf{k}-\mathbf{p}|)\times \\ \left[\mathcal{M}_{lnbf}(\hat{\mathbf{p}})\mathcal{M}_{mndf}(\widehat{\mathbf{k}-\mathbf{p}}) + \mathcal{M}_{lndf}(\hat{\mathbf{p}})\mathcal{M}_{mnbf}(\widehat{\mathbf{k}-\mathbf{p}})\right]\,. \end{aligned} \tag{2.137}$$

Finally, we have to perform the above product of three polarization tensors, defined as

in Eq. (2.32). To achieve this aim, we use the free source package "xAct" for Mathematica [133]: it is sufficient to define a three dimensional flat metric and the projection tensor $\mathcal{P}_{ij}(\hat{\mathbf{k}}) = \delta_{ij} - k^{-2}k_i k_j$ onto the plane normal to $\mathbf{k}$. Then, we can express $\mathcal{M}_{ijlm}(\hat{\mathbf{k}})$ in terms of this projector as

$$\mathcal{M}_{ijlm} \equiv \mathcal{P}_{il}\mathcal{P}_{jm} + \mathcal{P}_{im}\mathcal{P}_{jl} - \mathcal{P}_{ij}\mathcal{P}_{lm}\,.$$

Defining the angles between the three directions as $\alpha \equiv \hat{k} \cdot (\widehat{k-p})$, $\beta \equiv \hat{p} \cdot (\widehat{k-p})$ and $\gamma \equiv \hat{k} \cdot \hat{p}$, we obtain the expression given in Eq. (2.110).

Chapter 3

Can the observed large scale magnetic fields be seeded by helical primordial fields?

JOURNAL OF COSMOLOGY AND ASTROPARTICLE PHYSICS **0911**, 001 (2009)

Can the observed large scale magnetic fields be seeded by helical primordial fields?

Chiara Caprini, Ruth Durrer and Elisa Fenu

Gravitational wave production induces a strong constraint on the amplitude of a primordial magnetic field. It has been shown that the nucleosynthesis bound for a stochastic gravitational wave background implies that causally generated fields cannot have enough power on large scales to provide the seeds necessary for the observed magnetic fields in galaxies and clusters, even by the most optimistic dynamo amplification. Magnetic fields generated at inflation can have high enough amplitude only if their spectrum is very red. Here we show that helicity, which leads to an inverse cascade, can mitigate these limits. In particular, we find that helical fields generated at the QCD phase transition or at inflation with red spectrum are possible seeds for the dynamo. Helical fields generated at the electroweak phase transition are instead excluded as seeds at large scales. We also calculate the spectrum of gravitational waves generated by helical magnetic fields.

DOI: 10.1088/1475-7516/2009/11/001

3.1 Introduction

Magnetic fields are ubiquitous in the Universe. Wherever they can be measured, they are found. In stars, in galaxies [37], locally and at high redshift [39], and in clusters of galaxies [41]. There is also evidence of magnetic fields in super clusters [43]. However, the origin of these fields is still unclear. Have they emerged in the late Universe from charge separation processes or by ejection from stars and galaxies [36]? Or have they been amplified from primordial seed fields which may represent a relic from the early Universe, from the electroweak (EW) phase transition [51, 52, 53] or even from inflation [55, 56, 57, 58, 59]? If the second exciting possibility is realized, this means that we can learn about processes in the early universe from studying cosmological large scale magnetic fields.

In a previous paper [77] it has been shown that primordial magnetic fields lead to significant production of gravitational waves. If the magnetic field spectrum is blue, as it has to be if the production mechanism is causal [68], the nucleosynthesis limit for a gravitational wave (GW) background strongly constrains the amplitude of magnetic fields on large scales. This strong constraint comes from the fact that for causal magnetic fields, the energy density has to behave like

$$\frac{d\rho_B(k)}{d\log k} \propto k^5, \tag{3.1}$$

with comoving wave number k, on scales which are larger than the correlation scale. Hence even the moderate nucleosynthesis limit, since it comes from the smallest scales, highest wave numbers, at which the magnetic field is maximal, leads to a very strong limit on the field amplitude at large, cosmological scales. The detailed results are given in [77, 82]. For the derivation of this limit it is assumed that the magnetic field spectrum evolves solely via the damping of fields on small scales and via flux conservation. On large scales, the magnetic field spectrum scaled to today is assumed to remain constant.

However, if the magnetic field has non-vanishing helicity, the conservation of helicity leads to an inverse cascade, *i.e.* it can move power from small to large scales. A derivation of this result can be found in the review [48]. This can mitigate the magnetic field limit which precisely comes from the fact that for causally produced magnetic fields there is so little power on large scales. The production of helical magnetic fields has been proposed for both, inflation [134, 135, 136] and the EW phase transition where the magnetic field helicity is linked to the baryon number [137, 138, 139]. Furthermore, the formation of maximally helical magnetic fields at the QCD phase transition has been proposed in Ref. [54].

The evolution of helical magnetic fields and the inverse cascade have been studied in numerical simulations, and simple fits which describe the evolution of the correlation scale $L(t)$ and of the magnetic field energy density $\rho_B(t)$ have been derived in Refs. [80, 78, 79]. Using these results, we want to determine upper bounds on the amplitude of *helical* magnetic fields from the induced GWs. These bounds are summarised in Table 3.1.

In Section 3.2 we present the basic definitions and discuss the evolution of normal and helical magnetic fields. Here we make use of the results for the inverse cascade discussed in Ref. [79]. In Section 3.3 we calculate the induced GW spectrum. In Section 3.4 we derive the limits on helical magnetic fields on cosmological scales. In Section 6.5 we conclude.

Notation: Throughout this paper we neglect curvature and the cosmological constant, which are not relevant for our discussion. The cosmological metric is given by

$$ds^2 = a^2(t)\left(-dt^2 + \delta_{ij}dx^i dx^j\right) , \tag{3.2}$$

where t denotes conformal time and the scale factor, normalized to 1 today, is given to a good approximation by

$$a(t) \simeq H_0 t \left[\frac{H_0 t}{4} + \sqrt{\Omega_{\rm rad}}\left(\frac{g_0}{g_{\rm eff}(t)}\right)^{1/6}\right] , \tag{3.3}$$

where H_0 denotes the present value of the Hubble parameter, $g_{\rm eff}(t)$ is the number of effective relativistic degrees of freedom at time t, $g_0 \equiv g_{\rm eff}(t_0) = 2$, and $\Omega_{\rm rad}$ is the radiation density parameter today. In the following, the density parameter is defined as $\Omega_X(t) = \rho_X(t)/\rho_c(t)$, where $\rho_c(t)$ denotes the critical energy density at time t.

Spatial vectors are indicated in bold face, 3d spatial indices are lower case Latin letters while 4d spacetime indices are lower case Greek letters.

3.2 The evolution of helical magnetic fields

3.2.1 Basic definitions

The high conductivity of the cosmic plasma implies that, to lowest order, magnetic fields evolve by flux conservation, so that $B \propto a^{-2}$. We are mainly interested in the part of

the time dependence of our quantities which is not simply due to the expansion of the Universe but to the growth of the magnetic correlation length and to the additional decay of the magnetic energy density due to dissipation and to the MHD cascade [80, 78, 79]. Therefore we eliminate the scaling with redshift by expressing all the quantities in terms of comoving ones scaled to today which we denote by a tilde. For example the comoving magnetic energy density is given by [82]

$$\langle \tilde{B}^2(t) \rangle = \langle B^2(t) \rangle a^4(t) \ . \tag{3.4}$$

Here $\langle \tilde{B}^2(t) \rangle$ depends on time via the evolution of the correlation length and because of energy dissipation. Comoving quantities are not multiplied by powers of the scale factor $a^2(t)$ when lowering and rising indices.

The power spectrum of the magnetic field can be written as [130]

$$\langle \tilde{B}_i(\mathbf{k},t) \tilde{B}_j^*(\mathbf{q},t) \rangle = \frac{(2\pi)^3}{2} \delta^3(\mathbf{k}-\mathbf{q}) \left[\left(\delta_{ij} - \hat{k}_i \hat{k}_j \right) S(k,t) + i \epsilon_{ijn} \hat{k}_n A(k,t) \right] \ . \tag{3.5}$$

The functions S and A denote the parity even and the parity odd parts of the two point correlator respectively and $\mathbf{k}$ is the comoving wave vector (on the quantities where there is no danger of confusion because they always denote conformal quantities like $\mathbf{k}$, S or A, we omit the tilde). Using the above expressions, we compute the comoving magnetic energy density $\tilde{\rho}_B = (8\pi)^{-1} \tilde{B}^2$,

$$\tilde{\rho}_B(t) = \int_0^\infty \frac{dk}{k} \frac{d\tilde{\rho}_B(k,t)}{d\log k} \ , \qquad \frac{d\tilde{\rho}_B(k,t)}{d\log k} = \frac{k^3 S(k,t)}{2(2\pi)^3} \ . \tag{3.6}$$

Note that the antisymmetric part of the spectrum does not contribute to the energy density but its presence, which indicates non-vanishing helicity, influences the time dependence of $\tilde{\rho}_B$ and of the magnetic correlation length. In [79] the author derives analytically the expressions for the time evolution of the magnetic energy density and of the magnetic correlation length. These evolution laws have also been obtained in numerical simulations of a magnetic field in a turbulent MHD phase during the radiation dominated era [78]. On the other hand, the simulations of Ref. [80] indicate different exponents for the evolution laws. In the following analysis we adopt the analytical picture and the evolution laws derived in [79]. It is easy to show that during this epoch the MHD equations are identical to those of a non-expanding Universe, provided that all physical variables are replaced by comoving variables (see [140, 78]).

Our aim is to compute the GWs generated by an helical magnetic field and to use the GW energy density to derive constraints on the magnetic field strength on the comoving scale $\tilde{\lambda} \simeq 0.1$ Mpc. For this we express the results of Ref. [79] in terms of the quantities introduced above. Campanelli [79] defines the spectral energy density $\varepsilon_B(k,t)$ which is related to Eq. (3.6) by[1]

$$\frac{d\tilde{\rho}_B(k,t)}{d\log k} = \frac{k^3 S(k,t)}{2(2\pi)^3} = k\, \varepsilon_B(k,t) \ . \tag{3.7}$$

[1]Ref. [79] is using Heavyside-Lorentz units such that $\rho_B = (1/2)B^2$ while we are using Gaussian units with $\rho_B = (1/8\pi)B^2$. This leads to differences of factors of 4π in the relative expressions.

We adopt the following power spectrum for the magnetic field energy:

$$\varepsilon_B(k,t) = \begin{cases} \eta_B(t)\frac{\tilde{L}(t)K^{n+2}}{(1+K^2)^{(7+2n)/4}} & \text{for} \quad K \leq \frac{\tilde{L}(t)}{\tilde{l}_{\rm diss}(t)}\,, \\ 0 & \text{for} \quad K \geq \frac{\tilde{L}(t)}{\tilde{l}_{\rm diss}(t)}\,. \end{cases} \tag{3.8}$$

Here $\eta_B(t)$ parametrizes the time dependence of ρ_B (see Eq. (3.9)), $K \equiv k\tilde{L}(t)/(2\pi)$, $\tilde{L}(t)$ is the time dependent comoving correlation length which we infer from [79] and $\tilde{l}_{\rm diss}$ is the comoving dissipation scale (for smaller scales the magnetic power spectrum is exponentially suppressed and we thus can set it to zero). We derive the dissipation scale $\tilde{l}_{\rm diss}(t)$ in Appendix 3.6.1.2. Eq. (3.8) is inspired by Eq. (19) of [141], which provides a continuous expression for the turbulent velocity spectrum, interpolating between the large and small scale behaviours. We extend it here to the case of a magnetic field processed by MHD turbulence. The initial power spectrum at large scales, $k\tilde{L} \ll 1$ behaves like $k^2 S(k) \propto k^{n+2}$, n is the spectral index introduced in Refs. [82, 77]. If the initial correlation length is finite, the power spectrum given in Eq. (3.5) must be analytic and hence $n \geq 2$ must be an even integer [68]. A scale invariant spectrum corresponds to $n = -3$. We have chosen the form of $\varepsilon_B(k,t)$ such that it scales like $k^{-3/2}$ in the inertial range, $2\pi/\tilde{L}(t) < k < 2\pi/\tilde{l}_{\rm diss}$. This behavior corresponds to the Iroshnikov–Kraichnan spectrum, which can be realised in fully developed MHD turbulence [142, 143, 144]. Here we could have equally chosen the Kolmogorov or Goldreich-Sridhar spectral slopes: our main result does not depend significantly on this choice. Note that Ref. [79] does not account for the presence of the inertial range.

We adopt here the interpolating formula (3.8) in order to avoid joining the two asymptotic behaviours, at large and small scales, of the magnetic field spectrum up to the energy injection scale $\tilde{L}(t)$. This has been done for example in Ref. [77], and it leads to an overestimation of the peak amplitude. Note that we extend the formula of Ref. [141] to represent also magnetic fields with red spectra, generated during inflation.

Integrating Eq. (3.8) over k we obtain the total comoving magnetic field energy density,

$$\tilde{\rho}_B(t) = \rho_c(t_0)\tilde{\Omega}_B(t) \simeq \eta_B(t)\frac{\pi\Gamma\left(\frac{1}{4}\right)\Gamma\left(\frac{n+3}{2}\right)}{\Gamma\left(\frac{2n+7}{4}\right)}\,, \tag{3.9}$$

where we have set the upper limit of integration to infinity. Hence the function $\eta_B(t)$ reflects the time dependence of the total energy density. In the above expression we have introduced

$$\begin{aligned} \tilde{\Omega}_B(t) &\equiv \frac{\tilde{\rho}_B(t)}{\rho_c(t_0)} = \frac{\rho_B(t)a^4(t)}{\rho_c(t_0)} = \frac{\rho_B(t)a^4(t)}{\rho_{\rm rad}(t_0)}\,\Omega_{\rm rad} \\ &= \left(\frac{g_0}{g_{\rm eff}(t)}\right)^{1/3}\frac{\rho_B(t)}{\rho_{\rm rad}(t)}\,\Omega_{\rm rad} = \left(\frac{g_0}{g_{\rm eff}(t)}\right)^{1/3}\Omega_B(t)\,\Omega_{\rm rad}\,. \end{aligned} \tag{3.10}$$

We restrict to the analysis of magnetic fields in a radiation dominated universe. Furthermore, adiabatic expansion implies [132] that the entropy $S \propto g_{\rm eff}(aT)^3$ is independent of time, so that $\rho_{\rm rad}(t) = \rho_{\rm rad}(t_0)a(t)^{-4}[g_0/g_{\rm eff}(t)]^{1/3}$. At time t_*, which we define as the time

at which turbulence is fully developed (as we shall see in the following), one has

$$\Omega_B^* \equiv \Omega_B(t_*) = \frac{\tilde{\Omega}_B(t_*)}{\Omega_{\rm rad}} \left(\frac{g_*}{g_0}\right)^{1/3} \simeq \frac{\tilde{\Omega}_B(t_*)}{\Omega_{\rm rad}} \,, \tag{3.11}$$

where $g_* \equiv g_{\rm eff}(t_*)$. The comoving magnetic energy density parameter $\tilde{\Omega}_B(t)$ depends on time via the dissipation of magnetic energy.

In the following we will often neglect changes in $g_{\rm eff}(t)$. For example, we neglect the fact that the evolution of gravitational radiation is modified, even if the universe is radiation dominated, due to the fact that while $g_{\rm eff}(t)$ is evolving the scale factor does not expand like $a \propto t$ but somewhat faster. For the EW phase transition $(g_*/g_0)^{1/3} \simeq 3.7$. In the magnetic field limits this factor enters at most with power 1/2, which yields differences of less than a factor of two. In the amplitude of gravitational waves it can enter with a higher power and change it by up to an order of magnitude. But this is in any case roughly the precision of the results derived in this work.

3.2.2 Direct and inverse cascades

The main difference between non helical field evolution (which only exhibits direct cascade and dissipation on small scales) and helical field evolution (which leads to inverse cascade) can be expressed in the time evolution of the correlation scale $\tilde{L}(t)$ and the comoving magnetic field energy density $\tilde{\rho}_B(t)$, which we cast in the amplitude $\eta_B(t)$ [79].

We introduce the normalized conformal time τ

$$\tau = \frac{t - t_{\rm in}}{t_L^*} \,, \tag{3.12}$$

where t_L^* denotes the initial eddy turn-over time on the scale of energy injection $\tilde{L}_*$, and $t_{\rm in}$ is the time at which the magnetic field is generated. The eddy turnover time is defined as $t_L^* \simeq \tilde{L}_*/(2v_L)$, where v_L is the initial eddy turnover speed and the factor 1/2 comes from the fact the $\tilde{L}_*$ is the eddy diameter.

Starting from the asymptotic laws given in [79], we rewrite the time evolution of the comoving magnetic energy density and of the comoving magnetic correlation length in terms of the normalised conformal time (3.12). However, with respect to [79] we add a model of the initial evolution in which the magnetic energy density grows continuously from zero to the equipartition value, at which MHD is fully developed. We do this because later on we evaluate the GW spectrum generated by the magnetic source, and the time continuity of the source does affect the resulting GW spectrum (see Ref. [83] and section 3.3.4). Therefore, we assume that the magnetic field energy density is zero (continuous) at $t = t_{\rm in}$, $\tau = 0$; it then reaches its maximal value $\tilde{\rho}_B^*$ after a 'switching on' time which we set equal to the characteristic eddy turnover time, t_L^*, namely at $t_* = t_{\rm in} + t_L^*$. We therefore define $t_* \equiv t_{\rm in} + t_L^*$ as the time when turbulence is fully developed, and normalise also the energy injection scale as $\tilde{L}_* = \tilde{L}(t_*)$, $\tilde{L}(t_{\rm in}) = 0$.

- Direct cascade: the evolution laws are in this case

$$\tilde{\rho}_B(t) = \tilde{\rho}_B^* \begin{cases} \tau & \text{for } t_{\rm in} \le t < t_* \,, \quad \tau \le 1 \,, \\ \tau^{-2(n+3)/(n+5)} & \text{for } t \ge t_* \,, \quad \tau \ge 1 \,, \end{cases} \tag{3.13}$$

$$\tilde{L}(t) = \tilde{L}_* \tau^{2/(n+5)} \,, \tag{3.14}$$

where we may only consider $n > -2$ in order to recover the correct behavior with respect to time of the above quantities (*i.e.* decay for the energy and growth for the correlation scale). The above expressions go continuously to zero with $\tau \to 0$ and they have the asymptotic behavior found in Ref. [79] for $t \gg t_{\rm in} \geq t_L^*$, $\tau \gg 1$. Note that Ref. [79] uses a spectral index p which is related to n via $p = n + 2$. For simplicity, the parameter $\kappa_{\rm diss}$ of [79] is set to one, corresponding to $\gamma = 3\Gamma^2[(1+p)/2]/(3+p)/\Gamma^2[p/2]$.

The energy injection scale $\tilde{L}_*$ is determined by the physical process that generates the magnetic field and the turbulence. Generically it can be parametrised as a fraction of the horizon at the initial time. Therefore, we introduce the small parameter $\epsilon < 1$ defined by

$$\tilde{L}_* = \epsilon\, t_\in \ , \ \text{such that} \quad t_L^* \simeq \frac{\tilde{L}_*}{2v_L} = \frac{\epsilon}{2v_L} t_\in \ . \tag{3.15}$$

A typical value for causally generated turbulence is $\epsilon \simeq 10^{-2}$ (see for example [82]). The necessary condition to have a turbulent cascade is that $t_L^* \leq t_{\rm in}$, *i.e.* $v_L \geq \epsilon/2$. Eddies of the size of the horizon which move at the speed of light are the limiting case. Although it grows, the correlation length never becomes larger than the horizon. In fact one has

$$\frac{\tilde{L}(t)}{t} = \left[(2v_L)^2\, \epsilon^{n+3}\right]^{1/(n+5)} \left(1 - \frac{t_\in}{t}\right)^{2/(n+5)} \left(\frac{t_\in}{t}\right)^{(n+3)/(n+5)} \ , \tag{3.16}$$

which is smaller than one for all times $t \geq t_{\rm in}$. Indeed, for the initial period $t_\in \leq t \leq t_*$, the term $(1 - t_\in/t)^{2/(n+5)} \to 0$ and it dominates the above expression, while for $t \gg t_* > t_\in$ the asymptotic behaviour is controlled by the last term of the equation which keeps the correlation length smaller than the Hubble radius. This is shown in Fig. 3.1.

Even though the correlation length is growing, the spectral energy on a given comoving scale k is at best constant. On scales which are larger than the correlation scale, $k\tilde{L}(t) < 1$

$$\frac{d\tilde{\rho}_B(k,t)}{d\log k} \propto \tilde{\rho}_B(t)(k\tilde{L}(t))^{n+3} \, . \tag{3.17}$$

From Eqs. (3.13) and (3.14) it follows that during direct cascade $\tilde{L}^{n+3}(t)\tilde{\rho}_B(t) =$ constant, hence $d\tilde{\rho}_B/d\log k$ does not evolve on large scales. The same behaviour is observed in the free decay of the turbulent velocity field, and is related to the constancy in time of Loitsyansky invariant (see for example [145, 146, 147])

- Inverse cascade:
  During inverse cascade we assume that the magnetic field energy and correlation length evolve according to [79]

$$\tilde{\rho}_B(t) = \tilde{\rho}_B^* \begin{cases} \tau & \text{for } t_{\rm in} \leq t < t_* \, , \quad \tau \leq 1 \, , \\ \tau^{-2/3} & \text{for } t \geq t_* \, , \quad \tau \geq 1 \, , \end{cases} \tag{3.18}$$

$$\tilde{L}(t) = h_B \tilde{L}_* \tau^{2/3}, \tag{3.19}$$

where h_B is the initial fractional helicity: $h_B = 0$ corresponds to a non-helical mag-

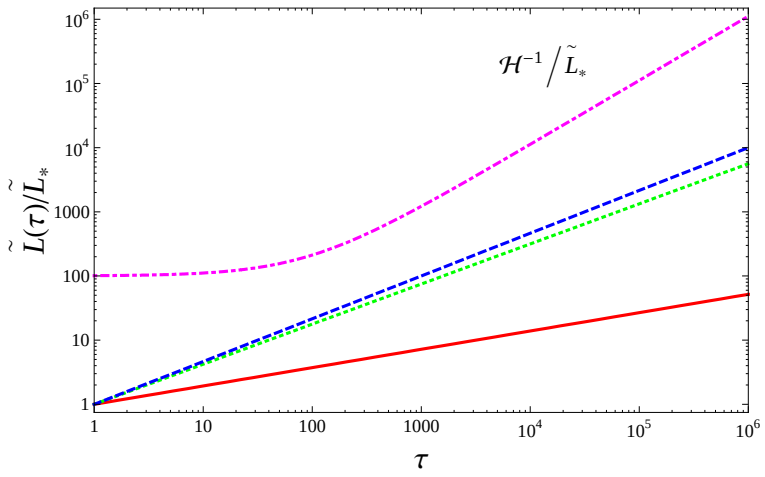

Figure 3.1: Time evolution of the comoving correlation length $\tilde{L}(\tau)$ as a function of τ for an inverse cascade (blue, dashed line) and for a direct cascade with the spectral indexes $n = 2$ (red, solid line) and $n = -1.8$ (green, dotted line). They are compared with the time evolution of the comoving Hubble radius in a radiation dominated background, in units of the correlation length $\tilde{L}_*$ (magenta, dot-dashed line).

netic field that remains non-helical for all its evolution (for which the above scaling relations do not apply), while $h_B = 1$ characterizes a maximally helical field. The above equations are again valid only for $p = n + 2 > 0$.

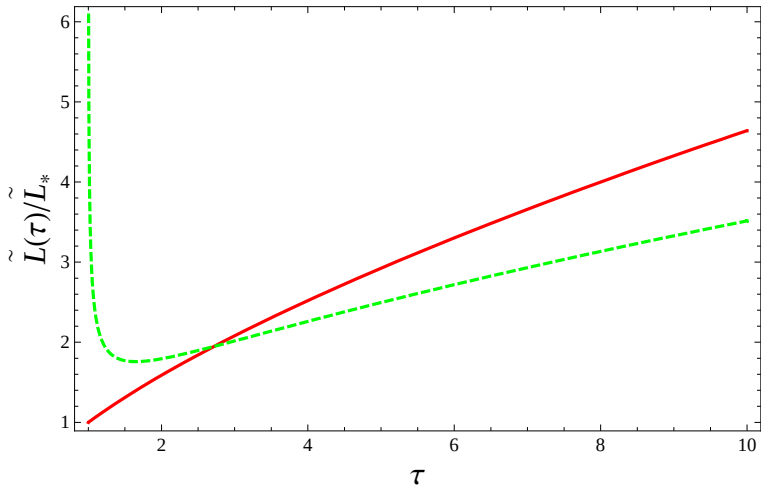

Figure 3.2: Time evolution of the comoving correlation length $\tilde{L}(\tau)$ as a function of τ during inverse cascade as given in Ref. [79] (green dashed line) and neglecting the logarithmic terms as in Eq. (3.19) (red solid line).

The original expression of Ref. [79] for $\tilde{L}(t)$ contains also a logarithmic term, and gives asymptotically a slower growth than Eq. (3.19), as can be seen in Fig. 3.2. In the following we neglect this logarithmic correction. Similarly, $\tilde{\rho}_B(t)$ given by Eq. (3.18) decays more rapidly than the full expression given in [79], due to the same

logarithmic correction (see Fig. 3.3). The limits on the magnetic field on large scales obtained using Eqs. (3.19) and (3.18) are less stringent than those one would obtain using the more accurate expression of [79]. Neglecting the logarithmic corrections is therefore a conservative assumption.

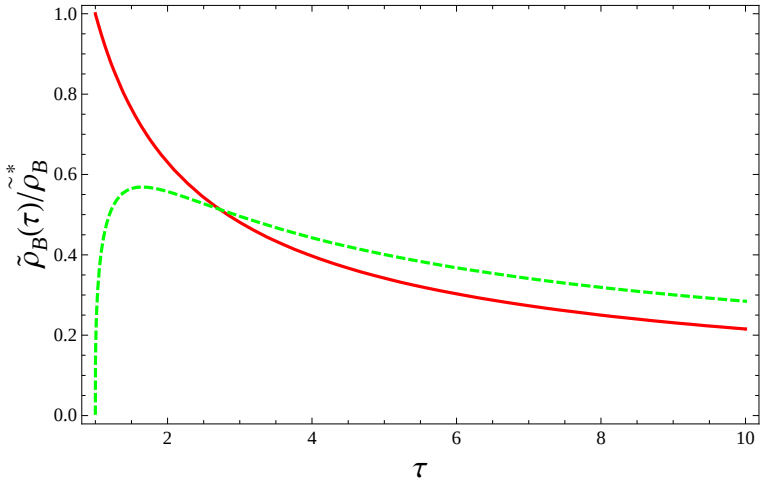

Figure 3.3: Time evolution of the magnetic energy density as a function of τ during inverse cascade as given in Ref. [79] (green dashed line) and neglecting the logarithmic terms as in Eq. (3.18) (red solid line).

Although the correlation length grows faster than in the direct cascade phase, it never becomes larger than the horizon even in this case (see Fig. 3.1). During the inverse cascade the product $\tilde{L}(t)\tilde{\rho}_B(t) = \tilde{L}_*\tilde{\rho}_B^*$ is constant. From Eq. (3.17) one sees that during the inverse cascade the spectral energy density is growing like $\tilde{L}^{n+2}(t)$ at large scales.

In Ref. [79] it is claimed that Eqs. (3.18), (3.19) apply only after a first phase during which the system behaves as if the magnetic helicity was zero, *i.e.* by direct cascade. Only when the magnetic field (with initial fractional helicity h_B) becomes maximally helical, the inverse cascade can start, and Eqs. (3.18) and (3.19) apply. This is probably a simplified picture: it seems more realistic that some amount of inverse cascade can happen as soon as an appreciable helical component has developed. For simplicity in our treatment we follow Ref. [79] and neglect this effect. Note however that this does not affect the final results, which are derived only for the case of a maximally helical magnetic field, for which the inverse cascade starts immediately. In the analysis of [79], in order to find the time at which the field becomes maximally helical one matches the product $\tilde{L}(t)\tilde{\rho}_B(t)$ (which is time dependent during direct cascade), to its constant value during the inverse cascade. This defines the transition time t_h

$$t_h = t_{\rm in}\left[1 + \frac{\epsilon}{2v_L} h_B^{-(n+5)/(2n+4)}\right] \ . \tag{3.20}$$

For a maximally helical magnetic field $t_h(h_B = 1) = t_*$. In general, for a given h_B, the second stage takes place for times $t > t_h \geq t_*$ and lasts until the time $t_{\rm fin}$ at which the turbulent phase ends (*c.f.* next section). Moreover, in the case of zero initial helicity, one has purely direct cascade: $t_h \to \infty$ when $h_B \to 0$ (this is true only if we restrict the value

of the spectral index to be $n > -2$, which we always do in the following).

3.2.3 The end of the turbulent phase and the dissipation scale

The turbulent phase ends when the Reynolds number on the scale of energy injection, $\tilde{L}(t)$, becomes of order unity [147]. In Appendix 3.6.1.1 we calculate the epoch at which turbulence ends for the EW and the QCD phase transitions, as well as for inflation with $T_* \sim 10^{14}$ GeV. The most important result from this calculation is that in all cases turbulence lasts for many Hubble times and therefore the source is not short lived. This finding and its consequences are the subject of [25]. For example, for a maximally helical field generated at the EW phase transition we find the final temperature $T_{\rm fin} \simeq 21\,{\rm MeV}$ (note that turbulence ends before nucleosynthesis [78]).

In Appendix 3.6.1.2 we determine the dissipation scale which is the scale $\tilde{l}_{\rm diss}(t)$ below which energy injection no longer leads to turbulence but is simply dissipated. This scale determines the time-dependent UV cutoff of our spectra. The evolution of both the correlation length $\tilde{L}(T)$ and the dissipation scale $\tilde{l}_{\rm diss}(T)$ for the EW phase transition is shown in Fig. 3.4. The dissipation scale grows faster than the correlation length and turbulence terminates roughly when the two curves cross.

In the evaluation of these scales, we often use the approximation $T_1/T_2 \simeq t_2/t_1$, which neglects changes in the number of effective relativistic degrees of freedom. Moreover in the following we do not distinguish among the temperatures corresponding to the initial time $t_{\rm in}$ and to the time at which turbulence is fully developed t_*, since they are separated by less than one Hubble time. Therefore, we generically indicate with T_* the temperature at which the generation mechanism for the magnetic field takes place.

After the end of turbulence the magnetic field simply stays frozen in the fluid at scales larger than the dissipation scale $\tilde{l}_{\rm diss}(T_{\rm fin}) \simeq \tilde{L}(T_{\rm fin})$. Eventually other dissipation processes, due to radiation viscosity, become active [84, 85].

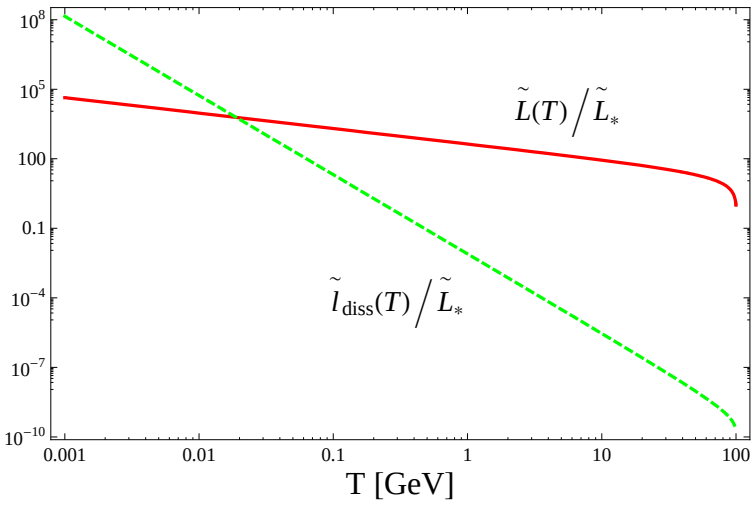

Figure 3.4: The evolution of the comoving magnetic correlation length (red solid line) and dissipation length (green dashed line), in the inverse cascade phase for the EW phase transition. Both quantities have been normalized with respect the initial value of the comoving correlation length $\tilde{L}_*$.

3.3 The GW spectrum

3.3.1 Generation of GWs from sources

In this section we calculate the spectrum of the GWs generated by a helical magnetic field. We restrict our analysis to the case of maximally helical fields. This calculation has also been performed in Ref. [148], where however stationarity in time of both the source and the GWs has been assumed. This invariance under time translation of the source seems to us justified only if the time over which the source is active is much shorter than a Hubble time. As we have argued in Section 3.2 and derived in Appendix 3.6.1.1, the Reynolds number remains larger than unity for the scales of interest over many Hubble times. Therefore we want to re-calculate the GW spectrum without the assumption of stationarity. We shall then compare our results with Ref. [148].

The parity invariant part the GW spectrum, which is the part which contributes to the energy density, is of the form [82, 130]

$$\langle \dot{h}_{ij}(\mathbf{k},t)\dot{h}^{*}_{ln}(\mathbf{q},t)\rangle \;=\; \frac{(2\pi)^3}{4}\mathcal{M}_{ijln}(\hat{\mathbf{k}})\delta^3(\mathbf{k}-\mathbf{q})|\dot{h}|^2(k,t)\ . \tag{3.21}$$

Here $\mathcal{M}_{ijln}(\hat{\mathbf{k}})$ is the GW polarization tensor normalized such that $\mathcal{M}_{ijij}=4$ and $|\dot{h}|^2(k,t)$ is related to the GW energy spectrum as follows [131, 82, 130]:

$$\begin{aligned}\tilde{\rho}_{\rm GW}(t) &= \frac{\langle \dot{h}_{ij}\dot{h}_{ij}\rangle}{32\pi G a^2(t)} = \int_0^\infty \frac{dk}{k}\frac{d\tilde{\rho}_{\rm GW}(k,t)}{d\log k}\ ,\\ \frac{d\tilde{\rho}_{\rm GW}(k,t)}{d\log k} &= \frac{k^3|\dot{h}|^2(k,t)}{8(2\pi)^3 G a^2(t)}\ .\end{aligned} \tag{3.22}$$

Our definition of the metric perturbations h_{ij} differs by a factor 2 with the one in [82, 130] and agrees with [131], $ds^2 = a^2(t)\left[-dt^2+(\delta_{ij}+h_{ij})dx^i dx^j\right]$. The Fourier space expression of the projection tensor onto the transverse traceless component, $\mathcal{M}_{ijln}(\hat{\mathbf{k}})$, is given explicitly *e.g.* in Ref. [130].

The evolution equation which governs the generation of GWs in an expanding universe is simply, see *e.g.* [132]

$$\ddot{h}_{ij}+2\frac{\dot{a}}{a}\dot{h}_{ij}+k^2 h_{ij} = 16\pi G a^2 \Pi_{ij}\ , \tag{3.23}$$

where the source term is the tensor contribution to the anisotropic stress of the energy momentum tensor of the source. In our case these come from the magnetic field and we relate the tensor anisotropic stress spectrum to the magnetic field spectrum in the next section. In terms of the comoving anisotropic stress $\tilde{\Pi}_{ij} = a^4\Pi_{ij}$ the above equation becomes

$$\ddot{h}_{ij}+2\frac{\dot{a}}{a}\dot{h}_{ij}+k^2 h_{ij} = 16\pi G\frac{\tilde{\Pi}_{ij}}{a^2}\ . \tag{3.24}$$

For GWs generated by a primordial magnetic field we cannot neglect the expansion of the Universe, since this source is active over a period which is much longer than a Hubble time. In terms of the rescaled variable $\bar{h}_{ij}\equiv a h_{ij}$, Eq. (3.24) becomes

$$\ddot{\bar{h}}_{ij}+\left(k^2-\frac{\ddot{a}}{a}\right)\bar{h}_{ij} = 16\pi G\frac{\tilde{\Pi}_{ij}}{a}\ . \tag{3.25}$$

In a radiation dominated background with $a \propto t$ so that $\ddot{a} = 0$,

$$\ddot{\bar{h}}_{ij} + k^2 \bar{h}_{ij} = 16\pi G \frac{\tilde{\Pi}_{ij}}{a} \ . \tag{3.26}$$

Since initially $h_{ij} = \dot{h}_{ij} = 0$, the solution of the the above differential equation is given by the convolution of the source with the retarded Green function $\mathcal{G}(k, t_1, t_2) = \sin(k(t_1 - t_2))$,

$$\bar{h}_{ij}(\mathbf{k}, x < x_{\rm fin}) = \frac{16\pi G}{k^2} \int_{x_\in}^{x} dy \ \frac{\tilde{\Pi}_{ij}(\mathbf{k}, y)}{a(y)} \sin(x - y), \tag{3.27}$$

where we have introduced $x \equiv kt_1$ and $y \equiv kt_2$.

We assume that the source is active until the final time $t_{\rm fin}$ at which turbulence terminates and the anisotropic stress become negligible. This is not completely correct, since after this final time we have no longer an inverse cascade, but the magnetic field is frozen in and evolves according to flux freezing. However, this is relevant only for GW production at scales which are super-horizon at $t_{\rm fin}$, and therefore it does not affect the peak region of the GW spectrum and the value of the integrated energy density, which determines our constraints (see Ref. [82] and section 3.3.3).

Once the source has decayed, GWs are freely propagating. This behavior is described by the homogeneous solution of Eq. (6.33),

$$\bar{h}_{ij}(\mathbf{k}, t > t_{\rm fin}) = A_{ij}(\mathbf{k}) \sin(kt - kt_{\rm fin}) + B_{ij}(\mathbf{k}) \cos(kt - kt_{\rm fin}) \ . \tag{3.28}$$

The coefficients A_{ij} and B_{ij} are determined by requiring continuity of $\bar{h}_{ij}$ and $\dot{\bar{h}}_{ij}$ at $t = t_{\rm fin}$. Matching (3.28) to the result from Eq. (3.27) yields

$$\begin{aligned} A_{ij}(\mathbf{k}) &= \frac{16\pi G}{k^2} \int_{x_\in}^{x_{\rm fin}} dy \ \frac{\tilde{\Pi}_{ij}(\mathbf{k}, y)}{a(y)} \cos(x_{\rm fin} - y) \ , \\ B_{ij}(\mathbf{k}) &= \frac{16\pi G}{k^2} \int_{x_\in}^{x_{\rm fin}} dy \ \frac{\tilde{\Pi}_{ij}(\mathbf{k}, y)}{a(y)} \sin(x_{\rm fin} - y) \ . \end{aligned} \tag{3.29}$$

With Eq. (3.21), using the above solution for $\bar{h}_{ij}$, we obtain for $t > t_{\rm fin}$

$$\begin{aligned} |\dot{h}|^2(k, t > t_{\rm fin}) &= \frac{1}{2a^2}(k^2 + \mathcal{H}^2) \left(\langle A_{ij} A_{ij}^* \rangle + \langle B_{ij} B_{ij}^* \rangle \right) \\ &= \frac{(k^2 + \mathcal{H}^2)}{2a^2} \left(\frac{16\pi G}{k^2} \right)^2 \int_{x_\in}^{x_{\rm fin}} dy \int_{x_\in}^{x_{\rm fin}} dz \ \cos(z - y) \frac{\tilde{\Pi}_B(k, y, z)}{a(y) a(z)} \ , \end{aligned} \tag{3.30}$$

where we have set $y = kt_1$ and $z = kt_2$. Furthermore, we have introduced the anisotropic stress unequal time power spectrum,

$$\langle \tilde{\Pi}_{ij}(\mathbf{k}, t_1) \tilde{\Pi}_{ij}^*(\mathbf{q}, t_2) \rangle = (2\pi)^3 \delta^3(\mathbf{k} - \mathbf{q}) \tilde{\Pi}_B(k, t_1, t_2) \ . \tag{3.31}$$

To obtain Eq. (3.30) we have not only performed an ensemble average, but also averaged over several periods so that $\langle \sin^2(kt) \rangle = \langle \cos^2(kt) \rangle = 1/2$ and $\langle \cos(kt) \sin(kt) \rangle = 0$. At times t at which we can observe a GW with wave number k, the latter must be largely sub-horizon so that $kt \gg 1$. We therefore may neglect the second term in the pre-factor

$(k^2+\mathcal{H}^2) \simeq k^2(1+1/(kt)^2)$. Rewriting Eq. (3.30) as integral over time, we find with (6.37)

$$\frac{d\rho_{\rm GW}(k,t)}{d\log k} = \frac{2G}{\pi a^4(t)} k^3 \int_{t_\in}^{t_{\rm fin}} dt_1 \int_{t_\in}^{t_{\rm fin}} dt_2 \ \cos(kt_1 - kt_2) \frac{\tilde{\Pi}_B(k,t_1,t_2)}{a(t_1)a(t_2)} \ . \tag{3.32}$$

3.3.2 Magnetic anisotropic stresses

According to Eq. (3.32), in order to determine the GWs produced by a cosmic magnetic field, we need to calculate the unequal time correlator of the tensor type magnetic stress, $\tilde{\Pi}_B(k,t_1,t_2)$, which sources GWs. By statistical isotropy, the tensor type magnetic stress 2-point function has the same tensor structure as the one of GWs,

$$\langle \tilde{\Pi}_{ij}(\mathbf{k},t) \tilde{\Pi}_{ln}(\mathbf{q},t) \rangle = \frac{(2\pi)^3}{4} \delta^3(\mathbf{k}-\mathbf{q}) \left[\mathcal{M}_{ijln}(\hat{\mathbf{k}}) \tilde{\Pi}_B(k,t,t) + \mathcal{A}_{ijln}(\hat{\mathbf{k}}) \tilde{\Pi}_A(k,t,t) \right] \ . \tag{3.33}$$

In the above expression $\tilde{\Pi}_A(k,t,t)$ is the term of odd parity due to the non-vanishing helicity of the magnetic field. It it does not contribute to the GW energy density but only to their polarization [130]. The odd parity projection tensor is also given in [130].
Following [130], we use Wick's theorem to reduce this four point correlator to the convolution of two 2-point correlators. The ansatz (3.5) then gives for the equal time correlator

$$\tilde{\Pi}_B(k,t,t) = \mathcal{N}_1 \int \mathrm{d}^3q \left[(1+\gamma^2)(1+\alpha^2) S(q,t) S(|\mathbf{k}-\mathbf{q}|,t) + 4\gamma\alpha A(q,t) A(|\mathbf{k}-\mathbf{q}|,t) \right] \tag{3.34}$$

where we set $\mathcal{N}_1 = 2/(4\pi)^5$, $\alpha \equiv \hat{\mathbf{k}} \cdot (\widehat{\mathbf{k}-\mathbf{q}})$ and $\gamma \equiv \hat{\mathbf{k}} \cdot \hat{\mathbf{q}}$. In the case of a maximally helical magnetic field, the symmetric and antisymmetric parts of the magnetic field spectrum are equal on sub-horizon scales,

$$|A(k,t)| = S(k,t) \ , \quad kt > 1 \, . \tag{3.35}$$

On super-horizon scales helicity is suppressed (see *e.g.* [68]). In order to account for this dependence, we introduce the function $\Sigma(t,q,|\mathbf{k}-\mathbf{q}|)$ in the integral (3.34)

$$\Sigma(t,q,|\mathbf{k}-\mathbf{q}|) = \begin{cases} 1 \ , & \text{for } qt \geq 1 \text{ and } |\mathbf{k}-\mathbf{q}|t \geq 1 \, , \\ 0 \ , & \text{otherwise} \, , \end{cases} \tag{3.36}$$

and we set

$$\tilde{\Pi}_B(k,t,t) \simeq \mathcal{N}_1 \int \mathrm{d}^3q \left[(1+\gamma^2)(1+\alpha^2) + 4\gamma\alpha \Sigma(t,q,|\mathbf{k}-\mathbf{q}|) \right] S(q,t) S(|\mathbf{k}-\mathbf{q}|,t) \, . \tag{3.37}$$

The integral (3.37) for the equal time correlator is evaluated numerically and the results is approximated by an analytical fit. More details on this are given in Appendix 3.6.2.1. Here we simply present the results for two exemplary values of the spectral index, a causal spectrum with $n = 2$ and a red spectrum with $n = -1.8$:

$$\tilde{\Pi}_B(K,t) \simeq \frac{\mathcal{N}_2}{2\pi} \tilde{L}^3(t) \tilde{\rho}_B^2(t) \frac{0.034}{1 + (K/12)^4 + (K/6)^{7/2}} \, , \qquad n = 2 \ , \tag{3.38}$$

$$\tilde{\Pi}_B(K,t) \simeq \frac{\mathcal{N}_2}{2\pi} \tilde{L}^3(t) \tilde{\rho}_B^2(t) \frac{(K/40)^{-3/5}}{1 + (K/1.4)^{29/10}} \, , \qquad n = -1.8 \ . \tag{3.39}$$

Here

$$\mathcal{N}_2 \equiv \left[\frac{\Gamma\left(\frac{2n+7}{4}\right)}{\Gamma\left(\frac{1}{4}\right)\Gamma\left(\frac{n+3}{2}\right)}\right]^2 = \begin{cases} 0.11 & \text{for } n = 2\ , \\ 0.04 & \text{for } n = -1.8\ . \end{cases}$$

3.3.3 The GW spectrum produced by a maximally helical magnetic field

Let us now consider a magnetic field with maximal initial helicity $h_B = 1$, which immediately (*i.e.* at $t_* = t_{\rm in} + t_L^*$) develops an inverse cascade. To compute the GWs produced by this field, we have to make assumptions about the unequal time correlator of the anisotropic stress. There are different possibilities which are discussed in the literature [83, 117].

We consider a completely coherent source, namely a source with deterministic time evolution for which the unequal time correlator is just the product of the square root of the equal time correlators at the different times,

$$\tilde{\Pi}_B(k, t_1, t_2) = \sqrt{\tilde{\Pi}_B(k, t_1, t_1)}\sqrt{\tilde{\Pi}_B(k, t_2, t_2)}\ . \tag{3.40}$$

This is not only the simplest approximation, but the results obtained in this case are also quite close to the results from a model with exponential decoherence as discussed in Ref. [25]. Furthermore, for colliding bubbles where numerical simulations exist, the totally coherent approximation is in good agreement with the numerical results [83]. This justifies our hope that this approximation captures the main features of the resulting spectrum and, especially, that it gives a good estimate for the total GW energy density. Note also that this assumption has usually been made in previous works, for a magnetic field which is simply redshifting with the expansion of the universe [77, 149]. A comparision of different approximations can be found in Refs. [83, 117].

For a completely coherent source we obtain

$$\frac{d\rho_{\rm GW}(k,t)}{d\log k} \simeq \frac{2G}{\pi a^4(t)}k^3 \left\{ \left[\int_{t_\in}^{t_{\rm fin}} dt'\ \cos(kt')\frac{\sqrt{\tilde{\Pi}_B(k,t')}}{a(t')}\right]^2 + \left[\int_{t_\in}^{t_{\rm fin}} dt'\ \sin(kt')\frac{\sqrt{\tilde{\Pi}_B(k,t')}}{a(t')}\right]^2 \right\}\ . \tag{3.41}$$

In order to compute the above integrals, we substitute approximations (3.38) for the anisotropic stresses of a magnetic field with a blue spectrum ($n = 2$), or (3.39) for a red spectrum ($n = -1.8$).

We fix the final time at which the source of GWs ceases to be active as the time given by the end of turbulence, when $\mathrm{Re}\,(L(T_{\rm fin}^{(1)})) \simeq 1$. This corresponds to the time at which the inertial range ($K \gtrsim 1$) is entirely dissipated, when the dissipation scale has grown to reach the correlation length, $\tilde{l}_{\rm diss}(T_{\rm fin}^{(1)}) \simeq \tilde{L}(T_{\rm fin}^{(1)})$. This condition determines the value of the final temperature $T_{\rm fin}^{(1)}$ at which turbulence terminates (in principle, the magnetic field is not damped after this temperature, but simply stays frozen in the fluid and keeps on generating GWs; however, here for simplicity we restrict to GW production during the turbulent phase, an assumption which, as previously mentioned, does not affect our result in a relevant way).

In Appendix 3.6.1.1 we estimate the final temperature for inverse cascade turbulence initiated at different times:

$$T_{\rm fin}^{(1)} \simeq 21\,{\rm MeV} \text{ for the EW phase transition,} \tag{3.42}$$

$$T_{\rm fin}^{(1)} \simeq 5\,{\rm MeV} \text{ for the QCD phase transition,} \tag{3.43}$$

$$T_{\rm fin}^{(1)} \simeq 1\,{\rm GeV} \text{ for inflation.} \tag{3.44}$$

The final time $t_{\rm fin}^{(1)}$ corresponding to these temperatures is given by [132]

$$t_{\rm fin}^{(1)} = t(T_{\rm fin}^{(1)}) \simeq 0.5 \left(g_{\rm eff}(T_{\rm fin}^{(1)})\right)^{-1/6} \frac{m_{Pl}}{T_0 T_{\rm fin}^{(1)}}\,. \tag{3.45}$$

On the other hand, we know that the dissipation scale grows more rapidly than the correlation scale. Therefore, when a given wavelength, smaller than the correlation scale but initially larger than the dissipation scale, becomes of the order of the dissipation scale $2\pi/k \simeq \tilde{l}_{\rm diss}(T_{\rm fin}^{(2)}(k))$, turbulence is dissipated on this scale and the GW source has decayed. This defines a second, k-dependent final temperature $T_{\rm fin}^{(2)}(k) \geq T_{\rm fin}^{(1)}$ given by

$$\tilde{l}_{\rm diss}(T_{\rm fin}^{(2)}(k)) = 2\pi/k = \tilde{L}_*/K_*\,.$$

Since $T_{\rm fin}^{(2)}(k) > T_{\rm fin}^{(1)}$, the final time of integration for the wave number k is $t_{\rm fin}^{(2)}(k) = t(T_{\rm fin}^{(2)}(k)) < t_{\rm fin}^{(1)}$.

In Appendix 3.6.1.2 we derive analytical expressions for $t_{\rm fin}^{(2)}(k)$, taking into account the time evolution of the dissipation length, see Eqs. (3.92) and (3.93). The final time $t_{\rm fin}$ is given by

$$t_{\rm fin}(k) = \min\left[t_{\rm fin}^{(1)}, t_{\rm fin}^{(2)}(k)\right]\,. \tag{3.46}$$

Indeed, for scales smaller than $\tilde{L}(t_{\rm fin}^{(1)})$, hence $K(t_{\rm fin}^{(1)}) > 1$, $t_{\rm fin}(k)$ is equal to $t_{\rm fin}^{(2)}(k)$, while larger scales are dissipated only at the end of turbulence, $t_{\rm fin}^{(1)}$.

The K_*-dependence of $t_{\rm fin}$ for magnetic fields generated at the EW phase transition and at inflation is plotted in Fig. 3.5. The final time starts to decrease for small wavelengths, namely around $K_* = K_1^* \simeq 10^{-3}$ for the EW transition and at $K_* = K_1^* \simeq 10^{-9}$ for inflation. This value is given by

$$1 = K_1(T_{\rm fin}) = K_1^* \frac{\tilde{L}(T_{\rm fin})}{\tilde{L}_*} = K_1^* \tau_{\rm fin}^{2/3} \simeq K_1^* \left(\frac{2v_L}{\epsilon}\frac{T_*}{T_{\rm fin}}\right)^{2/3}\,, \tag{3.47}$$

so that

$$K_1^* \simeq \left(\frac{\epsilon}{2v_L}\frac{T_{\rm fin}}{T_*}\right)^{2/3}\,. \tag{3.48}$$

To calculate the integrals (3.41) we use Eqs. (3.38) and (3.39) for the time evolution of the magnetic anisotropic stress. More details on the explicit form of (3.41) are given in

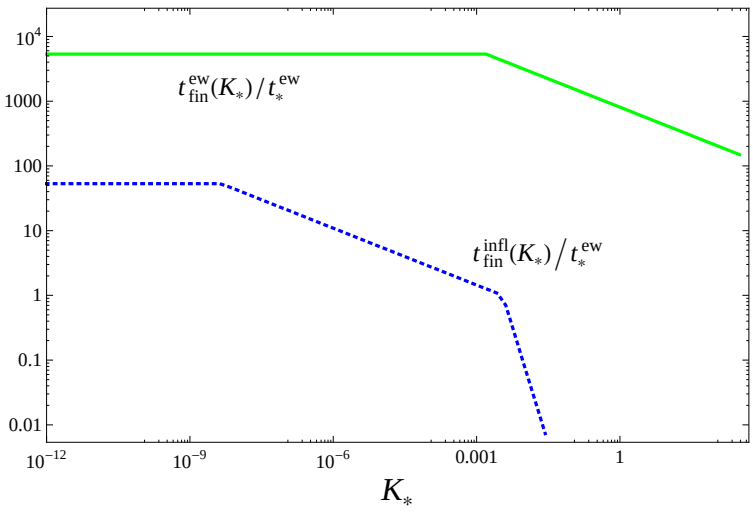

Figure 3.5: K_*-behavior of $t_{\rm fin}$ for the EW phase transition (green, solid line) and for inflation (blue, dotted line), both normalized with respect $t_*^{\rm ew}$.

Appendix 3.6.2.2. The GW energy spectrum can be written in the form

$$\frac{d\Omega_{\rm GW}(k,t_0)}{d\log k} \simeq 3\mathcal{N}_2 \left(\frac{\bar{g}}{g_0}\right)^{1/3} \frac{(\tilde{\Omega}_B^*)^2}{\Omega_{\rm rad}} \mathcal{I}_{\rm GW}(K_*) \,, \tag{3.49}$$

which holds for magnetic fields with both a blue and a red spectrum. Here $\bar{g}$ denotes an average number of relativistic degrees of freedom while the source is active. We neglect this factor in the following (it enters the limits for the magnetic field amplitude only as $(\bar{g}/g_0)^{1/12}$). The integral $\mathcal{I}_{\rm GW}(K_*)$ determines the spectral shape. We have calculated it numerically for both cases: a magnetic field generated at the EW phase transition with a blue spectrum, with parameters $n = 2$, $\epsilon = 0.01$ and $v_L^2 = 0.2$, and one generated at inflation with a red spectrum, setting the parameters to $n = -1.8$ and $\epsilon = v_L = 1$. This means that in the inflationary case, the initial stirring scale is set equal to the horizon size, and the eddy turnover time is half the initial Hubble time, $t_L^* = t_{\rm in}/2$ [2].

For a causal magnetic field spectrum with $n = 2$, the GW density parameter in units of $(\tilde{\Omega}_B^*)^2/\Omega_{\rm rad}$ is shown in Fig. 3.6.

Below the peak frequency, located at $k \simeq 2\pi/t_L^*$, the numerical result can be approximated by

$$\frac{d\Omega_{\rm GW}(k,t_0)}{d\log k} \simeq 3\mathcal{N}_2 \frac{(\tilde{\Omega}_B^*)^2}{\Omega_{\rm rad}} \begin{cases} \epsilon_1 K_*^3 & \text{for } 0 < K_* < \tilde{L}_*/(2\pi\, t_{\rm fin}) \,, \\ \epsilon_2 K_*^2 & \text{for } \tilde{L}_*/(2\pi\, t_{\rm fin}) < K_* < \tilde{L}_*/(2\pi\, t_*) \,, \\ \epsilon_3 K_*^{1/2} & \text{for } \tilde{L}_*/(2\pi\, t_*) < K_* < \tilde{L}_*/t_L^* \,. \end{cases} \tag{3.50}$$

[2] Note that in the inflationary case, we could as well have chosen the stirring scale to coincide with the horizon at any time. One could argue, in fact, that as soon as a scale enters the horizon, it causes a stirring of the cosmic fluid, acting as the stirring scale. We have evaluated the GW spectrum also setting $\tilde{L}(\tau) \propto \mathcal{H}^{-1} \propto \tau$ (instead of $\propto \tau^{2/3}$) and consequently $\tilde{\rho}_B(\tau) \propto \tau^{-1}$ to maintain the inverse cascade. We did not find an appreciable difference among the two resulting GW spectra.

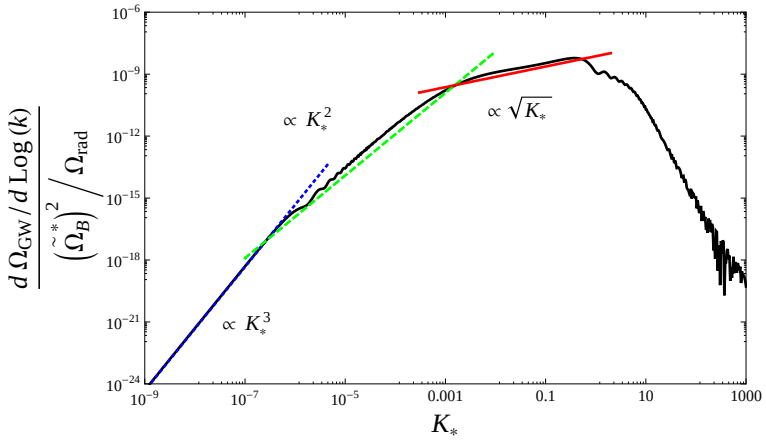

Figure 3.6: The GW energy density spectrum from a causal magnetic field $n = 2$ generated at the EW phase transition with maximal initial helicity $h_B = 1$. The spectrum grows like k^3 (blue, dotted line) up to the horizon at the end of the turbulent phase, $k \simeq t_{\rm fin}^{-1}$. Then the slope is given by k^2 (green, dashed line) up to the initial horizon $k \simeq t_*^{-1}$ and by $\sqrt{k}$ (red, solid line) up to the peak at $k \simeq (2\pi)/t_L^*$. Above the peak frequency the GW spectrum decays rapidly. For the EW phase transition one has $f/{\rm mHz} = 4\,K_*$. The wiggles in the spectrum are due to the coherent approximation (interference effects in the integration of Eq. (3.41)).

A part from the peak, the spectrum shows features at wave numbers corresponding to the characteristic times of the source: $k \simeq t_{\rm fin}^{-1}$ and $k \simeq t_*^{-1}$ ($t_{\rm in}$ is too close to t_* to be distinguishable). More details on the fit, including the values of the parameters ϵ_i, are given in Appendix 3.6.2.3. Using the above approximation (3.50), we find that the integrated energy density parameter of GWs today is approximately given by

$$\Omega_{\rm GW}(t_0) = \int_0^\infty \frac{dk}{k}\frac{d\Omega_{\rm GW}(k,t_0)}{d\log k} \simeq 6\,\mathcal{N}_2\frac{(\tilde{\Omega}_B^*)^2}{\Omega_{\rm rad}}\,\epsilon_3\sqrt{\frac{\tilde{L}_*}{t_L^*}} \simeq 2\times 10^{-8}\,\frac{(\tilde{\Omega}_B^*)^2}{\Omega_{\rm rad}}\,. \qquad (3.51)$$

Here we have neglected the decaying part of the GW spectrum, since the main contribution to the integrated energy density $\Omega_{\rm GW}$ comes from the part of the spectrum close to the peak $k \simeq 2\pi/t_L^*$. For the numerical value, we have inserted $\epsilon = 0.01$ and $v_L^2 = 0.2$ for a magnetic field generated at the EW phase transition with $T_* = 100\,{\rm GeV}$. The GW spectrum from a magnetic field generated at the QCD phase transition, $T_* = 100$ MeV, for the same values of ϵ and v_L is very similar, and in particular it has the same amplitude at the peak.

Next we consider an inflationary magnetic field with red spectrum $n = -1.8$. In this case we have to use the anisotropic stress given in Eq. (3.39). The resulting spectrum is

plotted in Fig. 3.7, and below the peak frequency it can be approximated by

$$\frac{\mathrm{d}\Omega_{\rm GW}(k,t_0)}{\mathrm{d}\log k} \simeq 3\mathcal{N}_2\frac{(\tilde{\Omega}_B^*)^2}{\Omega_{\rm rad}}\begin{cases}\epsilon_4 K_*^{2n+6}, & \text{for } 0<K_*<\frac{\tilde{L}_*}{2\pi\, t_{\rm fin}}\,,\\ \epsilon_5 K_*^{(2n+10)/3}, & \text{for } \frac{\tilde{L}_*}{2\pi\, t_{\rm fin}}<K_*<\left(\frac{(4\pi)^5}{R_*^9}\right)^{1/7},\\ \epsilon_6 K_*^{-(2+6n)/5}, & \text{for } \left(\frac{(4\pi)^5}{R_*^9}\right)^{1/7}<K_*<\frac{\tilde{L}_*}{t_L^*}\simeq 2\,.\end{cases} \tag{3.52}$$

Here, the K_*-dependence is written in terms of the general spectral index n, and it is valid for any $n<-3/2$. On the other hand, the values of the matching constants ϵ_i are derived in Appendix 3.6.2.3 under the assumption $n=-1.8$.

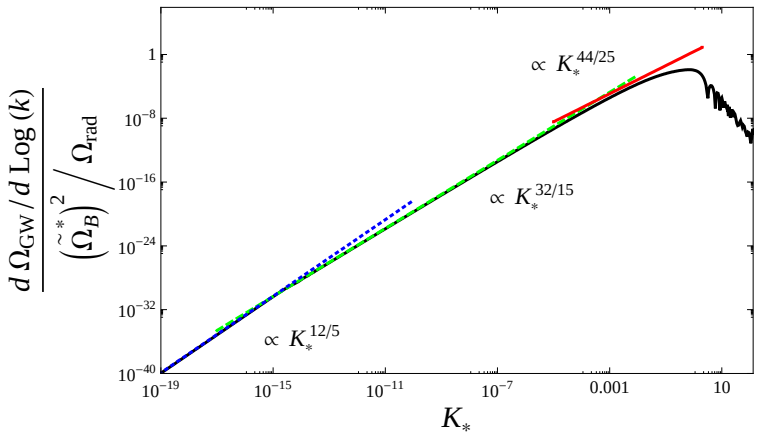

Figure 3.7: GW energy density spectrum from an inflationary magnetic field with red spectrum $n=-1.8$ and maximal initial helicity $h_B=1$. The analytically expected behavior is also indicated (*c.f.* Eq. (3.52)): $\propto K_*^{2n+6}$ (blue, dotted line), $\propto K_*^{(2n+10)/3}$ (green, dashed line) and $\propto K_*^{-(2+6n)/5}$ (red, solid line). For inflation one has $f/\mathrm{Hz}\simeq 10^7\,K_*$. Also here, the coherent approximation leads to wiggles on small scales.

Neglecting the decaying part of the GW spectrum, and using the slope $K_*^{-(2+6n)/5}$ up to the peak $k\simeq 2\pi/t_L^*$, we find the total GW energy density parameter:

$$\begin{aligned}\Omega_{\rm GW}(t_0) &\simeq 3\mathcal{N}_2\frac{(\tilde{\Omega}_B^*)^2}{\Omega_{\rm rad}}\left(\frac{-5}{2+6n}\right)\epsilon_6\left(\frac{\tilde{L}_*}{t_L^*}\right)^{-(2+6n)/5} \qquad n<-\frac{3}{2} \\ &\simeq 5.2\,\frac{(\tilde{\Omega}_B^*)^2}{\Omega_{\rm rad}}\,,\end{aligned} \tag{3.53}$$

Note that this approximation causes an overestimation of the total GW energy density of about three orders of magnitude. However, this does not affect the bounds on the magnetic field amplitude significantly: it translates into a bound that is stronger by about the 20% (see section 3.4). For the numerical value in the last equality of (3.53), we have inserted the value $n=-1.8$ and $\epsilon=v_L=1$.

Finally, to make contact with future observations, we express the GW spectra in terms

of the GW amplitude as function of the frequency f. For this we use [150]

$$h(f) = 1.26 \times 10^{-18} h_0 \sqrt{\Omega_{\rm GW}(f)} \left(\frac{\rm Hz}{f}\right) \ , \tag{3.54}$$

where the frequency is $f = k/(2\pi)$ and

$$\Omega_{\rm GW}(f) \equiv \left.\frac{{\rm d}\Omega_{\rm GW}(k,t_0)}{{\rm d}\log k}\right|_{k=2\pi f} .$$

The behavior of $h(f)$ for a causal and for an inflationary produced magnetic field, choosing a maximal magnetic field amplitude of $\Omega_B^* \simeq 0.1$, is plotted in Fig. 3.8. For another magnetic field density parameter the resulting amplitude $h(f)$ is simply rescaled by the factor $\Omega_B^*/0.1$.

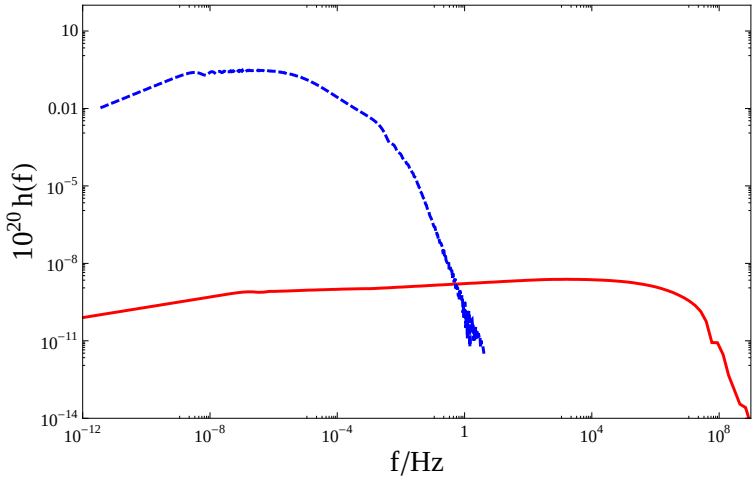

Figure 3.8: The GW amplitude $h(f)$ as a function of frequency from a maximally helical magnetic field with $\Omega_B^* \simeq 0.1$. Blue, dotted: causal generation at the EW phase transition with $n = 2$; red, solid: generation during inflation with $n = -1.8$.

The result for a magnetic field with a blue spectrum, shown in Fig. 3.8, agrees qualitatively with the one obtained in Ref. [148] . The position of the peak is the same, although the amplitude is higher in Ref. [148] by nearly one order of magnitude. This may come from the different assumptions for the unequal time correlator: in [148] the source is assumed to be stationary with exponential decorrelation, while we choose a completely coherent source. Moreover, in the magnetic energy spectrum, we have modelled the transition from the $k^{n+2}-$behaviour at low wave number to the inertial range, while Ref. [148] extends the Kolmogorov spectrum down to $k = 2\pi/\tilde{L}_*$. We have experienced that this leads to a significant overestimation of the peak amplitude [82]. Furthermore, the low frequency tail of the spectrum in [148] grows as $\sqrt{f}$, whereas in our case it becomes constant for $f > 1/t_{\rm fin}$: this is due to the fact that our source is long lasting, while theirs lasts for less than one Hubble time (see [25]).

For $\Omega_B^* \simeq 0.1$, the EW result is somewhat below the sensitivity range of LISA [13, 14, 15, 16]. On the other hand, the inflationary result is much below any proposed experiment: even though the energy density is higher, much of it is at high frequency, resulting in a

very low gravitational wave amplitude (see Fig. 3.8).

3.3.4 The peak position

In Ref [83] it has been argued that approximating the source of GWs by a discontinuous function might influence the decay law and even the peak position of the resulting GW spectrum. Therefore, as already discussed in section 3.2.2, in this work we model the 'switching on' process and avoid a discontinuous source function. Here we compare our result with what we would have obtained assuming a discontinuous source.

Fig. 3.9 shows the results for a continuous source and for a discontinuous one where the inverse cascade starts instantaneously at $t = t_*$. The predictions of Ref. [83] are confirmed: in the discontinuous case the peak is no longer at t_L^* but rather at $\tilde{L}_* \simeq t_L^*/(2v_L)$, leading to an over estimate of the resulting GW output. Therefore, it is important to take into account continuity.

In order to further clarify this issue, we vary the initial speed v_L, which relates the initial correlation length $\tilde{L}_*$ and the characteristic turnover time $t_L^* \simeq \tilde{L}_*/(2v_L)$. We fix it to $v_L = 10^{-2}$ so that $\tilde{L}_*$ and t_L^* are clearly separated: $t_L^* \simeq 10^2 \tilde{L}_*$. As can be seen in Fig. 3.9, in the discontinuous case the peak position is independent of the velocity v_L, while in the continuous one it is located at $k = 2\pi/t_L^*$.

Summarising, having assumed that the magnetic field processed by MHD turbulence needs a characteristic time of order t_L^* to 'form' induces a peak in the GW spectrum at a wave number corresponding to this characteristic time. If the field builds up much faster, almost instantaneously, the peak can move to $k = 2\pi/\tilde{L}^*$.

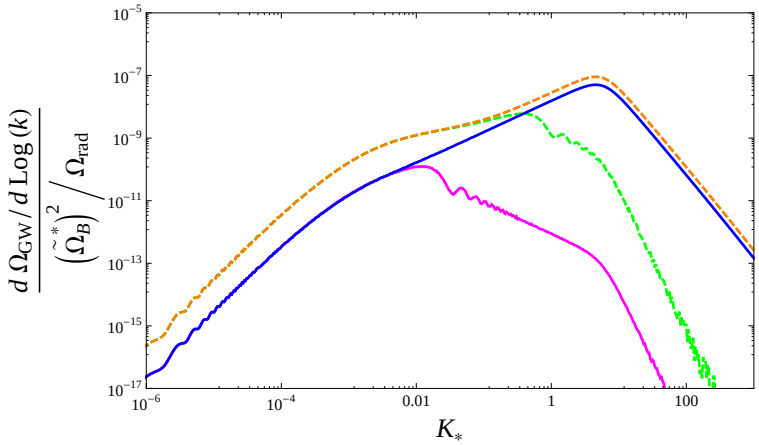

Figure 3.9: The GW spectrum, normalised to the magnetic energy density, for a causal magnetic field $n = 2$ with maximal initial helicity $h_B = 1$. Continuous source: green, dashed line with $v_L^2 = 0.2$ and magenta, solid line with $v_L^2 = 10^{-4}$. Discontinuous source: orange, dashed line with $v_L^2 = 0.2$ and blue, solid line with $v_L^2 = 10^{-4}$. In the continuous case the spectrum peaks at $k \simeq 2\pi/t_L^*$ while in the discontinuous one it peaks at $k \simeq 2\pi/\tilde{L}_*$.

3.4 Limits

The main aim of this paper is to derive constraints on the amplitude of a primordial magnetic field scaled to today, smoothed over an interesting characteristic scale. We choose

the comoving scale $\tilde{\lambda} \simeq 0.1$ Mpc. On one hand, this is approximately the largest correlation scale of cluster magnetic fields today, on the other hand it is only a little larger than the smallest scale which survived dissipation prior to recombination [84, 85]. Note however that, accounting for the full evolution of the magnetic field, Ref. [78] found a smaller dissipation scale at recombination, of about 1 kpc.

To constrain the magnetic field amplitude, we use the GW energy density generated by the magnetic field and we apply the nucleosynthesis bound to these GWs, the same strategy followed in Ref. [77]. We define the comoving magnetic field smoothed on the comoving scale $\tilde{\lambda}$ by

$$\tilde{B}_i(\tilde{\lambda}) = \frac{1}{V_1} \int d^3x \, \tilde{B}_i(\mathbf{x}) \exp\left(-\frac{x^2}{\tilde{\lambda}^2}\right), \tag{3.55}$$

where V_1 is the normalization volume given by

$$V_1 = \int d^3y \exp\left(-\frac{y^2}{\tilde{\lambda}^2}\right) = (\sqrt{\pi}\tilde{\lambda})^3, \tag{3.56}$$

and $\tilde{B}$ is the magnetic field scaled to today, $B(\mathbf{x}, t) = \tilde{B}(\mathbf{x})/a^2(t)$. A short calculation gives the smoothed amplitude

$$\tilde{B}_\lambda^2 = \frac{1}{V_2} \int d^3x \langle \tilde{\mathbf{B}}(\mathbf{x}) \cdot \tilde{\mathbf{B}}(\mathbf{x}+\mathbf{y}) \rangle \exp\left(-\frac{y^2}{2\tilde{\lambda}^2}\right), \tag{3.57}$$

whit $V_2 = (\sqrt{2\pi}\tilde{\lambda})^3$. Translating the above expression to Fourier space we obtain

$$\tilde{B}_\lambda^2 = \frac{1}{2\pi^2} \int_0^\infty dk \, k^2 S(k,t) \exp\left(-\frac{k^2\tilde{\lambda}^2}{2}\right) = 8\pi \int_0^\infty dk \, \varepsilon_B(k,t) \exp\left(-\frac{k^2\tilde{\lambda}^2}{2}\right) . \tag{3.58}$$

We relate this amplitude to the comoving magnetic density parameter $\tilde{\Omega}_B^*$ using Eqs. (3.8), (3.9) for $\varepsilon_B(k,t)$ which are valid for both direct and inverse cascade. Performing the above integral we find

$$\tilde{B}_\lambda^2(t) = 8\pi\rho_c(t_0)\tilde{\Omega}_B(t) \frac{\Gamma\left(\frac{2n+7}{4}\right)}{\Gamma\left(\frac{1}{4}\right)} \, \mathcal{U}\left[\frac{n+3}{2}, \frac{3}{4}, 2\pi^2\left(\frac{\tilde{\lambda}}{\tilde{L}}\right)^2\right] , \tag{3.59}$$

where $\mathcal{U}$ denotes the confluent hyper-geometric function, see *e.g.* [129].

We assume that the initial helicity of the cosmic magnetic field responsible for GW production is maximal, $h_B = 1$. Therefore, during the inverse cascade phase, the magnetic correlation length evolves as given in Eq. (3.19), and the product $\tilde{L}(t)\tilde{\Omega}_B(t)$ is constant in time. The inverse cascade goes on until the temperature $T_{\rm fin}$ at which MHD turbulence terminates. In the maximally helical case, this can vary from a temperature of a few MeV to approximately 1 GeV depending on the epoch of generation of the field (see Eqs. (3.42)-(3.44)). Up to this final time, the correlation length has grown substantially, but one readily confirms that it remains several orders of magnitude smaller than our scale of interest, $\tilde{\lambda} = 0.1$ Mpc $\simeq 10^{13}$sec,

$$\tilde{L}(t_{\rm fin}) \simeq \tilde{L}_* \left(\frac{t_{\rm fin}}{t_L^*}\right)^{2/3} \ll \tilde{\lambda} \, . \tag{3.60}$$

Therefore, we can expand the function $\mathcal{U}(a,b,z) = z^{-a}[1+\mathcal{O}(z^{-1})]$. With this we find

$$\tilde{B}_\lambda^2(t) = \frac{8\pi\Gamma\left(\frac{2n+7}{4}\right)}{(\sqrt{2}\pi)^{n+3}\Gamma\left(\frac{1}{4}\right)}\rho_c(t_0)\tilde{\Omega}_B(t)\left(\frac{\tilde{L}(t)}{\tilde{\lambda}}\right)^{n+3} . \tag{3.61}$$

Taking into account that during inverse cascade $\tilde{\Omega}_B(t)\tilde{L}(t) =$ constant and $\tilde{L}(t) = \tilde{L}_*\tau^{2/3}$, we obtain at $t_* \ll t \leq t_{\rm fin}$

$$\tilde{B}_\lambda^2(t) = \tilde{B}_\lambda^2(t_*)\tau^{2(n+2)/3} \text{ , with} \tag{3.62}$$

$$\tilde{B}_\lambda^2(t_*) \equiv \frac{8\pi\Gamma\left(\frac{2n+7}{4}\right)}{(\sqrt{2}\pi)^{n+3}\Gamma\left(\frac{1}{4}\right)}\rho_c(t_0)\tilde{\Omega}_B^*\left(\frac{\tilde{L}_*}{\tilde{\lambda}}\right)^{n+3} . \tag{3.63}$$

For $t > t_{\rm fin}$ the primordial fluid enters in the viscous phase and the magnetic field energy density is dissipated by radiation viscosity [84, 85]. During this phase, the evolution on large scales is similar to direct cascade, *i.e.* such that the large scale part of the power spectrum remains constant: $\tilde{\Omega}_B(t)\tilde{L}^{n+3}(t) =$ constant. From the general evolution of $\tilde{B}_\lambda$ given in Eq. (3.61), we see that it is justified to assume that, on the scale $\tilde{\lambda}$, after $t_{\rm fin}$ the magnetic field energy density evolves only by redshifting. Therefore, the comoving quantity $\tilde{B}_\lambda(t)$ remains constant:

$$\tilde{B}_\lambda^2 \equiv \tilde{B}_\lambda^2(t \geq t_{\rm fin}) \simeq \tilde{B}_\lambda^2(t_*)\left(\frac{t_{\rm fin}}{t_L^*}\right)^{2(n+2)/3} . \tag{3.64}$$

Like every contribution to radiation energy density prior to nucleosynthesis, $\Omega_{\rm GW}$ is constrained by the nucleosynthesis bound [151]

$$\Omega_{\rm GW} \leq \Omega_{\rm lim} \simeq 0.1\,\Omega_{\rm rad}\,. \tag{3.65}$$

Via Eqs. (3.51), (3.53) this yields a constraint on the magnetic field energy density parameter $\tilde{\Omega}_B^*$, in terms of $\tilde{L}_*/t_{\rm in} = \epsilon$ and $\tilde{L}_*/t_L^* \simeq 2v_L$:

$$\tilde{\Omega}_B^* \lesssim \frac{36}{(\epsilon^{11}\,v_L^2)^{1/12}}\Omega_{\rm rad} \qquad \text{blue case } n=2,\ \text{EW}\,, \tag{3.66}$$

$$\tilde{\Omega}_B^* \lesssim 0.14\,v_L^{(2+6n)/10}\,\Omega_{\rm rad} \qquad \text{red case } n=-1.8,\ \text{inflation}\,. \tag{3.67}$$

With the help of Eqs. (3.62)-(3.64) we translate this into a constraint on $\tilde{B}_\lambda$. Using $\rho_{\rm rad}(t_0) = \rho_c(t_0)\,\Omega_{\rm rad} \simeq 2\times10^{-51}{\rm GeV}^4 \simeq 0.4\times10^{-12}\,({\rm Gauss})^2$, we find for a blue magnetic field generated at the EW phase transition

$$\frac{\tilde{B}_\lambda}{1\mu{\rm Gauss}} \lesssim \frac{0.3}{(\epsilon^{11}\,v_L^2)^{1/24}}\left(\frac{\tilde{L}_*}{\tilde{\lambda}}\right)^{(n+3)/2}\left(\frac{t_{\rm fin}}{t_L^*}\right)^{(n+2)/3} , \tag{3.68}$$

for $n=2$, generated at the EW phase transition

and for a red magnetic field generated during inflation

$$\frac{\tilde{B}_\lambda}{1\mu\text{Gauss}} \lesssim 0.27\, v_L^{(2+6n)/20} \left(\frac{\tilde{L}_*}{\tilde{\lambda}}\right)^{(n+3)/2} \left(\frac{t_{\rm fin}}{t_L^*}\right)^{(n+2)/3}, \qquad (3.69)$$
$$\text{for } n = -1.8, \text{ generated at inflation.}$$

In these equations the pre-factors are calculated using the spectral indexes and the initial and final temperatures corresponding to the generation times. The dependence on v_L and ϵ is kept explicit for completeness.

It is interesting to see that the inverse cascade simply relaxes the limit by the factor $\tau_{\rm fin}^{(n+2)/3}$, absent in the non-helical case for which $\tilde{B}_\lambda(t) = \tilde{B}_\lambda^*$. This factor tends to 1 for $n \to -2$, the limiting value for which the inverse cascade relations (3.18) and (3.19) apply. For causal generation with $n = 2$ the limit for a magnetic field is substantially reduced, while for a red magnetic field spectrum with $n = -1.8$ the reduction is only by $\tau_{\rm fin}^{0.2/3}$.

Let us apply our findings to the two generation mechanisms considered above (EW phase transition and inflation), to which we add also the interesting case of the QCD phase transition [54]. As mentioned in Sec. 3.3.3, we have evaluated the spectrum also in this case, finding a very similar amplitude to the EW phase transition case, for the same values of v_L and ϵ. Therefore, we are confident that we can trivially extend the above Eq. (3.68) also to this case.

For a maximally helical field we find the following limits on $\tilde{B}_\lambda$:

- If the field is generated at the EW phase transition at 100 GeV, $t_{\rm in} \simeq 7.8 \times 10^4$ sec, assuming a causal spectrum with $n = 2$, taking the values $\epsilon = 0.01$, $v_L^2 = 0.2$, $T_{\rm fin} \simeq 21$ MeV, setting $g_{\rm eff}(T_{\rm fin}) = 43/4$ and using $\tilde{\lambda} = 0.1$ Mpc $\simeq 10^{13}$ sec, we obtain the constraint

$$\tilde{B}_{0.1\,\rm Mpc} \lesssim 8 \times 10^{-24}\,\text{Gauss}, \quad \text{EW phase transition, } T_* = 100\text{GeV} \qquad (3.70)$$

- If the field is generated at the QCD phase transition at 100 MeV, $t_{\rm in} \simeq 1.1 \times 10^8$ sec, with the same parameters as before but $T_{\rm fin} \simeq 5$ MeV, the constraint becomes

$$\tilde{B}_{0.1\,\rm Mpc} \lesssim 2 \times 10^{-19}\,\text{Gauss}, \quad \text{QCD phase transition, } T_* = 100\text{MeV} \qquad (3.71)$$

- If the field is generated during inflation at $T_* \simeq 10^{14}$GeV, $t_{\rm in} \simeq 7 \times 10^{-8}$sec, with an acausal red spectrum $n = -1.8$, choosing $\epsilon = v_L = 1$, $T_{\rm fin} \simeq 1$ GeV and $g_{\rm eff}(T_{\rm fin}) = 287/4$, we find the constraint

$$\tilde{B}_{0.1\,\rm Mpc} \lesssim 2 \times 10^{-18}\,\text{Gauss}, \quad \text{inflation, } n = -1.8 \qquad (3.72)$$

- If the field is generated during inflation but with a blue, acausal spectrum $n = 0$, with the same values of the parameters as before we find the stronger constraint

$$\tilde{B}_{0.1\,\rm Mpc} \lesssim 4 \times 10^{-28}\,\text{Gauss}, \quad \text{inflation, } n = 0\,. \qquad (3.73)$$

The above limits are summarised in Fig. 3.10 as a function of n, and in Table 3.1. These upper bounds on the amplitude of the primordial magnetic field are less stringent than the ones obtained from a direct cascade by the factor $\tau_{\rm fin}^{(n+2)/3}$. Moreover, they strongly depend

on the choice for the smoothing scale $\tilde{\lambda}$, in particular for blue spectra. The scaling with $\tilde{\lambda}$ is in fact given by (*c.f.* Eq. (3.61) and [68])

$$\tilde{B}_{\lambda_1} = \tilde{B}_{\lambda_2} \left(\frac{\tilde{\lambda}_2}{\tilde{\lambda}_1} \right)^{(n+3)/2} . \tag{3.74}$$

Therefore, for a smaller smoothing scale of *e.g.* $\tilde{\lambda} = 1$ kpc [78], the above bounds are relaxed by a factor of 10^5 in the EW and QCD generation cases, and by a factor of 10^3 in the inflationary case with flat spectrum $n = 0$. For red spectra the bound does not change much, *e.g.* in the inflationary case with $n = -1.8$ it is relaxed only by a factor of about 16.

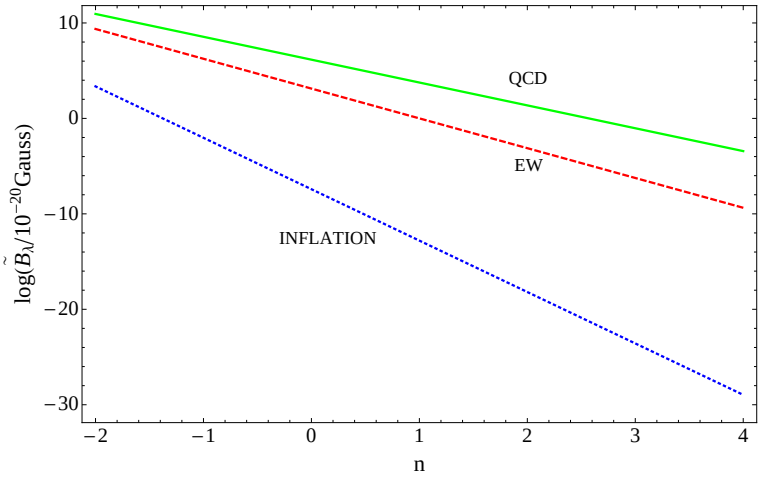

Figure 3.10: Upper bounds on the comoving amplitude of a primordial magnetic field from GW production as a function of n, for $\tilde{\lambda} = 0.1$ Mpc, for a field generated at inflation (blue, dotted), and at a phase transition (EW: red, dashed, QCD: green, solid). In these last two cases, the generation is causal, consequently only $n \geq 2$ is allowed.

More stringent bounds on the amplitude of a causally produced magnetic field can be obtained by imposing simply that the energy density of the magnetic field cannot overcome 10% of the total energy density in radiation at generation time:

$$\tilde{\Omega}_B^* \leq 0.1\, \Omega_{\rm rad} .$$

Comparing this last inequality with Eq. (3.66), one sees that in the latter the factor multiplying $\Omega_{\rm rad}$ is 5 orders of magnitude larger than 0.1 (with the usual values for the parameters). This shows that, in the causal case, the conversion of magnetic energy density into GW energy density, although quite efficient, is not at all complete. For example, using $\tilde{\Omega}_B^* \leq 0.1\, \Omega_{\rm rad}$, the bound on an helical magnetic field becomes $\tilde{B}_{0.1{\rm Mpc}} \lesssim 5 \times 10^{-26}$ Gauss for the EW phase transition. In the inflationary case, on the other hand, the bounds are not modified, since the conversion into GW is much more efficient (*c.f.* the pre-factor in Eq. (3.67)).

However, accounting for GW production seems to us more model independent. Once GWs are generated they do not interact with the cosmic fluid and simply redshift with the evolution of the universe. We are therefore sure that any GW energy density sourced

before nucleosynthesis is still present at that time and must respect the nucleosynthesis bound. On the other hand, magnetic energy density can be dissipated or converted into other forms of energy during the evolution of the universe. We could therefore invoke the extreme scenario in which a magnetic field is formed in the very early universe with amplitude higher than the presumed radiation energy density at that time. The magnetic energy can subsequently be transformed into other forms of energy in such a way that it satisfies the nucleosynthesis bound at nucleosynthesis. The main motivation to consider GW production is to obtain a bound which is safe from these exotic, but in principle possible, scenarios.

3.5 Conclusions

In this paper we have derived new upper bounds on the amplitude of primordial magnetic fields. We have considered helical magnetic field power spectra, which evolve via inverse cascade transferring power from small to large scales.

For the non-helical case, upper bounds on the magnetic field amplitude on the cosmologically relevant scale $\tilde{\lambda} \simeq 0.1$ Mpc have been derived in previous analyses [77, 82]. These bounds apply to magnetic fields generated before nucleosynthesis, for which the correlation scale at the moment of generation is $\tilde{L}_* \ll \tilde{\lambda}$. If the magnetic field spectrum is blue $n > -3/2$, the peak of the energy density per logarithmic scale sits at $\tilde{L}_*$, then the amplitude at the scale $\tilde{\lambda}$ is very constrained:

$$\tilde{B}_\lambda \simeq \tilde{B}_{L_*}(\tilde{L}_*/\tilde{\lambda})^{(n+3)/2} \ll \tilde{B}_{L_*}.$$

On the other hand, if an inverse cascade is active, the power at $\tilde{L}_*$ is moved to the larger correlation scale $\tilde{L}(\tau)$, following the evolution law $\tilde{L}(\tau) = \tilde{L}_* \tau^{2/3}$. At the end of the inverse cascade process, we have seen that the magnetic field on the scale $\tilde{\lambda}$ is finally

$$\tilde{B}_\lambda \simeq \tilde{B}_{L_*}(\tilde{L}_*/\tilde{\lambda})^{(n+3)/2} \tau_{\rm fin}^{(n+2)/3} \tag{3.75}$$

(naively one might expect a scaling like $\tau_{\rm fin}^{(n+3)/3}$, but some of the initial amplitude is lost during the inverse cascade process, so that $\tilde{\Omega}_B(t)\tilde{L}(t) =$ constant. This reduces the growth of $\tilde{B}_\lambda$ by a factor $\tau_{\rm fin}^{1/3}$).

The strong limits from magnetic fields which obey a direct cascade are therefore mitigated in the helical case by a factor

$$\begin{aligned} \tau_{\rm fin}^{(n+2)/3} &= \left[\frac{2v_L}{\epsilon}\,\frac{T_*}{T_{\rm fin}}\left(\frac{g_*}{g_{\rm fin}}\right)^{1/6}\right]^{(n+2)/3} \\ &\simeq \begin{cases} 5.3\times 10^7 & \text{for the EW transition,} \\ & n=2\ ,\ T_*=100\text{GeV} \\ 2\times 10^4 & \text{for the QCD transition,} \\ & n=2\ ,\ T_*=100\text{MeV} \\ 9.3 & \text{for inflation,} \\ & n=-1.8\ ,\ T_*=10^{14}\text{GeV} \\ 4.8\times 10^9 & \text{for inflation,} \\ & n=0\ ,\ T_*=10^{14}\text{GeV}\,. \end{cases} \end{aligned} \tag{3.76}$$

In this paper we have only considered spectral indexes $n > -2$, since Ref. [79] does not analyse smaller spectral indexes, and numerical simulations have always chosen either $n = 2$ [80], or $n = 0$ [78]. Consequently, we do not know whether for a red spectrum with $n \leq -2$ the inverse cascade is still active, or whether the limits are those of the direct cascade. For spectral indexes close to $n = -2$ the above mitigating factor is small, even if the magnetic field is generated in the very early universe. On the other hand, for blue magnetic fields generated at the QCD phase transition, the inverse cascade is not very efficient, since turbulence anyway stops after e^+e^- annihilation: therefore $\tau_{\rm fin}$ is not very large.

In Table 3.1 we summarise our results. We give the upper bounds on the magnetic field amplitude obtained both accounting for GW production and imposing that the magnetic energy does not overcome 10% of the radiation energy, for helical and non-helical magnetic fields smoothed on scales of 0.1 Mpc and 1 kpc. The upper bounds for a non-helical magnetic field are in agreement with those given in [77, 82].

We have found that only red magnetic field spectra from inflation or helical fields from the QCD phase transition can have the amplitude of $B_{0.1{\rm Mpc}} \gtrsim 10^{-22}$ Gauss which is necessary for amplification by a dynamo mechanism up to the observed μGauss field [48]. Especially, the well motivated helical fields from the EW phase transition are still too constrained, even after the inverse cascade.

This leads us to the conclusion that the observed magnetic fields in galaxies and clusters have either not been seeded by primordial fields, or these primordial fields have been produced during inflation and have a red spectrum $n \lesssim -1.8$, or they have been produced during the QCD phase transition. In this latter case it is crucial that these QCD fields be helical because the boost by the factor of about 20000 is absolutely needed, while for red ($-2 < n < -3/2$) inflationary fields the inverse cascade is not relevant.

To evade this conclusion one can argue that magnetic fields coherent on a smaller scale, of about 1 kpc, and with the required amplitude of 10^{-22} Gauss are sufficient to give rise to the fields observed today in galaxies and clusters [78]. If this is so, then the bounds derived here are relaxed in such a way that also helical fields from the EW phase transition can have a sufficiently high amplitude (however, for non-helical fields this is still not enough – see Table 3.1).

Ackowledgements
We thank K. Jedamzik, T. Kahniashvili, G. Servant, K. Subramanian and T. Vachaspati for useful discussions. EF thanks CEA-Saclay for hospitality. This work is supported by the Swiss National Science Foundation.

GW limits				
	helical		non-helical	
	$\lambda = 0.1$Mpc	$\lambda = 1$kpc	$\lambda = 0.1$Mpc	$\lambda = 1$kpc
EW	8×10^{-24}G	$\mathbf{8 \times 10^{-19}\ G}$	10^{-31}G	10^{-26}G
QCD	$\mathbf{2 \times 10^{-19}\ G}$	$\mathbf{2 \times 10^{-14}\ G}$	10^{-23}G	$\mathbf{10^{-18}\ G}$
Infl. $n = -1.8$	$\mathbf{2 \times 10^{-18}G}$	$\mathbf{3 \times 10^{-17}\ G}$	$\mathbf{2 \times 10^{-19}\ G}$	$\mathbf{3 \times 10^{-18}\ G}$
Infl. $n = 0$	4×10^{-28}G	4×10^{-25}G	8×10^{-38}G	8×10^{-35}G
limits from $\Omega_B^* < 0.1$				
EW	5×10^{-26}G	$\mathbf{5 \times 10^{-21}G}$	6×10^{-34}G	6×10^{-29}G
QCD	$\mathbf{10^{-21}G}$	$\mathbf{10^{-16}G}$	6×10^{-26}G	$\mathbf{6 \times 10^{-21}G}$
Infl. $n = -1.8$	$\mathbf{2 \times 10^{-18}G}$	$\mathbf{3 \times 10^{-17}G}$	$\mathbf{2 \times 10^{-19}G}$	$\mathbf{3 \times 10^{-18}G}$
Infl. $n = 0$	4×10^{-28}G	4×10^{-25}G	8×10^{-38}G	8×10^{-35}G

Table 3.1: This table summarises the upper bounds for the magnetic field amplitude averaged over the scales $\lambda = 0.1$ Mpc and $\lambda = 1$ kpc, for the different generation epochs discussed in the paper. Here we present the limits for maximally helical as well as non-helical fields. In the four top rows we give the limits from the production of GWs while in the lower part of the table we present the limits coming from the requirement that the magnetic field contribution be always subdominant: more precisely we require $\Omega_B^* < 0.1$. The values which may be sufficient for dynamo amplification are given in boldface.

3.6 Appendix

3.6.1 The end of turbulence and the dissipation scale

3.6.1.1 The end of turbulence

The turbulent phase ends when the Reynolds number on the scale of energy injection becomes of order unity [147]

$$\mathrm{Re}\,(L(T_{\rm fin}), T_{\rm fin}) = \left.\frac{v_L\, L}{\nu}\right|_{T_{\rm fin}} \simeq 1\,. \tag{3.77}$$

Here L denotes the *physical* energy injection scale, ν is the kinetic viscosity, and v_L is the eddy velocity on the scale L. We assume that in the MHD cascade kinetic and magnetic energy have the same time evolution (equipartition). Substituting $L(t) = \tilde{L}(t)a(t) = \tilde{L}(t)\,(T_0/T(t))\,(g_0/g_{\rm eff}(T))^{1/3}$, we find ($g_{\rm eff}(T_*) \equiv g_*$),

$$\mathrm{Re}\,(L(T), T) = R_*\frac{T_*}{T}\left(\frac{g_*}{g_{\rm eff}(T)}\right)^{1/3}\frac{\nu_*}{\nu(T)}\,\tau^\alpha\,, \qquad R_* \equiv \mathrm{Re}\,(L_*, T_*)\;, \tag{3.78}$$

where the power α represents the evolution of the product $\tilde{L}(t)v_L(t)$ and we use $v_L(t) \propto \sqrt{\tilde{\rho}_B}$. With Eqs. (3.13, 3.14) and (3.18, 3.19) we obtain

$$\alpha = \begin{cases} -(n+1)/(n+5) & \text{for non-helical fields (normal cascade),} \\ 1/3 & \text{for helical fields (inverse cascade).} \end{cases} \tag{3.79}$$

The kinetic viscosity is approximately given by the mean free path of the particle with the weakest interaction [131], $\nu \simeq \ell_{\rm mfp}/5$. During the early radiation dominated phase, neutrinos determine the viscosity until they decouple at $T \simeq 1$ MeV, when photon viscosity sets in. For $T > 1\,\mathrm{MeV}$ the mean free path of the neutrinos is given by

$$\ell^{(\nu)}_{\rm mfp} \simeq \frac{1}{3\,G_F^2\,T^5}\,, \qquad 1\,\mathrm{MeV} < T < 100\,\mathrm{GeV}\;, \tag{3.80}$$

where $G_F = (293\mathrm{GeV})^{-2}$ is the Fermi coupling constant. Below 1 MeV we have to consider the photon mean free path which can be approximated by Thomson scattering

$$\ell^{(\gamma)}_{\rm mfp} \simeq \frac{1}{\sigma_T\, n_e} \simeq \frac{3\,m_e^2\,m_p}{8\pi e^4\,\Omega_b\,\rho_c}\left(\frac{T_0}{T}\right)^3\,, \qquad 0.3\ \mathrm{eV} < T < 1\ \mathrm{MeV}\;, \tag{3.81}$$

where σ_T is the Thomson cross section, n_e is the electron density, Ω_b is the baryon density parameter and we neglect the short period of time during which electrons are still relativistic, after neutrino decoupling but before electron positron annihilation. The lower limit in (3.81) comes from recombination, when the electron density drops sharply and photons decouple. The situation also changes at very high temperature, when the EW symmetry is restored, $T \gtrsim 100\mathrm{GeV}$. Then the coupling constant is nearly independent of temperature, and the relativistic mean free path is of the order of the inverse temperature [152]

$$\ell_{\rm mfp} \simeq \frac{22}{T}\,, \qquad T > 100\,\mathrm{GeV}\;. \tag{3.82}$$

We first calculate the Reynolds number at the time of generation and at the initial correlation scale of the magnetic field, in order to confirm that a turbulent MHD phase is indeed present. With (3.78) we obtain

$$R_* = v_L\,\epsilon\,\frac{t_\in}{\nu_*}\,\frac{T_0}{T_*}\left(\frac{g_0}{g_*}\right)^{1/3}\,, \tag{3.83}$$

where we have identified the temperatures $T_\in \simeq T_*$. Furthermore, we use $\nu = \ell_{\rm mfp}/5$ and

$$\begin{aligned} t_\in &= \frac{1}{a_\in H_\in} \simeq 0.5\, g_*^{-1/6}\,\frac{m_{\rm Pl}}{T_* T_0}\,, \\ R_* &\simeq \frac{3\,v_L\,\epsilon}{\sqrt{g_*}}\,\frac{m_{\rm Pl}}{T_*^2 \ell_{\rm mfp}(t_*)}\,. \end{aligned} \tag{3.84}$$

We consider the two situations, $1\,{\rm MeV} \le T_* \le 100\,{\rm GeV}$ and $T_* > 100$ GeV, where the expressions (3.80) and (3.82) for the mean free path give

$$R_* \simeq \frac{9 v_L\,\epsilon}{\sqrt{g_*}} m_{\rm Pl} T_*^3 G_F^2\,, \quad 1\,{\rm MeV} \le T_* \le 100\,{\rm GeV} \tag{3.85}$$

$$R_* \simeq \frac{3}{22}\,\frac{v_L\,\epsilon}{\sqrt{g_*}}\,\frac{m_{\rm Pl}}{T_*}\,, \qquad T_* > 100\ {\rm GeV}\,. \tag{3.86}$$

Let us start by considering the generation of turbulence during the EW phase transition at 100 GeV. Setting $T_* = 100$ GeV, $\epsilon = 0.01$ and $v_L^2 = 0.2$, with $g_* \simeq 100$ we obtain $R_* \simeq 10^{13}$. The corresponding parameters for the QCD transition at $T_* = 100$ MeV and $g_* \simeq 10$ yield $R_* \simeq 10^4$. Both Reynolds numbers are much larger than one so that we can be certain that a first order phase transition will induce turbulence. To determine when turbulence terminates we use Eqs. (3.78) and (3.80), setting

$$1 = {\rm Re}\,(L(T_{\rm fin}), T_{\rm fin}) = R_* \tau^\alpha \left(\frac{g_*}{g_{\rm eff}(T_{\rm fin})}\right)^{1/3} \left(\frac{T_{\rm fin}}{T_*}\right)^4 \simeq R_* \left(\frac{2v_L}{\epsilon}\right)^\alpha \left(\frac{T_{\rm fin}}{T_*}\right)^{4-\alpha}\,. \tag{3.87}$$

For the last equal sign we have used $t_L^* = \tilde{L}_*/(2v_L) = \epsilon t_\in/(2v_L)$, $\tau \simeq t/t_L^*$ and we have approximated $t_{\rm fin}/t_{\rm in} \simeq T_*/T_{\rm fin}$. This corresponds to neglecting changes in the number of effective relativistic degrees of freedom.

For direct cascade with $n = 2$, hence $\alpha = -3/7$, we obtain $T_{\rm fin} \simeq 200$ MeV for the EW phase transition and $T_{\rm fin} \simeq 20$ MeV for the QCD phase transition.

In the helical case with inverse cascade $\alpha = 1/3$, turbulence is maintained longer and we find $T_{\rm fin} \simeq 21$ MeV for the EW phase transition and $T_{\rm fin} \simeq 5$ MeV for the QCD phase transition.

For generation of magnetic fields and turbulence at the end of inflation $T_* = 10^{14}$ GeV, no causality restriction holds and we choose $\epsilon = v_L = 1$. As long as $\nu(T) \propto \ell_{\rm mfp} \simeq 22/T$, the Reynolds number at the correlation length $L(T)$ evolves like $(t/t_{\rm in})^\alpha \simeq (T_*/T)^\alpha$ according to Eq. (3.78) (where we neglect changes in the effective number of relativistic degrees of freedom). At $T_* \simeq 10^{14}$ GeV, with $g_* \simeq 200$ we have $R_* \simeq 0.01\, m_{\rm Pl}/T_* \simeq 10^3$. As time evolves, the Reynolds number at $L(T)$ decays only in the non-helical case if $n > -1$, so that $\alpha = -(n+1)/(n+5) < 0$. In the helical case and for $n < -1$ the Reynolds number ${\rm Re}\,(L(T), T)$ grows as the temperature drops. Once $T = T_{ew} = 100$ GeV is reached, the viscosity ν starts decaying rapidly, like T^{-5}, and the Reynolds number then decreases.

We consider three cases

i) Direct cascade with $n = 0$, $\alpha = -1/5$

$$\mathrm{Re}\,(L(T_{ew}), T_{ew}) = R_*(T_*/T_{ew})^{\alpha} \simeq 6\,,$$

so $T_{\rm fin} \simeq 100$ GeV.
ii) Direct cascade with $n = -3/2$, $\alpha = 1/7$
In this case

$$\mathrm{Re}\,(L(T_{ew}), T_{ew}) = R_*(T_*/T_{ew})^{\alpha} \simeq 9 \times 10^4\,,$$

and

$$T_{\rm fin} = T_{ew}\mathrm{Re}\,(L(T_{ew}), T_{ew})^{\frac{-1}{4-\alpha}} \simeq 5\,\mathrm{GeV}\ .$$

iii) Inverse cascade, $\alpha = 1/3$
In this case

$$\mathrm{Re}\,(L(T_{ew}), T_{ew}) = R_*(T_*/T_{ew})^{\alpha} \simeq 2 \times 10^7\,,$$

and

$$T_{\rm fin} = T_{ew}\mathrm{Re}\,(L(T_{ew}), T_{ew})^{\frac{-1}{4-\alpha}} \simeq 1\,\mathrm{GeV}\ .$$

We draw the important conclusion that in all cases the MHD turbulent phase always lasts for many Hubble times before the total kinetic energy is dissipated [25].

3.6.1.2 The dissipation scale

In the previous subsection we have considered the energy injection scale $\tilde{L}(T)$ and determined first that turbulence is present on this scale, and second when turbulence ends (*i.e.* when the entire Kolmogorov range is dissipated). Now we want to know, for a given fixed time t (or temperature T), what is the scale below which kinetic energy is dissipated. This defines the comoving dissipation scale $\tilde{l}_{\rm diss}(T)$. The function $\tilde{l}_{\rm diss}(T)$ can be found considering that, on scales smaller than this scale, viscosity dominates, therefore there is no turbulence. Thus, $l_{\rm diss}$ corresponds to the physical scale at which the Reynolds number is equal to 1,

$$\mathrm{Re}\,(l_{\rm diss}, T) = \frac{v_l\, l_{\rm diss}}{\nu} \sim 1\,. \tag{3.88}$$

Here ν is the kinetic viscosity as in the previous section, and v_l is the eddy velocity at the dissipation scale. We determine $\tilde{l}_{\rm diss}(T)$ only for the helical case which is our main interest in this paper (see [25] for the non-helical one). In the inertial range the turbulent eddy velocity obeys a Kolmogorov spectrum so that [82]

$$v_l = v_L \left(\frac{\tilde{l}_{\rm diss}}{\tilde{L}(T)}\right)^{1/3}\ . \tag{3.89}$$

Now we use $\mathrm{Re}\,(L(T), T) = v_L(T)L(T)/\nu(T)$ so that, from Eq. (3.78) neglecting changes in the number of relativistic degrees of freedom, we find

$$\mathrm{Re}\,(l_{\rm diss}, T) = \mathrm{Re}\,(L(T), T)\left(\frac{\tilde{l}_{\rm diss}}{\tilde{L}(T)}\right)^{4/3} \simeq R_*\tau^{\alpha}\frac{T_*}{T}\frac{\nu_*}{\nu}\left(\frac{\tilde{l}_{\rm diss}}{\tilde{L}(t)}\right)^{4/3}\ . \tag{3.90}$$

Hence $\mathrm{Re}\,(l_{\rm diss}, T) = 1$ yields

$$\tilde{l}_{\rm diss}(T) \simeq \tilde{l}^*_{\rm diss}\,\tau^{5/12}\left(\frac{T}{T_*}\frac{\nu(T)}{\nu_*}\right)^{3/4}\,, \tag{3.91}$$

where we define $\tilde{l}^*_{\rm diss} \equiv \tilde{L}_*/R_*^{3/4}$. For the last equal sign we have used the behavior of the correlations scale with $\tau = (t - t_\in)/t^*_L$ as $\tau^{2/3}$, (3.19), and $\alpha = 1/3$ for the helical case.

The evolution of both the correlation length $\tilde{L}(T)$ and the dissipation scale $\tilde{l}_{\rm diss}(T)$ are compared in Fig. 3.4 for the EW phase transition. Turbulence stops roughly when the two curves cross. We call this time $t^{(1)}_{\rm fin}$.

Finally, we have to take into account that for a given comoving scale, $\tilde{l} = 2\pi/k$ the Reynolds number can become unity long before the end of turbulence. The time at which turbulence on the scale $\tilde{l}$ is dissipated is denoted $t^{(2)}_{\rm fin}(k)$ and it is defined by

$$\tilde{l} = 2\pi/k = \tilde{l}_{\rm diss}(t^{(2)}_{\rm fin}(k))\,.$$

Let us first consider $T_* \leq T_{ew} = 100$ GeV, so that for all times of interest the kinetic viscosity behaves as $\nu \propto T^{-5}$. This leads to

$$k = \frac{2\pi}{\tilde{l}_{\rm diss}(t^{(2)}_{\rm fin}(k))} \quad \Rightarrow \quad \frac{t^{(2)}_{\rm fin}(k)}{t_*} \simeq \left[\frac{1}{K_*}\frac{\tilde{L}_*}{\tilde{l}^*_{\rm diss}}\left(\frac{\epsilon}{2v_L}\right)^{5/12}\right]^{12/41}\,. \tag{3.92}$$

Here again, we neglect a possible difference in $g_{\rm eff}$ between t_* and $t^{(2)}_{\rm fin}$ and we set $\tau^{(2)}_{\rm fin} \simeq t^{(2)}_{\rm fin} 2v_L/(\epsilon t_\in)$. We also use $R_* = (\tilde{L}_*/\tilde{l}^*_{\rm diss})^{4/3}$.

The situation is somewhat more complicated for generation temperatures $T_* > T_{ew}$: until T_{ew} the kinematic viscosity decays roughly like $\nu \propto 1/T$. We therefore have to distinguish between scales which are damped at temperatures above T_{ew} and those which are damped below. Since we are in this situation only for the inflationary case, we set $\epsilon = v_L = 1$ for this case. We then obtain

$$t^{(2)}_{\rm fin}(k) \simeq \begin{cases} \frac{t_*}{2}\left(K_*^{-1}\frac{\tilde{L}_*}{\tilde{l}^*_{\rm diss}}\right)^{12/5} & \text{for } K_* \text{ such that } t^{(2)}_{\rm fin}(k) < t_{ew}\,, \quad K_* > K^*_{ew}\,, \\ t_{ew}\left(\frac{K^*_{ew}}{K_*}\right)^{12/41} 2^{-5/41} & \text{for } K_* < K^*_{ew}\,. \end{cases} \tag{3.93}$$

Here K^*_{ew} is the value of K_* for which turbulence terminates at T_{ew},

$$K^*_{ew} \simeq \left(\frac{T_{ew}}{2T_*}\right)^{5/12}\frac{\tilde{L}_*}{\tilde{l}^*_{\rm diss}}\,. \tag{3.94}$$

When applying these formulas for the calculation of GWs, we must choose the true final time given by

$$t_{\rm fin} = \min\left[t^{(1)}_{\rm fin}, t^{(2)}_{\rm fin}(k)\right]\,. \tag{3.95}$$

For turbulence from the EW phase transition and from inflation this function is plotted in Fig 3.5 . At $t^{(1)}_{\rm fin}$ turbulence is dissipated on all scales $\tilde{l} \leq \tilde{L}(t^{(1)}_{\rm fin})$ which is the scale of the largest eddies: therefore, the entire Kolmogorov range is dissipated.

3.6.2 The equal time correlator and other integrals

3.6.2.1 $\tilde{\Pi}_B(k,t)$

According to Eq. (3.37) we can write the equal time correlator as the following integral

$$\tilde{\Pi}_B(k,t) = \frac{\mathcal{N}_2}{2\pi}\tilde{L}^3(t)\tilde{\rho}_B^2(t)\left[I_1(k,t)+4I_2(k,t)\right] = \frac{\mathcal{N}_2}{2\pi}\tilde{L}^3(t)\tilde{\rho}_B^2(t)I(k,t)\ , \tag{3.96}$$

$$\begin{aligned} I_1(k,t) &= \int_0^{\tilde{L}(t)/\tilde{l}_{\rm diss}(t)} dQ \frac{Q^{n+2}}{(1+Q^2)^{(2n+7)/4}} \times \\ &\int_{\max\left(-1;\frac{K}{2Q}+\frac{Q}{2K}-\frac{\tilde{L}^2}{2KQ\tilde{l}_{\rm diss}^2}\right)}^{1} d\gamma(1+\gamma^2)\frac{x^{n-2}}{(1+x^2)^{(2n+7)/4}} \times \\ &[2K^2+(1+\gamma^2)Q^2-4\gamma KQ]\ , \end{aligned} \tag{3.97}$$

$$\begin{aligned} I_2(k,t) &= \int_{\tilde{L}(t)/(2\pi t)}^{\tilde{L}(t)/\tilde{l}_{\rm diss}(t)} dQ \frac{Q^{n+2}}{(1+Q^2)^{(2n+7)/4}} \times \\ &\int_{\max\left(-1;\frac{K}{2Q}+\frac{Q}{2K}-\frac{\tilde{L}^2}{2KQ\tilde{l}_{\rm diss}^2}\right)}^{\min\left(1;\frac{K}{2Q}+\frac{Q}{2K}-\frac{\tilde{L}^2}{2KQ(2\pi t)^2}\right)} d\gamma\ \frac{x^{n-1}}{(1+x^2)^{(2n+7)/4}}\gamma(K-Q\gamma)\ , \end{aligned} \tag{3.98}$$

where we have used $\alpha=(k-\gamma q)/\sqrt{k^2+q^2-2\gamma kq}$ and we have set $x\equiv\sqrt{K^2+Q^2-2\gamma KQ}$ and $Q(t)\equiv q\tilde{L}(t)/(2\pi)$. We have also introduced the constant $\mathcal{N}_2$ defined by

$$\mathcal{N}_2 \equiv \left[\frac{\Gamma\left(\frac{2n+7}{4}\right)}{\Gamma\left(\frac{1}{4}\right)\Gamma\left(\frac{n+3}{2}\right)}\right]^2 = \begin{cases} 0.11 & \text{for } n=2\ , \\ 0.08 & \text{for } n=0\ , \\ 0.05 & \text{for } n=-3/2\ , \\ 0.04 & \text{for } n=-1.8\ . \end{cases}$$

We have performed the double integrals $I_j(k,t)$ numerically for different values of the spectral index $n>-2$. In the numerical integration we neglect the time dependent cutoff in the above integrals and consider only the time dependence given by $K(t)=K_*\tau^\beta$, with $K_*\equiv k\tilde{L}_*/(2\pi)$, $\tau\equiv[(t-t_{\rm in})/t_L^*]$ and $\beta=2/(n+5)$ for the direct cascade regime while $\beta=2/3$ in the inverse cascade phase. In general we find that the antisymmetric contribution I_2 is negative (as it should be [130]), and negligible with respect to the symmetric contribution, namely $I_1\ll|I_2|$.

First we consider a blue magnetic field spectrum which is characterized by $n>-3/2$. The result of the numerical integration for $n=2$, which corresponds to a causal magnetic field, is shown in Fig. 3.11. The integral $I(K)$ can be approximated by the following analytical expression,

$$I(K)\simeq\frac{0.034}{1+\left(\frac{K}{12}\right)^4+\left(\frac{K}{6}\right)^{7/2}}\ . \tag{3.99}$$

With this approximation the equal time correlator $\tilde{\Pi}_B(K,t)$ can be written as

$$\tilde{\Pi}_B(K,t)\simeq\frac{\mathcal{N}_2}{2\pi}\tilde{L}^3(t)\tilde{\rho}_B^2(t)\frac{0.034}{1+\left(\frac{K}{12}\right)^4+\left(\frac{K}{6}\right)^{7/2}}\ . \tag{3.100}$$

For a red magnetic field spectrum with $n<-3/2$ we find a somewhat different power spectrum which is shown in Fig. 3.12 for the case $n=-1.8$. The integral can be approxi-

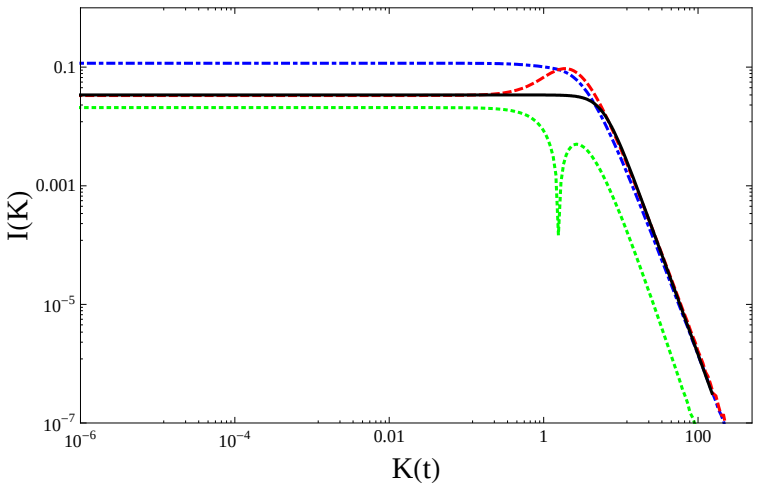

Figure 3.11: Symmetric part $I_1(K)$ (blue, dash-dotted line) and absolute value of the antisymmetric part $|I_2(K)|$ (green, dotted line) of the anisotropic stresses for a blue magnetic field with $n = 2$. The sum of the two parts $I(K) = I_1 + 4I_2$ (red, dashed line) and the fit (black, solid line) are also shown.

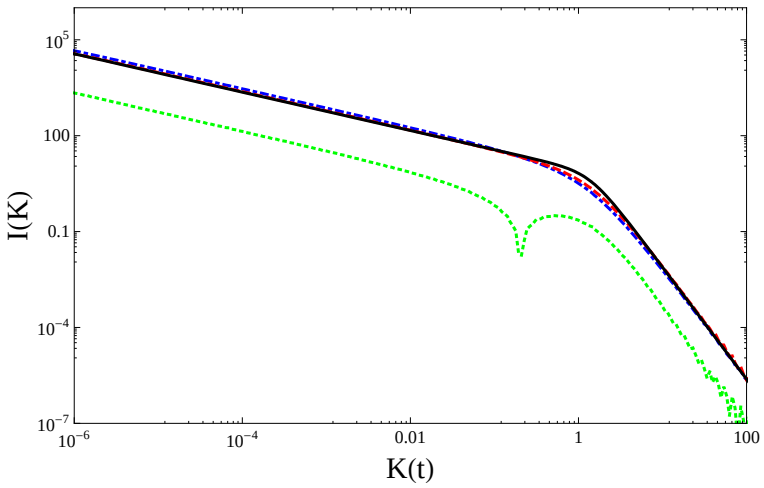

Figure 3.12: Symmetric part $I_1(K)$ (blue, dash-dotted line) and absolute value of the antisymmetric part $|I_2(K)|$ (green, dotted line) of the anisotropic stresses considering now a red magnetic field with $n = -1.8$. We plot also the sum of the two parts $I(K)$ (red, dashed line) and the fit (black, solid line).

mated by

$$I(K) \propto \frac{K^A}{1+(K/C)^B} \ , \tag{3.101}$$

where the constants A and B are given by $A = 2n+3 < 0$ and $B = A + 7/2 = 2n + 13/2$ and C varies with n and has been chosen to be equal to 1.4 in order to fit the numerical result. We recover the asymptotic behavior for the anisotropic stress of a red magnetic field found in [77], [82]:

$$\begin{aligned} I(K) &\simeq K^{2n+3} \qquad \text{for} \quad K \ll 1 \ , \\ I(K) &\simeq K^{-7/2} \qquad \text{for} \quad K \gg 1 \ . \end{aligned}$$

This explains also the higher amplitude of $I(K)$ in the red case compared to the one obtained for a blue magnetic field: we have an infrared divergence for small values of Q. Finally for $n = -1.8$ we find

$$\tilde{\Pi}_B(K,t) \simeq \frac{\mathcal{N}_2}{2\pi}\tilde{L}^3(t)\tilde{\rho}_B^2(t)\frac{(K/40)^{-3/5}}{1+(K/1.4)^{29/10}} \ . \tag{3.102}$$

3.6.2.2 GW integrals

To calculate the integrals (3.41) we use Eqs. (3.38), (3.39) for the time evolution of the magnetic anisotropic stress and we use the integration variable τ

$$\tau = \frac{t' - t_{\rm in}}{t_L^*} \ .$$

We can then write the GW energy spectrum as

$$\begin{aligned} \frac{d\rho_{\rm GW}(k,t)}{d\log k} \ &\simeq \ \frac{2G}{\pi a^4(t)}\frac{\mathcal{N}_2}{2\pi}\frac{(\tilde{\rho}_B^*)^2}{H_0^2\Omega_{\rm rad}}(2\pi)^3 K_*^3 \Big\{ [I_{c,\,I}(k) + I_{c,\,II}(k)]^2 \\ &\quad + [I_{s,\,I}(k) + I_{s,\,II}(k)]^2 \Big\} \ , \end{aligned} \tag{3.103}$$

which yields the following expression for the present density parameter of GWs

$$\begin{aligned} \frac{d\Omega_{\rm GW}(k,t_0)}{d\log k} \ &\simeq \ 3\mathcal{N}_2\frac{(\tilde{\Omega}_B^*)^2}{\Omega_{\rm rad}}\mathcal{I}_{\rm GW}(K_*) \ , \\ \mathcal{I}_{\rm GW}(K_*) \ &\equiv \ K_*^3 \Big\{ [I_{c,\,I}(K_*) + I_{c,\,II}(K_*)]^2 + [I_{s,\,I}(K_*) + I_{s,\,II}(K_*)]^2 \Big\} \ . \end{aligned} \tag{3.104}$$

The four integrals above distinguish the two different phases of the inverse cascade, namely the first one where the magnetic energy density is growing linearly up to its maximum value $\tilde{\rho}_B^*$ ($t_\in \leq t < t_*$) and the second one where $\tilde{\rho}_B(t)$ decays as $\tau^{-2/3}$ ($t \geq t_*$).

For the EW phase transition, $n = 2$ we have for $t_{\rm in} \leq t < t_*$

$$I_{c,\,I}(K_*) = \int_0^1 d\tau \frac{\sqrt{0.034}\ \tau^2}{\left(\tau + \frac{2v_L}{\epsilon}\right)\sqrt{1 + \left(\frac{K_*\tau^{2/3}}{12}\right)^4 + \left(\frac{K_*\tau^{2/3}}{6}\right)^{7/2}}} \times \cos\left[2\pi K_*\left(\frac{\tau}{2v_L} + \frac{1}{\epsilon}\right)\right] , \tag{3.105}$$

$$I_{s,\,I}(K_*) = \int_0^1 d\tau \frac{\sqrt{0.034}\ \tau^2}{\left(\tau + \frac{2v_L}{\epsilon}\right)\sqrt{1 + \left(\frac{K_*\tau^{2/3}}{12}\right)^4 + \left(\frac{K_*\tau^{2/3}}{6}\right)^{7/2}}} \times \sin\left[2\pi K_*\left(\frac{\tau}{2v_L} + \frac{1}{\epsilon}\right)\right] , \tag{3.106}$$

while for $t \geq t_*$ the integrals can be written as

$$I_{c,\,II}(K_*) = \int_1^{\frac{t_{\rm fin}}{t_L^*}} d\tau \frac{\sqrt{0.034}\ \tau^{1/3}}{\left(\tau + \frac{2v_L}{\epsilon}\right)\sqrt{1 + \left(\frac{K_*\tau^{2/3}}{12}\right)^4 + \left(\frac{K_*\tau^{2/3}}{6}\right)^{7/2}}} \times \cos\left[2\pi K_*\left(\frac{\tau}{v_L} + \frac{1}{\epsilon}\right)\right] , \tag{3.107}$$

$$I_{s,\,II}(K_*) = \int_1^{\frac{t_{\rm fin}}{t_L^*}} d\tau \frac{\sqrt{0.034}\ \tau^{1/3}}{\left(\tau + \frac{2v_L}{\epsilon}\right)\sqrt{1 + \left(\frac{K_*\tau^{2/3}}{12}\right)^4 + \left(\frac{K_*\tau^{2/3}}{6}\right)^{7/2}}} \times \sin\left[2\pi K_*\left(\frac{\tau}{2v_L} + \frac{1}{\epsilon}\right)\right] . \tag{3.108}$$

Secondly we consider a red magnetic field with $n = -1.8 < -3/2$, that implies $A = -3/5$, $B = 29/10$ and $C = 1.4$. In this case the four integrals read for $t_{\rm in} \leq t < t_*$

$$I_{c,\,I}(K_*) = \int_0^1 d\tau \frac{\tau^{9/5}(K_*/40)^{-3/10}}{\left(\tau + \frac{2v_L}{\epsilon}\right)\sqrt{1 + \left(\frac{K_*\tau^{2/3}}{1.4}\right)^{29/10}}} \times \cos\left[2\pi K_*\left(\frac{\tau}{2v_L} + \frac{1}{\epsilon}\right)\right] , \tag{3.109}$$

$$I_{s,\,I}(K_*) = \int_0^1 d\tau \frac{\tau^{9/5}(K_*/40)^{-3/10}}{\left(\tau + \frac{2v_L}{\epsilon}\right)\sqrt{1 + \left(\frac{K_*\tau^{2/3}}{1.4}\right)^{29/10}}} \times \sin\left[2\pi K_*\left(\frac{\tau}{2v_L} + \frac{1}{\epsilon}\right)\right] , \tag{3.110}$$

while for $t \geq t_*$ the integrals can be written as

$$I_{c,\,II}(K_*) = \int_1^{\frac{t_{\rm fin}}{t_L^*}} d\tau \frac{\tau^{2/15}(K_*/40)^{-3/10}}{\left(\tau + \frac{2v_L}{\epsilon}\right)\sqrt{1+\left(\frac{K_*\tau^{2/3}}{1.4}\right)^{29/10}}} \times \cos\left[2\pi K_*\left(\frac{\tau}{2v_L}+\frac{1}{\epsilon}\right)\right] , \tag{3.111}$$

$$I_{s,\,II}(K_*) = \int_1^{\frac{t_{\rm fin}}{t_L^*}} d\tau \frac{\tau^{2/15}(K_*/40)^{-3/10}}{\left(\tau + \frac{2v_L}{\epsilon}\right)\sqrt{1+\left(\frac{K_*\tau^{2/3}}{1.4}\right)^{29/10}}} \times \sin\left[2\pi K_*\left(\frac{\tau}{2v_L}+\frac{1}{\epsilon}\right)\right] . \tag{3.112}$$

Inserting typical values for the above quantities we perform a numerical integration, and we find that the first phase, the 'switching on' of the inverse cascade, is completely irrelevant for the final result for most of the spectrum. It does, however affect the peak position and the decay law as we discuss in Section 3.3.4. The numerical solutions of the integrals are shown in Figs. 3.6 and 3.7.

3.6.2.3 The fits for the GW spectrum

In deriving the analytical fits to the numerical GW spectra, Eqs. (3.50) and (3.52), we have been guided by analytic intuition of the behaviour of the integrals given in Eqs. (3.105) to (3.112) above. Here we give some details for the understanding of the fits.

Let us start with the causal case, $n = 2$. First of all, the main contribution to the GW spectrum comes from the integral in Eq. (3.107), *i.e.* the cosine part in (3.41). For very small values of K_*, below the characteristic wave number $k \leq 1/t_{\rm fin}$, the cosine does not oscillate: therefore, we expect to inherit directly the slope of the anisotropic stress. For the causal case this is flat, consequently we expect a K_*^3 behaviour, coming from (3.104). The constant ϵ_1 is fixed by the large wavelength limit of $\mathcal{I}_{\rm GW}(K_*)$, given mainly by the integral of Eq. (3.107) evaluated at the upper boundary $t_{\rm fin}$:

$$\mathcal{I}_{\rm GW}(K_* \to 0) \simeq 7.73\,\tilde{\Pi}(0)\left(\frac{T_*}{T_{\rm fin}}\frac{2v_L}{\epsilon}\right)^{2/3} K_*^3 \equiv \epsilon_1\, K_*^3 \, .$$

For higher values of the wave number, the main contribution to the integral comes roughly from the first oscillation of the cosine in Eq. (3.107) (note that the integrand decays with time). This can be accounted for by integrating only up to the time $t \simeq 1/k$, causing a change of slope of the GW spectrum, which now results in $\mathcal{I}_{\rm GW}(K_*) \propto K_*^{7/3}$. In the main text this slope is set to K_*^2, which corresponds to the best fit result from the numerical evaluation of the integral (see Fig. 3.6). These analytical considerations are in fact quite crude and lead to slopes which are not very precise. The parameter ϵ_2 is determined by the matching at the limiting value $k = 1/t_{\rm fin}$, which is the value of the wave number for which the cosine starts to oscillate:

$$\epsilon_2 \simeq 0.07\left(v_L^2\,\epsilon\,\frac{T_{\rm fin}}{T_*}\right)^{1/3} .$$

This behaviour continues until k becomes of the order of $1/t_*$. Above this value, the time dependence of the integrand is no longer $\tau^{-2/3}$ but $\tau^{1/3}$ (see Eq. (3.107)). This results in a further change in the slope of the spectrum, which now becomes $\mathcal{I}_{\rm GW}(K_*) \propto K_*^{1/3}$. In the main text this slope is set to $\sqrt{K_*}$, again according to the numerical evaluation of the integral. By continuity, the paramter ϵ_3 in Eq. (3.50) is

$$\epsilon_3 \simeq 4 \cdot 10^{-3} \left(v_L^2 \, \epsilon^{11/2} \, \frac{T_{\rm fin}}{T_*} \right)^{1/3} .$$

In the inflationary case, the main contribution to the GW spectrum comes again from the integral in Eq. (3.111). For very small values of K_*, below the characteristic wave number $k \leq 1/t_{\rm fin}$, we expect to inherit the slope of the anisotropic stress. The constant ϵ_4 is given by the large wavelength limit of $\mathcal{I}_{\rm GW}(K_*)$:

$$\mathcal{I}_{\rm GW}(K_* \to 0) \simeq 68 \, \tilde{\Pi}(K_*) \left(\frac{T_*}{T_{\rm fin}} \right)^{4/15} K_*^3 = \epsilon_4 \, K_*^{2n+6} . \tag{3.113}$$

The above formula is valid for $n = -1.8$. For higher values of the wave number, the same argument as in the causal case applies, and we integrate only up to $t \simeq 1/k$: the slope in wave number of the GW spectrum now results in $\mathcal{I}_{\rm GW}(K_*) \propto K_*^{(2n+10)/3}$. By continuity, we obtain (again for $n = -1.8$) $\epsilon_5 \simeq 619/(2\pi)^{4/15}$. This behaviour continues until the wave number for which the final time of turbulence $t_{\rm fin}(k)$, given in Eq. (3.46), becomes smaller than $1/k$: this happens for $K_* \simeq ((2\pi)^5/R_*^9)^{1/7}$, see the first line of Eq. (3.93). For higher wave numbers, the upper limit of integration has a different $k-$behaviour which translates to the slope $\mathcal{I}_{\rm GW}(K_*) \propto K_*^{-(2+6n)/5}$. By continuity, $\epsilon_6 \simeq 619/R_*^{12/25} \simeq 22$ for $n = -1.8$ and $R_* \simeq 10^3$ for inflation.

Chapter 4

The seed magnetic field generated during recombination

MONTHLY NOTICES OF THE ROYAL ASTRONOMICAL SOCIETY (2011)

The seed magnetic field generated during recombination

Elisa Fenu, Cyril Pitrou and Roy Maartens

Nonlinear dynamics creates vortical currents when the tight-coupling approximation between photons and baryons breaks down around the time of recombination. This generates a magnetic field at second order in cosmological perturbations, whose power spectrum is fixed by standard physics, without the need for any ad hoc assumptions. We present the fully general relativistic calculation of the magnetic power spectrum, including the effects of metric perturbations, second-order velocity and photon anisotropic stress, thus generalizing and correcting previous results. We also show that significant magnetogenesis continues to occur after recombination. The power spectrum $\sqrt{k^3 P_B}$ decays as k^4 on large scales, and grows as $k^{0.5}$ on small scales, down to the limit of our numerical computations, $\sim 1\,\mathrm{Mpc}$. On cluster scales, the created field has strength $\sim 3 \times 10^{-29}$ Gauss.

DOI: 10.1111/j.1365-2966.2011.18554.x

arXiv:1012.2958v2 [astro-ph.CO]

4.1 Introduction

Evidence is growing for magnetic fields on larger and larger scales in the Universe (see e.g. the reviews [35, 36]). In galaxies, the fields have strength of order μGauss, ordered on scales $\sim 1 - 10\,\mathrm{kpc}$. Fields of strength $\sim 1 - 10^{-2}\mu\mathrm{G}$ on scales $\sim 0.1 - 1\,\mathrm{Mpc}$ have been detected in galaxy clusters, and there is evidence of magnetic fields in superclusters. Recently, new evidence has been presented for intergalactic magnetic fields: high energy gamma-rays from distant sources can initiate electromagnetic pair cascades when interacting with the extragalactic photon background; the charged component of the cascades will be deflected by magnetic fields, affecting the images of the sources. Using observations from FERMI, a lower bound of order 10^{-16} G has been claimed for the strength of fields in the filaments and voids of the cosmic web [44, 45, 46, 47].

The origin of these fields is still unclear (see e.g. [48, 49, 50]). They could have been generated via astrophysical processes during the nonlinear collapse stage of structure formation. There remain unresolved difficulties in explaining how these astrophysical seed fields lead to fields of the observed strength and coherence scales. Alternatively, the fields could be primordial seed fields – created in the very early Universe, during inflation, or during subsequent phase transitions. In principle inflation can generate fields on all scales – but unknown physics must be invoked to achieve non-minimal coupling of the electromagnetic field. The electroweak and QCD transitions can only produce fields on very small scales, up to the Hubble radius at magnetogenesis (and their amplitude is strongly constrained by their gravitational wave production before nucleosynthesis [81]).

Primordial magnetogenesis also takes place in the cosmic plasma after particle/anti-particle annihilation. This avoids the problem of exotic physics that faces inflationary magnetogenesis – standard Maxwell theory and standard cosmological perturbations in the cosmic plasma inevitably lead to magnetic fields. It also avoids the small coherence scale problem facing electroweak and QCD fields. However, the problem is the weakness of the fields, since this effect occurs at second and higher order in cosmological perturbations.

The key question is how weak is the field and how does it vary with scale? Differing qualitative estimates of the field strength have been given by [87, 88, 89, 90, 91, 92]. The power spectrum was first numerically computed by [93], which differs significantly from ours. More recently, [94] presented a power spectrum that is closer to our result. We discuss below the differences between previous results and ours. Our analysis is the first complete general relativistic computation of the power spectrum, taking into account all effects.

Our result is shown in Fig. 4.1. The power spectrum behaves as

$$\sqrt{k^3 P_B} \propto \begin{cases} k^4 & k \ll k_{\rm eq} \\ k^{0.5} & k \gg k_{\rm eq}\,. \end{cases} \tag{4.1}$$

On cluster scales the comoving field strength is

$$B_{1\,\rm Mpc} \sim 3 \times 10^{-29}\,\rm G. \tag{4.2}$$

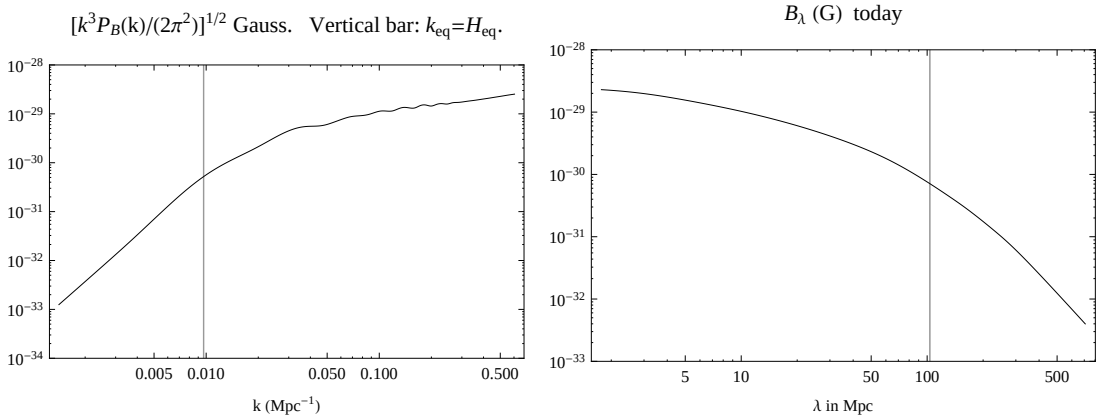

Figure 4.1: *Left:* Magnetic field spectrum today. *Right:* Comoving magnetic field strength today at a given scale.

Thus the field generated around recombination is too weak to act as a seed for the observed field strength of order μG. Adiabatic contraction of the magnetic flux lines during nonlinear collapse of structures provides an enhancement of $\sim 10^3$, while the nonlinear dynamo mechanism has an amplification factor $\sim 10^8$ (with many remaining uncertainties). Note that hydrodynamical and turbulence effects during nonlinear collapse themselves generate a field of order 10^{-20} G – which is also too small to account for the observed galactic and cluster fields [49].

The field (4.2) is also too weak to imprint detectable effects on the CMB. Nevertheless it is a real property of the standard cosmological model, and may have some impact on early structure formation during the 'dark ages' if it is the only primordial field. (See e.g.

[153, 154] for the role of magnetic fields in structure formation during the dark ages.)

As shown below, the magnetic field is given by

$$\left(a^2 B^i\right)' = -a^2 \epsilon^{ijk} \partial_j \Big[\left(1 + \Phi - \Psi\right) E_k \Big], \tag{4.3}$$

$$E^i \approx -\frac{4\rho_\gamma \sigma_{\rm T}}{3e} \Big(\Delta v^i_{{\rm b}\gamma} + \frac{2}{5} \Theta^i_j v^j_{\rm b} \Big), \tag{4.4}$$

where Φ, Ψ are first-order metric perturbations, $\Delta v^i_{{\rm b}\gamma} = v^i_{\rm b} - v^i_\gamma$ is the photon-baryon velocity difference, and Θ^i_j is the photon quadrupole moment, from anisotropic stress. This leads to three types of source terms for magnetogenesis:

$$\left(a^2 B\right)' = S_1 \big[\Delta v^{(2)}_{{\rm b}\gamma}\big] + S_2 \big[\big\{ \delta^{(1)}_\gamma + \Phi^{(1)} - \Psi^{(1)} \big\} \Delta v^{(1)}_{{\rm b}\gamma} \big] + S_3 \big[\Theta^{(1)}_\gamma v^{(1)}_{\rm b} \big]. \tag{4.5}$$

The first source term is second-order, while the other two are quadratic in first-order quantities. The contributions of the source terms to the power spectrum are shown in Fig. 6.1 (left).

Our paper builds on the physical analysis of nonlinear plasma dynamics presented in [155, 93, 94, 91, 156, 92, 96]. The key features of the dynamics are as follows.

- The electric field ensures that the proton-electron relative velocity is always strongly suppressed in comparison with the photon-electron relative velocity – even at high energies when the Compton interaction is stronger than the Coulomb interaction.
- Vorticity induced in the electron fluid is thus transferred almost entirely to the protons, and the baryon vorticity evolution is determined by the two-fluid dynamics of photons and baryons, which is very close to the equations of CMB dynamics. We use the second-order Boltzmann code of [96].
- The limit $v_{\rm e} - v_\gamma \to 0$ and $v_{\rm p} - v_{\rm e} \to 0$ is not equivalent to setting $v_{\rm p} = v_{\rm e} = v_\gamma$ in the momentum exchange equations, and the limit must be taken consistently.
- At first order, cosmological vector perturbations are zero after inflation, in the standard model. Magnetogenesis requires vortical currents, and these can therefore only be generated at second order, via mode-mode coupling of first-order scalar perturbations. This remains true even in the presence of topological defects, which are active sources for vector perturbations: at first order, the vector perturbations induced by the defects cannot break vorticity conservation in the cosmic plasma [98].
- On large scales there is some cancellation amongst the source terms in (4.5) (this is evident from Fig. 6.1). Neglecting any of the effects can thus lead to unreliable results.
- The magnetic field continues to be created after recombination, due to the residual nonzero ionization fraction. If the numerical integration is stopped at recombination, then the comoving field is under-estimated by a factor ~ 10 (see Fig. 6.1).

The plan of the paper is as follows. In the next section we review and clarify the magnetic and electric field generation beyond the tight-coupling limit. In Sec. 4.3, we detail the numerical integration of the differential evolution equations at second order in cosmological perturbations that we perform in order to solve for the magnetic field spectrum. We also provide analytical insight into the time and scale behaviors of the numerical results. We compare our results with previous work in Sec. 4.4. Details of some calculations are given in the Appendices.

4.2 Understanding the origin of the magnetic field

4.2.1 Interactions in the cosmic plasma

The stress-energy tensor of a species s satisfies

$$\nabla_\nu T_{\rm s}^{\mu\nu} = \sum_{\rm r} C_{\rm sr}^\mu \,, \quad \sum_{\rm s} \nabla_\nu T_{\rm s}^{\mu\nu} = 0 \,, \tag{4.6}$$

where $C_{\rm sr}^\nu (= -C_{\rm rs}^\nu)$ encodes all the effects of interactions with species r. Relative to observers with 4-velocity u^μ, the energy density transfer rate is $-u_\mu C_{\rm sr}^\mu$ and the momentum density transfer rate is $C_{\rm sr}^{\mu\perp} = h_\nu^\mu C_{\rm sr}^\nu$, where the projector is $h_\mu^\nu \equiv \delta_\mu^\nu + u_\mu u^\nu$.

The Euler equation for a species s is given in general by

$$\nabla_\nu T_{\rm s}^{\nu\mu\perp} = \sum_{\rm r} C_{\rm sr}^{\mu\perp} \,. \tag{4.7}$$

The kinematics of u^μ are described by decomposing its covariant derivative as [155, 157]

$$\nabla_\mu u_\nu = \frac{1}{3}\theta h_{\mu\nu} + \sigma_{\mu\nu} + \omega_{\mu\nu} - u_\mu \dot{u}_\nu \,, \tag{4.8}$$

where θ is the volume expansion, $\sigma_{\mu\nu}$ is the projected (i.e. orthogonal to u^μ), symmetric and tracefree shear, $\omega_{\mu\nu}$ is the projected antisymmetric vorticity, and $\dot{u}_\mu = u^\nu \nabla_\nu u_\mu$ is the projected acceleration. The vorticity vector is defined as

$$\omega_\nu \equiv \epsilon_{\mu\nu\lambda}\omega^{\nu\lambda} \,, \qquad \epsilon_{\mu\nu\lambda} \equiv u^\tau \epsilon_{\tau\mu\nu\lambda} \,, \tag{4.9}$$

where the totally antisymmetric tensor is defined by $\epsilon_{0123} = \sqrt{-g}$. (Note that our sign convention for $\omega_{\mu\nu}$ and definition of ω_μ recover the Newtonian limit, and differ from [155, 157].)

In the period of interest, from the end of particle/anti-particle annihilation up to now ($T_\gamma \lesssim 500{\rm keV}$, $z \lesssim 2\times 10^9$), the relevant species are protons, electrons, photons, and when recombination occurs, hydrogen atoms. Neutrinos affect only the background dynamics and the gravitational potentials in the Einstein equations. The Faraday tensor of the electromagnetic field defines electric and magnetic fields measured by u^μ observers:

$$E^\mu = F^{\mu\nu}u_\nu, \qquad B^\mu = \frac{1}{2}\epsilon^{\mu\nu\lambda}F_{\nu\lambda} \,. \tag{4.10}$$

Protons and electrons couple to the electromagnetic field through the term $C_{{\rm s}F}^\mu = F^\mu{}_\nu j_{\rm s}^\nu$, where $s = {\rm p,e}$ and j_s^ν is the electric 4-current. Then $\nabla_\nu T_F^{\mu\nu} = -\sum_{\rm s} F^\mu{}_\nu j_{\rm s}^\nu$. We have $j_{\rm s}^\mu = q_{\rm s} n_{\rm s} u_{\rm s}^\mu$, where $q_{\rm s}$ is the particle charge, $n_{\rm s}$ is the number density (in the rest frame) and the 4-velocity of species s is

$$u_{\rm s}^\mu = \gamma_{\rm s}(u^\mu + v_{\rm s}^\mu), \qquad u_\mu v_{\rm s}^\mu = 0, \qquad \gamma_{\rm s} = \left(1 - v_{\rm s}^2\right)^{-1/2} . \tag{4.11}$$

Here $\gamma_{\rm s} v_{\rm s}^\mu$ is the relative velocity of s measured by u^μ. Maxwell's equations are given in Appendix 4.6.1.

The momentum transfer rates are given by

$$C^{\mu\perp}_{\rm pe} = -e^2 n_{\rm e} n_{\rm p} \eta_{\rm C} \Delta v^\mu_{\rm pe}\,, \qquad \Delta v^\mu_{\rm pe} \equiv \gamma_{\rm p} v^\mu_{\rm p} - \gamma_{\rm e} v^\mu_{\rm e}\,, \tag{4.12}$$

$$C^{\mu\perp}_{\rm e\gamma} = -\frac{4}{3} n_{\rm e} \rho_\gamma \sigma_{\rm T} \Big(\Delta v^\mu_{\rm e\gamma} + \frac{2}{5} \Theta^\mu_\nu v^\nu_{\rm e} \Big), \tag{4.13}$$

$$C^{\mu\perp}_{\rm p\gamma} = -\frac{4}{3} \beta^2 n_{\rm p} \rho_\gamma \sigma_{\rm T} \Big(\Delta v^\mu_{\rm p\gamma} + \frac{2}{5} \Theta^\mu_\nu v^\nu_{\rm p} \Big), \qquad \beta \equiv \frac{m_{\rm e}}{m_{\rm p}}, \tag{4.14}$$

$$C^{\mu\perp}_{{\rm s}F} = q_{\rm s} n_{\rm s} \big(E^\mu + \epsilon_{\mu\nu\tau} v^\nu_{\rm s} B^\tau \big), \qquad {\rm s} = {\rm e}, {\rm p}\,. \tag{4.15}$$

The radiation energy density ρ_γ, the quadrupole of the radiation temperature anisotropy $\Theta_{\mu\nu}$, and the number densities $n_{\rm s}$, are as measured by u^μ observers. In the rest frame $u^\mu_{\rm s}$, the electrons and protons are well approximated by pressure-free matter, $T^{\mu\nu}_{\rm s} = \rho^{\rm rest}_{\rm s} u^\mu_{\rm s} u^\nu_{\rm s}$, where $\rho^{\rm rest}_{\rm s}$ is the rest-frame density measured by $u^\mu_{\rm s}$. In the u^μ frame, there is effective pressure, momentum density and anisotropic stress: $T^{\mu\nu}_{\rm s} = \rho_{\rm s} u^\mu u^\nu + P_{\rm s} h^{\mu\nu} + 2 q^{(\mu}_{\rm s} u^{\nu)} + \pi^{\mu\nu}_{\rm s}$, where [155],

$$\rho_{\rm s} \equiv m_{\rm s} n_{\rm s} = \gamma^2_{\rm s} \rho^{\rm rest}_{\rm s}\,, \qquad P_{\rm s} = \frac{1}{3} v^2_{\rm s} \rho_{\rm s}\,, \tag{4.16}$$

$$q^\mu_{\rm s} = \rho_{\rm s} v^\mu_{\rm s}\,, \qquad \pi^{\mu\nu}_{\rm s} = \rho_{\rm s} \Big(v^\mu_{\rm s} v^\nu_{\rm s} - \frac{1}{3} v^2_{\rm s} h^{\mu\nu} \Big). \tag{4.17}$$

The Thomson cross-section is $\sigma_{\rm T} = 8\pi\alpha^2/(3m^2_{\rm e})$, and the Coulomb interaction is governed by the electrical resistivity

$$\eta_{\rm C} = \frac{\pi e^2 \sqrt{m_{\rm e}} \ln\Lambda}{T^{3/2}} \simeq 10^{-12} {\rm sec} \left(\frac{1+z}{10^3} \right)^{-3/2} \left(\frac{\ln\Lambda}{10} \right), \tag{4.18}$$

where Λ is the Coulomb logarithm. On cosmological time scales the magnetic field diffuses below a length scale $\sim \sqrt{\eta_{\rm C}/H_0} \sim 100\,{\rm AU}$, so that diffusion can safely be ignored [94]. The characteristic time scales for electrons interacting via the Coulomb and Thomson interactions are

$$\tau_{\rm C} = \frac{m_{\rm e}}{e^2 n_{\rm e} \eta_{\rm C}} \simeq \frac{20\,{\rm sec}}{x_{\rm e}} \left(\frac{1+z}{10^3} \right)^{-3/2}, \qquad x_{\rm e} \equiv \frac{n_{\rm e}}{n_{\rm e} + n_{\rm H}}, \tag{4.19}$$

$$\tau_{\rm T} = \frac{m_{\rm e}}{\sigma_{\rm T} \rho_\gamma} \simeq 5 \times 10^8 {\rm sec} \left(\frac{1+z}{10^3} \right)^{-4}, \tag{4.20}$$

where $n_{\rm e}$ is the number density of free electrons and $x_{\rm e}$ is the fraction of free electrons. We used $n_{\rm e0} + n_{\rm H0} \simeq 3 \times 10^{-7}\,{\rm cm}^{-3}$ [158]. The time scale which characterizes the evolution of the plasma can be taken as

$$\begin{aligned} \tau_{\rm evo}(z) &= \min\left\{ \tau_{\rm S}(z),\, \tau_{1\,{\rm Mpc}}(z) \right\} \\ &= \min\left\{ \frac{1}{\sqrt{H(z) \sigma_{\rm T} n_{\rm e}(z)}},\, \frac{1}{(1+z) k_{1\,{\rm Mpc}}} \right\}. \end{aligned} \tag{4.21}$$

Here $\tau_{\rm S}$ is the Silk damping time and 1 Mpc is taken as the minimum comoving scale on which we can trust a second-order perturbative analysis up to redshift $z = 0$.

4.2.2 Electric field

The Euler equation (4.7) for the proton and electron velocities is given by [155]:

$$m_{\rm s}n_{\rm s}\Big(\dot{v}_{\rm s}^{\mu\perp}+\dot{u}^{\mu}+K_{\rm s}^{\mu}\Big)=C_{\rm sr}^{\mu\perp}+C_{{\rm s}\gamma}^{\mu\perp}+C_{{\rm s}F}^{\mu\perp}, \tag{4.22}$$

where $\mathrm{s},\mathrm{r}=\mathrm{p},\mathrm{e}$ and

$$\begin{aligned} K_{\rm s}^{\mu} &= \Big(\frac{\dot{n}_{\rm s}}{n_{\rm s}}+\frac{4}{3}\theta+\dot{u}_{\nu}v_{\rm s}^{\nu}+\frac{1}{n_{\rm s}}v_{\rm s}^{\nu}{\rm D}_{\nu}n_{\rm s}+{\rm D}_{\nu}v_{\rm s}^{\nu}\Big)v_{\rm s}^{\mu} \\ &\quad +\left(\sigma^{\mu}{}_{\nu}-\omega^{\mu}{}_{\nu}\right)v_{\rm s}^{\nu}+v_{\rm s}^{\nu}{\rm D}_{\nu}v_{\rm s}^{\mu}. \end{aligned} \tag{4.23}$$

The covariant spatial derivative D_{μ} is defined in (4.84). The first term on the right of (4.23) describes not only the evolution due to the expansion of the universe which conserves the particles, but also the evolution of the number density due to recombination which does not conserve the particles when hydrogen atoms are formed around recombination.

From now on we expand in perturbations around a Friedmann background, up to second order. The metric in Poisson gauge is

$${\rm d}s^2=a^2\left[-(1+2\Phi){\rm d}\eta^2+2S_i{\rm d}x^i{\rm d}\eta+(1-2\Psi){\rm d}\boldsymbol{x}^2\right] \tag{4.24}$$

where S_i is a vector perturbation ($\partial^i S_i=0$) and enters only at second order. Perturbed quantities are expanded according to $X=\bar{X}+X^{(1)}+X^{(2)}$. Only the first order of scalar perturbations Φ and Ψ will enter the evolution equation of the magnetic field, so we omit the superscripts for them. The explicit form of the term $\dot{v}_{\rm s}^{\mu\perp}+\dot{u}^{\mu}+K_{\rm s}^{\mu}$ in (4.22) is then given by (4.95), with $w_{\rm s}=0=c_{\rm s}^2$.

We set $n_{\rm e}=n_{\rm p}\equiv n$, since we find that the final expression of the resulting electric field is not affected by $n_{\rm e}-n_{\rm p}$, in agreement with [156].

In order to obtain a dynamical equation for the velocity difference $\Delta v_{\rm pe}^{\mu}=v_{\rm p}^{\mu}-v_{\rm e}^{\mu}$, we use (4.22) to obtain

$$m_{\rm e}n\Big(\Delta\dot{v}_{\rm pe}^{\mu\perp}+\Delta K_{\rm pe}^{\mu}\Big)=(1+\beta)enE^{\mu}+C_{\rm pe}^{\mu\perp}-C_{{\rm e}\gamma}^{\mu\perp}+\beta\left(C_{\rm pe}^{\mu\perp}+C_{{\rm p}\gamma}^{\mu\perp}\right). \tag{4.25}$$

The Lorentz force term in (4.15) has been neglected since it is higher order. We define the baryon velocity as the velocity of the centre of mass of the charged particles; then

$$(m_{\rm p}+m_{\rm e})v_{\rm b}^{\mu}=m_{\rm p}v_{\rm p}^{\mu}+m_{\rm e}v_{\rm e}^{\mu}\,, \tag{4.26}$$

$$v_{\rm p}^{\mu}=v_{\rm b}^{\mu}+\frac{\beta}{1+\beta}\Delta v_{\rm pe}^{\mu}\,,\qquad v_{\rm e}^{\mu}=v_{\rm b}^{\mu}-\frac{1}{1+\beta}\Delta v_{\rm pe}^{\mu}\,. \tag{4.27}$$

In principle, the baryon velocity can be different from the velocity of hydrogen, i.e. of electrons and protons recombined, but thermal collision ensure that hydrogen atoms follow closely the electrons and protons.

Using (4.25)–(4.27) and the explicit forms (4.12)–(4.14) of the collision terms, we obtain

$$m_{\rm e}\Big(\Delta\dot{v}^{\mu\perp}_{\rm pe}+\Delta K^{\mu}_{\rm pe}\Big)=(1+\beta)eE^{\mu}-(1+\beta)e^2n\eta_{\rm C}\Delta v^{\mu}_{\rm pe}\\ +\frac{4}{3}\sigma_{\rm T}\rho_{\gamma}\Big[(1-\beta^3)\Big(\Delta v^{\mu}_{{\rm b}\gamma}+\frac{2}{5}\Theta^{\mu}_{\nu}v^{\nu}_{\rm b}\Big)-\frac{1+\beta^4}{1+\beta}\Big(\Delta v^{\mu}_{\rm pe}+\frac{2}{5}\Theta^{\mu}_{\nu}\Delta v^{\nu}_{\rm pe}\Big)\Big]. \tag{4.28}$$

We show below that the $\Theta^{\mu}_{\nu}\Delta v^{\nu}_{\rm pe}$ term can be neglected, since it is higher order.

Equation (4.28) shows that an electric field can be generated by nonzero velocity differences $\Delta v_{\rm pe}$ and $\Delta v_{\gamma{\rm b}}$. The Maxwell equation (4.80) shows that then B^{μ} can be generated, provided that E^{μ} is transverse. We will show that the generated electric field keeps electrons and protons more bound together and therefore leads to a decrease in $\Delta v_{\rm pe}$, which becomes negligible compared to $\Delta v_{\gamma{\rm e}}$.

Neglecting third order terms, the Maxwell equation (4.81) can be rewritten in terms of the velocity difference $\Delta v^{\mu}_{\rm pe}$ as

$$\Delta v^{\mu}_{\rm pe}=\frac{1}{en}\Big(\mathrm{curl}\,B^{\mu}-\dot{E}^{\mu\perp}-\frac{2}{3}\theta E^{\mu}+\sigma^{\mu\nu}E_{\nu}\Big), \tag{4.29}$$

where we used (4.83).

In order to estimate the magnitudes of the various contributions in the stationary regime, we expand all evolving quantities in frequency space:

$$M^{\mu}(\boldsymbol{x},\eta)=\int_0^{\infty}\partial\omega\hat{M}^{\mu}(\boldsymbol{x},\omega)\mathrm{e}^{\mathrm{i}\omega\eta}\ , \tag{4.30}$$

where the mode $\hat{M}^{\mu}$ has characteristic oscillation frequency $\omega\simeq\tau_{\rm evo}^{-1}$. In terms of the characteristic timescales (4.19) and (4.20), we find from (4.28) and (4.29) that

$$\hat{E}^{\mu}\Big[(1+\beta)+\mathcal{O}\Big(\frac{\eta_{\rm C}\tau_{\rm C}}{\tau^2_{\rm evo}}+\mathrm{i}\frac{4}{3}\frac{\eta_{\rm C}}{\tau_{\rm evo}}+\mathrm{i}\frac{\eta_{\rm C}\tau_{\rm C}}{\tau_{\rm evo}\tau_{\rm T}}\Big)\Big]=\\ \eta_{\rm C,eff}\Big[(1+\beta)+\mathcal{O}\Big(\mathrm{i}\frac{\eta_{\rm C}\tau_{\rm C}}{\eta_{\rm C,eff}\tau_{\rm evo}}\Big)\Big]\mathrm{curl}\,\hat{B}^{\mu}-\frac{4m_{\rm e}}{3e\tau_{\rm T}}(1-\beta^3)\Big[\Delta\hat{v}^{\mu}_{{\rm b}\gamma}+\frac{2}{5}\Theta^{\mu}_{\nu}\hat{v}^{\nu}_{\rm b}\Big], \tag{4.31}$$

where we used $\Delta K_{\rm pe}=\mathcal{O}(\Delta\dot{v}_{\rm pe})$, and we defined [94]

$$\eta_{\rm C,eff}\equiv\eta_{\rm C}\Big[1+\frac{4(1+\beta^4)}{3(1+\beta)^2}\frac{\tau_{\rm C}}{\tau_{\rm T}}\Big]. \tag{4.32}$$

Given the hierarchy of the different timescales involved in (4.31), it follows that the largest contribution to the resulting electric field is given by the velocity difference $\Delta v^{\mu}_{{\rm b}\gamma}$. This can be seen in Fig. 4.2, where we plot the different ratios of typical timescales that enter in (4.31). Specifically, all the plotted ratios are always well below unity for the period of interest, from very large redshift until today, even accounting for recombination around $z\simeq1080$. This allows us to write

$$E^{\mu}\simeq\eta_{\rm C,eff}\,\mathrm{curl}\,B^{\mu}-\frac{4m_{\rm e}}{3e\tau_{\rm T}}\frac{1-\beta^3}{1+\beta}\Big(\Delta v^{\mu}_{{\rm b}\gamma}+\frac{2}{5}\Theta^{\mu}{}_{\nu}v^{\nu}_{\rm b}\Big). \tag{4.33}$$

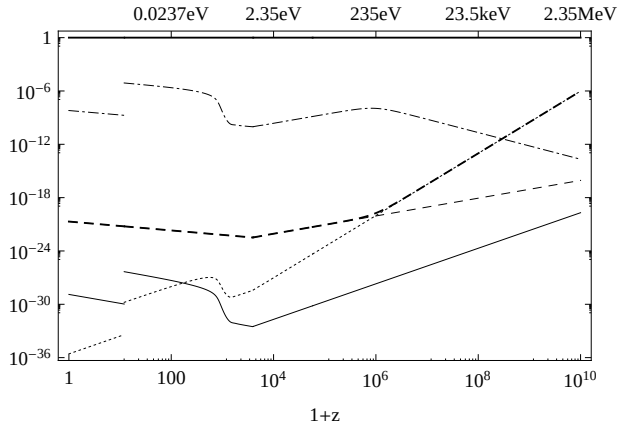

Figure 4.2: Evolution with redshift of different ratios between characteristic times that arise in (4.31), compared with unity (thick black line): $\eta_{\rm C}\tau_{\rm C}/(\tau_{\rm evo}^2)$ (thin solid), $\eta_{\rm C}/\tau_{\rm evo}$ (thin dashed), $\eta_{\rm C}\tau_{\rm C}/(\tau_{\rm evo}\tau_{\rm T})$ (dotted), $\eta_{\rm C}\tau_{\rm C}/(\eta_{\rm C,eff}\tau_{\rm evo})$ (dot-dashed) and $\eta_{\rm C,eff}/\tau_{\rm evo}$ (thick dashed). (The jumps in the curves occur at reionization.)

In order to compute the final magnetic field produced by such an electric field, we consider the curl of the electric field, governed by Maxwell's equation (4.80). In frequency space

$$\mathrm{i}\frac{\hat{B}^\mu}{\tau_{\rm evo}} \simeq -\eta_{\rm C,eff}\,\mathrm{curl}\,\mathrm{curl}\,\hat{B}^\mu + \frac{4m_{\rm e}}{3e\tau_{\rm T}}\frac{1-\beta^3}{1+\beta}\mathrm{curl}\Big(\Delta\hat{v}^\mu_{\rm b\gamma} + \frac{2}{5}\Theta^\mu_\nu\hat{v}^\nu_{\rm b}\Big). \tag{4.34}$$

Remembering that the magnetic field is divergence free, we can compare the first two terms of the above equation. Their ratio in Fourier space is of order $(\tau_{\rm evo}\eta_{\rm C,eff}k^2)^{-1} \simeq \tau_{\rm evo}/\eta_{\rm C,eff}$. Therefore, on all scales of interest, we can conclude that the contribution of the $\eta_{\rm C,eff}\,\mathrm{curl}\,\hat{B}^\mu$ term in (4.33) is negligible compared to the last term.

The above considerations remain valid once we approach recombination time, as long as the residual fraction of free electrons $x_{\rm e}$ is not too small. This is to ensure that the approximations of the ratios of time scales made to obtain (4.33) remain valid. This is indeed the case, and it can be checked from Fig. 4.2, since $x_{\rm e} \sim 10^{-3} - 10^{-4}$ after last scattering [159, 158] until reionization.

We are therefore left with the following expression for the electric field produced by the tiny velocity difference between electrons and protons:

$$E^\mu \;=\; -\frac{1-\beta^3}{1+\beta}\frac{4\rho_\gamma\sigma_{\rm T}}{3e}\Big(\Delta v^\mu_{\rm b\gamma} + \frac{2}{5}\Theta^\mu_\nu v^\nu_{\rm b}\Big). \tag{4.35}$$

It is important to note that this expression does not contain the number density of free electrons $n_{\rm e}$. Therefore the electric field produced by this mechanism before recombination is still present after last scattering (see also [158]) and can in principle continue to generate a magnetic field after recombination.

We can now also finally prove that

$$\Delta v^\mu_{\rm pe} \ll \Delta v^\mu_{\rm e\gamma}\,. \tag{4.36}$$

Using (4.35) and (4.34) without the $\eta_{\rm C,eff}$ term, and in the Maxwell equation (4.29) leads

to an estimation of the order of magnitude of velocity differences:

$$\Delta v^{\mu}_{\rm pe} \propto \frac{\eta_{\rm C}\tau_{\rm C}}{\tau_{\rm evo}\tau_{\rm T}}\Delta v^{\mu}_{\rm b\gamma}\,, \quad \Delta v^{\mu}_{\rm p\gamma} \simeq \Delta v^{\mu}_{\rm b\gamma} \simeq \Delta v^{\mu}_{\rm e\gamma}\,. \tag{4.37}$$

The order of magnitude of the ratio $\Delta v^{\mu}_{\rm pe}/\Delta v^{\mu}_{\rm b\gamma}$ is shown in Fig. 4.2 and remains well below unity for all relevant times, even when Coulomb scattering becomes less efficient than Compton scattering, that is for $z \gtrsim 10^6$.

It also follows from (4.37) and (4.13) that we can rewrite (4.35) as

$$e(n_{\rm e} + n_{\rm H})x_{\rm e}E^{\mu} = C^{\mu\perp}_{\rm b\gamma} = \nabla_{\nu}T^{\mu\nu\perp}_{\rm b}, \tag{4.38}$$

where we neglect terms of order β and where here the baryon index b encompasses protons, electrons and hydrogen atoms.

As a conclusion of this section, we stress again that when we assume that electrons and photons are tightly coupled, as was originally considered in [86], then the electrons and protons are even more tightly coupled by the electromagnetic field which is generated, so that the electrons and protons can still be considered, from the point of view of photons, as a single fluid of baryons. As a consequence, taking $\Delta v^{\mu}_{\rm e\gamma} \to 0$ at early times has to be performed consistently by keeping $\Delta v^{\mu}_{\rm pe} \ll \Delta v^{\mu}_{\rm e\gamma}$ when taking the limit. For the tight-coupled limit, this is crucial, since it corresponds exactly to the limit $v_{\rm e} = v_{\gamma} = v_{\rm p} = 0$, and the collision terms cannot be evaluated directly from their expressions (4.12)–(4.15).

4.2.3 Local inertial frame (tetrad)

It is convenient to express all quantities in a local inertial frame, defined by an orthonormal tetrad $\boldsymbol{e}_{\underline{a}}$ ($\underline{a} = 0, 1, 2, 3$):

$$e_{\underline{a}}{}^{\mu}e_{\underline{b}}{}^{\nu}g_{\mu\nu} = \eta_{\underline{ab}}, \quad e^{\underline{a}}{}_{\mu}e^{\underline{b}}{}_{\nu}g^{\mu\nu} = \eta^{\underline{ab}}. \tag{4.39}$$

The tetrad indices are distinguished from general coordinate indices by underlining, and $\underline{i}, \underline{j}, \underline{k} \cdots = 1, 2, 3$. We choose a comoving tetrad, so that $\boldsymbol{e}_{\underline{0}}$ is the fundamental observer 4-velocity: $e_{\underline{0}}{}^{\mu} = u^{\mu}$. In the background, $\bar{e}_{\underline{0}}{}^{\mu} = \bar{u}^{\mu} = (a^{-1}, 0)$. The perturbed tetrad is given in Appendix 4.6.2. Derivatives along the tetrad vectors are defined by

$$\partial_{\underline{a}} \equiv e_{\underline{a}}{}^{\nu}\partial_{\nu}\,. \tag{4.40}$$

Covariant derivatives in the tetrad frame are computed using the affine connections given in Appendix 4.6.2.

Tetrads make the physical meaning of all nonscalar quantities more transparent. In linear perturbation theory, it is common practice to decompose perturbed quantities in a background tetrad. For instance the velocity is often decomposed as $u^{i}_{(1)} \equiv a^{-1}v^{i}_{(1)}$, together with $u^{(1)}_{i} = av^{(1)}_{i}$, which means implicitly that $v^{(1)}_{i} \equiv \delta_{ij}v^{j}_{(1)}$. Thus $v^{i}_{(1)}$ coincides with $v^{\underline{i}}_{(1)} = \bar{e}^{\underline{i}}_{j}u^{j}_{(1)}$. Introducing tetrads is the natural generalization of this standard procedure when considering higher order perturbations, and this has already been used for example to decompose velocities [160, 161]. The nonlinear evolution of the distribution of photons is well suited to computation in a tetrad frame [96].

4.2.4 Magnetic field

The Maxwell equation (4.80) becomes in the tetrad basis

$$\partial_{\underline{0}}(a^2 B^{\underline{i}}) = -a^2 \epsilon^{\underline{i\ell k}} \partial_{\underline{\ell}} \left[(1 + \Phi - \Psi)\, E_{\underline{k}} \right], \tag{4.41}$$

Equivalently we can use derivatives in the coordinate basis:

$$\left(a^2 B^{\underline{i}}\right)' = -a^2 \epsilon^{\underline{i\ell k}} \partial_{\ell} \left[(1 + \Phi - \Psi)\, E_{\underline{k}} \right], \tag{4.42}$$

where we have used the fact that the electric field is at least a first order quantity, and the magnetic field a second order quantity. The gravitational potentials in this expression occur only at first order. Equation (4.42) is compatible with [92], which can be seen via $E_{\underline{k}} = e_{\underline{k}}{}^{i} E_i$.

To obtain (4.41), we need

$$(\mathrm{curl}\, E)^{\underline{i}} = \epsilon^{\underline{i\ell k}} \nabla_{\underline{\ell}} E_{\underline{k}} = \epsilon^{\underline{i\ell k}} \partial_{\ell} \left[(1 - \Psi) E_{\underline{k}} \right], \tag{4.43}$$

which uses the affine connections up to first order given in Appendix 4.6.2. Also,

$$e^{\underline{i}}{}_{\mu} \epsilon^{\mu\nu\lambda} \dot{u}_{\nu} E_{\lambda} = \epsilon^{\underline{i\ell k}}\, \dot{u}_{\underline{\ell}} E_{\underline{k}} = -\epsilon^{\underline{i\ell k}} E_{\underline{\ell}} \partial_{\underline{k}} \Phi\,, \tag{4.44}$$

which follows from

$$\dot{u}_{\underline{i}} = (u^{\mu} \nabla_{\mu} u_{\nu}) e_{\underline{i}}{}^{\nu} = (\nabla_{\underline{0}} e^{\underline{0}}{}_{\nu}) e_{\underline{i}}{}^{\nu} = \Omega_{\underline{0}}{}^{\underline{0}}{}_{\underline{i}} = \partial_{\underline{i}} \Phi\,. \tag{4.45}$$

In addition, we omitted terms like $\Phi \epsilon^{\underline{i\ell k}} \partial_{\underline{\ell}} E_{\underline{k}}$ and $\Psi \epsilon^{\underline{i\ell k}} \partial_{\underline{\ell}} E_{\underline{k}}$ in deriving (4.42), since the electric field contributes only at first order – and at this order, it is curl-free. For the same reason, we can also replace $\partial_{\underline{\ell}}$ by $a^{-1}\partial_{\ell}$.

In summary, magnetogenesis is governed by (4.42) and (4.38), i.e.

$$\begin{aligned} \left(a^2 B_{\underline{i}}\right)' &= -\frac{a^2}{e(n_{\mathrm{e}} + n_{\mathrm{H}}) x_{\mathrm{e}}} \epsilon_{\underline{i\ell k}} \partial^{\ell} \left[(1 + \Phi - \Psi)\, C^{\underline{k}}_{\mathrm{b}\gamma} \right] \\ &= -\frac{a^2}{e(n_{\mathrm{e}} + n_{\mathrm{H}}) x_{\mathrm{e}}} \epsilon_{\underline{i\ell k}} \partial^{\ell} \left[(1 + \Phi - \Psi)\, \nabla_{\nu} T^{\nu\underline{k}}_{\mathrm{b}} \right], \end{aligned} \tag{4.46}$$

where here, as in (4.38), the baryon index b encompasses electrons, protons and hydrogen atoms. Finally, note that the value of the magnetic field depends of course on the observer. Its value in the baryon frame is related to its value (4.42) in the fundamental frame by

$$B^{\underline{i}}_{\mathrm{b}} = B^{\underline{i}} - \epsilon^{\underline{i\ell k}}\, v_{\mathrm{b}\,\underline{\ell}} E_{\underline{k}}\,. \tag{4.47}$$

4.2.5 Numerical computation

In order to solve the evolution equation for the magnetic field, we need to solve the Boltzmann hierarchy for baryons and photons, to compute the source of the electric field in (4.35). The basic idea is to decompose the directional dependence of radiation in the local

inertial frame into multipoles:

$$\Theta_{\underline{i}_1\cdots\underline{i}_\ell}(\boldsymbol{x})n^{\underline{i}_1}\cdots n^{\underline{i}_\ell} = \int\frac{\partial^3\boldsymbol{k}}{(2\pi)^{3/2}}\sum_m\Theta^m_\ell(\boldsymbol{k})G_{\ell m}(\boldsymbol{k},\boldsymbol{x},\boldsymbol{n}) \tag{4.48}$$

$$G_{\ell m}(\boldsymbol{k},\boldsymbol{x},\boldsymbol{n}) = \mathrm{i}^{-\ell}\Big(\frac{4\pi}{2\ell+1}\Big)^{1/2}\mathrm{e}^{\mathrm{i}k_ix^i}Y^{\ell m}(n^{\underline{i}})\,. \tag{4.49}$$

We suppress the time dependence for convenience.

Terms quadratic in first order perturbations appear as convolutions, and we introduce the notation

$$\mathcal{K}\{f_1f_2\}(\boldsymbol{k}) \equiv \int\frac{\partial^3\boldsymbol{k}_1\partial^3\boldsymbol{k}_2}{(2\pi)^{3/2}}\,\delta^3_{\mathrm{D}}(\boldsymbol{k}_1+\boldsymbol{k}_2-\boldsymbol{k})f_1(\boldsymbol{k}_1)f_2(\boldsymbol{k}_2)\,. \tag{4.50}$$

A Fourier mode q_i is decomposed on the helicity basis of the background spacetime as

$$q^i = \delta^{ij}q_j = q_{(+)}\bar{e}^i_{(+)} + q_{(-)}\bar{e}^i_{(-)} + q_{(0)}\bar{e}^i_{(0)}\,, \tag{4.51}$$

$$q_{(h)} = q_i\bar{e}^{*i}_{(h)}\,. \tag{4.52}$$

The background helicity basis vectors $\bar{\boldsymbol{e}}_{(h)}$, with helicity $h=0,\pm$ are defined in [96]. The azimuthal direction $h=0$ corresponds to scalar perturbations and is aligned with the total Fourier mode, i.e. $\bar{\boldsymbol{e}}_{(0)}=\hat{\boldsymbol{k}}$, while $h=\pm$ correspond to vector perturbations. At first order, when the mode is aligned with the azimuthal direction since $\boldsymbol{q}=\boldsymbol{k}$, there are only scalar perturbations. For vector quantities like the electric field, we need to use a helicity basis $\boldsymbol{e}_{(h)}$ on the perturbed spacetime, and this is built by the identification of $\bar{\boldsymbol{e}}_{(h)}$ with $\boldsymbol{e}_{(h)}$, i.e. $\bar{e}^i_{(h)} = e^{\underline{i}}_{(h)}$. Vector quantities like the electric field $E_{\underline{i}}$ are then expanded as

$$X^{\underline{i}} = X_{(+)}e^{\underline{i}}_{(+)} + X_{(-)}e^{\underline{i}}_{(-)} + X_{(0)}e^{\underline{i}}_{(0)}\,, \tag{4.53}$$

$$X_{(h)} = X_{\underline{i}}e^{*\underline{i}}_{(h)}\,. \tag{4.54}$$

In this basis, the Maxwell equation (4.42) becomes (explicitly giving the perturbative order of quantities)

$$\Big[a^2B^{(2)}_{(\pm)}(\boldsymbol{k})\Big]' = \mp ka^2\Big[E^{(2)}_{(\pm)}(\boldsymbol{k}) + \mathcal{K}\Big\{\big[\Phi^{(1)}-\Psi^{(1)}\big]E^{(1)}_{(\pm)}\Big\}(\boldsymbol{k})\Big]. \tag{4.55}$$

We projected (4.42) along $e^{(h)*}_{\underline{i}}$ and used

$$\mathrm{i}\epsilon^{\underline{i\ell k}}k_{\underline{\ell}}e^{(\pm)}_{\underline{k}} = \pm ke^{\underline{i}}_{(\pm)}\,, \qquad \mathrm{i}e^{(\pm)*}_{\underline{i}}\epsilon^{\underline{i\ell k}}k_{\underline{\ell}}X_{\underline{k}} = \pm kX_{(\pm)}\,. \tag{4.56}$$

Note that there are only contributions from $h=\pm$ and we thus recover that scalar perturbations cannot generate a magnetic field and vortical perturbations are required to source the magnetic field. Using the multipole decomposition of (4.35), and neglecting $\beta\ll 1$, we

obtain finally,

$$\begin{aligned}\left[a^2 B^{(2)}_{(\pm)}(\boldsymbol{k})\right]' &= \pm ka^2 \frac{4\sigma_{\rm T}\bar{\rho}_\gamma}{3e}\Big[V^{(2)}_{(\pm)}(\boldsymbol{k}) + \mathcal{K}\Big\{\left[\delta^{(1)}_\gamma + \Phi^{(1)} - \Psi^{(1)}\right]V^{(1)}_{(\pm)}\Big\}(\boldsymbol{k}) \\ &\quad -\mathcal{K}\Big\{\sum_h \frac{\kappa(\pm 1,h)}{5}\Theta_2^{\pm 1+h(1)} v^{(1)}_{{\rm b}(-h)}\Big\}(\boldsymbol{k})\Big] \\ &\equiv \pm ka^2 \frac{4\sigma_{\rm T}\bar{\rho}_\gamma}{3e}\left[S^{(\pm)}_1(\boldsymbol{k}) + S^{(\pm)}_2(\boldsymbol{k}) + S^{(\pm)}_3(\boldsymbol{k})\right], \end{aligned} \tag{4.57}$$

where $V_{(h)} \equiv v_{{\rm b}(h)} - v_{\gamma(h)}$ and $\delta_\gamma = \delta\rho_\gamma/\bar{\rho}_\gamma$. Also,

$$\kappa(h,0) = \sqrt{(4-h^2)},\ \kappa(h,\pm 1) = -\sqrt{\frac{(2\pm h)(3\pm h)}{2}}. \tag{4.58}$$

The last equality in (4.57) defines the contribution of each line above: $S^{(\pm)}_1$ is the purely second order contribution from $V^{(2)}$; $S^{(\pm)}_2$ is the $\delta_\gamma V$ contribution and $S^{(\pm)}_3$ is the $\Theta_2 v_{\rm b}$ contribution.

Although $V^{(1)}_{(\pm)}(k)$ vanishes at first order since there are no vector perturbations, $V^{(1)}_{(\pm)}(\boldsymbol{k}_1)$ and $V^{(1)}_{(\pm)}(\boldsymbol{k}_2)$ do not vanish in general, since the modes $\boldsymbol{k}_1$ and $\boldsymbol{k}_2$ are not necessarily aligned with the azimuthal direction $\hat{\boldsymbol{k}} = \boldsymbol{k}/k$. We first need to obtain their expression when the modes $\boldsymbol{k}_1$ or $\boldsymbol{k}_2$ are aligned with the azimuthal direction, and then we perform a rotation of the azimuthal direction [96].

In order to explicitly take into account the symmetry of the convolution products in (4.57), we can symmetrize the source terms. At first order there are only scalar perturbations, and all first order tensorial quantities are gradients of scalar functions, so that $X^{(1)}_{\underline{i}_1\ldots\underline{i}_n} = X^{(1)}_{i_1\ldots i_n} = \partial_{i_1}\ldots\partial_{i_n}X^{(1)}$. Most of the source terms are of the form $\epsilon^{\underline{i\ell k}}\partial_\ell\left(X\,Y_k\right) = \epsilon^{\underline{i\ell k}}\partial_\ell\left(X\partial_k Y\right)$, and once projected along $e^{(\pm)*}_{\underline{i}}$ they contribute to the generation of the magnetic field proportionally to

$$\bar{e}^{*\,i}_{(\pm)}[X\partial_i Y](\boldsymbol{k}) = \frac{\rm i}{2}\int \frac{\partial^3\boldsymbol{q}}{(2\pi)^{3/2}} q_{(\pm)}\left[X(\boldsymbol{k}-\boldsymbol{q})Y(\boldsymbol{q}) - X(\boldsymbol{q})Y(\boldsymbol{k}-\boldsymbol{q})\right]. \tag{4.59}$$

Here X and Y denote $\delta_\gamma, V^{(1)}, v_{\rm b}, \Phi, \Psi$.

This symmetrization, which is always possible, shows that for these types of terms, the configurations of $(\boldsymbol{k},\boldsymbol{k}_1,\boldsymbol{k}_2)$ with $k_1 = k_2$ will not contribute in the convolution. Only couplings from a quadrupolar quantity to gradient terms, which are of the type

$$\epsilon^{\underline{i\ell k}}\partial_\ell\left(X_k{}^j\partial_j Y\right) = \epsilon^{\underline{i\ell k}}\partial_\ell\left(\partial_k\partial^j X\partial_j Y\right), \tag{4.60}$$

as in the last line of (4.57), can have contributions to the convolution coming from configurations with $k_1 = k_2$. The generated magnetic field is thus severely suppressed at early times for these configurations since the quadrupole of radiation is suppressed in the tight-coupling regime.

4.3 Numerical results

4.3.1 Transfer functions

In order to obtain the final magnetic field spectrum produced via this mechanism, we integrate numerically the evolution equations for cosmological perturbations up to second order, since we have to take into account even the behavior of the second order velocity difference between baryons and photons $V^{(2)}_{(h)}(k,\eta)$. We use throughout the cosmological parameters of WMAP7 [162].

For a variable X, the first order transfer function is $X^{(1)}(\boldsymbol{k},\eta) = \mathcal{X}^{(1)}(k,\eta)\Phi_{\rm in}(\boldsymbol{k})$, where $\Phi_{\rm in}$ is the gravitational potential deep in the radiation era. Because of statistical isotropy, the first order transfer function depends only on the magnitude of the Fourier mode and not on its direction. This is however only strictly true for multipoles like Θ^m_2 and $V_{(h)}$ defined from non-scalar quantities if the azimuthal direction is aligned with $\hat{\boldsymbol{k}}$, and considering only scalar perturbations at first order the contributions for $h \neq 0$ vanish. However, when using these first order transfer functions in the quadratic terms of the second order equations, we must rotate these multipoles according to the angles between $\hat{\boldsymbol{k}}_1, \hat{\boldsymbol{k}}_2$ and $\hat{\boldsymbol{k}}$. This is to ensure that the multipoles remain defined with respect to the total momentum $\hat{\boldsymbol{k}}$ [96].

The second order transfer function $\mathcal{X}^{(2)}(\boldsymbol{k}_1,\boldsymbol{k}_2,\eta)$ is defined by

$$X^{(2)}(\boldsymbol{k},\eta) = \mathcal{K}\left\{\mathcal{X}^{(2)}(\boldsymbol{k}_1,\boldsymbol{k}_2,\eta)\Phi_{\rm in}(\boldsymbol{k}_1)\Phi_{\rm in}(\boldsymbol{k}_2)\right\}(\boldsymbol{k}). \tag{4.61}$$

Without loss of generality we enforce $\mathcal{X}^{(2)}(\boldsymbol{k}_1,\boldsymbol{k}_2,\eta) = \mathcal{X}^{(2)}(\boldsymbol{k}_2,\boldsymbol{k}_1,\eta)$ in numerical calculations. The transfer functions of the first and second order quantities needed in the source terms are obtained by a joint solution of the Boltzmann equation (for photons and neutrinos), the conservation and Euler equations (for baryons and cold dark matter) and the Einstein equations (for metric perturbations). They are found numerically using the same techniques as in [163].

The transfer function of the magnetic field can be split into the different contributions of the $S_i^{(\pm)}$ sources defined in (4.57). The transfer functions of these contributions are related to the transfer functions of the sources through

$$\mathcal{B}^{S_i}_{(\pm)}(\boldsymbol{k}_1,\boldsymbol{k}_2,\eta) = \frac{4\sigma_{\rm T}k}{3ea^2}\int^{\eta}\partial\eta' a^2\bar{\rho}_\gamma\mathcal{S}_i^{(\pm)}(\boldsymbol{k}_1,\boldsymbol{k}_2,\eta')\,, \tag{4.62}$$

and this is how we obtain the complete time behavior of the magnetic field. A crucial point that will turn out to have important consequences is that the final redshift for numerical integration should be taken after the recombination epoch. The electric field that results from the small electron-proton velocity difference and that gives rise to a magnetic field is still present after last scattering, when the fraction of free electrons $x_{\rm e}$ is tiny but still does not completely vanish (see also [158]).

In order to compute the equal time correlation functions of the magnetic field, we need the power spectrum of the initial potential, defined by

$$\langle\Phi_{\rm in}(\boldsymbol{k})\Phi^*_{\rm in}(\boldsymbol{q})\rangle \equiv \delta(\boldsymbol{k}-\boldsymbol{q})P(k). \tag{4.63}$$

If the source terms are Gaussian random variables, we can apply Wick's theorem, and the

contributions of the two polarizations $h = \pm$ add up quadratically:

$$\begin{aligned}\langle \boldsymbol{B}(\boldsymbol{k},\eta)\boldsymbol{B}^*(\boldsymbol{k'},\eta)\rangle &= \frac{2\delta^3_{\rm D}(\boldsymbol{k}-\boldsymbol{k'})}{(2\pi)^3}\int \partial^3\boldsymbol{q}\, P(q)P(|\boldsymbol{k}-\boldsymbol{q}|)\times \\ &\quad \left\{|\mathcal{B}_{(+)}(\boldsymbol{q},\boldsymbol{k}-\boldsymbol{q},\eta)|^2 + \mathcal{B}_{(+)}(\boldsymbol{q},\boldsymbol{k}-\boldsymbol{q},\eta)\mathcal{B}^*_{(+)}(\boldsymbol{k}-\boldsymbol{q},\boldsymbol{q},\eta)\right\} \\ &= \frac{4\delta^3_{\rm D}(\boldsymbol{k}-\boldsymbol{k'})}{(2\pi)^3}\int \partial^3\boldsymbol{q}\, P(q)P(|\boldsymbol{k}-\boldsymbol{q}|)|\mathcal{B}_{(+)}(\boldsymbol{q},\boldsymbol{k}-\boldsymbol{q},\eta)|^2 \\ &\equiv \delta^3_{\rm D}(\boldsymbol{k}-\boldsymbol{k'})P_B(k,\eta), \end{aligned} \tag{4.64}$$

where $\mathcal{B}_{(\pm)} = \sum_i \mathcal{B}^{S_i}_{(\pm)}$. In the last line we have defined the power spectrum of the magnetic field P_B. Its value today is plotted in Fig. 6.1.

In order to have a deeper analytical understanding of the resulting magnetic field spectrum, we study each contribution S_i independently. There are cross correlations in (4.64), but our aim is to assess the relative importance of the different contributions; the $P_B^{S_i}$ are defined by replacing $\mathcal{B}_{(+)}$ with $\mathcal{B}^{S_i}_{(+)}$ in (4.64).

4.3.2 $\delta_\gamma \Delta v_{{\rm b}\gamma}$ contribution

The velocity difference between baryons and photons is severely suppressed in the tight-coupling limit relative to other perturbations like δ_γ; we expand this tiny velocity difference in terms of the expansion parameter $k/\tau' \ll 1$, where $\tau' = n_{\rm e}\sigma_{\rm T}a$ is the derivative of the optical depth for Thomson scattering. At first order in k/τ', in the radiation-dominated background on super-Hubble scales,

$$V^{(1)}_{(0)}(k,\eta) \simeq R\frac{k}{\tau'}\left(\frac{\delta_\gamma}{4} - \frac{\mathcal{H}v_{{\rm b}(0)}}{k}\right) \propto k^3\frac{\eta^5}{\eta^2_{\rm eq}}\,, \tag{4.65}$$

$$\delta_\gamma(k,\eta) \simeq \text{const}\,. \tag{4.66}$$

Using $R = 3\bar\rho_{\rm b}/(4\bar\rho_\gamma) \propto a$, $1/\tau' \propto a^{-2}$ and $a \propto \eta$, we get

$$\mathcal{S}^{(+)}_2(|\boldsymbol{k}-\boldsymbol{q}|,q,\eta) \propto \hat q_{(+)}\left(q^3 - |\boldsymbol{k}-\boldsymbol{q}|^3\right)\frac{\eta^5}{\eta^2_{\rm eq}}\,. \tag{4.67}$$

Then (4.62) gives the early-time and large-scale behaviour of $\mathcal{B}^{S_2}_{(\pm)}$, and the resulting magnetic field power spectrum behaves as

$$P_B^{S_2}(k,\eta) \propto k^2\int \partial^3 q\,|\hat q_{(+)}|^2 P(q)P(|\boldsymbol{k}-\boldsymbol{q}|)\left[q^6 - q^3|\boldsymbol{k}-\boldsymbol{q}|^3\right]\frac{\eta^4}{\eta^4_{\rm eq}}\,. \tag{4.68}$$

For a scale-invariant initial power spectrum, $P(q) \propto q^{-3}$,

$$P_B^{S_2}(\lambda k,\eta) = \lambda^5 P_B^{S_2}(k,\eta), \tag{4.69}$$

as can be seen just by a change of variable in the integral of (4.68). In [94] it is found that $P_B^{S_2}(\lambda k,\eta) = \lambda^4 P_B^{S_2}(k,\eta)$. The disagreement appears to arise since [94] infer the dependence on k from the $q \gg k$ contribution to the integral in (4.68) – but the main contribution to that integral are also limited to $q \lesssim k$ given the argument at the end of section 4.2.5. We finally find that for the S_2 source term, the power spectrum of the

magnetic field behaves as

$$\sqrt{k^3 P_B^{S_2}(k,\eta)} \propto k^4 \frac{\eta^2}{\eta_{\rm eq}^2}\,. \tag{4.70}$$

This behaviour in k and η at early times when the mode is still super-Hubble, is confirmed by numerical integration, as is evident from Fig. 4.3 (left).

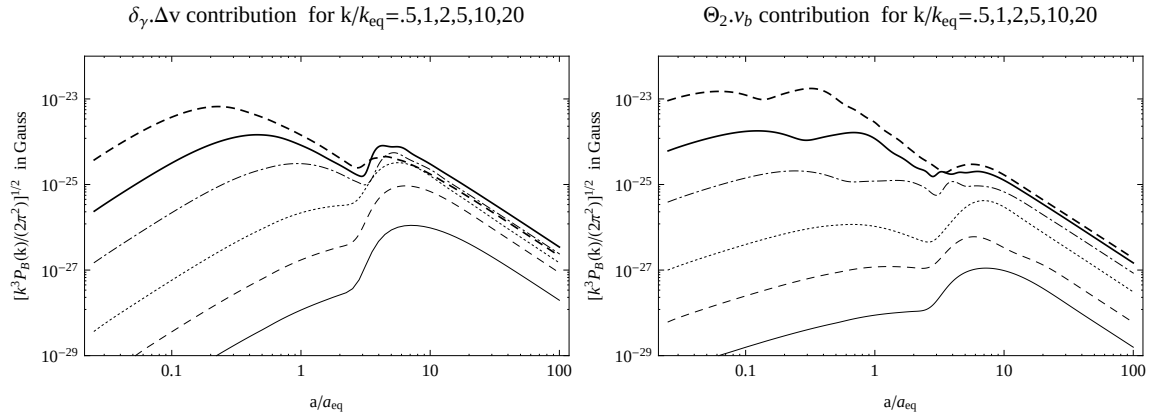

Figure 4.3: *Left:* Magnetic field spectrum $P_B^{S_2}(k,\eta)$ from only the S_2 contribution in (4.57), for different $k/k_{\rm eq}$, with values increasing from bottom to top. *Right:* Magnetic field spectrum $P_B^{S_3}(k,\eta)$ from only the S_3 contribution in (4.57).

4.3.3 $\Theta_2 v_{\rm b}$ contribution

Similar analytical arguments apply to the magnetic field generated by the source S_3. The tight coupling expansion of the source is

$$\Theta_2^0(k,\eta) \propto \frac{k}{\tau'} v_0^\gamma \propto k^2 \frac{\eta^3}{\eta_{\rm eq}}, \qquad v_{\rm b(0)}(k,\eta) \propto k\eta, \tag{4.71}$$

in a radiation background on super-Hubble scales. This implies that the S_3 contribution to the magnetic field power spectrum behaves as

$$\sqrt{k^3 P_B^{S_3}(k,\eta)} \propto k^4 \frac{\eta}{\eta_{\rm eq}}\,. \tag{4.72}$$

It has the same k dependence as (4.70) but a different η dependence. The analytical form is verified by the numerical output shown in Fig. 4.3 (right).

4.3.4 $\Delta v_{\rm b\gamma}^{(2)}$ contribution

For the purely second order part S_1, the only way to assess its contribution is to consider the tight coupling expansion of the evolution equation for the vorticity of baryons. Indeed, we need to evaluate first the total contribution $\sum_i \mathcal{S}_i$ at lowest order in tight-coupling, and the detail of this derivation is given in Appendix 4.6.3.2. It follows that $\sum_i \mathcal{S}_i$ behaves as

$(k/\tau')(k\eta)^2 \propto k^3\eta^5/\eta_{\rm eq}^2$, which implies that for the total magnetic field

$$\sqrt{k^3 P_B(k,\eta)} \propto k^4 \frac{\eta^2}{\eta_{\rm eq}^2}\,. \tag{4.73}$$

This behaviour is confirmed by numerical integration, as shown in Fig. 4.4 (right). Since

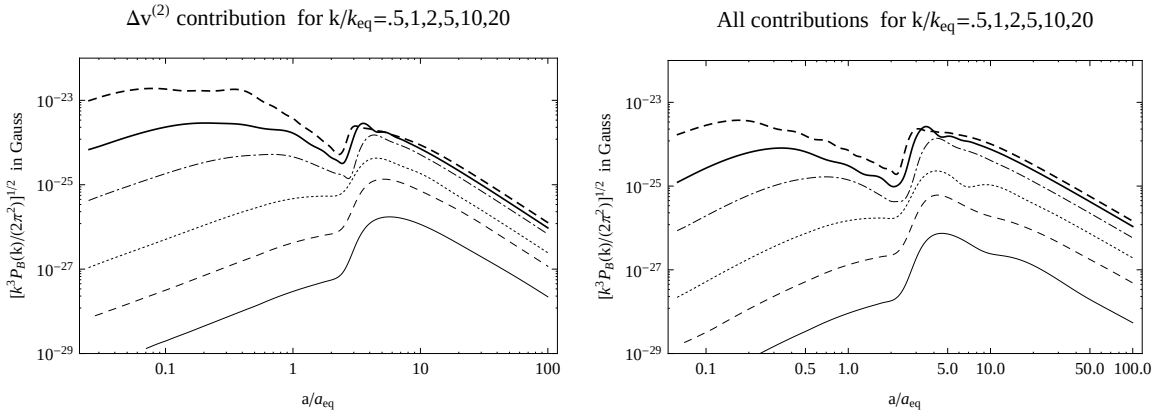

Figure 4.4: *Left:* Magnetic field spectrum $P_B^{S_1}(k,\eta)$ from only the S_1 contribution in (4.57), for different $k/k_{\rm eq}$, with values increasing from bottom to top. *Right:* Magnetic field spectrum $P_B(k,\eta)$ for all contributions.

$\mathcal{S}_2 \propto k^3\eta^5/\eta_{\rm eq}^2$, $\mathcal{S}_3 \propto k^3\eta^4/\eta_{\rm eq}$, and $\sum_i \mathcal{S}_i \propto k^3\eta^5/\eta_{\rm eq}^2$, we obtain that $\mathcal{S}_1 \propto k^3\eta^4/\eta_{\rm eq}$. Thus S_3 contributes to the magnetic field power spectrum as

$$\sqrt{k^3 P_B^{S_1}(k,\eta)} \propto k^4 \frac{\eta}{\eta_{\rm eq}}\,, \tag{4.74}$$

which is verified in Fig. 4.4 (left).

4.3.5 Magnetic power spectrum

From these plots it is evident that the magnetic field is still generated after recombination. This is the reason that it is important, to set the final time of integration after recombination, since the largest contribution comes from this last period of generation. Indeed, before reaching the usual 'final' stage where the magnetic field is no longer sourced but only redshifts with time ($B \propto a^{-2}$), we observe a bump in the resulting magnetic field spectrum, corresponding to the recombination time. This should be interpreted as an increase in magnetic field generation due to decoupling of photons and baryons.

In the decoupling regime the fluid of photons and baryons is no longer equivalent to a perfect fluid. The departure from tight coupling may be interpreted via non-adiabatic pressure perturbations, which can source the total vorticity [91, 164, 97, 165]. It is not a priori evident that this could lead to an increase in the magnetic field generation. On the one hand, the total vorticity is sourced when interactions between baryons and photons are less efficient, but on the other hand, there is less vorticity exchange between photons and baryons since the collisions are less efficient. In the ideal limit where the decoupling is complete, the vorticity of photons and baryons is adiabatically evolving according to (4.100), whereas the total vorticity is sourced by the gradients in the total non-adiabatic

pressure. This is possible because the vorticities of the different fluids do not add up linearly to give the total vorticity as can been seen from (4.98).

However, when decoupling occurs, we observe that there is in fact an increased generation of magnetic field in that phase, and this essentially comes from the factor $x_{\rm e}$ in (4.46), i.e. from the fact that the magnetic field is generated via the residual ionized fraction. More precisely, the generation of the magnetic field is proportional to $\partial_{[j}\nabla_\mu T^\mu_{{\rm b}\,\underline{k}]}/x_{\rm e}$ and not only to $\partial_{[j}\nabla_\mu T^\mu_{{\rm b}\,\underline{k}]}$, so even when $\nabla_\mu T^\mu_{{\rm b}\,\underline{k}} \to 0$ around decoupling, $\nabla_\mu T^\mu_{{\rm b}\,\underline{k}}/x_{\rm e}$ can still have sizeable values. This last significant stage of magnetic field generation is counterbalanced and finally stopped by the redshifting of photon energy density ($\bar\rho_\gamma \propto a^{-4}$). It can be seen from (4.57) that the background radiation energy density controls the efficiency of the total magnetic field production after recombination.

The power spectrum of the magnetic field is shown in Fig. 6.1 (left). The behaviour on large scales ($\propto k^4$) is explained above. The behaviour on small scales is complex, since it depends mainly on the generation between horizon crossing time and Silk damping time. During that period, the analysis which we restricted to super-Hubble scales does not apply – and the adiabatic redshifting does not apply either, since the magnetic field continues to be generated. For $k \gg k_{\rm eq}$, a reasonable linear approximation is $\log\left(\sqrt{k^3 P_B}\right) \propto 0.5 \log k$.

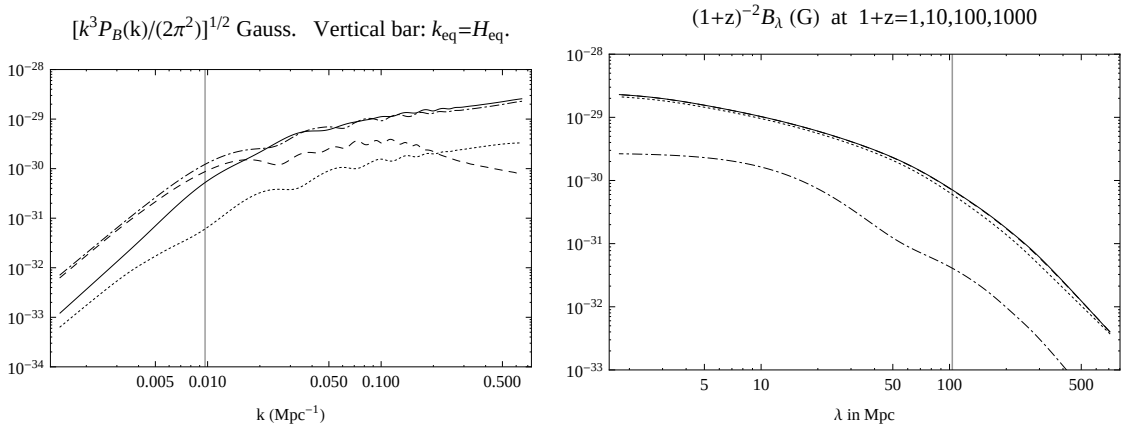

Figure 4.5: *Left:* Magnetic field spectrum today (solid). Contributions from the different sources in (4.5) are distinguished: second order velocity term S_1 (dot-dashed), quadratic term S_2 in velocity and density (dashed), quadratic term S_3 in anisotropic stress and velocity (dotted). *Right:* Comoving magnetic field strength at a given scale at times $1+z = 1, 10, 100, 1000$ corresponding respectively to solid, dashed, dotted and dot-dashed lines. (Dashed and solid lines cannot be distinguished).

4.3.6 Magnetic amplitude

The magnetic field amplitude smoothed over a comoving scale λ is

$$\begin{aligned} B_\lambda^2 &= \frac{1}{V}\int \partial^3\boldsymbol{y}\langle \boldsymbol{B}(\boldsymbol{x})\boldsymbol{B}^*(\boldsymbol{x}+\boldsymbol{y})\rangle \exp\left(-\frac{y^2}{2\lambda^2}\right) \\ &= \frac{1}{2\pi^2}\int_0^{k_{\rm damp}} \partial k\, k^2 P_B(k) \exp\left(-\frac{k^2\lambda^2}{2}\right), \end{aligned} \tag{4.75}$$

where the normalization volume is $V = \int \partial^3 \boldsymbol{y} \exp[-y^2/(2\lambda^2)] = \lambda^3 (2\pi)^{3/2}$. Note that the integral is insensitive to the upper cutoff, which may be taken to infinity, since $\lambda \gg \lambda_{\rm damp}$. The magnetic field strength is shown in Fig. 6.1 (right).

The field strength at 10 Mpc is approximately 10^{-29} Gauss and three times as much on cluster scales 1 Mpc. Given the slope of the spectrum, this is expected to grow to larger values for smaller scales. Our numerical integration does not allow us to investigate smaller scales since the numerical integration time increases dramatically with $k_{\rm max}$. In addition, the results become unreliable on small scales where density perturbations have become nonlinear by $z = 0$. On the comoving scale of the Hubble radius at equality, the strength is $\sim 10^{-30}$ G.

4.3.7 Frame dependence

At early times when photons and baryons are tightly coupled, the magnetic field measured in the baryon-photon fluid is not generated at lowest order in the tight coupling expansion. This is shown in Appendix 4.6.4.2. Only higher orders in the tight-coupling expansion contribute to magnetogenesis. However, since most of the magnetic field production occurs when the tight-coupling expansion breaks down around recombination, this suppression is only relevant at early times, before recombination, and for modes which remain for the longest time in the tight-coupled regime, i.e. for large scales. Therefore the difference between the magnetic field in the fundamental frame and in the baryon frame decreases, and they are nearly equal today, as shown in Fig. 4.6. This shows that at $1+z = 1000$ there is a suppression for large scales in the baryon frame, but today there is no more suppression since most of the magnetic field has been generated around recombination time.

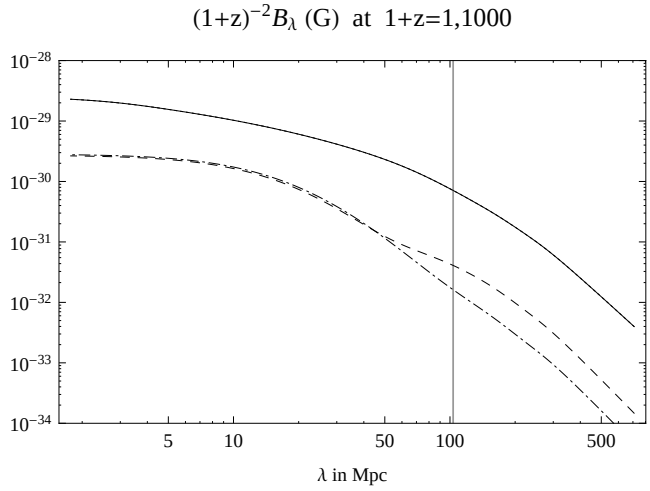

Figure 4.6: Magnetic field strength at a given scale as measured in the fundamental frame at $1 + z = 1$ (continuous) and $1 + z = 1000$ (dashed), and as measured in the baryon frame at $1 + z = 1$ (dotted) and $1 + z = 1000$ (dot-dashed). Dotted and continuous lines cannot be distinguished.

4.4 Discussion and comparison with previous results

Our approach is the first complete analysis of magnetogenesis around recombination, in the sense that it does not neglect any term in the second order equation for the generation of the magnetic field – previous work has omitted at least one of the terms. Therefore our results will necessarily differ from existing partial results and we discuss briefly how some of these differences arise.

Two general points can be highlighted:

- Numerical computation is essential to obtain the magnetic power spectrum – and even for a reliable estimate of the magnetic field strength. For example, [92, 91] use similar analytical methods and incorporate the same source terms, but the two estimated field strengths on the recombination Hubble scale differ by orders of magnitude. A full numerical integration is needed, especially to take into account all orders in the tight-coupling expansion. This was initiated by [94], and we have built on their work.
- Neglecting any of the source terms for magnetogenesis not only leads to inaccurate predictions – it also misses the fact the separate source terms do not simply add up linearly. The total of the different contributions is suppressed in the tight-coupling regime on large scales by a factor $(k\eta)^2$: the details are given in Appendix 4.6.4.1. As a consequence, discarding some terms implies that this suppression in the tight-coupling regime is neglected – which leads to an overestimate of the magnetic field generated. This is especially critical for the largest scales where tight-coupling is valid at the latest times.

In [87, 89, 90] the anisotropic stress contribution, S_3 in (4.57), and the second-order velocity contribution, S_1, are neglected. It is apparent from the power spectrum plot in Fig. 6.1 that both of these contributions are substantial and cannot be neglected for a reliable prediction of the magnetic field. In addition, these references omit the scalar metric perturbations. Metric perturbations and the second order velocity are included in [93, 91, 92], but the anisotropic stress is neglected.

In [94] the anisotropic stress is included, but the second order velocity contribution is neglected. In addition to this difference from our work, we find a different time and momentum dependence for the large-scale and early-time behaviour of the S_2 and S_3 contributions. We then find $\sqrt{k^3 P_B} \propto k^4$ while they find $\propto k^{7/2}$.

The first numerical prediction of the magnetic power spectrum was given by [93], neglecting anisotropic stress but including second order velocity. However, our power spectrum is significantly different from theirs. Part of the difference is due to anisotropic stress, but there is a further difference arising from the treatment of velocities. The evolution equation for the magnetic field can be given by (4.46). It is true that in the tight-coupled regime (see Appendix 4.6.3 for details), the velocities of electrons, protons and photons can be approximated to be equal. However, it is erroneous to use $\epsilon^{\underline{i\ell k}} \partial_\ell \nabla_\mu T^\mu_{\gamma\,\underline{k}} = 0$ to estimate the vorticity evolution. Indeed, in order to cancel the collision term when taking the tight-coupling limit, we have to consider a combination which uses the action reaction law and for which the collision terms do not appear. It is given by the total fluid vorticity conservation equation:

$$\epsilon^{\underline{i\ell k}} \partial_\ell \nabla_\mu T^\mu_{\gamma\,\underline{k}} + \epsilon^{\underline{i\ell k}} \partial_\ell \nabla_\mu T^\mu_{\mathrm{b}\,\underline{k}} = 0\,. \tag{4.76}$$

In the tight-coupled limit, the fluid of baryons and the fluid of radiation exchange vorticity, essentially because the dilution of their energy density is different, and this exchange of

vorticity is then required to maintain equal velocities at all times. In [93] it is implicitly assumed that $C^{\mu\perp}_{\gamma e}$ can be neglected because the velocity of electrons is assumed to be close to that of photons. However, as we discussed in Sec. 4.2, the limit has to be consistent with (4.37), and this collision term is precisely responsible for the vorticity exchange between photons and electrons, and thus between photons and baryons – and it cannot be ignored. The vorticity evolution in the tight-coupling limit should be computed using (4.107), i.e. by substituting the tight-coupling solution of velocities and energy densities perturbations in (4.46).

In [91] it is shown that there can be no generation of magnetic field in the photon frame at strictly less than the first order in tight coupling (if there is no initial vorticity). Note that what we call first order in tight-coupling (see also [166]) is called second order in tight coupling by [91, 92]. In our case, we focus on $C^{\mu}_{b\gamma}$, whereas they focus on $(k/\tau')C^{\mu}_{b\gamma}$ where τ' is the interaction rate and k/τ' is the parameter of the tight-coupling expansion. The result of [91] is compatible with our results in Appendix 4.6.4.2, since in the tight-coupled regime the photon frame is the baryon frame. Thus the magnetic field in the photon frame will be generated only starting from the next order, i.e. at first order in the tight-coupling expansion. Our numerical approach does not rely on a tight-coupling expansion since we integrate the full system of equations, and in that sense we consider necessarily the full tight-coupling expansion in our computation. We checked numerically that at early times, when photon-baryon coupling is efficient, the magnetic field in the baryon frame is severely suppressed compared to the magnetic field in the fundamental frame.

4.5 Conclusion

We have performed for the first time a full numerical computation of the seed magnetic field generated by nonlinear dynamics, taking into account all general relativistic effects and all source terms. We discussed the range of applicability of the mechanism on cosmological scales and concluded that the generation of the magnetic field is directly related to the Compton drag by photons on baryons. Even in the tight coupling regime, photons exchange vorticity with baryons and the magnetic field is created. Since the electric field that sources the magnetic field does not depend on the fraction of free electrons, the magnetic field is still generated after recombination, given that there is a relic fraction of charged particles, and we find that the largest production takes place in this final stage.

Our results are summarized in Fig. 4.1. The power spectrum (left plot) behaves as

$$\sqrt{k^3 P_B} \propto \begin{cases} k^4 & k \ll k_{\rm eq} \\ k^{0.5} & k \gg k_{\rm eq} \end{cases} \tag{4.77}$$

On cluster scales the comoving field strength is (right plot)

$$B_{1\,\rm Mpc} \sim 3 \times 10^{-29}\,\rm G. \tag{4.78}$$

Acknowledgements

EF is supported by the Swiss National Science Foundation. CP is supported by STFC (UK) grant ST/H002774/1. RM is supported by STFC (UK) grants ST/H002774/1 and ST/F002335/1, by a Royal Society (UK)–NRF (South Africa) exchange grant, and by

an SKA (South Africa) Research Chair. EF thanks the ICG, Portsmouth for hospitality during part of this work. CP thanks K. Takahashi and K. Ichiki for kind hospitality at the University of Nagoya, and especially for fruitful discussions on magnetic fields. RM thanks the ACGC, University of Cape Town, where part of this work was done, and NITHheP (South Africa) for a grant to support his visit to ACGC.

4.6 Appendix

4.6.1 Maxwell's equations

Maxwell's equations $\nabla_{[\lambda}F_{\mu\nu]} = 0$ and $\nabla_\nu F^{\mu\nu} = j^\mu$ in a general spacetime take the form [91, 157]

$$\mathrm{D}_\mu B^\mu = -\omega_\mu E^\mu\,, \qquad \mathrm{D}_\mu E^\mu = \omega_\mu B^\mu + \varrho\,, \tag{4.79}$$

$$\dot{B}^\perp_\mu + \frac{2}{3}\theta B_\mu - \big(\sigma_{\mu\nu} - \omega_{\mu\nu}\big)B^\nu = -\mathrm{curl}\, E_\mu - \epsilon_{\mu\nu\lambda}\dot{u}^\nu E^\lambda\,, \tag{4.80}$$

$$\dot{E}^\perp_\mu + \frac{2}{3}\theta E_\mu - \big(\sigma_{\mu\nu} - \omega_{\mu\nu}\big)E^\nu = \mathrm{curl}\, B_\mu + \epsilon_{\mu\nu\lambda}\dot{u}^\nu B^\lambda - J_\mu\,, \tag{4.81}$$

where E^μ, B^μ are defined by (4.10). Here the total 4-current is $j^\mu = j^\mu_{\rm e} + j^\mu_{\rm p}$ and it is split as

$$j^\mu = \varrho u^\mu + J^\mu\,, \qquad \varrho = -u_\mu j^\mu\,, \qquad J^\mu = h^\mu_\nu j^\nu\,, \tag{4.82}$$

where ϱ, J^μ are the charge density and current measured by u^μ observers. By (4.11),

$$\varrho = e(\gamma_{\rm p} n_{\rm p} - \gamma_{\rm e} n_{\rm e}), \qquad J^\mu = e(\gamma_{\rm p} n_{\rm p} v^\mu_{\rm p} - \gamma_{\rm e} n_{\rm e} v^\mu_{\rm e}). \tag{4.83}$$

The derivative D_μ is the projected covariant derivative and it defines a covariant curl [155, 157]:

$$\mathrm{D}_\mu f = h^\nu_\mu \nabla_\nu f, \;\; \mathrm{D}_\mu S^\nu = h^\lambda_\mu h^\nu_\tau \nabla_\lambda S^\tau, \tag{4.84}$$

$$\mathrm{curl}\, S^\mu = \epsilon^{\mu\nu\lambda}\mathrm{D}_\nu S_\lambda\,. \tag{4.85}$$

We work in Gaussian units so that the fine structure constant is $\alpha = e^2/(4\pi) = 1/137.036$ and the magnetic field strength is measured in Gauss.

4.6.2 Tetrads

The tetrad basis is given up to second order in scalar perturbations by

$$e_{\underline{0}}{}^\mu = \frac{1}{a}\Big(1 - \Phi + \frac{3}{2}\Phi^2\Big)\delta^\mu_{\underline{0}} - \frac{1}{a}S^i\delta^\mu_{\underline{i}}\,, \tag{4.86}$$

$$e_{\underline{i}}{}^\mu = \frac{1}{a}\Big(1 + \Psi + \frac{3}{2}\Psi^2\Big)\delta^\mu_{\underline{i}}\,, \tag{4.87}$$

$$e^{\underline{0}}{}_\mu = a\Big(1 + \Phi - \frac{1}{2}\Phi^2\Big)\delta^{\underline{0}}_\mu\,, \tag{4.88}$$

$$e^{\underline{i}}{}_\mu = a\Big(1 - \Psi - \frac{1}{2}\Psi^2\Big)\delta^{\underline{i}}_\mu + \frac{1}{a}S^i\delta^{\underline{0}}_\mu\,. \tag{4.89}$$

This choice of tetrad is discussed in [96] (see also [167, 160, 168]). The covariant derivative of a tensor in the tetrad basis is given by

$$\nabla_{\underline{a}} X_{\underline{b}}{}^{\underline{c}} = e^{\mu}_{\underline{a}} \partial_\mu X_{\underline{b}}{}^{\underline{c}} - \Omega_{\underline{a}}{}^{\underline{d}}{}_{\underline{b}} X_{\underline{d}}{}^{\underline{c}} + \Omega_{\underline{a}}{}^{\underline{c}}{}_{\underline{d}} X_{\underline{b}}{}^{\underline{d}}\,, \tag{4.90}$$

where indices are lowered and raised with $\eta_{\underline{ab}}$ and $\eta^{\underline{ab}}$. The affine connections in the background are

$$\bar{\Omega}_{\underline{i0k}} = -\bar{\Omega}_{\underline{ik0}} = -\frac{\mathcal{H}}{a}\delta_{\underline{ik}}\,, \qquad \mathcal{H} \equiv \frac{a'}{a}\,, \tag{4.91}$$

and the perturbed forms are

$$\Omega^{(1)}_{\underline{00i}} = -\Omega^{(1)}_{\underline{0i0}} = -\frac{1}{a}\partial_i \Phi^{(1)}\,, \quad \Omega^{(1)}_{\underline{0ik}} = 0\,, \tag{4.92}$$

$$\Omega^{(1)}_{\underline{i0k}} = -\Omega^{(1)}_{\underline{ik0}} = \frac{1}{a}\left[\mathcal{H}\Phi^{(1)} + \Psi^{(1)\prime}\right]\delta_{ik}\,, \tag{4.93}$$

$$\Omega^{(1)}_{\underline{\ell ik}} = -\Omega^{(1)}_{\underline{\ell ki}} = -\frac{2}{a}\partial_{[k}\Psi^{(1)}\delta_{i]\ell}\,. \tag{4.94}$$

4.6.3 Euler and vorticity equations

4.6.3.1 Euler equation

For a perfect fluid with equation of state $w_{\rm s} \equiv \bar{P}_{\rm s}/\bar{\rho}_{\rm s}$ and speed of sound $c_{\rm s}^2 \equiv \partial P_{\rm s}/\partial\rho_{\rm s}$, the term on the left of the Euler equation (4.7) is given to second order in the tetrad basis by [96, 169]:

$$\begin{aligned}
\frac{a\nabla_\mu T^\mu_{{\rm s}\,\underline{i}}}{\bar{\rho}_{\rm s}(1+w_{\rm s})} &= u^{\rm s}_{\underline{i}}{}' + (1-3c_{\rm s}^2)\mathcal{H}u^{\rm s}_{\underline{i}} + \frac{c_{\rm s}^2}{1+w_{\rm s}}\partial_i\delta_{\rm s} + \partial_i\Phi + \frac{1+c_{\rm s}^2}{1+w_{\rm s}}\left[(\delta_{\rm s}u^{\rm s}_{\underline{i}})'\right. \\
&\quad \left. +\mathcal{H}(1-3w_{\rm s})\delta_{\rm s}u^{\rm s}_{\underline{i}} + \delta_{\rm s}\partial_i\Phi\right] - 4\Psi' u^{\rm s}_{\underline{i}} + \partial_j(u^{\rm s}_{\underline{i}}u^j_{\rm s}) - (\Phi+\Psi)\left[u^{\rm s}_{\underline{i}}{}' + \right. \\
&\quad \left. \mathcal{H}(1-3c_{\rm s}^2)u^{\rm s}_{\underline{i}}\right] - \partial_i(\Phi^2) + \Psi\left[u^{\rm s}_{\underline{i}}{}' + (1-3c_{\rm s}^2)\mathcal{H}u^{\rm s}_{\underline{i}} + \frac{c_{\rm s}^2}{1+w_{\rm s}}\partial_i\delta_{\rm s} + \partial_i\Phi\right] \\
&\quad + \frac{c_{\rm s}^{2\prime}}{1+w_{\rm s}}\delta_{\rm s}u^{\rm s}_{\underline{i}} - \frac{c_{\rm s}^{2\prime}}{3\mathcal{H}(1+w_{\rm s})^2}\,\delta_{\rm s}\partial_i\delta_{\rm s}.
\end{aligned} \tag{4.95}$$

4.6.3.2 Vorticity evolution

The vorticity tensor of species s is

$$\omega^{\rm s}_{\mu\nu} = h^{{\rm s}\,\alpha}_{\mu} h^{{\rm s}\,\beta}_{\nu} \nabla_{[\alpha} u^{\rm s}_{\beta]}\,, \tag{4.96}$$

and the vorticity vector is given by (4.9). In the tetrad basis, up to second order,

$$\omega^{\rm s}_{\underline{i}} = \epsilon_{\underline{ik\ell}}\omega^{\underline{k\ell}}_{\rm s} \tag{4.97}$$

$$a\omega^{\rm s}_{\underline{ik}} = \partial_{[\underline{i}}u^{\rm s}_{\underline{k}]} + u^{\rm s}_{[\underline{i}}\partial_{\underline{k}]}(\Psi+\Phi) + u^{\rm s}_{[\underline{i}}u^{\rm s}_{\underline{k}]}{}'\,. \tag{4.98}$$

The evolution of the vorticity is deduced from (4.7) and (4.95). For a non-interacting perfect fluid, up to second order [97, 164]

$$\frac{1}{\bar{\rho}_{\rm s}(1+w_{\rm s})}\partial_{[\underline{i}}\nabla_\mu T^\mu_{{\rm s}\,\underline{k}]} = \omega^{\rm s}_{\underline{ik}}{}' + (2-3c_{\rm s}^2)\mathcal{H}\omega^{\rm s}_{\underline{ik}} = 0\,. \tag{4.99}$$

This can be recast as

$$\left[\bar{\rho}_{\rm s}(1+w_{\rm s})a^5\omega^{\rm s}_{\underline{i}}\right]' = 0\,. \tag{4.100}$$

For an interacting fluid,

$$\omega^{\rm s}_{\underline{ik}}{}' + (2-3c_{\rm s}^2)\mathcal{H}\omega^{\rm s}_{\underline{ik}} = \frac{1}{a}\sum_{\rm r}\Big\{u^{\rm s}_{[\underline{i}}C^{\rm sr\prime}_{\underline{k}]} + \partial_{[i}\Big(1-\Psi-\frac{1+c_{\rm s}^2}{1+w_{\rm s}}\,\delta_{\rm s}\Big)C^{\rm sr}_{\underline{k}]}\Big\}. \tag{4.101}$$

4.6.4 Magnetogenesis in tight-coupling

4.6.4.1 Magnetic field in fundamental frame

In the case where there are only interactions between baryons and photons, $C^\mu_{{\rm b}\gamma} + C^\mu_{\gamma{\rm b}} = 0$, and

$$\partial_{[i}\nabla_\mu T^\mu_{{\rm b}\,\underline{k}]} + \partial_{[i}\nabla_\mu T^\mu_{\gamma\,\underline{k}]} = 0\,. \tag{4.102}$$

In the tight-coupled limit where the interaction rate becomes very high, photons and baryons behave like a single fluid, with

$$w_{\rm f} = \frac{1}{3+4R}\,, \qquad c^2_{s,{\rm f}} = \frac{1}{3(1+R)}\,, \qquad R \equiv \frac{3\bar{\rho}_{\rm b}}{4\bar{\rho}_\gamma}\,. \tag{4.103}$$

The energy density contrasts at first order are

$$\delta^{(1)}_{\rm f} \simeq (1+w_{\rm f})\delta^{(1)}_{\rm b}\,, \qquad \delta^{(1)}_{\rm b} \simeq \frac{3}{4}\delta^{(1)}_\gamma\,. \tag{4.104}$$

The velocities of baryons and photons are the same in this regime

$$u^{\rm b}_{\underline{i}} \simeq u^\gamma_{\underline{i}} \simeq u^{\rm f}_{\underline{i}} \;\Rightarrow\; \omega^{\underline{i}}_{\rm f} \simeq \omega^{\underline{i}}_\gamma \simeq \omega^{\underline{i}}_{\rm b}\,. \tag{4.105}$$

By (4.99) and (4.102),

$$0 \simeq \omega^{\rm f}_{\underline{ik}}{}' + \mathcal{H}(2-3c_{\rm f}^2)\omega^{\rm f}_{\underline{ik}} = \frac{[\bar{\rho}_{\rm f}(1+w_{\rm f})a^5\omega^{\rm f}_{\underline{ik}}]'}{\bar{\rho}_{\rm f}(1+w_{\rm f})a^5}\,. \tag{4.106}$$

This can be used to infer the source term for magnetogenesis in (4.46). In the tight-coupled regime, $\partial_{[i}\nabla_\mu T^\mu_{{\rm b}\,\underline{k}]}$ can be estimated by using (4.105) and (4.104) in the baryon version of (4.95). Then, subtracting $\partial_{[i}\nabla_\mu T^\mu_{{\rm f}\,\underline{k}]} = 0$, we obtain

$$\begin{aligned}\frac{1}{\bar{\rho}_{\rm b}}\partial_{[i}\nabla_\mu T^\mu_{{\rm b}\,\underline{k}]} &= 3c_{\rm f}^2\mathcal{H}\omega^{\rm f}_{\underline{ik}} + \frac{c_{\rm f}^2}{a}\Big\{\frac{3\mathcal{H}}{1+w_{\rm f}}(1-c_{\rm f}^2+Rc_{\rm f}^2)\partial_{[i}\delta_{\rm f}v^{\rm f}_{\underline{k}]} + 3\mathcal{H}\partial_{[i}(\Psi-\Phi)v^{\rm f}_{\underline{k}]}\\ &\quad +\partial_{[i}\left(-3\Psi' + \partial_j v^j_{\rm f}\right)v^{\rm f}_{\underline{k}]} - \frac{1}{1+w_{\rm f}}\partial_{[i}\Psi\partial_{k]}\delta_{\rm f}\Big\}.\end{aligned} \tag{4.107}$$

From (4.46) it then follows that in the tight-coupled regime, the evolution of the magnetic field is given by

$$\begin{aligned}\frac{ex_{\rm e}}{m_{\rm p}}\frac{\left(a^2B^{\underline{i}}\right)'}{a^2} &= \frac{3}{2}c_{\rm f}^2\mathcal{H}\omega^{\underline{i}}_{\rm f} - \frac{c_{\rm f}^2}{a}\epsilon^{i\ell k}\Big\{\frac{3\mathcal{H}}{1+w_{\rm f}}(1-c_{\rm f}^2+Rc_{\rm f}^2)\partial_{[\ell}\delta_{\rm f}v^{\rm f}_{\underline{k}]}\\ &\quad +\partial_{[\ell}\left(-3\Psi' + \partial_j v^\ell_{\rm f}\right)v^{\rm f}_{\underline{\ell}]} - \frac{1}{1+w_{\rm f}}\partial_{[\ell}\Phi\partial_{k]}\delta_{\rm f}\Big\}\,,\end{aligned} \tag{4.108}$$

where we used $\rho_{\rm b} = (m_{\rm p} + m_{\rm e})(n_{\rm e} + n_{\rm H}) \simeq m_{\rm p}(n_{\rm e} + n_{\rm H})$. Note that $3c_{\rm f}^2\mathcal{H} = \partial \ln[\bar\rho_{\rm b}/(\bar\rho_{\rm b} + 4/3\bar\rho_\gamma)]/\partial\eta$. Since the vorticity in the tight-coupled plasma obeys (4.106), the first term on the right hand side of (4.108), which is linear in the vorticity, can only source the magnetic field if there is initially vorticity in the plasma. This is the term responsible for the Harrison mechanism [86, 98]. All other terms which are quadratic can source the magnetic field even if there is no initial vorticity.

However, *on large scales in the radiation era there is a suppression of the total contribution of these quadratic terms*. From the large-scale radiation era relations at first order,

$$2\mathcal{H}\partial_i v_{\rm f}^{\underline{i}} \simeq \nabla^2\Phi\,, \qquad \delta_{\rm f} \simeq -2\Phi\,, \tag{4.109}$$

it follows that at lowest order the quadratic terms are estimated by $\partial_i X \partial_j Y \sim \partial_i\Phi\partial_j\Phi$. Hence the quadratic source terms are suppressed by a factor $(k\eta)^2$, since at lowest order all contributions are of the type $\sim \partial_{[i}\Phi\partial_{j]}\Phi = 0$. This implies that $\sqrt{k^3 P_B(k,\eta)} \propto k^4\eta^2/\eta_{\rm eq}^2$, that is $\sum_i \mathcal{S}_i \propto k^3\eta^5/\eta_{\rm eq}^2$.

4.6.4.2 Magnetic field in baryon frame

From (4.47) we obtain

$$\begin{aligned} B_{\rm b}^{\underline{i}} - B^{\underline{i}} &= -\epsilon^{\underline{i\ell k}} v_{\underline{\ell}}^{\rm b} E_{\underline{k}} = -\frac{1}{e(n_{\rm e}+n_{\rm H})x_{\rm e}}\epsilon^{\underline{i\ell k}} v_{\underline{\ell}}^{\rm b}\nabla_\mu T^\mu_{{\rm b}\,\underline{k}} \\ &= \frac{m_{\rm p}}{aex_{\rm e}}\frac{c_{\rm f}^2}{(1+w_{\rm f})}\epsilon^{\underline{i\ell k}} v_{\underline{\ell}}^{\rm f}\partial_{\underline{k}}\delta_{\rm f}\,, \end{aligned} \tag{4.110}$$

where the second equality holds in the tight-coupled regime. Using the first order version of the Euler equation (4.95) for the plasma, i.e. with $\nabla_\mu T_{\rm f}^{\mu\underline{i}} = 0$, and using also the first order evolution equation for the plasma density contrast,

$$\Big(\frac{\delta_{\rm f}}{1+w_{\rm f}}\Big)' = 3\Psi' - \partial_i v^{\underline{i}}, \tag{4.111}$$

we deduce that in the tight-coupled regime

$$\frac{ex_{\rm e}}{m_{\rm p}}\frac{\big(a^2 B_{\rm b}^{\underline{i}}\big)'}{a^2} = 3c_{\rm f}^2\mathcal{H}\omega_{\rm f}^{\underline{i}} = -\frac{\big(a^2\omega_{\rm f}^{\underline{i}}\big)'}{a^2}\,. \tag{4.112}$$

At early times in the radiation era we have $x_{\rm e} \simeq 1$, and then we obtain a conservation equation up to second order:

$$\Big[a^2\Big(\frac{e}{m_{\rm p}}B_{\rm b}^{\underline{i}} + \omega_{\rm f}^{\underline{i}}\Big)\Big]' \simeq 0\,. \tag{4.113}$$

This is precisely the Harrison mechanism, but up to second order.

In the tight-coupled regime, in the plasma frame, the magnetic field can only be generated if there is initial vorticity, i.e. through the Harrison mechanism. We recover here the results in [91, 92]. The magnetic field measured in a different frame is only due to the contribution of the electric field to this change of frame. In the fundamental frame, this contribution in the tight-coupled regime is given by the second and third lines of (4.108). Note that the electric field is generated at first order in cosmological perturbations even in

the lowest order of the tight-coupling approximation and even in the plasma frame.

Chapter 5

A large scale coherent magnetic field: interactions with free streaming particles and limits from the CMB

JOURNAL OF COSMOLOGY AND ASTROPARTICLE PHYSICS **06**, 017 (2011)

A large scale coherent magnetic field: interactions with free streaming particles and limits from the CMB

Julian Adamek, Ruth Durrer, Elisa Fenu and Marc Vonlanthen

We study a homogeneous and nearly-isotropic Universe permeated by a homogeneous magnetic field. Together with an isotropic fluid, the homogeneous magnetic field, which is the primary source of anisotropy, leads to a plane-symmetric Bianchi I model of the Universe. However, when free-streaming relativistic particles are present, they generate an anisotropic pressure which counteracts the one from the magnetic field such that the Universe becomes isotropized. We show that due to this effect, the CMB temperature anisotropy from a homogeneous magnetic field is significantly suppressed if the the neutrino masses are smaller than 0.3 eV.

arXiv:1102.5235v1 [astro-ph.CO]

5.1 Introduction

On very large scales, the observed Universe is well approximated by a homogeneous and isotropic Friedmann solution of Einstein's equations. This is best verified by the isotropy of the Cosmic Microwave Background (CMB). The small fluctuations observed in the CMB temperature are fully accounted for by the standard model of structure formation from small initial fluctuations which are generated during an inflationary phase. Nevertheless, these small fluctuations are often used to limit other processes or components which may be present in the early Universe, like e.g. a primordial magnetic field.

The generation of the magnetic fields observed in galaxies and clusters [38, 41] is still unclear. It has been shown that phase transitions in the early Universe, even if they do generate magnetic fields, have not enough power on large scale to explain the observed large scale coherent fields [81, 77]. These findings suggest that primordial magnetic fields must be correlated over very large scales.

In this paper, we discuss limits on fields which are coherent over a Hubble scale and which we can therefore treat as a homogeneous magnetic field permeating the entire Universe. We want to derive limits on a homogeneous field from CMB anisotropies. This question has been addressed in the past [170, 99, 100] and limits on the order of $B \lesssim 2 \times 10^{-9}$ Gauss have been derived from the CMB anisotropies [60]. A similar limit can also be obtained from Faraday rotation [101, 7].

We show that the limits from the CMB temperature anisotropy actually are invalid if free streaming neutrinos with masses $m_\nu < T_{\rm dec}$ are present, where $T_{\rm dec}$ denotes the photon

temperature at decoupling. This is the case if the neutrino masses are not degenerate, i.e. the largest measured mass splitting is of the order of the largest mass, hence $m_\nu \lesssim 0.04$eV. The same effect can be obtained from any other massless free streaming particle species, like e.g. gravitons, if they contribute sufficiently to the background energy density. This is due to the following mechanism which we derive in detal in this paper: In an anisotropic Bianchi-I model, free streaming relativistic particles develop an anisotropic stress. If the geometric anisotropy is due to a magnetic field, which scales exactly like the anisotropic stress of the massless particles, this anisotropic stress cancels the one from the magnetic field and the Universe is isotropized. Hence the quadrupole anisotropy of the CMB due to the magnetic field is erased. This 'compensation' of the magnetic field anisotropic stress by free-streaming neutrinos has also been seen in the study of the effects of stochastic magnetic fields on the CMB [171, 172, 173, 174] for the large scale modes. In our simple analysis the mechanism behind it finally becomes clear.

The limits from Faraday rotation are not affected by our arguments.

In the next section we derive the CMB anisotropies in a Bianchi I Universe. In Section 5.3 we show that relativistic free streaming neutrinos in a Bianchi I model develop anisotropic stresses and that these back-react to remove the anisotropy of the Universe if the latter is due to a massless mode. In Section 5.4 we discuss isotropization due to other massless free streaming particles, with special attention to a gravitational wave background. In Section 5.5 we conclude.

5.2 Effects on the CMB from a constant magnetic field in an ideal fluid Universe

We consider a homogeneous magnetic field in $z-$direction, $\boldsymbol{\nu} = B\boldsymbol{e}_z$ in a Universe filled otherwise with an isotropic fluid consisting, e.g. of matter and radiation. The metric of such a Universe is of Bianchi type I,

$$ds^2 \;=\; -dt^2 + a_\perp^2(t)(dx^2+dy^2) + a_\parallel^2(t)\,dz^2\,, \tag{5.1}$$

where t is cosmic time. The Einstein equations in cosmic time read

$$2\frac{\dot a_\parallel}{a_\parallel}\frac{\dot a_\perp}{a_\perp} + \left(\frac{\dot a_\perp}{a_\perp}\right)^2 \;=\; 8\pi G\rho\;, \tag{5.2}$$

$$\frac{\ddot a_\parallel}{a_\parallel} + \frac{\ddot a_\perp}{a_\perp} + \frac{\dot a_\parallel}{a_\parallel}\frac{\dot a_\perp}{a_\perp} \;=\; -8\pi G P_\perp\;, \tag{5.3}$$

$$2\frac{\ddot a_\perp}{a_\perp} + \left(\frac{\dot a_\perp}{a_\perp}\right)^2 \;=\; -8\pi G P_\parallel\;. \tag{5.4}$$

The dot denotes the derivative with respect to t. We have introduced the total energy density $\rho = \rho_B + \rho_m + \rho_\gamma + \rho_\nu + \rho_\Lambda$, where $\rho_B = B^2/8\pi$ is the energy density in the magnetic field, and $\rho_m, \rho_\gamma, \rho_\nu, \rho_\Lambda$ are as usual the energy densities of matter (assumed to be baryons and cold dark matter), photons, neutrinos, and dark energy (assumed to be a cosmological constant), respectively.

All the above constituents of the Universe, except matter (which is assumed to be pressureless) also contribute to the pressure components $P_\parallel, P_\perp$. The contribution from

the magnetic field is intrinsically anisotropic and given by

$$P_{B,\perp} = -P_{B,\parallel} = \rho_B \,, \tag{5.5}$$

as can be read off from the corresponding stress-energy tensor. Note that the magnetic field B decays as $a_\perp^{-2}$, so that ρ_B scales as $a_\perp^{-4}$.

For later reference we define an 'average' scale factor

$$a \equiv a_\perp^{2/3} a_\parallel^{1/3} \,, \tag{5.6}$$

which is chosen such that it correctly describes the volume expansion.

Let us also introduce the expansion rates $H_\perp = \dot{a}_\perp/a_\perp$ and $H_\parallel = \dot{a}_\parallel/a_\parallel$. The anisotropic stress of the homogeneous magnetic field sources anisotropic expansion, which can be expressed as the difference of the expansion rates, $\Delta H = H_\perp - H_\parallel$. We combine eqs. (5.4) and (5.3) to obtain an evolution equation for ΔH,

$$\dot{\Delta H} + \left(2H_\perp + H_\parallel\right) \Delta H = 8\pi G \left(P_\perp - P_\parallel\right) \,. \tag{5.7}$$

This pressure difference is actually simply the anisotropic stress. More precisely,

$$\begin{aligned} \Pi_i{}^j &\equiv T_i{}^j - P\delta_i{}^j \,, \qquad P = T_i^i/3 = (2P_\perp + P_\parallel)/3 \,, \\ \Pi_1{}^1 &= \Pi_2{}^2 = P_\perp - P = \frac{1}{3}\left(P_\perp - P_\parallel\right) \,, \quad \Pi_3{}^3 = P_\parallel - P = -\frac{2}{3}\left(P_\perp - P_\parallel\right) \,. \end{aligned} \tag{5.8}$$

At very high temperatures, both photons and neutrinos are tightly coupled to baryons. Their pressure is isotropic and thus their contribution to the right-hand-side of (5.7) vanishes. The collision term in Boltzmann's equation tends to isotropize their momentum-space distribution. Under these conditions the only source of anisotropic stress is the magnetic field. The above equation can then easily be solved to leading order in ΔH, as will be carried out in section 5.3.

However, as soon as the neutrinos decouple and start to free-stream, their momentum-space distribution will be affected by the anisotropic expansion caused by the magnetic field and thus they will develop anisotropic stress. As we will show, the neutrino anisotropic stress counteracts the one from the magnetic field. This behavior will be maintained until the neutrinos become non-relativistic, then their pressure decays. For the temperature anisotropy in the CMB it is relevant whether this happens before or after photon decoupling. This depends, of course, on the neutrino masses.

We introduce the energy density parameters

$$\Omega_x(t) \equiv \frac{8\pi G \rho_x(t)}{3H^2(t)} = \frac{\rho_x(t)}{\rho_c(t)} \,,$$

corresponding respectively to the magnetic field, matter and radiation etc., such that e.g. $\Omega_B = B^2/8\pi\rho_c$, $\Omega_m = \rho_m/\rho_c$ and $\Omega_\gamma = \rho_\gamma/\rho_c$. Here we define the 'average' Hubble parameter by

$$H^2 \equiv \frac{1}{3}\left[\left(\frac{\dot{a}_\perp}{a_\perp}\right)^2 + 2\frac{\dot{a}_\perp \dot{a}_\parallel}{a_\perp a_\parallel}\right] \,. \tag{5.9}$$

With this, eq. (5.2), implies

$$\Omega_{\rm T} \equiv \Omega_B + \Omega_\gamma + \Omega_\nu + \Omega_m + \Omega_\Lambda = 1 \quad \text{ at all times.} \tag{5.10}$$

As an alternative, one could have defined the 'average' Hubble parameter as

$$H_a \equiv \frac{1}{3}\left[2\frac{\dot{a}_\perp}{a_\perp} + \frac{\dot{a}_\parallel}{a_\parallel}\right] .$$

It can easily be verified that the difference between these definitions is of the order of the small quantity $\Delta H = H_\perp - H_\parallel$. More precisely,

$$H^2 \;=\; H_a^2\left[1 - \frac{2}{3}\frac{\Delta H}{H_a} - \frac{1}{3}\left(\frac{\Delta H}{H_a}\right)^2\right] . \tag{5.11}$$

We shall mainly use the definition which yields the constraint (5.10).

The scaling of the energy densities corresponding to every species follows from the stress energy conservation of every single fluid

$$\rho_\gamma = \rho_\gamma^0\left(\frac{a_0}{a}\right)^4 , \quad \rho_m = \rho_m^0\left(\frac{a_0}{a}\right)^3 , \quad \rho_B = \rho_B^0\left[\frac{a_\perp(t_0)}{a_\perp}\right]^4 . \tag{5.12}$$

To obtain the above behavior for radiation, it is important to impose that the fluid is ideal, i.e. that pressure is isotropic. This is the case if there are sufficiently many collisions, but does not hold for free streaming particles as we shall see in the next section.

At a fixed initial time one may set $a_\perp = a_\parallel$ as initial condition. Motivated by observations, we assume that the scale factor difference always remains small,

$$\frac{a_\perp - a_\parallel}{a} \equiv \delta \ll 1 . \tag{5.13}$$

To first order in $\Delta H \ll H$, as long as the magnetic field is the only anisotropic component, eq. (5.7) becomes (see also [175])

$$\dot{\Delta H} + 3H\Delta H = 8\pi G\left(P_\perp - P_\parallel\right) = 6H^2\Omega_B . \tag{5.14}$$

In the following we consider both Ω_B and ΔH as small quantities and want to calculate effects to first order in them. To first order, $\rho_B \propto a^{-4} \propto \rho_\gamma$. We can therefore introduce the ratio

$$r = \frac{\rho_B}{\rho_\gamma} = \frac{\Omega_B}{\Omega_\gamma} , \tag{5.15}$$

which (to first order) is constant.

In fig. 5.1 we plot the scale factor difference $\delta_0 - \delta$ and $\Delta H/H$ as functions of the temperature in a first stage where neutrinos, photons and baryons are all tightly coupled and the magnetic field is the only source of anisotropy.

5.2.1 Lightlike geodesics in Bianchi I

Let us now determine the CMB anisotropies in a Bianchi I Universe. We are not interested in the usual anisotropies from primordial perturbations, which we disregard in our treat-

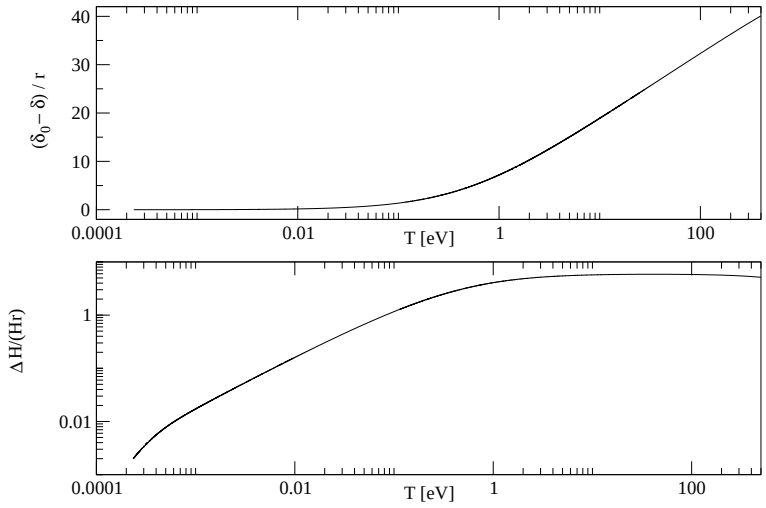

Figure 5.1: Temperature evolution of the scale factor difference $\delta_0 - \delta$ and $\Delta H/H$ in units of $r = \Omega_B/\Omega_\gamma$ when no free-streaming particle compensates the anisotropy produced by the magnetic field anisotropic stress. Here δ_0 denotes the scale factor difference δ today. The evolution of the 'average' scale factor a is the one of a ΛCDM Universe. As it is shown in section 3, $\Delta H/H$ is constant during the radiation dominated era and δ is growing. During the matter dominated era $\Delta H/H$ is decaying, $\Delta H/H \propto 1/a \propto T$, and δ asymptotes to a constant.

ment, but we concentrate on the effect of the global anisotropy, which to leading order will result in a temperature quadrupole.

We choose the tetrad basis $e_0 = \partial_t$, $e_i = a_\perp^{-1}\partial_i$ for $i = 1, 2$ and $e_3 = a_\parallel^{-1}\partial_3$. The dual basis of 1-forms is given by $\theta^0 = dt$, $\theta^i = a_\perp dx^i$, for $i = 1, 2$ and $\theta^3 = a_\parallel dx^3$. The first structure equation,

$$d\theta^a + \omega^a{}_b \wedge \theta^b = 0\,,$$

yields

$$\omega^i{}_0 \;=\; \frac{\dot{a_\perp}}{a_\perp}\theta^0\,, \quad i = 1, 2\,, \qquad \text{and} \quad \omega^3{}_0 = \frac{\dot{a_\parallel}}{a_\parallel}\theta^0\,. \tag{5.16}$$

The other non-vanishing connection 1-forms are determined by anti-symmetry, $\omega_{ab} = -\omega_{ba}$. After photon decoupling, the photon 4-momentum $\boldsymbol{p} = p^a \boldsymbol{e}_a$ satisfies the geodesic equation

$$\frac{dp^a}{d\lambda} + \omega^a{}_c(\boldsymbol{e}_b)\, p^b\, p^c = 0\,. \tag{5.17}$$

Considering the constraint relation for massless particles $p_a p^a = 0$ and setting $\alpha T_0 \equiv p^0 = p = \sqrt{\sum_{i=1}^3 (p^i)^2}$, where T_0 is a constant with the dimension of energy (or temperature) that multiplies all the components p^a, the above equation is solved by

$$(p^a) = T_0 \left(\alpha, \frac{n^1}{a_\perp}, \frac{n^2}{a_\perp}, \frac{n^3}{a_\parallel}\right)\,, \tag{5.18}$$

where n is a unit vector in the direction of the particle momentum and α is determined by the condition $p_a p^a = 0$.

$$n^1 = \sin\theta\sin\phi\,, \quad n^2 = \sin\theta\cos\phi \quad \text{and} \quad n^3 = \cos\theta\,.$$

The temperature of photons in such an anisotropic Universe for a comoving observer, $u = \partial_t$, is then given by

$$T(t,\theta) = \eta_{ab}u^a p^b = p^0 = T_0\alpha = T_0\sqrt{\frac{\sin^2\theta}{a_\perp^2} + \frac{\cos^2\theta}{a_\parallel^2}} \simeq \frac{T_0}{a}\left[1 + \delta\cos^2\theta + \mathcal{O}(\delta^2)\right]\,. \quad (5.19)$$

We set

$$\bar{T} = \frac{1}{4\pi}\int T(t,\theta)\sin\theta d\theta d\phi = \frac{T_0}{a}\left[1 + \frac{1}{3}\delta + \mathcal{O}(\delta^2)\right]$$

to be the temperature averaged over directions. Note that for $\delta = 0$ and $a_0 = 1$, T_0 is simply the CMB temperature at time t_0. For the temperature fluctuations to first order in δ we obtain

$$\frac{\Delta T}{T} \equiv \frac{T(t,\theta) - \bar{T}}{\bar{T}} = \frac{1}{3}\delta(3\cos^2\theta - 1) + \mathcal{O}(\delta^2) = \delta\frac{2}{3}\sqrt{\frac{4\pi}{5}}Y_{20}(\mathbf{n}) + \mathcal{O}(\delta^2)\,. \quad (5.20)$$

Hence, to lowest order in δ a homogeneous magnetic field generates a quadrupole which is given by

$$C_2 = \frac{1}{5}\sum_{m=-2}^{2}|a_{2m}|^2 = \frac{1}{5}|a_{20}|^2 = \frac{16\pi}{225}\delta^2 \simeq 0.22\times\delta^2\,. \quad (5.21)$$

Of course, in principle one can set $\delta(t_1) = 0$ at any given moment t_1 which then leads to $\frac{\Delta T}{T}(t_1) = 0$. However, for the CMB we know that photons start free-streaming only at $t_{\rm dec}$ when they decouple from electrons. Before that, scattering isotropizes the photon distribution and no quadrupole can develop[1]. In other words, we have to make sure that the anisotropy-induced quadrupole is fixed to zero at decoupling and only appears as a result of differential expansion between last scattering and today. This can be taken into account by simply choosing the initial condition $\delta(t_{\rm dec}) = 0$. Without this initial condition we have to replace $\delta(t)$ by $\delta(t) - \delta(t_{\rm dec})$ in eq. (5.21) [2]. The general result for the CMB quadrupole today is therefore

$$C_2 = \frac{16\pi}{225}\left[\delta(t_0) - \delta(t_{\rm dec})\right]^2\,. \quad (5.22)$$

5.2.2 The Liouville equation

At this stage it is straightforward to check that the exact expression found above for the temperature, eq. (5.19), satisfies the Liouville equation for photons (see, e.g. [168])

$$p^a \boldsymbol{e}_a(f_\gamma) - \omega^i{}_b(\boldsymbol{p})p^b\frac{\partial f_\gamma}{\partial p^i} = 0\,, \quad (5.23)$$

[1] This is not strictly true and neglects the slight anisotropy of non-relativistic Thomson scattering.

[2] More generally, one can say that δ itself is not a quantity with a physical meaning as long as no reference value is specified. In physical terms, only the difference of δ between two instants of time can be a relevant quantity.

when we make the following Ansatz for the distribution function of massless bosonic particles in our Bianchi I Universe

$$p_\perp \equiv \sqrt{(p^1)^2 + (p^2)^2}\,, \quad p_\parallel = p^3, \quad p = \sqrt{p_\perp^2 + p_\parallel^2} = p^0\,, \tag{5.24}$$

$$f_\gamma(t,T) = \frac{N_\gamma}{(2\pi)^3}\frac{1}{\mathrm{e}^{p/T}-1}, \qquad T = T(t,\theta)\,. \tag{5.25}$$

Indeed, using eqs. (5.16), we find the following differential equation for the temperature T

$$\frac{\partial f_\gamma}{\partial T}\frac{\partial T}{\partial t} - \frac{\dot{a_\perp}}{a_\perp}\frac{\partial f_\gamma}{p_\perp}p_\perp - \frac{\dot{a_\parallel}}{a_\parallel}\frac{\partial f_\gamma}{\partial p_\parallel}p_\parallel = 0\,. \tag{5.26}$$

With (5.25) this can be written as

$$\frac{\dot{T}}{T} + \frac{\dot{a_\perp}}{a_\perp}\left(\frac{p_\perp}{p}\right)^2 + \frac{\dot{a_\parallel}}{a_\parallel}\left(\frac{p_\parallel}{p}\right)^2 = 0\,. \tag{5.27}$$

The time behavior of the different components of the photon momentum are given by eq. (5.18) and one immediately sees that expression (5.19) for the temperature solves the above differential equation.

Moreover, defining the time dependent unit vectors $\hat{p}^i \equiv p^i/p$ and the shear tensor

$$\sigma_{ab} \equiv \vartheta_{ab} - \frac{1}{3}\vartheta^c_c h_{ab}\,, \quad \text{where } \vartheta_{ab} \equiv \frac{1}{2}\left(\nabla_a u_b + \nabla_b u_a\right) \quad \text{and} \quad h_{ab} \equiv \eta_{ab} + u_a u_b\,,$$

one can rewrite the above Liouville equation as

$$(\tilde{p})^{\cdot} = -\tilde{p}\sigma_{ij}\hat{p}^i\hat{p}^j\,, \tag{5.28}$$

where $\tilde{p}$ denotes the redshift-corrected photon energy defined as $\tilde{p} \equiv ap$. This last expression agrees with the corresponding equation given in [176].

Using the expression for the distribution function of massless fermions, we can also compute the pressure of neutrinos once they start free-streaming. Indeed, given the fact that neutrinos can be considered massless before they become non-relativistic, their geodesic equation has the same solution as the one for photons found above, therefore we immediately obtain the time behavior of their temperature in an anisotropic Bianchi I background. Taking also into account the fact that neutrinos are fermions, their distribution function reads

$$f_\nu(t,T) = \frac{N_\nu}{(2\pi)^3}\frac{1}{\mathrm{e}^{p/T}+1}, \quad \text{with} \quad T(t,\theta) = \frac{T_\nu}{a}\left[1 + \delta\cos^2\theta + \mathcal{O}(\delta^2)\right]\,. \tag{5.29}$$

Note that the parameter T appearing in the neutrino distribution function in not a temperature in the thermodynamical sense as the neutrinos are not in thermal equilibrium. It is simply a parameter in the distribution function and its time evolution has been determined by requiring the neutrinos to move along geodesics i.e. to free-stream.

This distribution function remains valid also in the case where neutrinos are massive, i.e. $T_\nu < m_\nu$. The only difference is that the relation $p^0 = p$ changes to $p^0 = \sqrt{p^2 + (m_\nu a)^2}$ which of course affects the momentum integrals for the neutrino energy density and pressure.

The energy T_ν/a_0 is the present neutrino 'temperature' in the absence of a homogeneous magnetic field ($\delta = 0$). The energy density ρ_ν and the pressure $P_{\nu,i}$ in direction i with respect to our orthonormal basis are

$$\rho_\nu = N_\nu \int d^3p\, f_\nu(t,T) p^0 \tag{5.30}$$

$$P_{\nu,i} = N_\nu \int d^3p\, f_\nu(t,T)\, \frac{p_i^2}{p^0}\,. \tag{5.31}$$

Calculating the integral (5.31) for relativistic neutrinos to first order in δ in the directions perpendicular and parallel to the magnetic field direction, one finds for the neutrino anisotropic stress in the ultra-relativistic limit

$$P_{\nu,\perp} - P_{\nu,\parallel} \simeq -\frac{8}{15}\rho_\nu\,(\delta - \delta_*)\ , \tag{5.32}$$

where δ_* is the value of δ at neutrino decoupling and can be fixed to zero for convenience.

The temperature dependence of the neutrino pressure is shown in fig. 5.2. To leading order, this also gives the temperature dependence of the neutrino anisotropic stress. From the plot it is clear how the pressure scales as a^{-4} as long as the neutrinos are ultra-relativistic. Once they have become effectively non-relativistic, their pressure decays more rapidly, as a^{-5}. The break in the power law is not precisely at $T = m_\nu$, but at a somewhat lower temperature. Because the neutrinos still have the highly relativistic Fermi-Dirac distribution from the time of their thermal freeze-out, it takes some additional redshift until they behave effectively non-relativisic. This will have some effect on the estimates for the residu scussion of fig. 5.5.

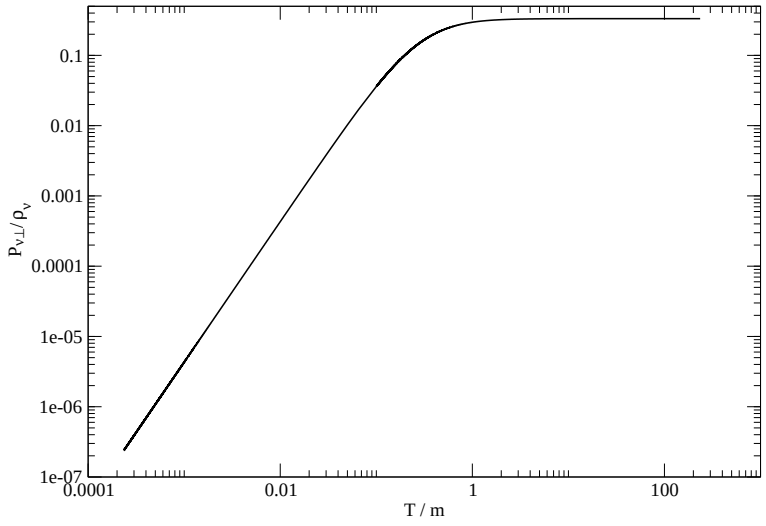

Figure 5.2: Temperature evolution of the neutrino pressure $P_{\nu,\perp}$ normalized to the neutrino energy density ρ_ν. The temperature is given in units of the neutrino mass. Note that the break in the power law is not at $T = m$, but at somewhat lower temperature. This is due to the highly relativistic Fermi-Dirac distribution of the neutrinos, see also the discussion of fig. 5.5 in sec. 5.3.3.

5.3 Neutrino free-streaming and isotropization

5.3.1 Massless free-streaming neutrinos

We now calculate the effect of free-streaming neutrinos perturbatively, i.e. to first order in δ, $\Delta H/H$ and Ω_B. We linearize eq. (5.7), taking into account the contribution of a free-streaming relativistic component to the right-hand side. We have shown that this contribution, to leading order in δ, is given by eq. (5.32). Furthermore, up to $\mathcal{O}(\delta^2)$ corrections, δ is just the integral of ΔH,

$$\int_{t_*}^{t} \Delta H(t')dt' = \ln \frac{a_\perp(t)}{a_\parallel(t)} - \ln \frac{a_\perp(t_*)}{a_\parallel(t_*)} \simeq \delta - \delta_* \ , \tag{5.33}$$

so that to first order we can identify $\Delta H \simeq \dot{\delta}$.

Inserting this back into eq. (5.7) we find, to linear order in δ,

$$\ddot{\delta} + 3H\dot{\delta} + \frac{8}{5}H^2\Omega_\nu(\delta - \delta_*) = 6H^2\Omega_B \ . \tag{5.34}$$

Note that, because we are working at linear order, it is not important with respect to which scale factor H, Ω_ν and Ω_B are defined in (5.34). We will now give analytic solutions to this equation for different regimes in the evolution of the Universe.

Let us begin at very high temperature where the neutrinos are still strongly coupled to baryons. In this case they do not contribute to eq. (5.34) since their pressure is isotropic ($P_{\nu,\perp} - P_{\nu,\parallel} \sim 0$) given the high rate of collisions. Furthermore, since we are in the **radiation dominated era** ($a \propto t^{1/2}$), we have $H = 1/2t$, and Ω_B is constant. The solution to eq. (5.34) in this case is

$$\dot{\delta}(t) = \Delta H(t) = \frac{3\Omega_B}{t} + \frac{C}{t^{3/2}} \ . \tag{5.35}$$

The dimensionless quantity $\Delta H/H$ hence asymptotes to a constant, since the homogeneous piece decays like a^{-1}:

$$\frac{\Delta H}{H} \to 6\Omega_B \ . \tag{5.36}$$

ΔH soon becomes insensitive to the initial conditions and only depends on Ω_B. This also shows that in the absence of an anisotropic source ($\Omega_B = 0$), the expanding Universe isotropizes. Integrating this equation and remembering that $\Omega_B =$ constant to first order in a radiation dominated Universe, we obtain

$$\delta(t) - \delta(t') = 3\Omega_B \ln(t/t') \, . \tag{5.37}$$

As the Universe reaches a temperature of roughly 1.4 MeV, the neutrinos decouple and begin to free-stream, giving rise to the corresponding term in eq. (5.34). In the radiation dominated era, Ω_ν remains constant as long as neutrinos are ultra-relativistic[3]. This is certainly true for temperatures well above a few eV. In this regime, the general solution of

[3] Actually, Ω_ν changes slightly when electron-positron annihilation takes place, a process which heats up the photons but not the neutrinos. This happens at a temperature close to the electron mass. After that, Ω_ν/Ω_γ remains constant until the neutrinos become non-relativistic.

eq. (5.34) is given by

$$\delta(t) - \delta_* = \frac{15}{4}\frac{\Omega_B}{\Omega_\nu} + t^{-1/4}\left(C_+ t^{i\sqrt{2\Omega_\nu/5-1/16}} + C_- t^{-i\sqrt{2\Omega_\nu/5-1/16}}\right) . \tag{5.38}$$

For $\Omega_\nu > 5/32$, the homogeneous part is oscillating with a damping envelope $\propto t^{-1/4} \propto a^{-1/2}$. This means that $\Delta H = \dot{\delta}$ will decay within a few Hubble times, which is a matter of seconds at the temperatures we are talking about. After that, $\delta - \delta_*$ will remain constant at the value of $(15/4)\,\Omega_B/\Omega_\nu$ until the neutrinos become non-relativistic. Then their pressure drops dramatically and so does their anisotropic stress. Until this time, the Universe expands isotropically, because the anisotropic stress of the magnetic field is precisely cancelled by the one of the neutrinos. Remember that a constant δ can always be absorbed in a re-scaling of the coordinates and has no physical effect. Fig. 5.3 shows the temperature evolution of $\delta - \delta_*$ in the radiation dominated era from neutrinos decoupling until $T = 100$eV.

This mechanism rests on two important facts. Firstly, as long as neutrinos are ultra-relativistic, they redshift in the same way as the magnetic field, meaning that Ω_B/Ω_ν is constant. Once the anisotropic stress of the neutrinos has adjusted to the magnetic field, their sum remains zero independent of the expansion of the Universe which is now in a Friedmann phase. Secondly, the efficiency of the effect hinges on the absolute value of Ω_ν. In the radiation dominated era (after positron annihilation), we have $\Omega_\nu \simeq 0.4$ so that $\Omega_\nu > 5/32$, and hence the system behaves as an underdamped oscillator with a damping envelope $\propto t^{-1/4}$. Had the density parameter of the free-streaming particles been less than 5/32, the behavior would be that of an overdamped oscillator. As it is evident from eq. (5.38), for $\Omega_\nu \ll 5/32$ there would be a mode which decays extremely slowly, roughly as $t^{-4\Omega_\nu/5}$. This is why a strongly subdominant free-streaming component cannot damp the anisotropy efficiently. As we shall discuss in section 5.4, a primordial gravitational wave background could play the role of such a free-streaming component if $\Omega_{GW} \gtrsim 5/32$.

5.3.2 Massive neutrinos

The neutrinos become non-relativistic roughly at the time when their temperature drops below their mass scale. Current bounds on the neutrino mass [177] are such that the highest-mass eigenstate is somewhere between ~ 1 eV and ~ 0.04 eV. Since the neutrino mass splitting is much below 1 eV, an eigenstate close to the upper bound would mean that the neutrinos are almost degenerate and hence become non-relativistic all at the same time. If this happens *before* photon decoupling, i.e., if $m_\nu > 0.3$ eV, the isotropization effect will not be present and the CMB will be affected by the anisotropic expansion sourced by the magnetic field. However, if the neutrinos remain ultra-relativistic until long *after* photon decoupling, the CMB quadrupole due to anisotropic expansion will be reduced because the neutrinos maintain expansion isotropic until they become non-relativistic.

In order to quantify this statement, we repeat the above calculations for the **matter dominated era**. For our purposes, this is a reasonable approximation for the time between photon decoupling and today. At decoupling, radiation is already subdominant, and on the other hand vacuum energy only begins to dominate at redshift $z \sim 0.5$. We therefore expect that both give small corrections only.

For completeness, we also give the solution of eq. (5.34) in a matter dominated Universe for the case where we ignore any contributions from free-streaming particles (neutrinos

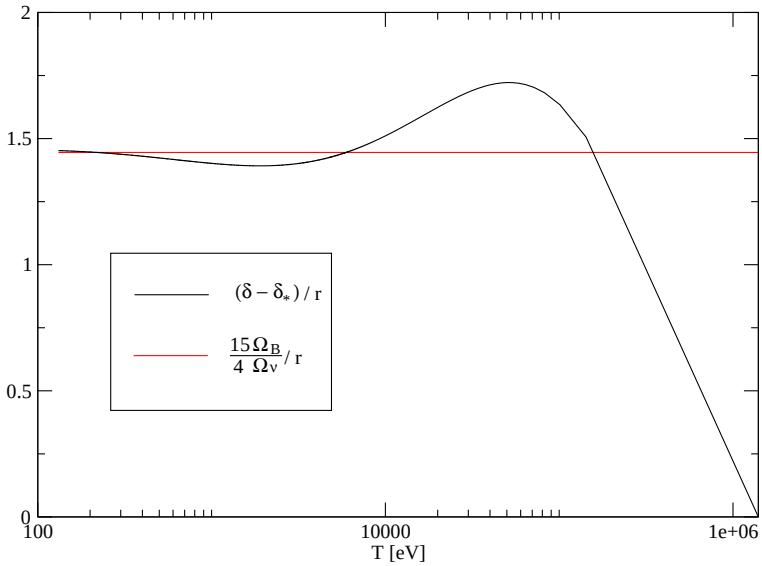

Figure 5.3: Temperature evolution of $\delta - \delta_*$ from neutrinos decoupling to $T = 100\text{eV}$. After decoupling, $\delta - \delta_*$ begins to oscillate with a decreasing amplitude around the constant $\frac{15}{4}\frac{\Omega_B}{\Omega_\nu}$, as predicted by the analytical solution (5.38). This qualitative behavior is independent of the initial conditions.

and, after decoupling, also photons). During matter domination we have $H = 2/3t$ and $\Omega_B \propto a^{-1} \propto t^{-2/3}$. The solution to (5.14) hence reads

$$\dot{\delta}(t) = \Delta H(t) = \frac{8\Omega_B(t)}{t} + \frac{C}{t^2} \ . \tag{5.39}$$

The homogeneous mode again decays more rapidly than the particular solution, so that the dimensionless quantity $\Delta H/H$ is again asymptotically proportional to Ω_B. Instead of eqs. (5.36), (5.37), we have

$$\frac{\Delta H}{H} \to 12\Omega_B \ , \qquad \delta(t) - \delta(t_{\rm eq}) = \int_{t_{\rm eq}}^{t} \Delta H dt \simeq 12\left[\Omega_B(t_{\rm eq}) - \Omega_B(t)\right] \ . \tag{5.40}$$

Let us now take into account a free-streaming component. We want to estimate the effect on the photon distribution function caused by anisotropic expansion in two cases. Case A: the neutrinos become non-relativistic *before* photon decoupling. Case B: the neutrinos become non-relativistic *after* photon decoupling. As an approximation, we assume that this happens instantaneously to all neutrino species, such that the contribution of neutrinos to eq. (5.34) disappears abruptly. We know that the neutrinos are in fact spread out in momentum space and also have a certain spread in the mass spectrum, so in reality this will be a gentle transition. However, we only want to estimate the order of magnitude of the effect and are not interested in these details at this point. More precice numerical results will be presented in sec. 5.3.3. Let us consider case A first.

5.3.2.1 Case A: neutrinos become non-relativistic before photon decoupling

We know that ΔH is very nearly zero when the neutrinos become non-relativistic. After that, $\Delta H/H$ will start to grow again to approach the value $6\Omega_B$ during radiation domination and $12\Omega_B$ during matter domination. As boundary condition at photon decoupling, we will hence assume $\Delta H/H = x\Omega_B$ with $x \lesssim 12$. This number can in principle be computed given the neutrino masses and the evolution of the scale factor across matter-radiation equality. We shall solve the full equations in subsection 5.3.3; here we just want to understand the results which we obtain there by numerical integration. The free-streaming component we are interested in now are the photons after decoupling. We therefore identify $\delta_* = \delta(t_{\rm dec})$, where $t_{\rm dec}$ denotes the instant of photon decoupling. Furthermore, in eq. (5.34) we replace Ω_ν by Ω_γ, our new free-streaming species. With $\Omega_\gamma \propto t^{-2/3}$ in the matter dominated era, the (not so obvious) analytic solution to eq. (5.34) is

$$\delta(t) - \delta(t_{\rm dec}) = \frac{15}{4}\frac{\Omega_B}{\Omega_\gamma} + C\left[f(t)\cos f(t) - \sin f(t)\right] + D\left[f(t)\sin f(t) + \cos f(t)\right] \ , \quad (5.41)$$

where we have introduced $f(t) \equiv 4\sqrt{2\Omega_\gamma(t)/5}$. The time derivative of eq. (5.41) yields

$$\frac{\Delta H}{H} = \frac{16}{5}\Omega_\gamma\left[C\sin f(t) - D\cos f(t)\right] \ . \quad (5.42)$$

Note that the slowly decaying mode has the same asymptotic behavior as (5.40) – in the matter dominated era, the free-streaming radiation can never catch up to the magnetic field, since both fade away too quickly. In other words, this means that free-streaming photons are never able to counteract the magnetic field anisotropy in order to isotropize again the Universe, even if they represent the main contribution to the background radiation energy density, and the reason for this is that they decouple only after the end of radiation dominantion.

In order to estimate the value of δ today (t_0), we can simply take the limit of small $\Omega_\gamma(t_0) \ll 1$ of (5.41). Correction terms are suppressed at least by $\sqrt{\Omega_\gamma(t_0)} \sim 10^{-2}$. We find

$$\delta(t_0) - \delta(t_{\rm dec}) \simeq \frac{15}{4}\frac{\Omega_B}{\Omega_\gamma} + D \ . \quad (5.43)$$

The constant D is fixed by the boundary conditions at decoupling, given by $\Delta H/H = x\Omega_B$ and $\delta = \delta(t_{\rm dec})$. These boundary conditions translate to

$$\begin{aligned} D &= \frac{\Omega_B(t_{\rm dec})}{\Omega_\gamma(t_{\rm dec})}\left[\frac{\sin f(t_{\rm dec})}{f(t_{\rm dec})}\left(\frac{5}{16}x - \frac{15}{4}\right) - \frac{5}{16}x\cos f(t_{\rm dec})\right] \\ &= \frac{\Omega_B(t_{\rm dec})}{\Omega_\gamma(t_{\rm dec})}\left[-\frac{15}{4} + \left(4 + \frac{2x}{3}\right)\Omega_\gamma(t_{\rm dec}) + \mathcal{O}\left(\Omega_\gamma^2(t_{\rm dec})\right)\right] \ . \end{aligned} \quad (5.44)$$

In order to obtain the essential behavior we have expanded the boundary term as a Taylor series in $\Omega_\gamma(t_{\rm dec}) \ll 1$. Our final result is

$$\delta(t_0) - \delta(t_{\rm dec}) \simeq \left(4 + \frac{2x}{3}\right)\Omega_B(t_{\rm dec}) \lesssim 12\Omega_B(t_{\rm dec}) \ , \quad (5.45)$$

up to corrections suppressed by additional powers of $\Omega_\gamma(t_{\rm dec})$.

In this case, the CMB quadrupole is not affected by the presence of free-streaming

neutrinos and we obtain the same result as when neglecting their presence,

$$C_2 \simeq \frac{16\pi}{225}\left[\delta(t_0) - \delta(t_{\rm dec})\right]^2 \simeq \frac{768\pi}{75}\Omega_B^2(t_{\rm dec}) \simeq 0.1 r^2\,. \tag{5.46}$$

5.3.2.2 Case B: neutrinos become non-relativistic after photon decoupling

In this case, the presence of the neutrino anisotropic stress will delay the onset of anisotropic expansion until a time t_m when the neutrinos become effectively non-relativistic. As before, we will ignore that this is a gradual process and simply assume that one can define some kind of "effective" t_m at which the neutrino anisotropic stress drops to zero. The full numerical result is given in section 5.3.3. The effect of anisotropic expansion on the photon distribution function is estimated as follows. We assume there is no anisotropic expansion between photon decoupling and t_m. At later times, neutrino anisotropic stress can be ignored. The relevant solution (5.41) is hence obtained with boundary condition $\dot{\delta}(t_m) = 0$. Working through the steps above once again or simply taking the result (5.45) with $t_{\rm dec} \to t_m$ and $x \to 0$, one finds

$$\delta(t_0) - \delta(t_{\rm dec}) = \delta(t_0) - \delta(t_m) \simeq 4\,\Omega_B(t_m)\ . \tag{5.47}$$

Since Ω_B decays as a^{-1}, the effect of anisotropic expansion in case B is suppressed by roughly a factor of $a(t_{\rm dec})/(3a(t_m))$ with respect to case A. For light neutrinos with a highest-mass eigenstate close to the current lower bound, this factor can be as small as ~ 0.03, loosening the constraint on a constant magnetic field from the CMB temperature anisotropy correspondingly. Constraints coming from Faraday rotation are not affected.

Clearly, the heaviest neutrino becomes massive at redshift $z_m = m_\nu/T_\nu \gtrsim 0.04{\rm eV}/T_\nu \simeq 200$. One might wonder whether isotropization can be supported even if only one neutrino remains massless, since its contribution to the energy density is $\Omega_{\nu 1} \simeq 0.23\Omega_\gamma$. The problem is however that, as soon as one neutrino species becomes massive, the equilibrium between the magnetic field and the neutrino anisotropic stresses is destroyed and, as we have seen under case A, where one still has free streaming photons, it cannot be fully re-established in a matter dominated Universe.

5.3.3 Numerical solutions

In order to go beyond the estimates derived so far, we have solved eqs. (5.2-5.4) numerically with cosmological parameters corresponding to the current best-fit ΛCDM model [178]. We use cosmological parameters $\Omega_\Lambda = 0.73$, $\Omega_m = 0.27$ today, where Ω_m includes a contribution of massive neutrinos[4] which we approximate by $\Omega_\nu h^2 = N_\nu m_\nu/94{\rm eV}$ with $N_\nu \simeq 3$. The contribution to the right-hand side of eq. (5.7) from free-streaming neutrinos is obtained by integrating eq. (5.31) with the full distribution function for massive fermions. More precisely, we compute the full distribution function to first order in δ and perform the integration numerically, including the neutrino mass as a parameter. We begin to integrate deep inside the radiation dominated era, when the neutrinos are still relativistic but already free-streaming. The asymptotic behavior of solution (5.37) can be used as

[4]CMB observations actually constrain the matter density at decoupling, such that neutrinos with $m_\nu \lesssim 0.3$eV, which are still relativistic at that time, do not contribute to the measurement of Ω_m. However, since their density parameter today is then also very small, their contribution to the matter density remains practically irrelevant.

initial condition at neutrino decoupling. The constraint equation (5.2) provides the remaining initial condition. We then integrate until the desired time. We define today t_0 by $a(t_0) = 1$.

In fig. 5.4, we present the results of the numerical integration from neutrino decoupling until today. We plot both $\delta - \delta_*$ and $\Delta H/H$ in units of the parameter $r = \Omega_B/\Omega_\gamma$ so that the plots are valid for arbitrary magnetic field strengths, as long as $r \ll 1$. After neutrino decoupling, δ oscillates and reaches its constant value as in eqs. (5.38), (5.41), while $\Delta H = \dot{\delta}$ oscillates and decays. We choose as initial condition $\delta = \delta_* = 0$ at neutrino decoupling. Once the temperature of the Universe reaches the neutrinos mass scale, neutrino pressure decreases and they become non-relativistic. At this point, they can no longer compensate the anisotropic pressure of the magnetic field, and both δ and ΔH begin to grow. However, it is clear from fig. 5.4 (left plot) how, once neutrinos become non relativistic after photon decoupling (case B), the growth of δ is suppressed with respect to case A, where this happens before photon decoupling. Moreover, the solid black line in the lower plot represents the temperature evolution of $\Delta H/H$ in the case where only the magnetic field sources the anisotropy: this makes clear how the absence of any free-streaming particle able to counteract the magnetic anisotropic stress leaves the anisotropy of the Universe free to grow with respect to its value today.

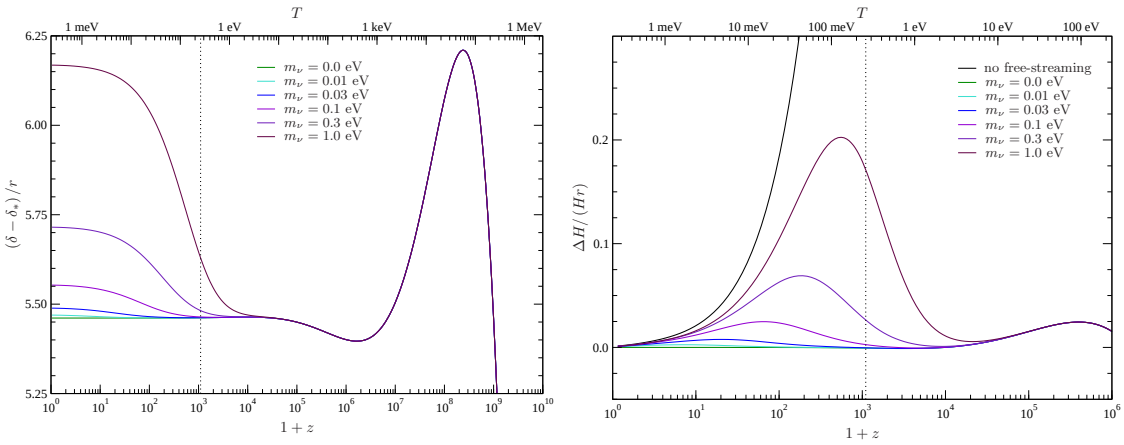

Figure 5.4: Temperature evolution of $\Delta H/H$ and $\delta - \delta_*$ for different neutrinos masses. We chose the initial conditions to be given by $\delta_* = 0$ at neutrino decoupling. The black solid line in the right plot represents the temperature evolution of $\Delta H/H$ in the case where only the magnetic field sources the anisotropy and no free-streaming particle is present to compensate this effect.

Our quantitative final result is shown in fig. 5.5, where we plot the value of the quadrupole generated by a constant magnetic field, rescaled by r^2, as function of the neutrino mass. We weight the final C_2 with respect to the quadrupole obtained without considering the isotropization induced by free-streaming particles, in order to underline the relative importance of this effect. These results clearly show that the CMB quadrupole is significantly reduced by neutrino free-streaming only if their mass is smaller than the temperature at photon decoupling, $m_\nu < T_{\rm dec} \simeq 0.26\,\text{eV}$. In fact, for neutrino masses in the range $0.3\,\text{eV} \lesssim m_\nu \lesssim 3\,\text{eV}$, the quadrupole C_2 is reduced by less than a factor 100 from the result without a free-streaming component, whereas for $0 \lesssim m_\nu \lesssim 0.3\,\text{eV}$, it decreases

by several orders of magnitude. Note, however, that the effect is not negligible even in the former case with relatively large neutrino masses. Fig. 5.5 also shows our analytical estimation for the final amplitude of the CMB quadrupole produced by this effect as given by eq. (5.47). Of course the value of eq. (5.47) depends on the time at which neutrinos become effectively non-relativistic, t_m. Once we choose t_m to be given by the time at which $T = m_\nu$, we overestimate the final quadrupole amplitude by one order of magnitude (dashed blue line). This is a consequence of the fact that the neutrino distribution function is highly relativistic and therefore it takes a further redshift for them to start behaving effectively as massive pressureless particles. This has been considered in the more elaborate estimate given by the dashed red line where we fix the time t_m to be given by the time at which $d^3P_\nu/d(\ln T)^3 = 0$, i.e. the time at which the pressure reaches the break in the power law. This is in excellent agreement with the numerical results.

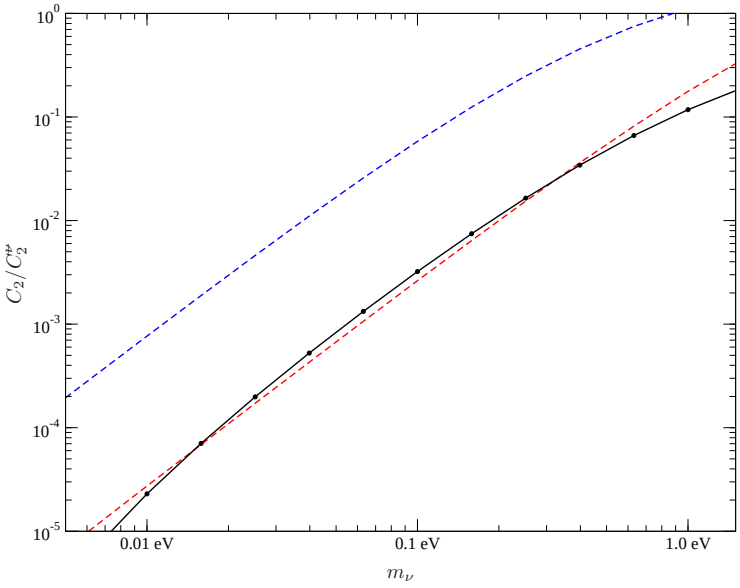

Figure 5.5: Effect of free-streaming neutrinos with different masses on the quadrupole generated by a homogeneous magnetic field, weighted on the quadrupole obtained without considering the effect of any free-streaming particles. The solid black line represents the result of the numerical integration, the dashed blue and red lines correspond to our analytical prediction given by eq. (5.47) for two different choices of t_m, the time at which neutrinos are effectively non-relativistic (see the text for clarification).

5.4 A gravitational wave background and other massless free-streaming components in an anisotropic Universe

From our previous discussion it is evident that any massless free-streaming particle species X can isotropize the Bianchi I model with a constant magnetic field, if present with sufficient contribution Ω_X already in the radiation dominated era. This has to be accounted for if we want to estimate the CMB quadrupole induced by a homogeneous magnetic field.

So far we have discussed the standard model neutrinos as an example of such a particle. However, also other massless particles can play this role, for instance gravitons, but also

particle species outside of the spectrum of the standard model. Interestingly, the current bounds on the number of relativistic degrees of freedom during nucleosynthesis, often parameterized by the *effective number of additional neutrino species* ΔN_ν, allow for the possibility that such a species could be sufficiently abundant. The present bound on N_ν from nucleosynthesis is [177]

$$\begin{aligned} N_\nu &= 3.2 \pm 1.2 \,, \\ g_* &= 2 + \frac{7N_\nu}{4}\left(\frac{4}{11}\right)^{4/3} = 3.36 + (N_\nu - 3) \times 0.454 \\ &= 3.36 + (0.2 \pm 1.2) \times 0.454 \quad \text{at } 95\% \text{ confidence.} \end{aligned} \tag{5.48}$$

Here we have taken into account that the photon and neutrino temperatures are related by $T_\nu = (4/11)^{1/3} T_\gamma$ [132]. The effective g_* from γ and three species of neutrino corresponds to $g_*(\gamma, 3\nu) = 3.36$. This is equivalent to a limit on an additional relativistic contribution at nucleosynthesis of $\Omega_X \lesssim 0.2$. From the solution (5.38) we know that a free-streaming relativistic species with a density parameter $\Omega_X \gtrsim 5/32 \simeq 0.156$ during the radiation dominated era will isotropize expansion within a few Hubble times. Since this species will presumably decouple before the neutrinos (otherwise it should have been discovered in laboratory experiments), expansion can be isotropic already at neutrino decoupling, and thus neither the cosmic neutrino background nor the CMB will be affected by anisotropic expansion. In this case therefore, unless we are able to detect the background of the species X, we will never find a trace of the anisotropic stress produced by a homogeneous magnetic field. An interesting example are gravitons, which we now want to discuss.

Inflationary models generically predict a background of cosmological gravitational waves which are produced from quantum fluctuations during the inflationary phase. The amplitude of this background, usually expressed by the so-called tensor-to-scalar ratio, r_T, has not yet been measured, but for a certain class of inflationary models, forthcoming experiments such as Planck might be able to detect these gravitational waves. This is in contrast to the cosmic neutrino background, for which there is no hope of direct detection with current or foreseeable technology. However, this background typically contributes only a very small energy density,

$$\Omega_{\mathrm{GW,\,inf}}/\Omega_\gamma \simeq 10^{-10} r_T \,, \qquad n_T \lesssim 0 \,.$$

Only non-standard inflationary models which allow for $n_T > 0$ can contribute a significant background, see [179].

Gravitational waves can also be produced during phase transitions in the early Universe [180, 83], after the end of inflation. Such gravitational wave backgrounds can easily contribute the required energy density. Let us therefore concentrate on this possibility.

If the highest energy scales of our Universe remain some orders of magnitude below the Planck scale, gravitational waves are *never* in thermal equilibrium and can be considered as free-streaming radiation throughout the *entire history*. Therefore, if the gravitational wave background was statistically isotropic at some very early time, then any amount of anisotropic expansion taking place between this initial time and today will affect the gravitons in a similar fashion as any other free-streaming component, and therefore our present gravitational wave background would be anisotropic. Loosely speaking, the intensity of gravitational waves would be larger in those directions which have experienced less expansion in total since the initial time when the gravitational wave background was

isotropic.

As we have specified above, with the current limits on ΔN_ν, the density parameter of gravitons $\Omega_{\rm GW}$ during nucleosynthesis can be as large as ~ 0.2. At higher temperatures (that is, at earlier times), the number of relativistic degrees of freedom increases (more particle species are effectively massless), such that $\Omega_{\rm GW}$ at earlier time can even be larger[5]. It is therefore conceivable that gravitons acquire sufficient anisotropic stress to compensate the magnetic field and hence take over the role which neutrinos have played in section 5.3. As already pointed out, in this case, neither neutrinos nor photons will ever experience any significant anisotropic expansion, since the Universe remains in a Friedmann phase after the gravitons have adjusted to the magnetic field. Of course, gravitons remain relativistic for all times and the mass effect which we discussed for the neutrinos does not occur.

In order to rule out this scenario, it would be very interesting not only to measure the background of cosmological gravitational waves but also to determine whether or not it shows a quadrupole anisotropy compatible with such a compensating anisotropic stress. Or in other words: just as the smallness of the CMB quadrupole is a direct indication for isotropic expansion between decoupling of photons and today, the smallness of the quadrupole of a gravitational wave background would inform us about the isotropy of expansion between today and a much earlier epoch where this background was generated.

5.5 Conclusions

In this paper we have studied a magnetic field coherent over very large scales so that it can be considered homogeneous. We have shown that in the radiation dominated era the well known Bianchi I solution for this geometry is isotropized if a free streaming relativistic component is present and contributes sufficiently to the energy density, $\Omega_X \gtrsim 5/32$. This is in tune with the numerical finding [171, 172, 174] that the neutrino anisotropic stresses 'compensate' large scale magnetic field stresses. A perturbative explanation of this effect is attempted in [173]. Here we explain the effect for the simple case of a homogeneous magnetic field: free streaming of relativistic particles leads to larger redshift, hence smaller pressure in the directions orthogonal to the field lines where the magnetic field pressure is positive and to smaller redshift, hence larger pressure in the direction parallel to the magnetic field, where the magnetic field pressure is negative. To first order in the difference of the scale factors this effect leads to a build up of anisotropic stress in the free streaming component until it exactly cancels the magnetic field anisotropic stress. This is possible since both these anisotropic stresses scale like a^{-4}.

In standard cosmology this free-streaming component is given by neutrinos. However, as soon as neutrinos become massive, their pressure, $P_\nu \propto a^{-5}$, decays much faster than their energy density, $\rho_\nu \propto a^{-3}$, and the effect of compensation is lost. If this happens significantly after decoupling, there is still a partial cancellation, but if it happens before decoupling, the neutrinos no longer compensate the magnetic field anisotropic stress. Furthermore, a component which starts to free-stream only in the matter era (like e.g. the photons) does not significantly reduce the anisotropic stress. Actually, inserting the

[5] During a transition from g_1 relativistic degrees of freedom to $g_2 < g_1$, the temperature changes from T_1 to T_2. Since entropy is conserved during the transition we have $g_1 T_1^3 = g_2 T_2^3$. Hence $\rho_2 = g_2 T_2^4 = g_2 \left[\left(\frac{g_1}{g_2}\right)^{1/3} T_1\right]^4 = \left(\frac{g_1}{g_2}\right)^{1/3} \rho_1 > \rho_1$. In other words, the energy density of all species which are still in thermal equilibrium increases if one reduces the number of degrees of freedom at constant entropy.

dominant part of the constant D from eq. (5.44) in (5.42) one finds

$$\frac{\Delta H}{H} = 12\Omega_B \,, \tag{5.49}$$

like without a free-streaming component.

This cancellation of anisotropic stresses does not affect Faraday rotation. A constant magnetic field with amplitude $B_0 \gtrsim 10^{-9}$Gauss can therefore be discovered either by the Faraday rotation it induces in the CMB [101], or, if a sufficiently intense gravitational wave background exists, by the quadrupole (anisotropic stress) it generates in it.

Finally, Planck and certainly future large scale structure surveys like Euclid will most probably determine the absolute neutrino mass scale. Once this is known, we can infer exactly by how much the CMB quadrupole from a constant magnetic field is reduced by their presence.

Acknowledgments

We thank Camille Bonvin and Chiara Caprini for discussions. JA wants to thank Geneva University for hospitality and the German Research Foundation (DFG) for financial support. This work is supported by the Swiss National Science Foundation.

Chapter 6

Gravitational waves from self-ordering scalar fields

JOURNAL OF COSMOLOGY AND ASTROPARTICLE PHYSICS **0910**, 005 (2009)

Gravitational waves from self-ordering scalar fields

Elisa Fenu, Daniel G. Figueroa, Ruth Durrer and Juan García-Bellido

Gravitational waves were copiously produced in the early Universe whenever the processes taking place were sufficiently violent. The spectra of several of these gravitational wave backgrounds on subhorizon scales have been extensively studied in the literature. In this paper we analyze the shape and amplitude of the gravitational wave spectrum on scales which are superhorizon at the time of production. Such gravitational waves are expected from the self ordering of randomly oriented scalar fields which can be present during a thermal phase transition or during preheating after hybrid inflation. We find that, if the gravitational wave source acts only during a small fraction of the Hubble time, the gravitational wave spectrum at frequencies lower than the expansion rate at the time of production behaves as $\Omega_{\rm GW}(f) \propto f^3$ with an amplitude much too small to be observable by gravitational wave observatories like LIGO, LISA or BBO. On the other hand, if the source is active for a much longer time, until a given mode which is initially superhorizon ($k\eta_* \ll 1$), enters the horizon, for $k\eta \gtrsim 1$, we find that the gravitational wave energy density is frequency independent, i.e. scale invariant. Moreover, its amplitude for a GUT scale scenario turns out to be within the range and sensitivity of BBO and marginally detectable by LIGO and LISA. This new gravitational wave background can compete with the one generated during inflation, and distinguishing both may require extra information.

DOI: 10.1088/1475-7516/2009/10/005

6.1 Introduction

Gravitational waves (GWs) are produced in the late Universe via cataclismic astrophysical events like hypernovae and inspiralling binaries. Because gravity is so weak, it is extremely difficult to detect directly with present day interferometers [181]. On the other hand, during the violent processes which we expect took place in the very early Universe, several stochastic backgrounds of GWs of significant energy may be produced, although their amplitude today is drastically reduced by the expansion of the Universe, making them equally difficult to detect [182, 183, 150]. Their discovery may however be possible in the near future, opening a completely new window into the uncharted territory of the very early Universe. For this we must determine the detailed GW spectrum, which strongly depends on the physical processes generating them.

In the last few years there has been significant progress in the experimental prospects for detecting GWs with interferometers like LIGO and VIRGO and the future satellite mission LISA. This has stimulated research for sources of primordial GWs from the early Universe,

either from hypothetical first order phase transitions [184, 185, 116, 149, 186, 187, 82, 117, 118] or from the process of reheating after inflation [108, 109, 110, 111, 112, 113, 114, 115].

The mechanism responsible for GW production during these early Universe phenomena is typically a causal process, like bubble collisions or turbulence, giving rise to spectra which peak at wavelengths that are well within the causal horizon during their generation. Thus, most of past analyses concentrate on contributions of GWs with wavelengths smaller than the horizon at the time of production, with the exception of those generated during inflation [188], which are stretched by the inflationary expansion.

In this paper we study the infrared behaviour of the GW spectrum produced either during preheating or during first order phase transitions, on scales which are superhorizon at the time of formation, *i.e.* $k < \mathcal{H}_*$, where k and $\mathcal{H}_*$ are the comoving momentum and inverse horizon. We want to study a causal process of symmetry breaking like hybrid preheating [189, 190, 191, 192, 193, 194, 195], where the order parameter has global $\mathcal{O}(N)$ symmetry in the false vacuum and, upon symmetry breaking, the N fields undergo self-ordering on a given scale as soon as they enter the horizon, in particular on scales much larger than the inverse mass of the field in the true vacuum.

We consider a multi-component scalar field which obtains a non-zero *vacuum expectation value* (*vev*) v and a mass m, during a symmetry breaking process. We shall assume that this mass m is much larger than the Hubble parameter H_* at the time of the transition, since if the *vev* in the true vacuum is much smaller than the Planck scale, then $H_* \sim m\,v/M_p \ll m$. Such a model could describe the symmetry breaking process which triggers the end of hybrid inflation or a thermal phase transition. As long as we are only interested in superhorizon scales, $k \gg \mathcal{H}_*$, we can neglect the radial, massive mode and treat the dynamics within the non-linear sigma-model (NLSM) approximation. On large scales, the anisotropic stresses are determined by gradient energy and the typical (comoving) scale is simply the time dependent horizon scale $\mathcal{H}^{-1}$. The field self-orders at the horizon scale, and the source of GWs decays inside the horizon. For scalar metric perturbations this process has been studied *e.g.* in Ref. [196]. It is very closely related to the scaling of global topological defects [31] even though for a number of components $N > 4$ there are no topological defects associated with such a scalar field in $3+1$ dimensions.

We work in the large N approximation within which the scalar field equation of motion, for scales larger than the inverse mass, $k \ll m$, can be solved analytically. The GW spectrum will then be estimated by analytical approximations, introducing the anisotropic stress tensor sourced by the field fluctuations at different scales.

Tensor perturbations from a NLSM in the large N approximation have also been studied in Ref. [197, 121], see also [198]. There the authors have calculated the tensor perturbation spectrum for scales which enter the horizon in the matter era and they have compared this with the inflationary signal in the CMB. Here we shall concentrate on the radiation dominated era and the detection of the signal in direct gravitational wave experiments like advanced LIGO [10, 11], LISA [13, 14, 15, 16] and BBO [199, 200, 201].

The paper is organized as follows. In the next section we describe the formalism, derive the scalar field solutions and calculate the unequal time anisotropic stress correlators which source GWs. In Section 6.3 we study the production of GWs from long wavelength modes of this source. We derive a general formula that can be applied to different situations, depending how long the GW source is acting. In Section 6.4 we use this result to determine the shape and amplitude of the GW spectrum in two situations, first the case of a source producing GWs only during a small fraction of the Hubble time and, second, the case in

which the source producing GWs acts for a much longer time, until a given mode which is initially superhorizon, $k\eta_* \ll 1$, enters the Hubble radius, $k\eta \simeq 1$. In Section 6.5 we summarize our results and conclude.

Notation Throughout this paper we assume a spatially flat Friedmann Universe with metric

$$ds^2 = a^2(\eta)\left(-d\eta^2 + \delta_{ij}dx^i dx^j\right) , \tag{6.1}$$

where η denotes conformal time and we normalize the scale factor to unity today, $a(\eta_0) = 1$. The comoving Hubble rate is $\mathcal{H} = a'/a$, while $H = a'/a^2$ is the physical one. The prime denotes derivative w.r.t. conformal time η.

6.2 Formalism

We first introduce the NLSM and the large N limit of a global $\mathcal{O}(N)$ symmetric scalar field, then we study the physics of the correlators of the anisotropic stress tensor.

6.2.1 The model

We consider an N-component scalar field with a Lagrangian

$$\mathcal{L} = \mathcal{L}_0 + \mathcal{L}_1 = -\partial_\mu \Phi^{\mathrm{T}} \partial^\mu \Phi - \lambda\left(\Phi^{\mathrm{T}}\Phi - \frac{v^2}{2}\right)^2 + \mathcal{L}_1 , \tag{6.2}$$

where $\Phi^{\mathrm{T}} = (\phi_1, \phi_2, ..., \phi_N)/\sqrt{2}$, λ is the dimensionless self-coupling of Φ and v is the *vev* in the true vacuum. In the case of a thermal bath at high temperature, the Lagrangian $\mathcal{L}_0$ obtains corrections of the form $\mathcal{L}_1 \sim -T^2\Phi^2$, so that its minimum is at $\Phi = 0$ which respects the global $\mathcal{O}(N)$ symmetry of the Lagrangian. At low temperature, $T < T_c \simeq v$, the thermal corrections are too small to the keep the minimum at $\Phi = 0$ and the global $\mathcal{O}(N)$ symmetry is spontaneously broken to $\mathcal{O}(N-1)$. In the context of hybrid preheating, there is no need for thermal restoration of the symmetry. The field Φ acquires a large mass during inflation through its coupling to the inflaton χ, $\mathcal{L}_1 = -g^2\Phi^{\mathrm{T}}\Phi\chi^2$. Above a critical value, $\chi > \chi_c \equiv \sqrt{\lambda}v/g$, the effective quadratic mass of Φ is positive and the field is fixed at $\Phi = 0$. When the quadratic mass becomes negative, $\chi < \chi_c$, a tachyonic instability triggers the end of inflation and symmetry breaking. Soon after the symmetry is broken, thermal corrections and tachyonic effects can be neglected, and Φ is closely confined (in most of space) to the vacuum manifold, given by $\sum_a \phi_a^2(\mathbf{x}, \eta) = v^2$. Nevertheless, in positions such that their comoving distance is $|\mathbf{x} - \mathbf{x}'| > \mathcal{H}^{-1}$, the values $\Phi(\mathbf{x}, \eta)$ and $\Phi(\mathbf{x}', \eta)$ are uncorrelated, which leads to a gradient energy density associated to the $N-1$ Goldstone modes, $\rho \sim (\partial_i \Phi)^2$. For $N > 2$, the dynamics of the Goldstone modes is well described by a NLSM [119, 31] where we force $\sum_a \phi_a^2 = v^2$ by a Lagrange multiplier. This corresponds to the limit $\lambda \to \infty$ in the above Lagrangian. This approximation is very good for physical scales with are much larger than $m^{-1} \equiv 1/(\sqrt{\lambda}v)$. Of course, on small scales the field fluctuations still oscillates around the true *vev*, but in this paper we only focus on the superhorizon modes which are free to wander around in the vacuum manifold, giving rise to a gradient energy density which will generate GWs on these scales.

Normalizing the symmetry breaking field to its *vev*, $\beta \equiv \Phi/v$, each component of the

field obeys the non-linear sigma model evolution equation [196]

$$\Box\beta^a - (\partial_\mu\beta\cdot\partial^\mu\beta)\beta^a \;=\; 0\;, \tag{6.3}$$

where $(\partial_\mu\beta\cdot\partial^\mu\beta)=\sum_a \eta^{\mu\nu}\partial_\mu\beta^a(\mathbf{x},\eta)\partial_\nu\beta^a(\mathbf{x},\eta)$ and $\sum_a \beta^a(\mathbf{x},\eta)\beta^a(\mathbf{x},\eta)=1$. In the large N-limit, we assume that the sum over components can be replaced by an ensemble average,

$$T(x)=\sum_a \eta^{\mu\nu}\partial_\mu\beta^a\partial_\nu\beta^a = N\langle\eta^{\mu\nu}\partial_\mu\beta^a\partial_\nu\beta^a\rangle = \bar{T}(\eta)\;. \tag{6.4}$$

By dimensional considerations, $T\propto\mathcal{H}^2$, or

$$\bar{T}(\eta)=T_o\eta^{-2}\,, \tag{6.5}$$

with $T_o>0$. Replacing the non-linearity in the sigma-model by this expectation value we obtain a linear equation which can be solved exactly. In Fourier space it reads

$$\beta_k^a{}'' + \frac{2\gamma}{\eta}\beta_k^a{}' + \left(k^2-\frac{T_o}{\eta^2}\right)\beta_k^a = 0\,, \tag{6.6}$$

where $\gamma = d\log a/d\log\eta$ and primes denote derivatives w.r.t. η. In a radiation dominated Universe $\gamma=1$ while in a matter dominated Universe $\gamma=2$. The solution to Eq. (6.6) for constant γ is given by

$$\beta^a(\mathbf{k},\eta)=(k\eta)^{\frac{1}{2}-\gamma}\Big[C_1(\mathbf{k})\,J_\nu(k\eta)+C_2(\mathbf{k})\,Y_\nu(k\eta)\Big]\,, \tag{6.7}$$

where

$$\nu^2=\left(\frac{1}{2}-\gamma\right)^2+T_o\;, \tag{6.8}$$

and C_1, C_2 are constants of integration. Thus, $\nu>1/2$ for a radiation dominated Universe and $\nu>3/2$ for matter domination. Since in general we have that $\nu>0$, Y_ν diverges for small argument, so we will keep only the regular mode of the solution J_ν, which can be written as

$$\beta^a(\mathbf{k},\eta) \;=\; \sqrt{A}\left(\frac{\eta}{\eta_*}\right)^{\frac{1}{2}-\gamma}\frac{J_\nu(k\eta)}{(k\eta_*)^\nu}\beta^a(\mathbf{k},\eta_*)\,, \tag{6.9}$$

where $\beta^a(k,\eta_*)$ is the a-th component of the field at the initial time η_*. We assume that β is initially Gaussian distributed with a scale-invariant spectrum on large scales and vanishing power on small scales

$$\langle\beta^a(\mathbf{k},\eta_*)\beta^{*b}(\mathbf{k}',\eta_*)\rangle = \begin{cases} (2\pi)^3\mathcal{C}\frac{\delta^{ab}}{N}\delta(\mathbf{k}-\mathbf{k}') & ,\; k\eta_*\ll 1 \\ 0 & ,\; k\eta_*>1\;. \end{cases} \tag{6.10}$$

This means that the field is aligned on scales smaller than the comoving horizon η_* and has arbitrary orientation on scales larger than η_*. The condition that $\beta^2=1$ actually introduces correlations between the different components of β but these lead to corrections of order $1/N$ to the above expression which we will neglect here. We also do not enter into the details of the decay of this function around $k\eta_*=1$. The constant $\mathcal{C}$ is chosen such

that the normalization condition is satisfied (up to corrections of order $1/N$),

$$\begin{aligned}\beta^2(\mathbf{x},\eta_*) &\equiv \langle\beta^2(\mathbf{x},\eta_*)\rangle\Big(1+\mathcal{O}(1/N)\Big)\\ &\simeq \int\frac{d^3k}{(2\pi)^3}\frac{d^3k'}{(2\pi)^3}\langle\beta^a(\mathbf{k},\eta_*)\beta^{*a}(\mathbf{k}',\eta_*)\rangle e^{i\mathbf{x}\cdot(\mathbf{k}-\mathbf{k}')}\simeq\frac{\mathcal{C}}{6\pi^2\eta_*^3}=1\,. \quad (6.11)\end{aligned}$$

In the large N-limit we neglect the corrections of order $1/N$ which come from the fluctuations in β^2. On large scales this is a very good approximation. However, on small scales, and in particular, on scales comparable with the inverse of the mass of the symmetry breaking field, m^{-1}, the fluctuations are certainly not negligible. In our analysis we consider only large scales, where the above approximation is valid.

In order for $\langle\beta^2\rangle$ to be time independent we need that the equal time correlator be fixed to one:

$$\begin{aligned}\langle\beta^2(\mathbf{k},\eta)\rangle &= A\,\mathcal{C}\int\frac{d^3k}{(2\pi)^3}\left(\frac{\eta}{\eta_*}\right)^{(1-2\gamma)}\frac{J_\nu^2(k\eta)}{(k\eta_*)^{2\nu}}\\ &\simeq 3A\left(\frac{\eta_*}{\eta}\right)^{2(1+\gamma-\nu)}\int_0^\infty dy y^{2(1-\nu)}J_\nu^2(y)\,=\,1\,, \quad (6.12)\end{aligned}$$

where we have substituted $\mathcal{C}=6\pi^2\eta_*^3$ and we have set $y=k\eta$. Note that the upper limit is actually η/η_*, but at late times, the (dimensionless) integral is insensitive to the upper boundary, so we can take it to infinity and thus make the integral free of any time scale. In order to obtain a time-independent *vev*, we then just require

$$\nu=\gamma+1\,. \quad (6.13)$$

Introducing this relation into Eq. (6.8), one obtains T_o in terms of γ as

$$T_o \;=\; 3(\gamma+1/4)\,. \quad (6.14)$$

The constant A is determined then by the condition

$$1=3A\int_0^\infty dy y^{2(1-\nu)}J_\nu^2(y)\,,\qquad \text{hence}\qquad A=\frac{4\Gamma(2\nu-1/2)\Gamma(\nu-1/2)}{3\Gamma(\nu-1)}\,. \quad (6.15)$$

Since $\nu=\gamma+1$, we can also write the amplitude of the field fluctuations, as

$$\beta^a(\mathbf{k},\eta)=\sqrt{A}\left(\frac{\eta}{\eta_*}\right)^{3/2}\frac{J_\nu(k\eta)}{(k\eta)^\nu}\beta^a(\mathbf{k},\eta_*)\,. \quad (6.16)$$

6.2.2 Unequal time correlators

From Eqs. (6.10) and (6.16) we obtain the following expression for the unequal time correlator of the field:

$$\begin{aligned}\left\langle \beta^a(\mathbf{k},\eta)\beta^{*b}(\mathbf{k}',\eta')\right\rangle &= A\left(\frac{\eta\eta'}{\eta_*^2}\right)^{3/2}\frac{J_\nu(k\eta)J_\nu(k'\eta')}{(k\eta)^\nu(k'\eta')^\nu}\left\langle \beta^a(\mathbf{k},\eta_*)\beta^{*b}(\mathbf{k}',\eta_*)\right\rangle \\ &= (2\pi)^3 6\pi^2 A(\eta\eta')^{3/2}\frac{J_\nu(k\eta)J_\nu(k\eta')}{(k\eta)^\nu(k\eta')^\nu}\frac{\delta_{ab}}{N}\delta(\mathbf{k}-\mathbf{k}') \\ &\equiv (2\pi)^3\delta(\mathbf{k}-\mathbf{k}')\mathcal{P}_\beta^{ab}(k,\eta,\eta')\,. \end{aligned} \tag{6.17}$$

We assume that the field β is Gaussian distributed initially. As its time evolution is linear, it will remain a Gaussian field and we can determine higher order correlators via Wick's theorem. This will be important in the next section when we determine the unequal time correlator of the anisotropic stresses which source the production of GWs. Furthermore, this source is *totally coherent* [31] in the sense that its unequal time correlator $\mathcal{P}_\beta^{ab}(k,\eta,\eta')$ is a product of a function of η and η',

$$\begin{aligned}\mathcal{P}_\beta^{ab}(k,\eta,\eta') &= \frac{\delta_{ab}}{N}6\pi^2 A(\eta\eta')^{3/2}\frac{J_\nu(k\eta)J_\nu(k\eta')}{(k\eta)^\nu(k\eta')^\nu} \equiv \frac{\delta_{ab}}{N}f(k,\eta)f(k,\eta')\,, \\ \text{with}\quad f(k,\eta) &= \sqrt{6\pi^2 A}\;k^{3/2}\frac{J_\nu(k\eta)}{(k\eta)^{\nu-3/2}}\,. \end{aligned} \tag{6.18}$$

Note the $k^{3/2}$ scaling law at horizon crossing ($k\eta\sim 1$) which is characteristic for quantum fluctuations from de Sitter, *i.e.* inflation. This already hints to the fact that we will find a scale-invariant spectrum also in this case.

6.3 The production of gravitational waves

In this section we derive a general formula for the GW power spectrum sourced by super-horizon modes of a self ordering field. We also comment about the frequency range for the GW background produced in this way.

Let us consider tensor perturbations (GWs) of the metric,

$$ds^2 = a^2(\eta)(\eta_{\mu\nu}+2h_{\mu\nu})dx^\mu dx^\nu\,, \tag{6.19}$$

where h_{ij} is traceless, $h_i^i=0$, and divergence free, $\partial^i h_{ij}=0$. Linearizing Einstein's equations yields the evolution equation of GWs sourced by the anisotropic stresses of the scalar fields Φ,

$$h_{ij}''(\mathbf{x},\eta)+2\mathcal{H}\,h_{ij}'(\mathbf{x},\eta)-\nabla^2 h_{ij}(\mathbf{x},\eta)=8\pi G\,\Pi_{ij}(\mathbf{x},\eta)\,, \tag{6.20}$$

where Π_{ij} represents the TT part of the (effective) anisotropic stress tensor

$$T_{ij}(\mathbf{x},\eta)=\partial_i\phi^a(\mathbf{x},\eta)\partial_j\phi^a(\mathbf{x},\eta)-\frac{1}{3}\delta_{ij}\left[\nabla\phi^a(\mathbf{x},\eta)\right]^2\,. \tag{6.21}$$

Fourier transforming the GW evolution equation (6.20) we obtain

$$h''_{ij}(\mathbf{k},\eta) + 2\mathcal{H}\, h'_{ij}(\mathbf{k},\eta) + k^2 h_{ij}(\mathbf{k},\eta) = 8\pi G\, \Lambda_{ij,lm}(\hat{\mathbf{k}}) T_{lm}(\mathbf{k},\eta) \tag{6.22}$$

where the projector

$$\begin{aligned} \Lambda_{ij,lm}(\hat{\mathbf{k}}) &\equiv P_{il}(\hat{\mathbf{k}})P_{jm}(\hat{\mathbf{k}}) - \frac{1}{2}P_{ij}(\hat{\mathbf{k}})P_{lm}(\hat{\mathbf{k}}) \ , \\ P_{ij}(\hat{\mathbf{k}}) &\equiv \delta_{ij} - \hat{\mathbf{k}}_i\hat{\mathbf{k}}_j \ , \qquad \hat{\mathbf{k}} \equiv \mathbf{k}/k \ , \end{aligned}$$

filters out the TT part of the Fourier transformed effective anisotropic stress tensor

$$\Pi_{ij}(\mathbf{k},\eta) = \Lambda_{ij,lm}(\hat{\mathbf{k}}) \int \frac{d^3q}{(2\pi)^3}\, q_l q_m\, \phi^a(\mathbf{q},\eta)\phi^a(\mathbf{k}-\mathbf{q},\eta) \ . \tag{6.23}$$

Note that we are summing over repeated indices both in coordinates and in field components.

The 2-point correlation function of the tensorial part of the anisotropic stress-tensor is of the form

$$\Big\langle \Pi_{ij}(\mathbf{k},\eta)\Pi^*_{lm}(\mathbf{k}',\eta') \Big\rangle \equiv (2\pi)^3\delta(\mathbf{k}-\mathbf{k}')\Pi^2(k,\eta,\eta')\mathcal{M}_{ijlm}(\hat{\mathbf{k}}) \ , \tag{6.24}$$

where

$$\mathcal{M}_{ijlm}(\hat{\mathbf{k}}) = \frac{1}{4}\Big[\Lambda_{ij,lm}(\hat{\mathbf{k}}) + \Lambda_{ij,ml}(\hat{\mathbf{k}})\Big] \ . \tag{6.25}$$

Since the trace $\mathcal{M}_{ijij} = 1$,

$$\Big\langle \Pi_{ij}(\mathbf{k},\eta)\Pi^*_{ij}(\mathbf{k}',\eta') \Big\rangle \equiv (2\pi)^3\delta(\mathbf{k}-\mathbf{k}')\Pi^2(k,\eta,\eta') \ . \tag{6.26}$$

To determine $\Pi^2(k,\eta,\eta')$, we compute $\Big\langle \Pi_{ij}(\mathbf{k},\eta)\Pi^*_{ij}(\mathbf{k}',\eta') \Big\rangle$ explicitly using Wick's theorem to reduce 4-point functions of the field to products of 2-point functions

$$\begin{aligned} &\Big\langle \Pi_{ij}(\mathbf{k},\eta)\Pi^*_{lm}(\mathbf{k}',\eta') \Big\rangle = \\ =\ & \Lambda_{ij,pq}(\hat{\mathbf{k}})\,\Lambda_{lm,rs}(\hat{\mathbf{k}}') \int \frac{d^3q}{(2\pi)^3}\frac{d^3q'}{(2\pi)^3}\, q_p q_q q'_r q'_s \Big\langle \phi^a(\mathbf{q},\eta)\phi^a(\mathbf{k}-\mathbf{q},\eta)\phi^{*b}(\mathbf{q}',\eta')\phi^{*b}(\mathbf{k}-\mathbf{q},\eta') \Big\rangle \\ =\ & \int \frac{d^3q\, d^3q'}{(2\pi)^6} \left(q^{\mathrm{T}}\Lambda q\right)_{ij} \left(q'^{\mathrm{T}}\Lambda q'\right)_{lm} \Big[\Big\langle \phi^a(\mathbf{q},\eta)\phi^{*a}(\mathbf{q}-\mathbf{k},\eta)\rangle\langle\phi^b(-\mathbf{q}',\eta')\phi^{*b}(\mathbf{k}'-\mathbf{q}',\eta') \Big\rangle + \\ &+ \Big\langle \phi^a(\mathbf{q},\eta)\phi^{*b}(\mathbf{q}',\eta') \Big\rangle \Big\langle \phi^a(\mathbf{k}-\mathbf{q},\eta)\phi^{*b}(\mathbf{k}'-\mathbf{q}',\eta') \Big\rangle + \\ &+ \Big\langle \phi^a(\mathbf{q},\eta)\phi^{*b}(\mathbf{k}'-\mathbf{q}',\eta') \Big\rangle \Big\langle \phi^a(\mathbf{k}-\mathbf{q},\eta)\phi^{*b}(\mathbf{q}',\eta') \Big\rangle \Big] \\ =\ & \int d^3q\, d^3q' \left(q^{\mathrm{T}}\Lambda q\right)_{ij} \left(q'^{\mathrm{T}}\Lambda q'\right)_{lm} \Big[\mathcal{P}^{aa}_\phi(|\mathbf{q}|,\eta,\eta)\mathcal{P}^{bb}_\phi(|\mathbf{q}'|,\eta',\eta')\,\delta(\mathbf{k})\delta(\mathbf{k}') \\ &+ \mathcal{P}^{ab}_\phi(|\mathbf{q}|,\eta,\eta')\mathcal{P}^{ab}_\phi(|\mathbf{k}-\mathbf{q}|,\eta,\eta')\,\delta(\mathbf{q}-\mathbf{q}')\delta(\mathbf{k}-\mathbf{q}-\mathbf{k}'+\mathbf{q}') \\ &+ \mathcal{P}^{ab}_\phi(|\mathbf{q}|,\eta,\eta')\mathcal{P}^{ab}_\phi(|\mathbf{k}-\mathbf{q}|,\eta,\eta')\,\delta(\mathbf{q}'+\mathbf{q}-\mathbf{k}')\delta(\mathbf{q}'+\mathbf{q}-\mathbf{k}) \Big] \end{aligned} \tag{6.27}$$

where we use the notation $\left(q^{\mathrm{T}}\Lambda q\right)_{ij} \equiv q_l \Lambda_{ij,lm} q_m$ and we have introduced the reality condition $\phi^*(\mathbf{k}) = \phi(-\mathbf{k})$ and the unequal time correlator of the field ϕ which is defined in the same way as the one for β,

$$\langle \phi^a(\mathbf{k},\eta)\phi^{*b}(\mathbf{k}',\eta')\rangle = (2\pi)^3\delta(\mathbf{k}-\mathbf{k}')\,\mathcal{P}_\phi^{ab}(k,\eta,\eta')\ . \tag{6.28}$$

The zero-mode of the anisotropic stresses vanishes due to isotropy so that the first term in the square bracket of the integral (6.27) does not contribute.

We now can compute the unequal time correlator $\left\langle \Pi_{ij}(\mathbf{k},\eta)\Pi_{ij}^*(\mathbf{k}',\eta')\right\rangle$. Using

$$\left(q^{\mathrm{T}}\Lambda q\right)_{ij}\left(q^{\mathrm{T}}\Lambda q\right)_{ij} = \frac{1}{2}q^4\left(1-(\hat{\mathbf{k}}\cdot\hat{\mathbf{q}})^2\right)^2\ , \tag{6.29}$$

we obtain

$$\Pi^2(k,\eta,\eta') = \int \frac{d^3q}{(2\pi)^3}\,q^4\left[1-(\hat{\mathbf{k}}\cdot\hat{\mathbf{q}})^2\right]^2 \mathcal{P}_\phi^{ab}(|\mathbf{q}|,\eta,\eta')\mathcal{P}_\phi^{ab}(|\mathbf{k}-\mathbf{q}|,\eta,\eta')\ . \tag{6.30}$$

We now relate the GW energy density spectrum to the unequal time anisotropic stress spectrum of the source, $\Pi^2(k,\eta,\eta')$. For this we first write the GW evolution equation in momentum space,

$$h_{ij}'' + 2\frac{a'}{a}h_{ij}' + k^2 h_{ij} = 8\pi G\,\Pi_{ij}\ . \tag{6.31}$$

Defining a new variable $\bar{h}_{ij} \equiv a h_{ij}$, one obtains

$$\bar{h}_{ij}'' + \left(k^2 - \frac{a''}{a}\right)\bar{h}_{ij} = 8\pi G a\,\Pi_{ij}\ . \tag{6.32}$$

In a radiation dominated background ($a \propto \eta$) this reduces to

$$\bar{h}_{ij}'' + k^2\bar{h}_{ij} = 8\pi G a\,\Pi_{ij}\ . \tag{6.33}$$

The solution of this differential equation with the initial conditions $h_{ij} = h_{ij}' = 0$ is given by the convolution of the source with the Green function $\mathcal{G}(k,\eta,\eta') = \sin(k\eta - k\eta')$,

$$\bar{h}_{ij}(\mathbf{k},\eta<\eta_{\rm fin}) = \frac{8\pi G}{k^2}\int_{x_*}^{x} dy\ a(y/k)\,\Pi_{ij}(\mathbf{k},y/k)\sin(x-y)\,, \tag{6.34}$$

where we have set $x \equiv k\eta$ and $y \equiv k\eta'$. The source of gravity waves is acting for a time interval $\delta\eta_* = (\eta_{\rm fin} - \eta_*) = \epsilon\eta_*$. If $\epsilon < 1$ we call the process short-lasting. This is the relevant case for example for GWs produced during a symmetry breaking phase transition where the source disappears after the phase transition since the latter typically lasts only for a fraction of the Hubble time. However, the Goldstone modes considered in this work may very well be long lived as they are not expected to interact with ordinary matter. In this case therefore a long lasting source may be better motivated. We discuss both cases below.

After the source has decayed, GWs are freely propagating, and thus described by the homogeneous solution of Eq. (6.33),

$$\bar{h}_{ij}(\mathbf{k},\eta>\eta_{\rm fin}) = A_{ij}(\mathbf{k})\sin(k\eta - k\eta_{\rm fin}) + B_{ij}(\mathbf{k})\cos(k\eta - k\eta_{\rm fin})\,. \tag{6.35}$$

The coefficients A_{ij} and B_{ij} are fixed by matching the homogeneous solution to the inhomogeneous one at $\eta = \eta_{\rm fin}$. Matching both $\bar{h}_{ij}$ and its derivative $\bar{h}'_{ij}$ yields

$$A_{ij}(\mathbf{k}) = \frac{8\pi G}{k^2}\int_{x_*}^{x_{\rm fin}} dy\; a(y/k)\Pi_{ij}(\mathbf{k}, y/k)\cos(x_{\rm fin}-y)\;,$$
$$B_{ij}(\mathbf{k}) = \frac{8\pi G}{k^2}\int_{x_*}^{x_{\rm fin}} dy\; a(y/k)\Pi_{ij}(\mathbf{k}, y/k)\sin(x_{\rm fin}-y)\;. \tag{6.36}$$

The GW energy density is given by (see *e.g.* [186, 187, 82])

$$\frac{d\rho_{\rm GW}}{d\log k} = \frac{k^3|h'|^2(k,\eta)}{2(2\pi)^3 G a^2}\;, \tag{6.37}$$

where the GW power spectrum has been normalized as follows:

$$\Big\langle h'_{ij}(\mathbf{k},\eta)h'^*_{ij}(\mathbf{q},\eta)\Big\rangle = 2\Big\langle h'_+(\mathbf{k},\eta)h'^*_+(\mathbf{q},\eta)+h'_\times(\mathbf{k},\eta)h'^*_\times(\mathbf{q},\eta)\Big\rangle = (2\pi)^3\delta^3(\mathbf{k}-\mathbf{q})\,|h'|^2(k,\eta)\;. \tag{6.38}$$

Here our normalization differs from that of Ref. [121]. Their definition of the power spectrum is related to ours by

$$\mathcal{P}(k,\eta) \equiv 2\pi k^3|h|^2(k,\eta) \tag{6.39}$$

and they infer $\frac{d\Omega_{GW}(k,\eta_0)}{d\log k} = \frac{k^2\mathcal{P}(k,\eta)}{6H_0^2}$ whereas we obtain, with (6.37) and $h' = kh$ for sub-horizon modes,

$$\frac{d\Omega_{GW}(k,\eta_0)}{d\log k} = \frac{k^5|h|^2(k,\eta)}{6\pi^2 H_0^2} = \frac{k^2\mathcal{P}(k,\eta)}{12\pi^3 H_0^2}\;.$$

This difference in the normalization, which we attribute to an error in Ref. [121], leads to a reduction of the final result by about a factor 60, which may be relevant for observations.

With the solution for $\bar{h}_{ij}$ above, we obtain for $\eta > \eta_{\rm fin}$

$$\begin{aligned}|h'|^2(k,\eta) &= \frac{1}{2a^2}\Big(k^2+\mathcal{H}^2\Big)\Big(\langle A_{ij}A^*_{ij}\rangle + \langle B_{ij}B^*_{ij}\rangle\Big)\\ &= \frac{k^2+\mathcal{H}^2}{2a^2}\left(\frac{8\pi G}{k^2}\right)^2\int_{x_*}^{x_{\rm fin}} dy\int_{x_*}^{x_{\rm fin}} dz\; a\left(\frac{y}{k}\right)a\left(\frac{z}{k}\right)\cos(z-y)\Pi^2\left(k,\frac{y}{k},\frac{z}{k}\right)\end{aligned} \tag{6.40}$$

where we have used Eq. (6.26). The GW energy density at time η is of course well defined only for waves with a wavelength well within the horizon, $k \gg \mathcal{H}$. Therefore we shall approximate $k^2+\mathcal{H}^2 \simeq k^2$ in the following.

The GWs are sourced by the anisotropic stress of the scalar field $\phi^a = v\beta^a$. The correlators are simply related by

$$\mathcal{P}^{ab}_\phi = v^2\mathcal{P}^{ab}_\beta\,.$$

With Eq. (6.30) we obtain the following expression for the GW energy density after the decay of the source, $\eta > \eta_{\rm fin}$,

$$\begin{aligned}\frac{d\rho_{\rm GW}(k,\eta)}{d\log k} &= \frac{G\,v^4}{4\pi^4}\frac{k^3}{a^4(\eta)}\int_{\eta_*}^{\eta_{\rm fin}} d\tau\int_{\eta_*}^{\eta_{\rm fin}} d\xi\; a(\tau)a(\xi)\;\cos(k\xi-k\tau)\\ &\quad\times\int d^3p\; p^4\sin^4\theta\;\mathcal{P}^{ab}_\beta(p,\tau,\xi)\,\mathcal{P}^{ab}_\beta(|\mathbf{k}-\mathbf{p}|,\tau,\xi)\,,\end{aligned} \tag{6.41}$$

where $\cos\theta \equiv \hat{\mathbf{k}}\cdot\hat{\mathbf{p}}$. Inserting the power spectrum of β in the above expression and summing over the field components, we find

$$\frac{d\rho_{\rm GW}(k,\eta)}{d\log k} = \frac{G\,v^4}{4\pi^4}\frac{k^3}{a^4(\eta)}\frac{36\pi^4 A^2}{N}\int_{\eta_*}^{\eta_{\rm fin}} d\tau \int_{\eta_*}^{\eta_{\rm fin}} d\xi\; a(\tau)a(\xi)\,\cos(k\xi - k\tau)$$
$$\times \int_{\substack{p\,<\,1/\eta_* \\ |\mathbf{k}-\mathbf{p}|\,<\,1/\eta_*}} d^3p\; p^4 \sin^4\theta\; \tau^3\xi^3\; \frac{J_\nu(p\tau)}{(p\tau)^\nu}\frac{J_\nu(p\xi)}{(p\xi)^\nu}\frac{J_\nu(|\mathbf{k}-\mathbf{p}|\tau)}{(|\mathbf{k}-\mathbf{p}|\tau)^\nu}\frac{J_\nu(|\mathbf{k}-\mathbf{p}|\xi)}{(|\mathbf{k}-\mathbf{p}|\xi)^\nu} \quad (6.42)$$

Here the constant A comes from the normalization of β, and it is given by Eq. (6.15). In the radiation dominated background considered here, we have $\nu = 1+\gamma = 2$ and $A = 5\pi/4$. Note also that we choose the normalization of the scale factor such that $a(\eta_0) = 1$. Hence the *comoving* wave number k is simply related to the present frequency of the GW by

$$f = \frac{k}{2\pi}\ .$$

In the next section we evaluate the present amplitude and frequency dependence of the GW spectrum generated in this way explicitly. For this, the following relation between temperature and time in a radiation dominated Universe are useful [132],

$$H^2(t) = \frac{1}{\eta^2\, a(\eta)^2} = \frac{8\pi G}{3}\frac{\pi^2}{30}\, g_{\rm eff}(\eta) T^4(\eta)\,. \quad (6.43)$$

Assuming an adiabatic expansion, $g_{\rm eff}(aT)^3 = $ const., one finds

$$\eta = \frac{M_{\rm Pl}}{T(\eta)T_0}\left(\frac{g_{\rm eff}(\eta)}{2}\right)^{1/3}\left(\frac{45}{4\pi^3 g_{\rm eff}(\eta)}\right)^{1/2} = 1.6\times 10^7 {\rm sec}\left(\frac{\rm GeV}{T}\right) g_{\rm eff}^{-1/6}(T)\ . \quad (6.44)$$

On the other hand, the expression for the temperature associated to a global $\mathcal{O}(N)$ symmetry breaking is [202]

$$T_* = \sqrt{\frac{24}{N+2}}v\ , \quad (6.45)$$

independent of the coupling λ.

Before moving to the evaluation of Eq. (6.42), let us briefly determine the frequencies for the GW sources discussed in this paper. We are studying the IR modes $k\eta_* < 1$ of the GW spectrum, corresponding to frequencies smaller than the expansion rate at the time of production, $f_* = \mathcal{H}_*/(2\pi)$,

$$f_* = \frac{1}{2\pi\eta_*} \approx 10^{-8}\left(\frac{T_*}{\rm GeV}\right)\ {\rm Hz}\ . \quad (6.46)$$

For the EW scale this corresponds to $f_*^{\rm EW} \sim 10^{-6}$ Hz, while for the GUT scale the associated frequency is $f_*^{GUT} \sim 10^8$ Hz. For a given energy scale $M \simeq T_*$ at the time of production, we are describing one frequency range or another, but always frequencies smaller than the one corresponding today to that energy scale, $f < f_*(M) \sim 10^{-8}{\rm Hz}(M/{\rm GeV})$. Clearly, only processes taking place in the radiation dominated Universe generate GWs with sufficiently high frequencies such that they can be observed by direct GW detection experiments. Indeed the frequency associated to the horizon at the matter-radiation equality is far too small, $f_*^{\rm eq} \sim 10^{-17}$ Hz, to be observed by direct GW detectors, like LIGO,

LISA or BBO will be working. Therefore we consider only processes in the radiation dominated Universe and $\gamma = 1$ and $\nu = 2$ are assumed for the rest of the paper.

6.4 The gravitational wave spectrum today

In this section we study two different cases, first the situation in which the source producing GWs lasts only a small fraction of the Hubble time at the moment of production and, second, the case in which the GW source acts for a much longer time, until the moment at which a given mode enters the horizon.

6.4.1 Short lived source

We first estimate the amplitude of the GW spectrum for large wavelengths, $k < \mathcal{H}_*$, from a short lived source which lasts from η_* to $\eta_{\rm fin}$, such that $(\eta_{\rm fin} - \eta_*)/\eta_* \equiv \epsilon \ll 1$ (as *e.g.* for the radial mode of ϕ in hybrid preheating [111, 113]). Let us first note the following facts: 1) From Eq. (6.42) we see immediately that for small wavenumbers, $k\eta_{\rm fin} \ll 1$, the result scales like

$$\frac{d\rho_{\rm GW}}{d\log k} \propto k^3 \ .$$

2) Since the source is short lived, $\eta_* \approx \eta_{\rm fin}$, and we deal with superhorizon modes, $k\eta_* \ll 1$, we may set $\cos(k\eta - k\eta') \approx 1$ and the time integral can be replaced simply by a factor $\epsilon\eta_*$. 3) To estimate the momentum integral, we use that Bessel functions at small arguments, $x \equiv k\eta < 1$, can be approximated by $J_\nu(x) \approx (x/2)^\nu/\Gamma(1+\nu)$. To obtain the dominant contribution at large wavelength (*i.e.* the least blue part) we may also set $|\mathbf{k} - \mathbf{q}|\eta_* \simeq q\eta_*$.

Using all the above considerations, we are left with a simple integral for the evaluation of the spectra of the IR modes ($k\eta_* \ll 1$) of GWs, at any time $\eta \gg \eta_*$ for which those modes have already crossed the horizon

$$\left.\frac{d\rho_{\rm GW}(\eta)}{d\log k}\right|_{k\eta_* \ll 1} \simeq \frac{Gv^4}{4\pi^4} 36\pi^4 A^2 \frac{k^3}{a^4(\eta)} \frac{2\pi}{N} \int_{-1}^{1} d\cos\theta \sin^4\theta \int_0^{1/\eta_*} dp \, \frac{p^6}{2^{2\nu}\Gamma^4(\nu+1)} \times \left(\int_{\eta_*}^{\eta_{\rm fin}} d\tau \, a(\tau)\tau^3\right)^2 = \frac{3\cdot 5\pi^3}{7\cdot 2^{11}} \frac{Gv^4}{N} \left(\frac{a_*}{a(\eta)}\right)^4 \epsilon^2 H_*^2 \, (k\eta_*)^3 \,, \tag{6.47}$$

where we used $A = 5\pi/4$, $\nu = 2$ and we approximated $\int_{\eta_*}^{\eta_{\rm fin}} d\tau a(\tau)\tau^3 \approx a(\eta_*)\eta_*^3\delta\eta_* = \epsilon\, a(\eta_*)\eta_*^4$, since we have set $\eta_{\rm fin} - \eta_* = \delta\eta_* \simeq \epsilon\eta_*$.

With this we can now evaluate the ratio of the GW energy density to the critical density today, for the IR modes $k\eta_* \ll 1$, as

$$\begin{aligned} \Omega_{\rm GW}(f) &= \frac{1}{\rho_c}\frac{d\rho_{\rm GW}(\eta_0)}{d\log k} \approx \frac{5\pi^4}{7\cdot 2^8}\left(\frac{v}{M_{\rm Pl}}\right)^4 \frac{\epsilon^2}{N}\,\Omega_{\rm rad}(k\eta_*)^3 \\ &\sim 10^{-5}\left(\frac{v}{M_{\rm Pl}}\right)^4 \frac{\epsilon^2}{N}\,(k\eta_*)^3 \ , \end{aligned} \tag{6.48}$$

where we used $H_*^2 = 8\pi G\rho_*/3$, we expressed the radiation density today as $\rho_{\rm rad} \approx \rho_*(a_*/a_0)^4$ and we introduced the the radiation density parameter today as $\Omega_{\rm rad} \approx 4.2 \times 10^{-5}$. We have also neglected the factors coming from the ratio of the effective relativistic

degrees of freedom since they appear only with the power 1/3.

Note that this formula is general for the IR spectrum of GWs generated at any process in which the source, a N-component scalar field, has rapidly acquired its true *vev* v at η_* and undergoes a short phase of self-ordering which lasts for a fraction $\epsilon < 1$ of the Hubble time.

Finally, note also that very generically we have $\eta_* \propto T_*^{-1} \propto 1/v$ so that $\Omega_{\rm GW} \propto v^4 \eta_*^3 k^3 \propto v\, k^3$ and not as v^4, as one could naively have concluded from Eq. (6.48).

6.4.1.1 The electroweak phase transition

The comoving horizon size at the electroweak (EW) phase transition is given by the EW energy scale $T_* \sim 100$ GeV, $g_{\rm eff}(T_*) = 106.75$,

$$\eta_* \simeq 7.5 \times 10^4 \text{ sec} .$$

Inserting this above with $f = k/(2\pi)$, we find

$$\Omega_{\rm GW}(f) \approx 4.2 \times 10^5 \, \frac{5\pi^4 (2\pi)^3}{7 \cdot 2^8} \, \Omega_{\rm rad} \left(\frac{v}{M_{\rm Pl}}\right)^4 \frac{\epsilon^2}{N} \left(\frac{f}{\rm mHz}\right)^3 \sim 10^{-65} \, \frac{\epsilon^2}{N} \left(\frac{f}{\rm mHz}\right)^3 . \quad (6.49)$$

For the last expression we have used $v \simeq T_*$. This result is of course unmeasurably small.

6.4.1.2 A GUT scale phase transition

To have any chance to measure this spectrum, we need a *vev* which is not too many orders of magnitude below that Planck scale, since the GW energy density is suppressed by a fourth power of the ratio of the *vev* to $M_{\rm Pl}$. The best change might be a GUT scale with a *vev* of the order of $v \simeq 10^{16}$GeV. But then of course η_* will be very small and the dominant contribution will come from very high frequencies, lower frequencies being suppressed by the factor $(k\eta_*)^3$. For $T_* = 10^{16}$GeV we have

$$\eta_* \simeq 5 \times 10^{-10} \text{ sec} ,$$

leading to

$$\Omega_{\rm GW}(f) \approx 0.125 \, \frac{5\pi^4 (2\pi)^3}{7 \cdot 2^8} \, \Omega_{\rm rad} \left(\frac{v}{M_{\rm Pl}}\right)^4 \frac{\epsilon^2}{N} \left(\frac{f}{\rm GHz}\right)^3 \sim 10^{-16} \, \frac{\epsilon^2}{N} \left(\frac{f}{\rm GHz}\right)^3 . \quad (6.50)$$

Apart from the fact that this result suffers severe additional suppression at measurable frequencies which are significantly below 1GHz $= 10^9$Hz, the sensitivity of $10^{-12}\Omega_{\rm rad} \simeq 10^{-16}$ cannot be reached with any presently proposed experiment at those frequencies.

Therefore, we can only conclude that the superhorizon GW spectrum generated from a short lived self ordering scalar field is much below presently proposed experimental sensitivities.

6.4.2 A long lived source

As we have seen in the previous subsection, short lived Goldstone modes cannot lead to a significant GW background. But since Goldstone modes are typically non-interacting and long lived, it is more natural to consider them for a time which is much longer than the horizon scale η_*. To compute the GW energy density produced by such a self ordering scalar field, we consider Eq. (6.42) and set $\eta_{\rm fin} = \eta_k \equiv 1/k$, since the solution (6.16) decays inside the horizon, when $k\eta > 1$. We then have to compute the following integral

$$\frac{d\rho_{\rm GW}(k,\eta_k)}{d\log k} = \frac{G\,v^4}{4\pi^4}\frac{k^3}{a^4(\eta_k)}\frac{36\pi^4 A^2}{N}\int_{\eta_*}^{1/k} d\tau \int_{\eta_*}^{1/k} d\xi\; a(\tau)a(\xi)\cos(k\xi - k\tau)\,\times$$
$$\int_{\substack{p\eta_* \,<\, 1 \\ |\mathbf{p}\,-\,\mathbf{k}|\eta_* \,<\, 1}} d^3p\; p^4 \sin^4\theta\; \tau^3\xi^3\; \frac{J_\nu(p\tau)}{(p\tau)^\nu}\frac{J_\nu(p\xi)}{(p\xi)^\nu}\frac{J_\nu(|\mathbf{k}-\mathbf{p}|\tau)}{(|\mathbf{k}-\mathbf{p}|\tau)^\nu}\frac{J_\nu(|\mathbf{k}-\mathbf{p}|\xi)}{(|\mathbf{k}-\mathbf{p}|\xi)^\nu} \quad (6.51)$$

Note that the range of integration of the variable p in the above expression is set to be $\{p\eta_* < 1,\ |\mathbf{p}-\mathbf{k}|\eta_* < 1\}$ since the initial two point correlator of the scalar field turns out to be different from zero only in this range of momenta [*c.f.* Eq. (6.10)].

In order to obtain an analytical result for the above integral, we perform the following approximations:

- We are interested in scales k that are superhorizon for all the time of GW production, namely $k\tau < 1$ and $k\xi < 1$ for times τ, ξ between η_* and $\eta_{\rm fin} = 1/k$, therefore we approximate $\cos(k\xi - k\tau) \simeq 1$.
- We neglect the angular dependence of $|\mathbf{p}-\mathbf{k}|$ so that the angular integral reduces to $2\pi\int \sin^4\theta d\cos\theta = 32\pi/15$.
- In the range of integration where $p\tau \gg 1$ we substitute $|\mathbf{k}-\mathbf{p}|\tau \simeq p\tau$, while when $p\tau \ll 1$ we approximate $|\mathbf{k}-\mathbf{p}|\tau \ll 1$.
- The range of momenta for which we can expand the Bessel functions in terms of small arguments is $p < \min(1/\tau, 1/\xi)$, while in the range $\min(1/\tau,1/\xi) < p < \max(1/\tau,1/\xi)$ we should distinguish between large and small argument expansions of the Bessel functions. Finally, in the range $\max(1/\tau,1/\xi) < p < 1/\eta_*$ one can consider the large argument limit for all the four Bessel functions of the above integral.

Taking into account all the above considerations, we find that the complete integral becomes

$$\int_{\eta_*}^{1/k} d\tau \int_{\eta_*}^{1/k} d\xi \int_0^\infty dp\, f(p,\tau,\xi) \;=\; 2\int_{\eta_*}^{1/k} d\tau \int_{\eta_*}^{\tau} d\xi \left(\int_0^{1/\tau} dp\, f + \int_{1/\tau}^{1/\xi} dp\, f + \int_{1/\xi}^{1/\eta_*} dp\, f\right),$$

which allows us to separate the integral in p using the asymptotic behaviour of the Bessel functions,

$$J_\nu(x) \simeq \frac{x^\nu}{2^\nu\Gamma(\nu+1)} \qquad \text{for } x \ll 1\ ,$$
$$J_\nu(x) \simeq \sqrt{\frac{2}{x\pi}}\cos\left(x - \frac{(2\nu+1)\pi}{4}\right) \qquad \text{for } x \gg 1\ .$$

We can distinguish three different intervals:

- The IR contribution, $I_1(k)$, for $0 < p < 1/\tau$, with $|\mathbf{k}-\mathbf{p}|\tau < 1$ and $|\mathbf{k}-\mathbf{p}|\xi < 1$.
- The mixed (UV+IR) contribution, $I_2(k)$, for $1/\tau < p < 1/\xi$, with $|\mathbf{k}-\mathbf{p}|\tau \simeq p\tau > 1$ but $|\mathbf{k}-\mathbf{p}|\xi \simeq p\xi < 1$.
- The UV contribution, $I_3(k)$, for $1/\xi < p < 1/\eta_*$, with $|\mathbf{k}-\mathbf{p}|\tau \simeq p\tau > 1$ and $|\mathbf{k}-\mathbf{p}|\xi \simeq p\xi > 1$.

Therefore we can finally write

$$\frac{d\rho_{\rm GW}(k,\eta_k)}{d\log k} = \mathcal{D}(k)\left[I_1(k)+I_2(k)+I_3(k)\right] \ , \tag{6.52}$$

where the pre-factor $\mathcal{D}(k)$ contains the coefficients in front of the integral in Eq. (6.51), the factor coming from the angular integration $(32\pi/15)$ and the factor 2 that comes from the symmetry of the double time integration, namely

$$\mathcal{D}(k) \equiv \frac{G\,v^4}{4\pi^4}\frac{k^3}{a^4(\eta_k)}\frac{36\pi^4 A^2}{N}\times\frac{32\pi}{15}\times 2 = \frac{G\,v^4}{N}\frac{k^3}{a^4(\eta_k)}15\cdot 4\pi^3 \ . \tag{6.53}$$

The three integrals of Eq. (6.52) are given by

$$\begin{aligned} I_1(k) &\equiv \int_{\eta_*}^{1/k} d\tau \int_{\eta_*}^{\tau} d\xi\ a(\tau)\ a(\xi)\ \tau^3\ \xi^3 \int_0^{1/\tau} dp\ p^6\ \frac{J_\nu(p\tau)}{(p\tau)^\nu}\frac{J_\nu(p\xi)}{(p\xi)^\nu}\frac{J_\nu(|\mathbf{k}-\mathbf{p}|\tau)}{(|\mathbf{k}-\mathbf{p}|\tau)^\nu}\frac{J_\nu(|\mathbf{k}-\mathbf{p}|\xi)}{(|\mathbf{k}-\mathbf{p}|\xi)^\nu} \\ &\simeq \frac{H_0^2\Omega_{\rm rad}}{4096}\int_{\eta_*}^{1/k} d\tau \int_{\eta_*}^{\tau} d\xi\ \tau^4\ \xi^4 \int_0^{1/\tau} dp\ p^6 \\ &= \frac{H_0^2\Omega_{\rm rad}}{4096\ k^3}\frac{1}{35}\left[\frac{1}{3}-\frac{5}{6}(k\eta_*)^3+\frac{1}{2}(k\eta_*)^5\right] , \end{aligned} \tag{6.54}$$

$$\begin{aligned} I_2(k) &\equiv \int_{\eta_*}^{1/k} d\tau \int_{\eta_*}^{\tau} d\xi\ a(\tau)\ a(\xi)\ \tau^3\ \xi^3 \int_{1/\tau}^{1/\xi} dp\ p^6\ \frac{J_\nu(p\tau)}{(p\tau)^\nu}\frac{J_\nu(p\xi)}{(p\xi)^\nu}\frac{J_\nu(|\mathbf{k}-\mathbf{p}|\tau)}{(|\mathbf{k}-\mathbf{p}|\tau)^\nu}\frac{J_\nu(|\mathbf{k}-\mathbf{p}|\xi)}{(|\mathbf{k}-\mathbf{p}|\xi)^\nu} \\ &\simeq \frac{H_0^2\Omega_{\rm rad}}{32\pi}\int_{\eta_*}^{1/k} d\tau \int_{\eta_*}^{\tau} d\xi\ \tau^4\ \xi^4 \int_{1/\tau}^{1/\xi} \frac{dp\ p^6}{(p\tau)^5}\ \cos^2\left(p\tau-\frac{5\pi}{4}\right) \\ &= \frac{H_0^2\Omega_{\rm rad}}{128\pi\ k^3}\left[\frac{2}{45}+\frac{1}{18}(k\eta_*)^3-\frac{1}{10}(k\eta_*)^5+\frac{(k\eta_*)^3}{3}\log(k\eta_*)\right] , \end{aligned} \tag{6.55}$$

and

$$\begin{aligned} I_3(k) &\equiv \int_{\eta_*}^{1/k} d\tau \int_{\eta_*}^{\tau} d\xi\ a(\tau)\ a(\xi)\ \tau^3\ \xi^3 \int_{1/\xi}^{1/\eta_*} dp\ p^6\ \frac{J_\nu(p\tau)}{(p\tau)^\nu}\frac{J_\nu(p\xi)}{(p\xi)^\nu}\frac{J_\nu(|\mathbf{k}-\mathbf{p}|\tau)}{(|\mathbf{k}-\mathbf{p}|\tau)^\nu}\frac{J_\nu(|\mathbf{k}-\mathbf{p}|\xi)}{(|\mathbf{k}-\mathbf{p}|\xi)^\nu} \\ &\simeq \frac{4\,H_0^2\Omega_{\rm rad}}{\pi^2}\int_{\eta_*}^{1/k} d\tau \int_{\eta_*}^{\tau} d\xi\ \tau^4\ \xi^4 \int_{1/\xi}^{1/\eta_*} \frac{dp\ p^6}{(p\tau)^5(p\xi)^5}\cos^2\left(p\tau-\frac{5\pi}{4}\right)\cos^2\left(p\xi-\frac{5\pi}{4}\right) \\ &= \frac{H_0^2\Omega_{\rm rad}}{3\pi^2\ k^3}\left[\frac{1}{9}-\frac{1}{9}(k\eta_*)^3-(k\eta_*)^3\left(\frac{1}{2}\log^2(k\eta_*)-\frac{1}{3}\log(k\eta_*)\right)\right] . \end{aligned} \tag{6.56}$$

More precisely, in the above computation we substituted each $\cos^2 x$ by its mean value $\langle\cos^2 x\rangle = 1/2$ averaged over a few oscillations, and we introduced the usual expression

for the scale factor in a radiation dominated background, $a(\eta) \simeq H_0\sqrt{\Omega_{\rm rad}}\eta$, which is consistent with $a_0 = 1$ today.

All three terms have a scale-invariant spectrum. Actually, the "UV" contribution given in Eq. (6.56) is the largest. Summing all the three contribution and considering the dominant part in the limit $k\eta_* \ll 1$ [hence also $(k\eta_*)^3 \log(k\eta_*) \ll 1$], we obtain the following scale-invariant spectrum

$$\begin{aligned}\frac{d\rho_{\rm GW}(k,\eta_k)}{d\log k} &\simeq 5\cdot 2^5\pi^4 \frac{\Omega_{\rm rad}\,\rho_c}{Na^4(\eta_k)}\left(\frac{v}{M_{\rm Pl}}\right)^4\left(\frac{1}{2^{12}\cdot 105}+\frac{1}{2^6\pi\cdot 45}+\frac{1}{27\pi^2}\right)\\ &\simeq 60\times\frac{\Omega_{\rm rad}\,\rho_c}{Na^4(\eta_k)}\left(\frac{v}{M_{\rm Pl}}\right)^4\,,\end{aligned} \tag{6.57}$$

where we have used the Friedmann equation $H_0^2 = 8\pi G\rho_c/3$. Redshifting the above expression until today, we obtain for the GW energy density parameter,

$$\Omega_{\rm GW}(k,\eta_0) \equiv \frac{d\rho_{\rm GW}(k,\eta_0)}{\rho_c d\log k} = \frac{d\rho_{\rm GW}(k,\eta_k)}{\rho_c d\log k}a^4(\eta_k) \simeq \frac{60}{N}\,\Omega_{\rm rad}\left(\frac{v}{M_{\rm Pl}}\right)^4. \tag{6.58}$$

This corresponds to a scale-invariant GW spectrum produced by a self-ordering scalar field in the large N-limit. This result is valid for all wave numbers k which enter the horizon when the Goldstone modes of our N-component field are still massless and the field has not yet decayed. Scales which enter the horizon after this time $\eta_{\rm fin}$, *i.e.* scales with $k\eta_{\rm fin} < 1$, are suppressed by a factor $(k\eta_{\rm fin})^3$, as for them the result for a short lived source with η_* replaced by $\eta_{\rm fin}$ applies.

6.4.3 Numerical integration

In order to obtain more accurate results, and to check the validity of our analytical approximations, we have also performed a numerical evaluation of the integrals in Eq. (6.42). If we set the final time of integration to be the horizon crossing, $\eta_{\rm fin} = 1/k$, as we did in the analytical evaluation for the long lasting source (6.51), we obtain the following result for the final GW density parameter today

$$\Omega_{\rm GW}(k,\eta_0) \simeq \frac{22}{N}\Omega_{\rm rad}\left(\frac{v}{M_{\rm Pl}}\right)^4\,, \qquad \eta_{\rm fin} = 1/k\,. \tag{6.59}$$

This suggests that the analytical approximation somewhat overestimates the result. However, we can continue the integration to later times when the wavelength has already entered the horizon.

The integral in Eq. (6.51) allows us to compute the GW energy density in the limit $k\eta_* \ll 1$, using the change of variables $u = \cos\theta,\ q = p/k,\ x = k\tau$,

$$\Omega_{\rm GW}(k,\eta) = \frac{G^2v^4\Omega_{\rm rad}}{Na^4(\eta)}\,75\pi^4\int_0^\infty dq\,q^2F(q)\left\{\left[\int_0^{k\eta}dx\,\cos x\,J_2^2(qx)\right]^2+\left[\int_0^{k\eta}dx\,\sin x\,J_2^2(qx)\right]^2\right\} \tag{6.60}$$

where the kernel $F(q)$ comes from the integration over angles,

$$F(q) = \int_{-1}^1 \frac{du\,(1-u^2)^2}{(q^2+1-2qu)^2} = \frac{1}{24q^5}\left[16q+12q(q^2-1)^2+3(q^2-1)^2(q^2+1)\log\frac{(q-1)^2}{(q+1)^2}\right]$$

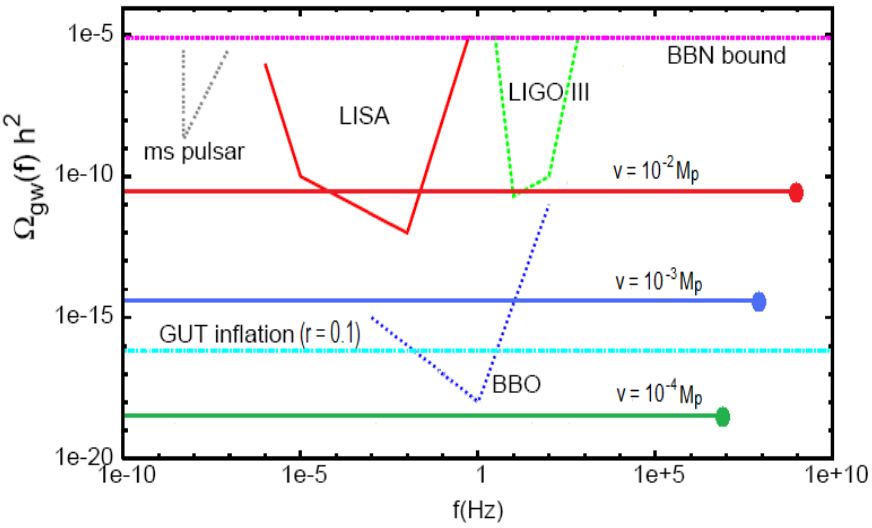

Figure 6.1: The sensitivity of present and future GW experiments are compared with our results for a long lasting source and inflation. We show, the amplitude of the scale-invariant GW background expected from a GUT scale inflation (blue, dashed) and from a self-ordering long lived source as studied in this paper, for a symmetry breaking field with $N = 4$ real components and a *vev* $v = 10^{-2} M_{\rm Pl}$ (top, red line), $v = 10^{-3} M_{\rm Pl}$ (middle, blue line, overlying with inflation) and $v = 10^{-4} M_{\rm Pl}$ (bottom, green line). The big dot at the right end of the horizontal lines represents the frequency (6.46) associated to the horizon at the initial time of production.

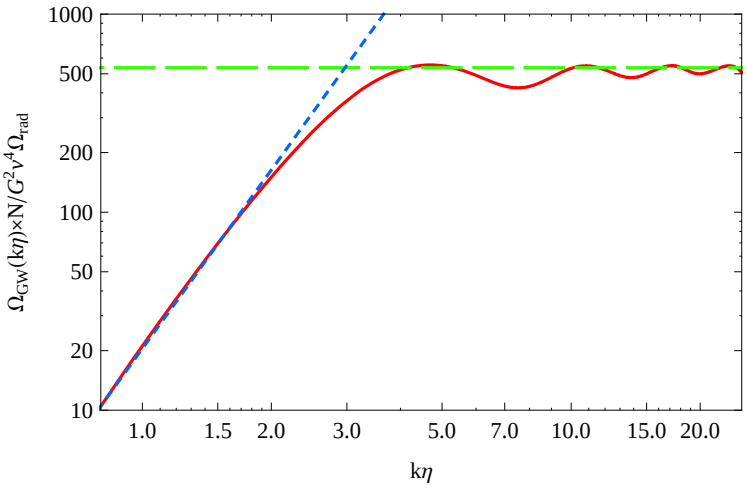

Figure 6.2: The density parameter in gravitational waves as a function of $k\eta$. For scales outside the horizon, $k\eta < \pi$, we observe the $(k\eta)^3$ dependence (short dashed line), while for scales that have entered the horizon, $k\eta > \pi$, the GW energy density saturates, at a normalized value of 511 (long dashed line). This result implies a significant scale-invariant GW spectrum today.

and we have made the approximation, $J_2(x\sqrt{q^2+1-2qu}) \to J_2(qx)$, inside the time integration. We have checked that for large times the result is correct within 0.1%.

Numerically evaluating (6.60), we find that the GW energy density continues to grow until horizon crossing, $k\eta \simeq \pi$, and saturates thereafter, see Fig. 6.2. This agrees with the result of Ref. [121], who find a peak in the power spectrum $\mathcal{P}(k,\eta)$ at approximately this value, and also explains the $1/a(\eta)^2$ dependence of the Power spectrum, $\mathcal{P} \propto \Omega_{\rm GW}/a^2$, for scales that have already entered the horizon.

For $k\eta \gg 4$ the gravitational wave energy density saturates at a value

$$\Omega_{\rm GW}(k,\eta_0) \simeq \frac{511}{N}\Omega_{\rm rad}\left(\frac{v}{M_{\rm Pl}}\right)^4 , \tag{6.61}$$

where we used again the usual normalization of the scale factor in a radiation dominated background. These results suggest that the GW spectrum produced by this mechanism still grows inside the horizon and reaches its final value somewhat after horizon crossing. This is consistent with the fact that the power of the scalar field that sources these GWs is not absent inside the horizon, but it is indeed given by the Bessel functions in Eq. (6.18), which decay rather slowly as functions of $k\eta$.

In the following analysis we will consider the numbers arising from the numerical integration, as given in Eq. (6.61).

6.4.4 Observational constraints

Our result for the amplitude of the GW spectrum (6.61) is inside the range of detectability of the BBO [199, 200, 201] experiment ($\Omega_{\rm GW}(k) \gtrsim 10^{-17}$) and is marginally detectable by LISA [13, 14, 15, 16] or advanced LIGO [10, 11] ($\Omega_{\rm GW}(k) \gtrsim 10^{-10}$). Indeed, with $\Omega_{\rm rad} \simeq 4.2 \times 10^{-5}$, we find that BBO would detect this signal if the symmetry breaking scale v satisfies

$$\left(\frac{v}{M_{\rm Pl}}\right)^4 \gtrsim 4.7 \cdot 10^{-16} N \qquad \Rightarrow \qquad \frac{v}{M_{\rm Pl}} \gtrsim 1.5 \cdot 10^{-4} N^{1/4} .$$

Concerning the sensitivity of LIGO or LISA, the signal is detectable if

$$\left(\frac{v}{M_{\rm Pl}}\right)^4 \gtrsim 4.7 \cdot 10^{-9} N \qquad \Rightarrow \qquad \frac{v}{M_{\rm Pl}} \gtrsim 0.008\, N^{1/4} .$$

In other words, for scales higher or around the GUT scale, $v \gtrsim 10^{16}$GeV, the very long wavelength tail which we have studied here could be observed.

In order to relate the above scale-invariant GW energy density to the GW spectrum from inflation, we compute the relative tensor-to-scalar ratio r. Following Ref. [203], one has the following expression for the GW density parameter from inflation

$$\Omega_{\rm GW}(k,\eta_0) = 4.36 \times 10^{-15}\, r \left(\frac{k}{k_0}\right)^{n_{\rm T}} , \qquad r \equiv \frac{\mathcal{P}_{\rm T}(k_0)}{\mathcal{P}_{\rm S}(k_0)} , \tag{6.62}$$

where $k_0 = 0.002\, h\,{\rm Mpc}^{-1}$, $\mathcal{P}_{\rm T}(k) = r\mathcal{P}_{\rm S}(k_0)(k/k_0)^{n_{\rm T}}$ and we used the WMAP result, $\mathcal{P}_{\rm S}(k_0) = 2.21 \times 10^{-9}$. This concerns only the wavelengths which enter the horizon in the radiation dominated era, before equality. Comparing the above expression for $n_T \simeq 0$ with

our Eq. (6.61), we obtain in our case

$$r \simeq \frac{3}{N}\left(\frac{v}{10^{16}\mathrm{GeV}}\right)^4 . \tag{6.63}$$

Another usefull comparison with inflation is the relative strength of the GW energy densities produced by the above two different mechanisms. Considering always wavelengths which enter the horizon in the radiation dominated epoch, we have [150]

$$\Omega_{GW}^{(\mathrm{inf})} = 10^{-13}\left(\frac{H_*}{10^{-4}M_{\mathrm{Pl}}}\right)^2 = 8.4\times 10^{-5}\left(\frac{M}{M_{\mathrm{Pl}}}\right)^4 , \tag{6.64}$$

where M denotes the energy scale of inflation, $H_*^2 \equiv 8\pi G M^4/3$. The ratio between the GW energy density produced by our mechanism and the one from inflation is then

$$\mathcal{R} \equiv \frac{\Omega_{\mathrm{GW}}(k,\eta_0)}{\Omega_{\mathrm{GW}}^{(\mathrm{inf})}(k,\eta_0)} \simeq \frac{256}{N}\left(\frac{v}{M}\right)^4 . \tag{6.65}$$

Comparing these results with those of Ref. [121], where the authors mainly concentrate on the spectrum of GWs produced in a matter dominated universe, we reproduce perfectly the amplitude of their spectrum $\mathcal{P}(k,\eta)$ defined as in Eq. (6.39), but their final relative strength $\mathcal{R}$ is nearly 2 orders of magnitude larger than what we find in Eq. (6.65). We believe this is due to the factor $1/(2\pi^3)$ missing in their expression for $\Omega_{\mathrm{GW}}(k,\eta_0)$ which has to be introduced for consistency with the definition of the power spectrum $\mathcal{P}(k)$.

6.5 Conclusions

In this paper we have estimated the contributions to the gravitational wave background from a symmetry breaking phase transition on large scales, $k\eta_* < 1$. We have concentrated on the analysis of the Goldstone modes and we obtained the following main conclusions.

If the modes are *short lived* with duration $\epsilon\eta_*$, $\epsilon < 1$ their contribution is blue and suppressed by a factor $\epsilon^2(k\eta_*)^3$. This result is actually generic, independent of the nature of the short lived source. Indeed, one typically obtains

$$\Omega_{\mathrm{GW}}(k) \simeq (k\eta_*)^3\Omega_{\mathrm{rad}}\Omega_X^2\epsilon^2 , \tag{6.66}$$

where Ω_X is the density parameter of the source of anisotropic stresses at the moment of creation. For the Goldstone modes the factor Ω_X^2 is replaced by $(v/M_{\mathrm{Pl}})^4$. This strong suppression factor renders GWs from short-lived Goldstone modes entirely unobservable.

The situation is different for *long lived* Goldstone modes. There the suppression factor $(k\eta_*)^3$ is absent. Therefore, if the Goldstone modes remain massless until a time η_{fin}, for modes with $k\eta_{\mathrm{fin}} \gtrsim 1$ the spectrum is scale invariant and the amplitude is given by

$$\Omega_{\mathrm{GW}}(k) \simeq \frac{511}{N}\Omega_{\mathrm{rad}}\left(\frac{v}{M_{\mathrm{Pl}}}\right)^4 , \tag{6.67}$$

which is marginally detectable with the experimental sensitivity of advanced LIGO or LISA and is well within the range of BBO for a GUT scale phase transition. The results for the long-lived source are summarized in Fig. 6.1.

If the Goldstone modes are still present at decoupling, $\eta_{\rm fin} \gtrsim \eta_{\rm dec}$, these GWs will also leave a signature in the cosmic microwave background where they lead to a scale-invariant contribution very similar to the one of global textures, i.e. a $N = 4$ global $\mathcal{O}(N)$ model [31].

Note that this new GW background from self-ordering fields after inflation (e.g. from hybrid preheating) has a power spectrum very similar to that coming from inflation, and therefore it may become important to disentangle both if they are present simultaneously, that is if the scale of inflation and that of symmetry breaking are related by parameters of order one, like in hybrid inflation.

Acknowledgments

DGF would like to express his gratitude to the Cosmology Group of Geneva University, for hospitality received during the fall 2008, when this project was initiated. EF is grateful to the Universidad Autónoma de Madrid for hospitality during the spring of 2009. JGB thanks the Theory Group at CERN for hospitality during the summer of 2009. DGF also acknowledges support from a FPU-Fellowship from the Spanish M.E.C., with Ref. AP-2005-1092. This work is supported by the Swiss National Science Foundation. We also acknowledge financial support from the Madrid Regional Government (CAM) under the program HEPHACOS P-ESP-00346, and the Spanish Science Research Ministry (MEC) under contract FPA2006-05807. DGF and JGB participate in the Consolider-Ingenio 2010 PAU (CSD2007-00060), as well as in the European Union Marie Curie Network "UniverseNet" under contract MRTN-CT-2006-035863.

Chapter 7

The local B-polarization of the CMB: a very sensitive probe of cosmic defects

PHYSICS LETTERS B **695**, 26-29 (2011)

The local B-polarization of the CMB: a very sensitive probe of cosmic defects

Juan García-Bellido, Ruth Durrer, Elisa Fenu, Daniel G. Figueroa and Martin Kunz

We present a new and especially powerful signature of cosmic strings and other topological or non-topological defects in the polarization of the cosmic microwave background (CMB). We show that even if defects contribute 1% or less in the CMB temperature anisotropy spectrum, their signature in the local $\tilde{B}$-polarization correlation function at angular scales of tens of arc-minutes is much larger than that due to gravitational waves from inflation, even if the latter contribute with a ratio as big as $r \simeq 0.1$ to the temperature anisotropies. We show that when going from non-local to local $\tilde{B}$-polarization, the ratio of the defect signal-to-noise with respect to the inflationary value increases by about an order of magnitude. Proposed B-polarization experiments, with a good sensitivity on arc-minute scales, may either detect a contribution from topological defects produced after inflation or place stringent limits on them. Already Planck should be able to improve present constraints on defect models by about an order of magnitude, to the level of $\epsilon = Gv^2 < 10^{-7}$. A future full-sky experiment like CMBpol, with polarization sensitivities of the order of 1μK-arcmin, will be able to constrain the defect parameter ϵ to less than a few $\times 10^{-9}$, depending on the defect model.

DOI: 10.1016/j.physletb.2010.11.031 **PACS** numbers 98.80.-k, 98.80.Cq, 11.27.+d

7.1 Introduction

Many inflationary models terminate with a phase transition which often also leads to the formation of cosmic strings and other topological defects [204, 205]. Furthermore, we have recently argued [120] that the end of hybrid inflation may involve the self-ordering of a N-component scalar field. Even though for $N > 4$ it does not lead to the formation of topological defects, the self-ordering dynamics leads to a scale-invariant spectrum of fluctuations which leaves a signature on the CMB [196, 31]. It has been shown long ago that topological defects do not generate acoustic peaks [32] and therefore they cannot provide the main contribution to the CMB anisotropies. However, they still may provide a fraction of about 10%, similar to a possible gravitational wave contribution [102, 103, 104, 105] in the temperature anisotropies of the CMB.

The perturbations from cosmic strings and other topological defects are proportional to the dimensionless variable $\epsilon = Gv^2$ where v is the symmetry breaking scale. For cosmic strings $\mu = v^2$ is the energy per unit length of the string [30]. Present CMB data limit the contribution from defects [102, 103, 104, 105] such that $\epsilon < 7 \times 10^{-7}$. Stronger limits on ϵ have been derived from the gravitational waves emitted from cosmic string loops [206, 207, 208], but these are quite model dependent and will not be discussed here.

In this Letter we show that measuring the local $\tilde{B}$-polarization correlation function of the CMB provides stringent limits on defects or, alternatively, detects them. The physical reason for this is twofold. First, defects lead not only to tensor but also to even larger vector perturbations [31]. What is more important, vector modes generate much stronger B-polarization than tensor modes with the same amplitude, see e.g. [132]. B-polarization is not only a 'smoking gun' for gravitational waves from inflation, but it is also extremely sensitive to the presence of vector perturbations (vorticity). Furthermore, the B-polarization of the angular power spectrum of topological defects, especially of cosmic strings, peaks on somewhat smaller scales than the one from tensors due to inflation. The local $\tilde{B}$-correlation function, which is obtained from the polarization by two additional derivatives, enhances fluctuations on small angular scales. As we shall see, measuring the local $\tilde{B}$ instead of the usual non-local B correlation function results in an enhancement of the signal to noise ratio from defects with respect to the inflationary one by about a factor 10.

7.2 The local $\tilde{B}$-polarization correlation function

Since Thomson scattering is direction dependent, a non-vanishing quadrupole anisotropy on the surface of last scattering leads to a slight polarization of the CMB [132]. This polarization is described as a rank-2 tensor field $\mathcal{P}_{ab}$ on the sphere, the CMB sky. It is usually decomposed into Stokes parameters, $\mathcal{P}_{ab} = (I\sigma^{(0)}_{ab} + U\sigma^{(1)}_{ab} + V\sigma^{(2)}_{ab} + Q\sigma^{(3)}_{ab})/2 = I\delta_{ab}/2 + P_{ab}$, where $\sigma^{(\mu)}$ are the Pauli matrices [132], and I corresponds to the intensity of the radiation and contains the temperature anisotropies. Thomson scattering does not induce circular polarization so we expect $V = 0$ for the CMB polarization, and hence P_{ab} to be real. We define an orthonormal frame $(\mathbf{e}_1, \mathbf{e}_2, \mathbf{n})$ and the circular polarization vectors $\mathbf{e}_\pm = \frac{1}{\sqrt{2}}(\mathbf{e}_1 \pm i\mathbf{e}_2)$, which allows us to introduce the components $P_{\pm\pm} = 2\mathbf{e}^a_\pm \mathbf{e}^b_\pm P_{ab} = Q \pm iU$ and $P_{+-} \sim V = 0$. The second derivatives of this polarization tensor are related to the local $\tilde{E}$- and $\tilde{B}$-polarizations,

$$\begin{aligned} \nabla_-\nabla_- P_{++} + \nabla_+\nabla_+ P_{--} &= 2\nabla_a\nabla_b P_{ab} \equiv \tilde{E}\,, \\ \nabla_-\nabla_- P_{++} - \nabla_+\nabla_+ P_{--} &= 2\epsilon_{cd}\epsilon_{ab}\nabla_c\nabla_a P_{bd} \equiv \tilde{B}\,. \end{aligned}$$

Here $\nabla_\pm$ are the derivatives in the directions $\mathbf{e}_\pm$ and ϵ_{cd} is the 2-dimensional totally anti-symmetric tensor. These functions are defined *locally*. The usual E- and B-modes can be obtained by applying the inverse Laplacian to the local $\tilde{E}$- and $\tilde{B}$-polarizations. Such inversions of differential operators depend on boundary conditions which can affect the result for local observations. The $\tilde{B}$-correlation function, $C^{\tilde{B}}(\theta) \equiv \langle \tilde{B}(\mathbf{n})\tilde{B}(\mathbf{n}')\rangle_{\mathbf{n}\cdot\mathbf{n}'=\cos\theta}$, is measurable locally. It is related to the B-polarization power spectrum C^B_ℓ by [132]

$$C^{\tilde{B}}(\theta) = \frac{1}{4\pi}\sum_{\ell=2}^{\infty}\frac{(\ell+2)!}{(\ell-2)!}(2\ell+1)P_\ell(\cos\theta)C^B_\ell\,. \tag{7.1}$$

Here $P_\ell(x)$ are the Legendre polynomials. Analogous formulae also hold for $C^{\tilde{E}}$. Note the additional factor $n_\ell = (\ell+2)!/(\ell-2)! = \ell(\ell^2-1)(\ell+2) \sim \ell^4$ as compared to the usual non-local E- and B-polarization correlation functions. At first sight one might argue that whether one expresses a result in terms of C^B_ℓ's or $C^{\tilde{B}}_\ell = n_\ell C^B_\ell$ should really not make a difference since both contain the same information. For an ideal full sky experiment which directly measures the C^B_ℓ with only instrumental errors this is true. But a CMB

experiment usually measures a polarization direction and amplitude with a given resolution over a patch of sky and with a significant noise level, and this makes a big difference as we shall show.

7.3 Results

In Fig. 7.1 we show the local $\tilde{B}$-polarization power spectra for tensor perturbations from inflation, cosmic strings, textures and the large-N limit of the non-linear sigma-model. All spectra are normalized such that they make up 10% of the temperature anisotropy at $\ell = 10$. Details of how these calculations are done can be found in [31] for global defects and the large-N limit and in [209] for cosmic strings. A comparison of the non-local B-polarization power spectra for cosmic strings and inflation can be found in [210].

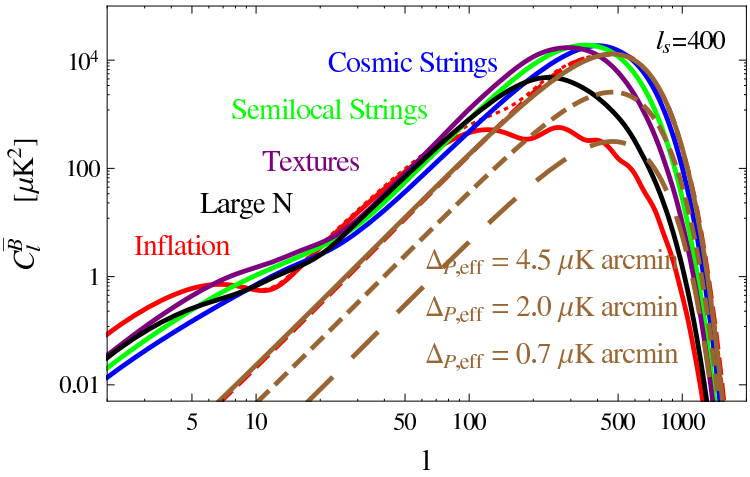

Figure 7.1: The local $\tilde{B}$-polarization power spectra for tensor perturbations from inflation, cosmic strings, textures and the large-N limit of the non-linear sigma-model. All spectra are normalized such that they make up 10% of the temperature anisotropy at $\ell = 10$. The dotted red line corresponds to the inflationary contribution taking into account the induced power from lensing of E-modes. The different noise levels (dashed brown curves) precisely mimic the effect of E-lensing. For a definition of the noise amplitude $\Delta_{P,\mathrm{eff}}$ and the smoothing scale ℓ_s see the text.

It had already been noted in Refs. [106] and [30] that the B-polarization power spectra for defects are larger than those from inflation for the same temperature anisotropy. Defects peak at somewhat higher ℓ's than inflationary perturbations, since B-modes from defects are dominated by their vector (vorticity) modes. This contribution is maximal on scales that are somewhat smaller than the horizon scale, while gravitational waves truly peak at the Hubble horizon at decoupling, which corresponds to $\ell \sim 100$. As a consequence, the *local* $\tilde{B}$-polarization spectra for defects are even larger than those from inflation because of the factor $n_\ell \simeq \ell^4$. This is most pronounced for cosmic strings, which have considerable power on small scales, but it is also true for other defects.

Due to the extra factor n_ℓ, in the local $\tilde{B}$-power spectra shown in Fig. 7.1, power at small scales (high ℓ) counts significantly more than power at larger scales (low ℓ). This is the reason why defect models dominate over the inflationary B-modes of the same amplitude.

This is seen very prominently in the 2-point angular correlation function shown in Fig. 7.2 where we can compare the defect peaks coming from cosmic strings, textures and large-N. Note the decreasing height but increasing width of the peak as we go from cosmic strings to large-N models.

For $0.2 < \theta < 1^o$, where the inflationary $\tilde{B}$-polarization is about -2 mK^2, that from cosmic strings is -150 mK^2, about a factor 100 larger. For textures and the large-N model, the difference is somewhat smaller, roughly a factor of 50 and 10 respectively. The very pronounced peak on very small scales is not visible due to the noise.

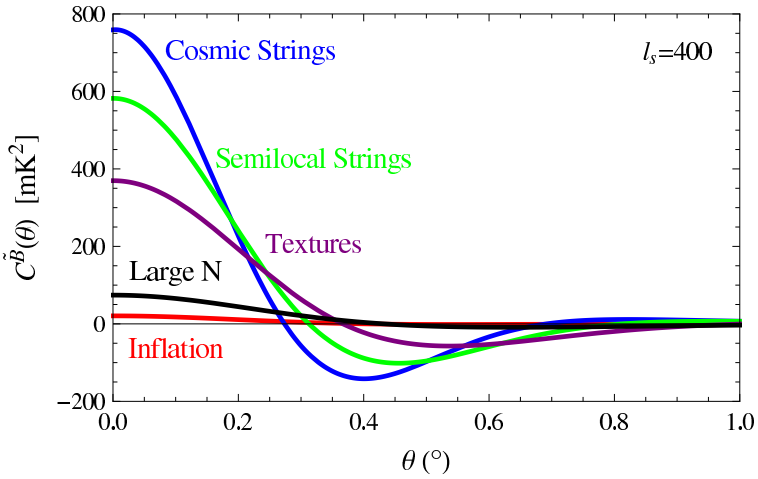

Figure 7.2: The local $\tilde{B}$-polarization angular correlation functions for $\theta < 1^o$ for inflation and the defect models of Fig. 1, with a smoothing scale $l_s = 400$.

Even though constructed ad hoc, coherent causal seed models (but not topological defects) can have acoustic peaks, see Ref. [211], which thus cannot be used as a differentiating signature from inflation. But the fact that polarization is generated at the last scattering surface implies that it cannot have power on scales larger than the horizon at decoupling, corresponding to about $\ell \sim 100$, or angles $\theta > 2^o$, unless something like inflation has taken place [107]. This can only be circumvented if one allows for acausality, i.e. superluminal motion, of the seeds [212], however improbable. In Ref. [123] the authors have shown that this superhorizon signature appears not only in the TE-cross correlation spectrum, but also in the local $\tilde{B}$-polarization spectrum. We find that this is somewhat weakened by re-ionization, which adds power on large scales to the B-polarization from defects, see Fig. 7.1.

7.4 Observational prospects

It is clear from Fig. 7.2 that cosmic defects with equal amplitude as the tensor component from inflation (note $\epsilon = 7 \times 10^{-7}$ is equivalent to $r = 0.1$) would have a significant peak in the two-point correlation function of the local $\tilde{B}$-polarization, on angular scales of order tens of arc-minutes. A relevant issue is whether this peak could be measured with full-sky probes like Planck [8] or CMBpol [213], or even with small-area experiments. This is difficult because, although CMB experiments typically have a flat (white) noise power spectrum for the Stokes parameters, the *local* $n_\ell \sim \ell^4$ factor induces a very blue spectrum for the noise in the local $\tilde{B}$-modes, which erases the significance of the broad defect peak at $\ell \sim 500$

in the $C_\ell^{\tilde{B}}$ power spectrum. Moreover, in order to extract the cosmological $\tilde{B}$-polarization signal it is necessary first to clean the map from the contribution coming from gravitationally lensed $\tilde{E}$-modes. This induces an extra 'lensing noise' $\Delta_{P,\rm eff} \sim 4.5\,\mu$K·arcmin for uncleaned maps that can be reduced to $\sim (0.1 - 0.7)\,\mu$K·arcmin by iterative cleaning or a simple quadratic estimator respectively [214]. Furthermore, CMB experiments have an angular resolution determined by the microwave horn beam width, $\theta_{\rm FWHM}$, which induces an uncertainty in the C_ℓ's that can be described by an exponential factor $\exp[\ell(\ell+1)\sigma_b^2]$, with $\sigma_b = \theta_{\rm FWHM}/\sqrt{8\log 2}$. Resolutions of order 10 arcminutes, like those of the Planck HFI experiment, correspond to multipoles $\ell_b = 1/\sigma_b \sim 800$. Adding the steep polarization noise, with typical amplitude $\Delta_{P,\rm eff} = (0.5 - 12)\,\mu$K·arcmin, would make the signal disappear under the small-scale noise. In order to regulate this divergence, we smooth both the signal and the noise with a Gaussian smoothing of width σ_s, corresponding to a smoothing scale $\ell_s < \ell_b$. We choose $\ell_s = 400$ in our analysis.

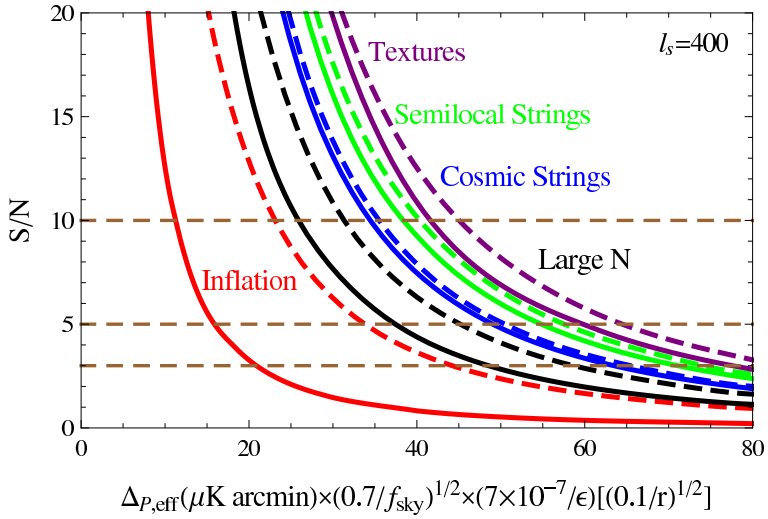

Figure 7.3: The signal-to-noise ratio as a function of the normalized polarization sensitivity, for inflation, cosmic strings, textures and the large-N limit of the non-linear sigma-model. Solid curves: using angular scales up to 1^o and dashed curves: using angular scales up to 4^o, with 6 arcmin resolution bins.

In order to compute the signal-to-noise ratio S/N for detection of the defect peak in the local $\tilde{B}$-correlation function, we split the interval $\theta \in [0, 1^o]$ in 10 equal bins [1]. We then evaluate the theoretical correlation function at the center of those bins, $\mathsf{S}_i = C^{\tilde{B}}(\theta_i)$, and write the covariance matrix of the correlated bins as

$$\mathsf{C}_{ij} = \sum_\ell \frac{2\ell+1}{8\pi^2 f_{\rm sky}} (\mathcal{C}_\ell^{\tilde{B}})^2 P_\ell(\cos\theta_i) P_\ell(\cos\theta_j)\,,$$

where the covariance matrix in ℓ-space is assumed to be diagonal, $\mathrm{cov}[\mathcal{C}_\ell^{\tilde{B}}, \mathcal{C}_{\ell'}^{\tilde{B}}] = 2(\mathcal{C}_\ell^{\tilde{B}})^2\delta_{\ell\ell'}/(2\ell+1)f_{\rm sky}$, with $\mathcal{C}_\ell^{\tilde{B}} = (C_\ell^{\tilde{B}} + N_\ell)\exp[-\ell(\ell+1)/\ell_s^2]$. Here $f_{\rm sky}$ is the fraction of the observed sky which we set to 0.7 for satellite probes. The signal-to-noise ratio for the defect model

[1] Note that Planck has this resolution only for the higher frequency bands, above 200 GHz, where the sensitivity is somewhat reduced.

is $S/N = \sqrt{\mathsf{S}_i \mathsf{C}_{ij}^{-1} \mathsf{S}_j}$. In Fig. 7.3 we show this ratio as a function of the normalized polarization sensitivity for all types of defects as well as for inflation (where $7 \times 10^{-7}/\epsilon$ has to be replaced by $\sqrt{0.1/r}$). The horizontal lines correspond to 3, 5 and 10-σ respectively. To show why the choice of $\theta_{\rm max} = 1^o$ is optimal we also plot (dashed lines) the S/N for $\theta_{\rm max} = 4^o$, at fixed resolution ($6'$). For the latter, the noise level allowed for a 3-σ detection increases by more than a factor of 2 for inflation while it does not change much for defects. This behaviour is a telltale sign for defects, and shows that their signal is strongly localised in the angular correlation function, which distinguishes them e.g. from inflationary tensor perturbations and lensed E-modes: the S/N curve from defects does not change much for angles above $\sim 1^o$, while the one from inflation increases significantly.

In Table 7.1 we give the values of ϵ which are measured at 3σ by Planck (assuming $\Delta_{P,\rm eff} = 11.2\,\mu$K·arcmin [123], where the de-lensing error is added in quadrature), a CMBpol-like experiment with polarization sensitivity $\Delta_{P,\rm eff} = 0.7\,\mu$K·arcmin, and a dedicated CMB experiment with $\Delta_{P,\rm eff} = 0.01\,\mu$K·arcmin. Note, however, that it is not clear how to perform the de-lensing of the B-modes to the level of precision needed for the last case.

In Fig. 7.4 we show the ratio of S/N from defects to the one from inflation for non-local (dashed) and local $\tilde{B}$-modes (solid curves). Clearly, in the local polarization the defect signal is substantially enhanced. It is interesting to note that actually textures fare better than cosmic strings even though they have less power on small scales. The reason is that the very small scales are dominated by noise and the signal mainly comes from the intermediate scales around 0.3^o where textures dominate, see Fig. 2.

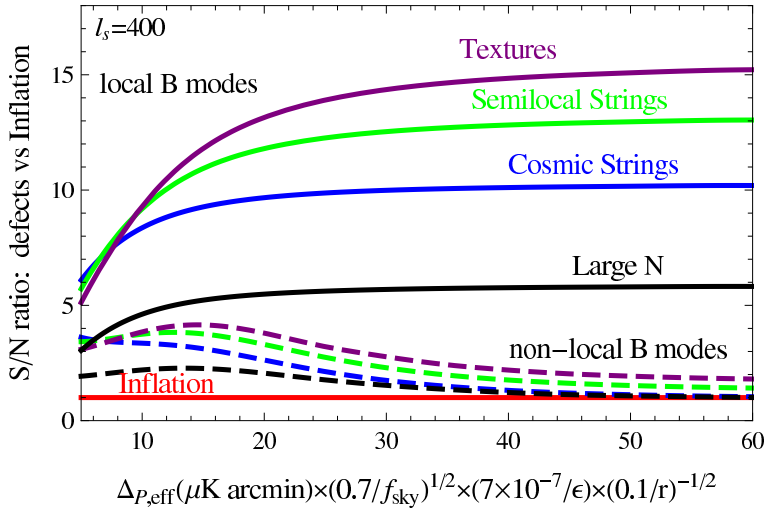

Figure 7.4: The ratio of the signal-to-noise from defects to the one from inflation. Solid curves: measuring the local $\tilde{B}$ correlation function. Dashed curves: measuring the non-local B correlation function.

7.5 Conclusions

In this Letter we have shown that measuring the local $\tilde{B}$-polarization correlation function on small scales, $\theta \lesssim 1^o$ is a superb way to detect topological and non-topological defects,

Table 7.1: The limiting amplitude, $\epsilon = Gv^2$, of various defects, at 3-σ in the range $\theta \in [0, 1^o]$, for Planck ($\Delta_{P,\rm eff} = 11.2\,\mu$K·arcmin), CMBpol-like exp. ($\Delta_{P,\rm eff} = 0.7\,\mu$K·arcmin) and a dedicated CMB experiment with ($\Delta_{P,\rm eff} = 0.01\,\mu$K·arcmin). We set $f_{\rm sky} = 0.7$.

$S/N = 3$	Strings	Semi-local	Textures	Large-N
Planck	$1.2 \cdot 10^{-7}$	$1.1 \cdot 10^{-7}$	$1.0 \cdot 10^{-7}$	$1.6 \cdot 10^{-7}$
CMBpol	$7.7 \cdot 10^{-9}$	$6.9 \cdot 10^{-9}$	$6.3 \cdot 10^{-9}$	$1.0 \cdot 10^{-8}$
$\tilde{B}$ exp	$1.1 \cdot 10^{-10}$	$1.0 \cdot 10^{-10}$	$0.9 \cdot 10^{-10}$	$1.4 \cdot 10^{-10}$

or alternatively to constrain their contribution to the CMB. For simple inflationary models which lead to defect formation at the end of inflation, a value of $\epsilon \simeq 10^{-7} \div 10^{-8}$ seems rather natural, hence the achieved limits include the relevant regime. The fact that the local $\tilde{B}$-polarization from defects is dominated by the vector mode, which peaks on scales smaller than the horizon, is responsible for a significant enhancement of the local $\tilde{B}$-polarization correlation function on tens of arc-minute scales.

Even though the Planck satellite is not the ideal probe for constraining these models, if it finally reaches down to $r \leq 0.025$, see Ref. [215], it will either lead to the detection of a defect contribution, or it will constrain it to $\epsilon = Gv^2 \lesssim 10^{-7}$, depending on the defect model (textures being the most constrained and Large-N non-topological defects the least). Future CMB experiments, with 0.1 arc-minute resolution and sensitivities at the level of $0.1\,\mu$K in polarization, could in principle reach the bound $\epsilon < 10^{-10}$ for most defect types, which would rule out a large fraction of present models.

Acknowledgements

We thank Neil Bevis, Mark Hindmarsh and Jon Urrestilla for allowing us to use their C_ℓ's from cosmic string and texture simulations. D.G.F. acknowledges support from a Marie Curie Early Stage Research Training Fellowship associated with the EU RTN "UniverseNet" during his stay at CERN TH-Division. J.G.B. thanks the Institute de Physique Theorique de l'Universite de Geneve for their generous hospitality during his sabbatical in Geneva. This work is supported by the Spanish MICINN under project AYA2009-13936-C06-06 and by the EU FP6 Marie Curie Research and Training Network "UniverseNet" (MRTN-CT-2006-035863).

Chapter 8

Conclusions

In this Thesis I have investigate the primordial Universe through the imprints that high energy mechanisms may have left in the CMB and GWB. This represents one of the most challenging aspects of modern Cosmology: the new incoming data will reach a level of precision that allows us to gain a deeper understanding of the processes that characterized our Universe just after the Big Bang, and Cosmology represents a unique possibility to get insights and eventually test the Physics at so high temperatures.

In particular, I concentrate my research on two different fundamental features that may have characterized the early Universe: primordial magnetic fields and cosmological defects.

On one hand, we address the basic question concerning the origin of the MF observed today in galaxies and clusters: it is still unclear whether this MF is seeded by a primordial field originated in the early Universe through some high energy physical processes, or it is the result of charge separation scenarios during late structure formation. Assuming that the primordial option is the correct one, we might be able to detect the imprints that such a seed field would have left in the CMB. Through this analysis important constraints on the initial amplitude that such a primordial MF had before recombination have already been obtained in the literature.

First we analyze the interaction between MFs and GWs, confirming that this is not a cause of amplification of none of these two physical quantities. Considering other consequences of this interaction, we follow an idea presented previously in the literature according to which this allows us to obtain more stringent upper-bounds than through a CMB analysis on the amplitude of a primordial MF in case it is produced by causal mechanisms. Applying the nucleosynthesis limit on the GW energy density produced by a seed field, we are able to exclude most of the primordial mechanisms proposed to generate MFs in the early Universe. Indeed, we confirm that causally generated MFs do not have enough power on large scale even if they present initially an helical component that leads to an inverse cascade. The limits in the case of helical MFs are relaxed with respect the ones obtained for standard non-helical fields, but they cannot seed the observed MF in galaxies and clusters, even considering the most efficient dynamo amplification. Only MFs generated during inflation with a red spectrum, or the ones produced during a later QCD phase transition may have enough power to seed the present field.

In order to cover another chapter concerning the generation of a primordial MF in the early Universe, we study the possibility of producing a small seed field through non-linear

dynamics that create vortical currents when the tight-coupling approximation between photons and baryons breaks down near the last scattering surface. This mechanism is necessarily present in the early Universe and it has been already analyzed by several authors. With the aim of reviewing this process in all its completeness, we take into account for the first time in the literature all the contributions to the resulting MF power spectrum. With the help of a numerical computation we obtain as final result a MF amplitude of 10^{-29} Gauss on a comoving smoothing scale of 1 Mpc. This means that the seed field generated by magnetogenesis around recombination is too weak to sustain the amplification mechanisms that can amplify it in order to explain the observed field today.

Another important step concerning the MF puzzle consists in the analysis of the influence that massless particles free-streaming before recombination have on the imprints that a constant MF leaves on the CMB anisotropies. While a constant seed field gives mainly a quadrupole contribution, we observe how this quadrupole can be erased through a compensation of the anisotropic stresses of the MF and of massless particles free-streaming in an anisotropic Universe. This compensation results in a subsequent isotropization of the Universe and, in the case where this remains true even during recombination, in a complete cancelation of the quadrupole generated by the MF alone. Once we consider primordial neutrinos to have the role of the above free-streaming particles, of course this argument will depend on their masses and the final cancelation will be more effective the longer they are relativistic.

Even if no conclusive understanding concerning the origin of the observed MF today has been reached yet, more clear answers have been provided to some of the fundamental questions about the option of a primordial origin. Of course more work is needed in order to fully complete the MF puzzle.

Another aspect of my research is focused on the investigation of the remnants produced by cosmological defects that may have played a role in the early Universe.

A first study concentrate on the GWs produced by a self-ordering scalar field once it broke a global symmetry. We underline that the super-horizon tail of such GWs is characterized by a flat spectrum whose amplitude is, for some value of the true vacuum expectation, in the range of sensitivity of some GW observers. This means that it is very similar to the one produced by primordial tensor perturbations generated during inflation. Therefore, it is important to find an efficient way to disentangle these two spectra in the case they have also similar amplitudes. This is the motivation that pushes us toward the analysis of the B-polarization spectrum produced by defects a the second project on this same topic.

With the aim of detecting or better constraining the defect contribution to CMB anisotropies, we investigate the local $\tilde{B}$-polarization of the CMB as produced by different kind of cosmological defects and by primordial inflationary perturbations. We first underlined that, since real CMB experiments are not full sky ideal probes of the temperature anisotropies, the analysis of the local $\tilde{B}$-modes, which do not depend on the boundary conditions, gives rather big advantages than the standard non-local B-modes. Indeed, in the local polarization the defect signal is substantially enhanced with respect to the inflationary one, while, if we consider the non-local one, this is not the case, namely the signal to noise ratios for the two models are almost comparable. Moreover, we also show that the comparison between the two signal to noise ratios corresponding to different sky patch

sizes shows that, once we enlarge the patch of the sky that we observe, the inflation signal to noise ratio increases significantly, while the one for defects does not change much. This is a consequence of the a-causal nature of inflation, that presents its main features in a range of angles corresponding to distances bigger than the Hubble size at recombination. Therefore, once we consider sky patches corresponding to smaller angles we better extract the signal corresponding to causal processes such as defect perturbation generation. With our proposed sky analysis, we forecast an improvement on the current upper-bounds on the defect contribution to the CMB anisotropies by several orders of magnitude.

The research present in this Thesis represents important bricks on the way of building a more complete and deep understanding of the physical mechanisms the characterized the first few seconds after the creation of our Universe, a regime of temperatures and energies that is impossible to access otherwise in a normal laboratory. Moreover, it also underlines the open questions that still remain unsolved. It is therefore crucial to keep investigating both on the theoretical and experimental points of view, with the certitude that, for every answered query, many more new and interesting issues will arise.

Bibliography

[1] http://www.aip.org/history/cosmology/.

[2] Kolb, R., *Blind watchers of the sky: the people and ideas that shaped our view of the universe*, Basic Book, 1996.

[3] Penzias, A. A. and Wilson, R. W., The Astrophysical Journal**142** (1965) 419.

[4] Smoot, G. F. et al., Astrophys.J. **437** (1994) 1.

[5] Liddle, A. R. and Lyth, D. H., *Cosmological Inflation and Large-Scale Structure*, 2000.

[6] Bennett, C. et al., Astrophys.J.Suppl. **148** (2003) 1.

[7] Komatsu, E. et al., Astrophys.J.Suppl. **180** (2009) 330.

[8] http://www.esa.int/specials/planck/index.html.

[9] Hulse, R. A. and Taylor, J. H., Astrophys.J. **195** (1975) L51.

[10] http://www.ligo.caltech.edu/.

[11] Abbott, B. et al., Astrophys.J. **659** (2007) 918.

[12] https://wwwcascina.virgo.infn.it/.

[13] http://lisa.jpl.nasa.gov/.

[14] http://www.srl.caltech.edu.

[15] http://lisa.esa.int.

[16] Hughes, S. A., (2007), arXiv:0711.0188 (gr-qc).

[17] Smith, T. L., Kamionkowski, M., and Cooray, A., Phys.Rev. **D73** (2006) 023504.

[18] Abadie, J. et al., (2011).

[19] Abadie, J. et al., Astrophys.J. **722** (2010) 1504.

[20] Ashoorioon, A. and Konstandin, T., JHEP **0907** (2009) 086.

[21] Stevens, T. and Johnson, M. B., Phys.Rev. **D80** (2009) 083011.

[22] Stevens, T. and Johnson, M. B., (2010), arXiv:1001.3694.

[23] Rummukainen, K., Tsypin, M., Kajantie, K., Laine, M., and Shaposhnikov, M. E., Nucl.Phys. **B532** (1998) 283.

[24] Rummukainen, K., Kajantie, K., Laine, M., Shaposhnikov, M. E., and Tsypin, M., (1998), arXiv:hep-ph/9809435.

[25] Caprini, C., Durrer, R., and Servant, G., JCAP **0912** (2009) 024.

[26] Aoki, Y., Fodor, Z., Katz, S., and Szabo, K., Phys.Lett. **B643** (2006) 46.

[27] Aoki, Y. et al., JHEP **0906** (2009) 088.

[28] Boyarsky, A., Ruchayskiy, O., and Shaposhnikov, M., Ann.Rev.Nucl.Part.Sci. **59** (2009) 191.

[29] Schwarz, D. J. and Stuke, M., JCAP **0911** (2009) 025.

[30] Durrer, R., Kunz, M., and Melchiorri, A., Phys.Rept. **364** (2002) 1.

[31] Durrer, R., Kunz, M., and Melchiorri, A., Phys.Rev. **D59** (1999) 123005.

[32] Durrer, R., Gangui, A., and Sakellariadou, M., Phys.Rev.Lett. **76** (1996) 579.

[33] Pen, U.-L., Seljak, U., and Turok, N., Phys.Rev.Lett. **79** (1997) 1611.

[34] Bevis, N., Hindmarsh, M., Kunz, M., and Urrestilla, J., Phys.Rev. **D82** (2010) 065004.

[35] Giovannini, M., Int.J.Mod.Phys. **D13** (2004) 391.

[36] Subramanian, K., PoS **MRU** (2007) 071.

[37] Battaglia, N., Pfrommer, C., Sievers, J., Bond, J., and Ensslin, T., Mon.Not.Roy.Astron.Soc. **393** (2009) 1073.

[38] Kronberg, P. P., Rept. Prog. Phys. **57** (1994) 325.

[39] Pentericci, L., Van Reeven, W., Carilli, C., Rottgering, H., and Miley, G., Astron.Astrophys.Suppl.Ser. **145** (2000) 121.

[40] Bernet, M. L., Miniati, F., Lilly, S. J., Kronberg, P. P., and Dessauges-Zavadsky, M., Nature **454** (2008) 302.

[41] Clarke, T. E., Kronberg, P. P., and Boehringer, H., Astrophys. J. **547** (2001) L111.

[42] Govoni, F. and Feretti, L., Int. J. Mod. Phys. **D13** (2004) 1549.

[43] Xu, Y., Kronberg, P. P., Habib, S., and Dufton, Q. W., Astrophys.J. **637** (2006) 19.

[44] Neronov, A. and Vovk, I., Science **328** (2010) 73.

[45] Ando, S. and Kusenko, A., Astrophys.J. **722** (2010) L39.

[46] Dolag, K., Kachelriess, M., Ostapchenko, S., and Tomas, R., Astrophys.J. **727** (2011) L4.

[47] Essey, W., Ando, S., and Kusenko, A., (2010), arXiv:1012.5313 (astro-ph.HE).

[48] Brandenburg, A. and Subramanian, K., Phys.Rept. **417** (2005) 1.

[49] Kulsrud, R. M. and Zweibel, E. G., Rept.Prog.Phys. **71** (2008) 0046091.

[50] Kandus, A., Kunze, K. E., and Tsagas, C. G., (2010), arXiv:1007.3891 (astro-ph.CO).

[51] Enqvist, K. and Olesen, P., Phys.Lett. **B319** (1993) 178.

[52] Joyce, M. and Shaposhnikov, M. E., Phys.Rev.Lett. **79** (1997) 1193.

[53] Grasso, D. and Riotto, A., Phys.Lett. **B418** (1998) 258.

[54] Boeckel, T. and Schaffner-Bielich, J., Phys.Rev.Lett. **105** (2010) 041301.

[55] Turner, M. S. and Widrow, L. M., Phys. Rev. **D37** (1988) 2743.

[56] Ratra, B., Astrophys. J. **391** (1992) L1.

[57] Giovannini, M. and Shaposhnikov, M. E., Phys.Rev. **D62** (2000) 103512.

[58] Bamba, K., Phys.Rev. **D75** (2007) 083516.

[59] Bamba, K., Geng, C., and Ho, S., JCAP **0811** (2008) 013.

[60] Barrow, J. D., Ferreira, P. G., and Silk, J., Phys.Rev.Lett. **78** (1997) 3610.

[61] Mack, A., Kahniashvili, T., and Kosowsky, A., Phys.Rev. **D65** (2002) 123004.

[62] Ohno, H., Takada, M., Dolag, K., Bartelmann, M., and Sugiyama, N., Astrophys.J. **584** (2003) 599.

[63] Durrer, R., Ferreira, P., and Kahniashvili, T., Phys.Rev. **D61** (2000) 043001.

[64] Seshadri, T. and Subramanian, K., Phys.Rev.Lett. **103** (2009) 081303.

[65] Caprini, C., Finelli, F., Paoletti, D., and Riotto, A., JCAP **0906** (2009) 021.

[66] Trivedi, P., Subramanian, K., and Seshadri, T., Phys.Rev. **D82** (2010) 123006.

[67] Yamazaki, D. G., Ichiki, K., Kajino, T., and Mathews, G. J., Phys.Rev. **D78** (2008) 123001.

[68] Durrer, R. and Caprini, C., JCAP **0311** (2003) 010.

[69] Durrer, R., New Astron.Rev. **51** (2007) 275.

[70] http://www.skatelescope.org/.

[71] Tsagas, C. G., Phys.Rev. **D72** (2005) 123509.

[72] Betschart, G., Zunckel, C., Dunsby, P., and Marklund, M., Phys. Rev. **D72** (2005) 123514.

[73] Zunckel, C., Betschart, G., Dunsby, P. K. S., and Marklund, M., Phys. Rev. **D73** (2006) 103509.

[74] Fenu, E. and Durrer, R., Phys.Rev. **D79** (2009) 024021.

[75] Tsagas, C. G., Phys.Rev. **D75** (2007) 087901.

[76] Betschart, G., Zunckel, C., Dunsby, P. K., and Marklund, M., Phys.Rev. **D75** (2007) 087902.

[77] Caprini, C. and Durrer, R., Phys.Rev. **D65** (2001) 023517.

[78] Banerjee, R. and Jedamzik, K., Phys.Rev. **D70** (2004) 123003.

[79] Campanelli, L., Phys.Rev.Lett. **98** (2007) 251302.

[80] Christensson, M., Hindmarsh, M., and Brandenburg, A., (2000), arXiv:astro-ph/0011321.

[81] Caprini, C., Durrer, R., and Fenu, E., JCAP **0911** (2009) 001.

[82] Caprini, C. and Durrer, R., Phys.Rev. **D74** (2006) 063521.

[83] Caprini, C., Durrer, R., Konstandin, T., and Servant, G., Phys.Rev. **D79** (2009) 083519.

[84] Jedamzik, K., Katalinic, V., and Olinto, A. V., Phys.Rev. **D57** (1998) 3264.

[85] Subramanian, K. and Barrow, J. D., Phys.Rev. **D58** (1998) 083502.

[86] Harrison, E. R., Mon. Not. Roy. Astron. Soc. **147** (1970) 279.

[87] Hogan, C. J., (2000), arXiv:astro-ph/0005380.

[88] Berezhiani, Z. and Dolgov, A. D., Astropart. Phys. **21** (2004) 59.

[89] Gopal, R. and Sethi, S., Mon. Not. Roy. Astron. Soc. **363** (2005) 521.

[90] Siegel, E. R. and Fry, J. N., Astrophys. J. **651** (2006) 627.

[91] Kobayashi, T., Maartens, R., Shiromizu, T., and Takahashi, K., Phys. Rev. **D75** (2007) 103501.

[92] Maeda, S., Kitagawa, S., Kobayashi, T., and Shiromizu, T., Class. Quant. Grav. **26** (2009) 135014.

[93] Matarrese, S., Mollerach, S., Notari, A., and Riotto, A., Phys. Rev. **D71** (2005) 043502.

[94] Ichiki, K., Takahashi, K., Sugiyama, N., Hanayama, H., and Ohno, H., (2007), arXiv:astro-ph/0701329.

[95] Fenu, E., Pitrou, C., and Maartens, R., (2010), arXiv:1012.2958 (astro-ph.CO).

[96] Pitrou, C., Class. Quant. Grav. **26** (2009) 065006.

[97] Christopherson, A. J., Malik, K. A., and Matravers, D. R., Phys. Rev. **D79** (2009) 123523.

[98] Hollenstein, L., Caprini, C., Crittenden, R., and Maartens, R., Phys.Rev. **D77** (2008) 063517.

[99] Barrow, J. D., Canadian Journal of Physics **64** (1986) 152.

[100] Barrow, J. D., Juszkiewicz, R., and Sonoda, D. H., Monthly Notice of the Royal Astronomical Society**213** (1985) 917.

[101] Scannapieco, E. S. and Ferreira, P. G., Phys.Rev. (1997) 7493.

[102] Seljak, U. and Slosar, A., Phys.Rev. **D74** (2006) 063523.

[103] Bevis, N., Hindmarsh, M., Kunz, M., and Urrestilla, J., Phys.Rev.Lett. **100** (2008) 021301.

[104] Pogosian, L. and Wyman, M., Phys.Rev. **D77** (2008) 083509.

[105] Urrestilla, J., Bevis, N., Hindmarsh, M., Kunz, M., and Liddle, A. R., JCAP **0807** (2008) 010.

[106] Seljak, U., Pen, U.-L., and Turok, N., Phys.Rev.Lett. **79** (1997) 1615.

[107] Spergel, D. N. and Zaldarriaga, M., Phys.Rev.Lett. **79** (1997) 2180.

[108] Khlebnikov, S. and Tkachev, I., Phys.Rev. **D56** (1997) 653.

[109] Garcia-Bellido, J., (1998), arXiv:hep-ph/9804205.

[110] Easther, R. and Lim, E. A., JCAP **0604** (2006) 010.

[111] Garcia-Bellido, J. and Figueroa, D. G., Phys.Rev.Lett. **98** (2007) 061302.

[112] Easther, R., Giblin, John T., J., and Lim, E. A., Phys.Rev.Lett. **99** (2007) 221301.

[113] Garcia-Bellido, J., Figueroa, D. G., and Sastre, A., Phys.Rev. **D77** (2008) 043517.

[114] Dufaux, J. F., Bergman, A., Felder, G. N., Kofman, L., and Uzan, J.-P., Phys.Rev. **D76** (2007) 123517.

[115] Dufaux, J. F., Felder, G. N., Kofman, L., and Navros, O., JCAP **0903** (2009) 001.

[116] Kamionkowski, M., Kosowsky, A., and Turner, M. S., Phys.Rev. **D49** (1994) 2837.

[117] Caprini, C., Durrer, R., and Servant, G., Phys.Rev. **D77** (2008) 124015.

[118] Huber, S. J. and Konstandin, T., JCAP **0809** (2008) 022.

[119] Turok, N. and Spergel, D. N., Phys. Rev. Lett. **66** (1991) 3093.

[120] Fenu, E., Figueroa, D. G., Durrer, R., and Garcia-Bellido, J., JCAP **0910** (2009) 005.

[121] Jones-Smith, K., Krauss, L. M., and Mathur, H., Phys.Rev.Lett. **100** (2008) 131302.

[122] Garcia-Bellido, J., Durrer, R., Fenu, E., Figueroa, D. G., and Kunz, M., Phys.Lett. **B695** (2011) 26.

[123] Baumann, D. and Zaldarriaga, M., JCAP **0906** (2009) 013.

[124] Tsagas, C. G., Dunsby, P. K., and Marklund, M., Phys.Lett. **B561** (2003) 17.

[125] Ichiki, K., Takahashi, K., Ohno, H., Hanayama, H., and Sugiyama, N., Science **311** (2006) 827.

[126] Ryu, D., Kang, H., Cho, J., and Das, S., (2008), arXiv:0805.2466 (astro-ph).

[127] Barrow, J. D., Maartens, R., and Tsagas, C. G., Phys.Rept. **449** (2007) 131.

[128] Tsagas, C. G., Class.Quant.Grav. **22** (2005) 393.

[129] Abramowitz, M. and Stegun, I., *Handbook of Mathematical Functions*, Dover Publications, 1972.

[130] Caprini, C., Durrer, R., and Kahniashvili, T., Phys.Rev. **D69** (2004) 063006.

[131] Weinberg, S., *General Relativity and Gravitation*, Weyley and Sons, 1972.

[132] Durrer, R., *The Cosmic Microwave Background*, Cambridge University Press, 2008.

[133] Martin-Garcia, J., xPerm and xAct, http://metric.iem.csic.es/Martin-Garcia/xAct/index.html.

[134] Anber, M. M. and Sorbo, L., JCAP **0610** (2006) 018.

[135] Campanelli, L., Int.J.Mod.Phys. **D18** (2009) 1395.

[136] Campanelli, L., Cea, P., and Fogli, G., Phys.Lett. **B680** (2009) 125.

[137] Cornwall, J. M., Phys.Rev. **D56** (1997) 6146.

[138] Vachaspati, T., Phys.Rev.Lett. **87** (2001) 251302.

[139] Copi, C. J., Ferrer, F., Vachaspati, T., and Achucarro, A., Phys.Rev.Lett. **101** (2008) 171302.

[140] Lemoine, D. and Lemoine, M., Phys.Rev. **52** (1995) 1955.

[141] von Karman, T., Proceedings of the National Academy of Science **34** (1948) 530.

[142] Kazantsev, A. P., Soviet Journal of Experimental and Theoretical Physics **26** (1968) 1031.

[143] Schekochihin, A. A., Maron, J. L., Cowley, S. C., and McWilliams, J. C., The Astrophysical Journal**576** (2002) 806.

[144] Shore, S., *Astrophysical Hydrodynamics: an Introduction*, WILEY-VCH Verlag GmbH, Weinheim, 2007.

[145] Davidson, P. A., Journal of Turbulence **1** (2000) 6.

[146] Davidson, P., *Turbulence*, Oxford University Press, 2004.

[147] Landau, L. and Lifshitz, E., *"Hydrodynamik", Lehrbuch der theoretischen Physik Band VI*, Akademie Verlag Berlin, 1990.

[148] Kahniashvili, T., Campanelli, L., Gogoberidze, G., Maravin, Y., and Ratra, B., Phys.Rev. **D78** (2008) 123006.

[149] Kosowsky, A., Mack, A., and Kahniashvili, T., Phys.Rev. **D66** (2002) 024030.

[150] Maggiore, M., Phys.Rept. **331** (2000) 283.

[151] Fields, B. and Sarkar, S., ArXiv Astrophysics e-prints (2006), arXiv:astro-ph/0601514.

[152] Arnold, P., Moore, G. D., and Yaffe, L. G., Journal of High Energy Physics **11** (2000) 1.

[153] Sethi, S. K. and Subramanian, K., JCAP **0911** (2009) 021.

[154] Schleicher, D. R. G. et al., (2010), arXiv:1003.1135 (astro-ph.CO).

[155] Maartens, R., Gebbie, T., and Ellis, G. F. R., Phys. Rev. **D59** (1999) 083506.

[156] Takahashi, K., Ichiki, K., and Sugiyama, N., Phys. Rev. **D77** (2008) 124028.

[157] Tsagas, C. G., Challinor, A., and Maartens, R., Phys. Rept. **465** (2008) 61.

[158] Takahashi, K., (2008), arXiv:0804.3578 (astro-ph).

[159] Seager, S., Sasselov, D. D., and Scott, D., Astrophys. J. **523** (1999) L1.

[160] Senatore, L., Tassev, S., and Zaldarriaga, M., JCAP **0908** (2009) 031.

[161] Fitzpatrick, A. L., Senatore, L., and Zaldarriaga, M., JCAP **1005** (2010) 004.

[162] Komatsu, E. et al., (2010), arXiv:1001.4538 (astro-ph).

[163] Pitrou, C., Uzan, J., and Bernardeau, F., JCAP **7** (2010) 3.

[164] Lu, T. H.-C., Ananda, K., Clarkson, C., and Maartens, R., JCAP **0902** (2009) 023.

[165] Christopherson, A. J. and Malik, K. A., (2010), arXiv:1010.4885 (gr-qc).

[166] Pitrou, C., (2010), arXiv:1012.0546 (astro-ph.CO).

[167] Pitrou, C., Class. Quant. Grav. **24** (2007) 6127.

[168] Durrer, R., Fund. Cosmic Phys. **15** (1994) 209.

[169] Pitrou, C., Uzan, J.-P., and Bernardeau, F., Phys. Rev. **D78** (2008) 063526.

[170] Novikov, I. D., Sov. Astron. **12** (1968) 427.

[171] Paoletti, D., Finelli, F., and Paci, F., Mon.Not.Roy.Astron.Soc. **396** (2009) 523.

[172] Shaw, J. and Lewis, A., Phys.Rev. **D81** (2010) 043517.

[173] Bonvin, C. and Caprini, C., JCAP **1005** (2010) 022.

[174] Kunze, K. E., Phys.Rev. **D83** (2011) 023006.

[175] Graham, P. W., Harnik, R., and Rajendran, S., Phys.Rev. **D82** (2010) 063524.

[176] Pontzen, A. and Challinor, A., Mon.Not.Roy.Astron.Soc. (2007).

[177] Amsler, C. et al., Phys. Lett. **B667** (2008) 1.

[178] Larson, D. et al., Astrophys. J. Supp. **192** (2011) 16.

[179] Camerini, R. et al., Phys.Rev. **D77** (2008) 101301.

[180] Durrer, R., J.Phys.Conf.Ser. **222** (2010) 012021.

[181] Maggiore, M., *Gravitational Waves. Vol. 1: Theory and Experiments*, Oxford University Press, 2007.

[182] Hogan, C. J., AIP Conf.Proc. **873** (2006) 30.

[183] Buonanno, A., (2007), arXiv:0709.4682 (gr-qc).

[184] Kosowsky, A., Turner, M. S., and Watkins, R., Phys. Rev. **D45** (1992) 4514.

[185] Kosowsky, A. and Turner, M. S., Phys.Rev. **D47** (1993) 4372.

[186] Grojean, C. and Servant, G., Phys.Rev. **D75** (2007) 043507.

[187] Kahniashvili, T., Kosowsky, A., Gogoberidze, G., and Maravin, Y., Phys.Rev. **D78** (2008) 043003.

[188] Starobinskii, A. A., Spectrum of Relict Gravitational Radiation and the Early State of the Universe - JETP Lett. 30, 682 (1979), in *30 Years of the Landau Institute*, edited by I. M. Khalatnikov & V. P. Mineev, pages 767–+, 1996.

[189] Garcia-Bellido, J. and Linde, A. D., Phys.Rev. **D57** (1998) 6075.

[190] Garcia-Bellido, J., Grigoriev, D. Y., Kusenko, A., and Shaposhnikov, M. E., Phys.Rev. **D60** (1999) 123504.

[191] Felder, G. N. et al., Phys.Rev.Lett. **87** (2001) 011601.

[192] Felder, G. N., Kofman, L., and Linde, A. D., Phys.Rev. **D64** (2001) 123517.

[193] Garcia-Bellido, J. and Ruiz Morales, E., Phys.Lett. **B536** (2002) 193.

[194] J. Garcia-Bellido, M. G. P. and Gonzalez-Arroyo, A., Phys. Rev. **D67** (2003) 103501.

[195] Diaz-Gil, A., Garcia-Bellido, J., Garcia Perez, M., and Gonzalez-Arroyo, A., Phys.Rev.Lett. **100** (2008) 241301.

[196] Kunz, M. and Durrer, R., Phys.Rev. **D55** (1997) 4516.

[197] Krauss, L. M., Phys. Lett. **B284** (1992) 229.

[198] Jones-Smith, K., Krauss, L. M., and Mathur, H., (2009), arXiv:0907.4857(astro-ph.CO).

[199] http://universe.nasa.gov/new/program/bbo.html.

[200] Corbin, V. and Cornish, N. J., Class. Quant. Grav. **23** (2006) 2435.

[201] Harry, G. M., Fritschel, P., Shaddock, D. A., Folkner, W., and Phinney, E. S., Class. Quant. Grav. **23** (2006) 4887.

[202] Durrer, R., New Astronomy Reviews **43** (1999) 111.

[203] Chongchitnan, S. and Efstathiou, G., Phys.Rev. **D73** (2006) 083511.

[204] Jeannerot, R., Rocher, J., and Sakellariadou, M., Phys.Rev. **D68** (2003) 103514.

[205] Rocher, J. and Sakellariadou, M., JCAP **0503** (2005) 004.

[206] Vachaspati, T. and Vilenkin, A., Phys. Rev. **D30** (1984) 2036.

[207] Durrer, R., Nucl. Phys. **B328** (1989) 238.

[208] Jenet, F. A. et al., Astrophys.J. **653** (2006) 1571.

[209] Bevis, N., Hindmarsh, M., Kunz, M., and Urrestilla, J., Phys. Rev. **D75** (2007) 065015.

[210] Urrestilla, J. et al., Phys. Rev. **D77** (2008) 123005.

[211] Turok, N., Phys.Rev.Lett. **77** (1996) 4138.

[212] Scodeller, S., Kunz, M., and Durrer, R., Phys.Rev. **D79** (2009) 083515.

[213] http://cmbpol.uchicago.edu/.

[214] Seljak, U. and Hirata, C. M., Phys.Rev. **D69** (2004) 043005.

[215] Esa document 'planck-incannexes' on the r-limit from 4 sky coverages.